University of Nevada, Reno

Advancing Gait Identification and Analysis with a Soft, Compact 3D Force Sensing Insole System

A thesis submitted in partial fulfillment of the

requirements for the degree of Master of Science in

Biomedical Engineering

by

Jared A. Vlach

Dr. Yantao Shen/Thesis Advisor

May, 2024

THE GRADUATE SCHOOL

We recommend that the thesis prepared under our supervision by

JARED VLACH

entitled
Advancing Gait Identification and Analysis with a Soft, Compact 3D Force Sensing

Insole System

be accepted in partial fulfillment of the requirements for the degree of

MASTER OF SCIENCE

Yantao Shen, Ph.D.
Advisor

Jeongwon Park, Ph.D.
Co-advisor

Sergiu Dascalu, Ph.D
Graduate School Representative

Markus Kemmelmeier, Ph.D.
Dean, Graduate School

May, 2024

Abstract

The field of smart insoles has seen tremendous improvement throughout the last 25 years, driven primarily by the miniaturization of technology and introduction of novel sensing methods. These innovations have broadened the scope of applications in areas such as general health monitoring, disease identification, and sports analysis. However, despite these strides, many research-driven insole advancements still suffer from limitations, including rigidity, bulkiness, high costs, discomfort, and a focus on measurements predominantly in the normal direction.

This research targets to address these shortcomings by developing a small, soft, flexible, cost-effective, resilient, and ergonomically designed insole system. Moreover, the goal is to optimize sensing locations to enable three-dimensional measurement capabilities, encompassing both normal and shear stress.

Three distinct iterations of insole designs were tested during this study, each targeting improvements across the aforementioned parameters. The initial design underwent experimental validation, achieving an average accuracy of 89.51% with a maximum normalized error metric of 16.41%. Subsequent iterations focused on enhancing durability and practical usability. The second design exhibited promising results, demonstrating an average accuracy of 92.79% with a maximum normalized error metric of 12.22%. Notably, it showcased expected performance across various gait patterns, capturing data from three different force directions at each analysis point. The third design, while still undergoing refinement, displayed considerable improvements, boasting an average accuracy of 94.35% with a maximum normalized

error metric of 7.79%. Ongoing research is addressing early limiting factors encountered during practical testing, with the aim of further enhancing performance and robustness.

Overall, these designs promote the development of compact, comfortable insole systems featuring optimized sensing capabilities for comprehensive force detection in three dimensions. Moreover, the cost-effectiveness of these designs underscores their accessibility and potential for widespread adoption. Future investigations will focus on leveraging smaller sensors for refined sensing locations and enhancing adhesive properties to bolster the durability of miniaturized sensors.

Dedication

Thank you to my sister, Brianna, my father, Frank, and my mother, Bonnie, for their unwavering support throughout my life. Thank you to my friends and my partner for their kindness during my graduate years and beyond.

Acknowledgements

This research would not be possible without the support of countless individuals throughout each step. Firstly, thank you to my advising committee: Dr. Yantao Shen as my main faculty advisor, Dr. Jeongwon Park as my faculty co-advisor, and Dr. Sergiu Dascalu as my graduate representative. Thank you to Dr. Shen for your tremendous assistance and guidance throughout my graduate years. Thank you to Dr. Park for your unwavering support and insistence that I will succeed in all I do. Thank you to Dr. Dascalu, for all the kind words, immediate willingness to be a part of my advising committee, and the opportunity to travel to Romania. You three made my graduate years truly memorable and successful.

I would also like to thank my bosses who provided me a means of attending this university for a Master's in Biomedical Engineering. Thank you to Candice Bauer for believing in me, Gabbi Bachand for your support and kindness, and Jamie Gutual for helping me learn how to teach and enjoy instructing.

I would like to thank my family. Thank you to my mother Bonnie and father Frank for providing me a means to attend university in the first place and a wonderful upbringing. Thank you to my sister Brianna for your support and your willingness to listen to the stressors in my life.

Thank you to my partner Maddie McLain. I do not think I would have had the mental fortitude to continue with my research if it were not for your endless support throughout my graduate education.

Also, thank you to the workers in the Maker's Space in the De La Mare Library at the University of Nevada, Reno. Much of my research relied heavily on resin and 3D printing for my molds and the workers there were instrumental toward my success and research.

Finally, thank you to the University of Nevada, Reno, for the opportunity to receive both a Bachelor's and a Master's in Biomedical Engineering. I am incredibly grateful for the research and learning that took place while I was here.

Table of Contents

List of Tables

List of Figures

Body of Manuscript

Chapter 1: Introduction

Insole research currently focuses on applications of gait analysis, incorporating variable sensing mechanisms and capabilities. Gait analysis typically involves research into sensing technologies such as piezoresistive or capacitive measurements, correlating data to force inputs. Research also includes applications toward areas such as disease identification, general health monitoring, and demographic differentiation. However, research focuses typically include several limiting factors, including size, cost, and directional sensing capabilities, often relying solely on normal force detection. In light of this, improvements can be made to research efforts of insole systems.

This research on this paper advances gait analysis and identification with the application of 3-dimensional self-decoupled piezoresistive force sensor systems to measure normal and shear force simultaneously. The subsequent sections will include a literature review investigating the field of gait analysis conducted with insole technologies (Chapter 2), a description of the methodologies such as the materials used and the sensing principles present in the experimental setup (Chapter 3), the results collected from the experimental and practical testing of each iterative insole system (Chapter 4), a discussion of the results and the conclusions that can be drawn from the trends presented (Chapter 5), and elaboration of future work to be done with this technology to further test and validate the findings exemplified in this paper (Back Matter).

Chapter 2: Literature Review

Research toward insole technologies and gait analysis has increased in prevalence dramatically over the last several decades, spanning many different applications and analysis methods [1]. Initially, the field of insole research focused on parasitic energy harvesting during walking as a means to reduce environmental impacts of energy consumption [2]. However, the focus of this field of research eventually moved away from energy harvesting and more toward gait analysis.

Research of gait analysis by measurement of insole systems has evolved rapidly with the introduction of micro electromechanical systems, incorporating sensing technologies miniaturized for less invasive sensing capabilities. Researchers began incorporating multiple technologies in tandem such as resistive force sensors and gyroscopes to measure force, angular measurements, and acceleration data to correlate to gait analysis [3,4]. However, researchers have explored many different analysis methods. Some researchers utilized Piezoelectric Force Sensors (PFS), which rely on electrical properties in piezoelectric materials that react to mechanical signal inputs [5, 6, 7], demonstrated in Figure 1.

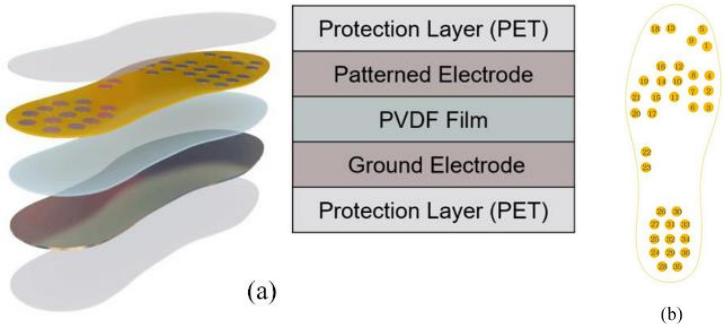

Fig. 1: One example of a piezoelectric force sensor, measuring 36 unique locations [6].

Other research groups have focused on Force Sensing Resistor (FSR) based system, incorporating resistance change measurements due to force inputs [8, 9]. Less common methods of force measurement methods found in insole systems include Optical Pressure Sensors (OPS) relying on increased reflective unique light magnitudes for force application [10], Polymer Optical Fibers (POF) which rely on variable power attenuation and are relatively new in this field of research [11], or even temperature sensors measuring thermal readings [12]. However, pressure and force sensors remain the predominant analysis method in the field of insole research advancement. In any sense, the force application would alter the sensing mechanisms, allowing for detection of force based on this change, only in the normal direction or force applied toward the ground initially.

Often, research incorporates larger and more rigid designs, sometimes built into shoes themselves to incorporate more sensing capabilities. Research groups often organize their design into layers with seemingly less of a focus into comfortability, incorporating the system into a shoe permanently, shown in Figure 2 [13]. Other research groups go beyond this limitation and implement these systems below shoes, accounting for the entire body weight of an individual and therefore the entire force they exhibit on the system [14]. Researchers have even considered gait identification with worn sensors away from the feet, utilizing sensors implemented in clothing more similar to pants rather than shoes or insoles [15].

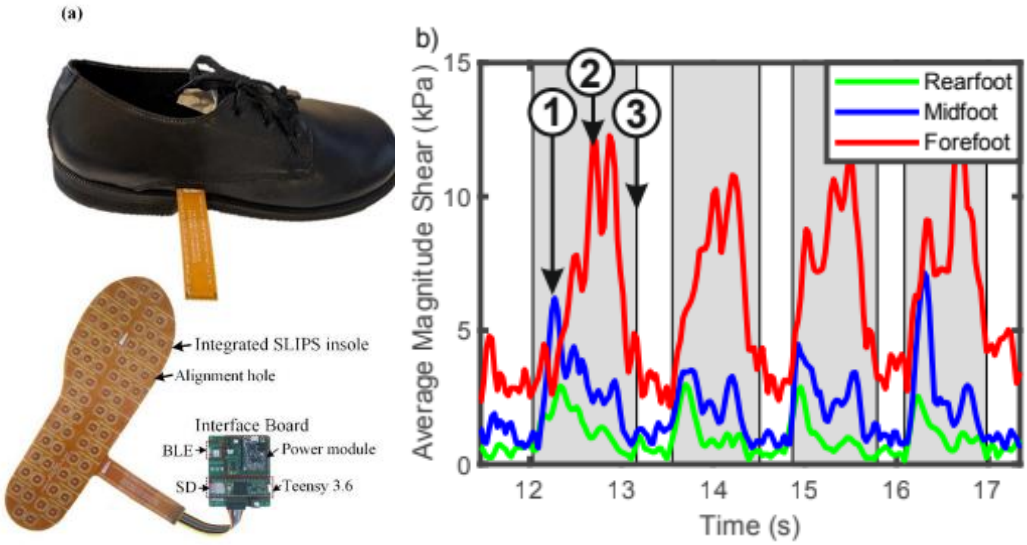

Fig. 2: An integrated shoe system consisting of three rigid layers and one elastomer layer. The right visual indicates typical trends in force magnitude analysis, where peaks indicate steps [13].

Regardless of sensing mechanism, there are generally similar trends for data outputs from insole systems. Research in this field presents data indicating predominant shear force measurements found in the sole of the foot rather than the heel [14, 16-18].

Additionally, data collection typically correlates with a large array of sensing locations [6, 13, 19-21]. However, these arrangements of sensing arrays are largely found to be unoptimized, analyzing locations in the foot that are not required to analyze the users overall gait pattern. Ohnishi et. al propose the idea that rather than using large sensing array to detect the entire area of the foot when walking, gait can be analyzed with two or three optimally placed sensing locations [22]. They indicate that most array locations were not critical in gait analysis, nor do they provide valuable data for gait detection. Despite using an array of 36 sensing locations for their design, they theorize the best two or three sensing locations are located in the locations demonstrated in Figure 3.

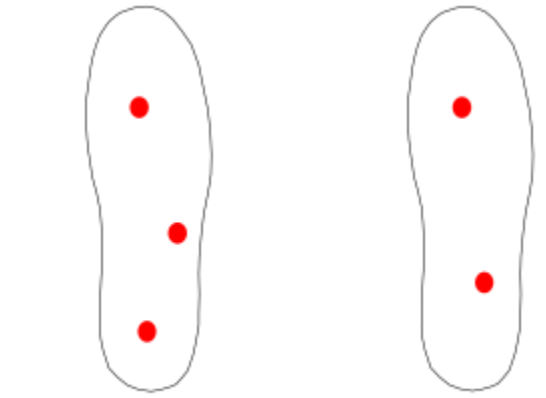

(a) 3 points that increased versatility

(b) Best 2 points

Fig. 3: These are the most optimal sensing locations for gait analysis proposed by Ohnishi et. al [22]

In light of this, research efforts could be made to improve sensing locations found in the insole systems during use. Sazanov et. al implement only three sensing locations, one in the heel and two in the sole, capable of differentiating between sitting, standing, and walking motions while wearing the insole [23]. Roden et. al incorporate four sensing locations, two force sensors located in the sole and two located in the heel, while also incorporating a gyroscope with the advent of improving physical therapy efforts as well as enhancing sports analysis [24]. Jo et. al utilize three RFID sensing locations positioned optimally to create an insole system that does not necessitate a power source [25]. This optimization would also be implemented in the research found in this thesis as well.

Concurrently, alternative measurement methods for gait detection were explored. Cameras were introduced into similar research fields and applications, namely motion capture and video augmentation in a three-dimensional space. Subsequently, cameras were introduced into gait analysis with the implementation of marker-based gait analysis and detection. Marker based detection became increasingly popular in the mid-2000s, incorporating visual analysis of markers located on segments of the legs, providing the

advent of analyzing individual walking phase patterns [26]. Marker-based gait analysis relies on marker detection from video data collected by cameras and cross correlation to create relative trajectories for each marker as well as relationships between markers, enabling pattern analysis in both 2-dimensional and 3-dimensional spaces [27]. Marker-based gait analysis also encourages the reconstruction of datasets in order to incorporate pattern recognition capabilities with the use of innovations such as convolutional neural networks [27, 28]. Alternatively, markerless gait detection was introduced, allowing for keypoint detection such as hips and knees without the addition of markers to the subject [29]. In some cases, cameras would not appear from an external perspective to monitor markers placed on a user, but instead would be attached to the user to analyze infrared markers from the perspective of the user themselves as seen in Figure 4 [30].

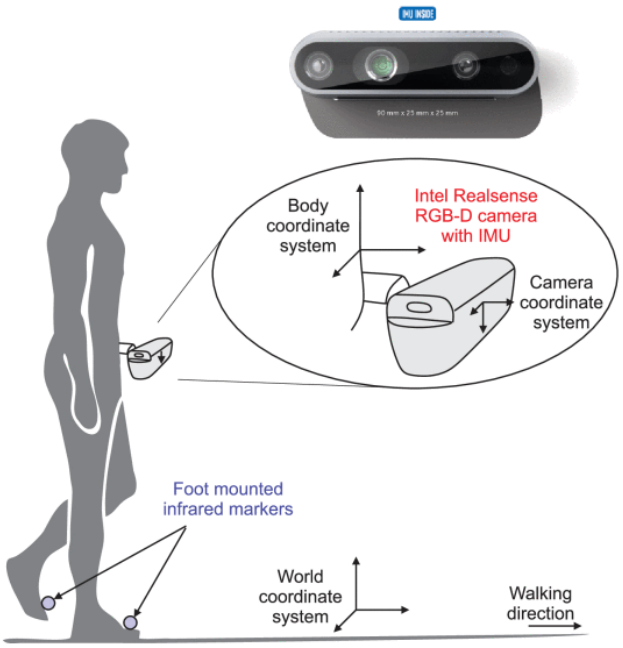

Fig. 4: One such example of marker-based gait detection, incorporating a camera attached to the user [30].

High-accuracy camera implementations often results in increased costs for research purposes and questionability when applying to the end-user. For the purpose of

this research, the focus of design was an insole system. However, for gait phase identification and force input analysis, visual analysis was incorporated in order to improve the viability of the data collected from the testing of the insole system as well as identifying different phases of the gait during testing.

Although normal force was the primary focus in this field of research since its inception, research efforts explored the creation of insole systems that could measure both normal and shear forces, or forces parallel and perpendicular relative to the direction of movement and in the same plane as the insole system itself. Rajala et. al provides an in-depth analysis of the development of shear measurement capabilities found in different insole research focuses throughout the years, including analyses using sensing methods discussed before such as piezoelectric films, force sensing resistors, or optical fiber sensing systems [31]. Tavares et. al introduced an optical fiber sensing system that was capable of sensing both normal force during use as well as a distinct measurement for shear force in two directions by diversifying the fibers into two channels, one for normal force and one for shear force [32]. Mertodikromo et. al and Mohammad et. al focus solely on shear force analysis, disregarding normal force entirely to ideally improvement measurement capabilities in the desired direction [33-34]. However, research would ultimately incorporate a focus into three directions of force analysis, including both normal force and shear force [6, 13, 35-37].

The 3-dimensional self-decoupling method utilized in this research was originally proposed by Luo et. al at the University of Nevada, Reno [38]. Luo et. al designed a microforce sensor that incorporates four Flexpoint bilateral bend sensors in a 3-dimensionally symmetrical configuration placed in an air medium, shown in Figure 5.

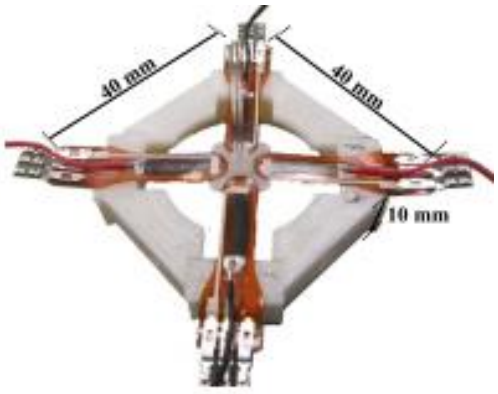

Fig. 5: The original design orientation of the four flex sensors, enabling decoupling in three directions of force due to oppositional but symmetrical resistor pairs [38].

In doing so, oppositional resistors across the central point from one another can act as reference points, where force in a given direction will cause these pairs of resistors to act inversely from one another. Moreover, where one resistor would be increasing in resistance due to the force application stretching the resistor, the opposite relational resistor would be compressing and therefore reducing in resistance. The relationship between force input direction and resultant resistance change in each resistor can further be demonstrated in Figure 6.

	F_{x+}	F_{x-}	F_{y+}	F_{y-}	F_{z+}	F_{z-}
R_{T1}	$-$	$+$	0	0	$+$	$-$
R_{B1}	$+$	$-$	0	0	$-$	$+$
R_{T2}	0	0	$+$	$-$	$+$	$-$
R_{B2}	0	0	$-$	$+$	$-$	$+$
R_{T3}	$+$	$-$	0	0	$+$	$-$
R_{B3}	$-$	$+$	0	0	$-$	$+$
R_{T4}	0	0	$-$	$+$	$+$	$-$
R_{B4}	0	0	$+$	$-$	$-$	$+$

Fig. 6: The resistance relationships found at each resistor in the configuration, indicating an increase in resistance (+), decrease in resistance (-), or no change (0). RT_1 would refer to the resistance of the top resistor in the first position, which would be symmetrical to the resistor found in the third position [38].

With this relationship, a voltage passing through these pairs of resistors can also be decoupled utilizing half-Wheatstone bridges, incorporating each of these paired voltages as the two analytes of this circuit [39]. When force is applied in a given direction, the output voltages of these analytes will respond according to the relationships in the Figure above, providing consistent and analyzable decoupled voltage outputs between each half-Wheatstone bridge circuit, indicated in Figure 7.

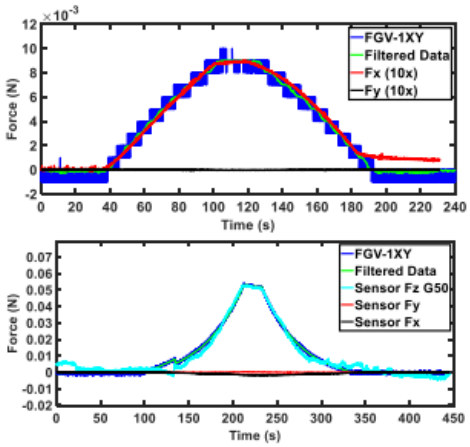

Fig. 7: Two examples of voltage outputs during force input to the system. The top visual indicates a force in the X direction, where there is little response in the Y direction. The bottom indicates a force in the Z direction with little response in the X or Y direction [38].

Within this research, Luo et. al investigate the robustness, thermal drift, hysteresis, and sensitivity of these sensors, ensuring the decoupling method will function properly under varied conditions and is reliable in most cases as well [38]. However, the Flexpoint bend sensors in this research have also been experimented with and analyzed outside of the research conducted by Luo et. al. Researchers such as Saggio et. al have analyzed bending capabilities in variably sized bend sensors as well as the resistance response due to deflection angle, analyzing the sensitivity of the sensors for force detection [40]. Additionally, this research group also investigated sensor modifications of

cutting the sensors slightly to control output resistance responses after cutting [40]. Gerboni et. al implemented the system into a soft robotic system, analyzing the sensitivity of the sensing mechanism as well as the low hysteresis between force application and subsequent release of force [41]. Zheng et. al indicate their preference for these sensors due to low drift and high sensing capability [42].

Within the field of insole research, there have also been many different applications. Most predominantly, this field of research incorporates analysis into disease identification, most notably diabetes and Parkinson's. Diabetic foot ulcers pose a large risk in the diabetic community, often leading to uneven distribution of weight, instability, and increased joint deterioration commonly caused by related limps [43]. To counteract this, many research groups test diabetic populations prone to developing diabetic foot ulcers with the focus of early detection in order to lead to early treatment [44-48]. This can lead to developments into treatment in tandem with gait analysis, such as the implementation of heel wedges, orthotic inserts placed into shoes to deter instability and uneven weight distribution [49]. Parkinson's is often detectable or monitorable with incorporation of an inertial momentum unit (IMU), enabling detection of certain gait trends and characteristics including weight distribution and balance, largely benefitting the improvements to constant monitoring capability due to a non-invasive insole system characterizing their movements [50-53]. Common testing methods are comparisons are visualized in Figure 8, including analysis of user capability during different walking methods, such as walking straight or turning at variable speeds.

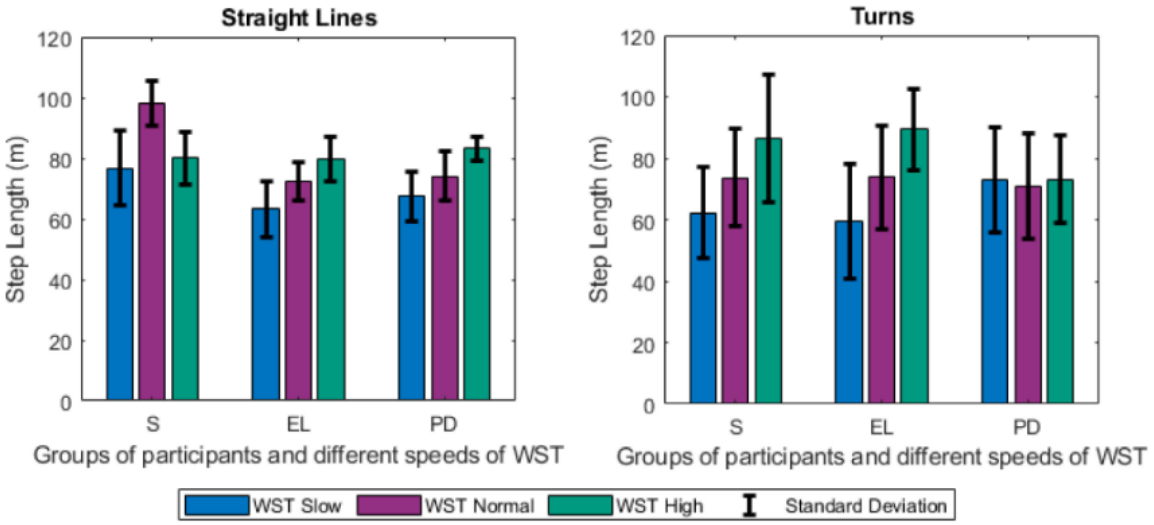

Fig. 8: Comparisons between varied gait motions, analyzing users for their step lengths at varied speeds [51].

Similar to disease detection is demographic identification by varied gait disorders present in certain populations, including walking disorder such as knee buckling, cerebral palsy, or simply gait identification correlated with age [54]. Increased age often correlates with uneven gait distribution during walking, exemplified by research identifying older age as well as implementing fall detection or prevention in these older populations [55, 56].

There are also several commercially available products, providing valuable insight into the products available to end-users as well as the limitations these products may have. One such example is Kitronyx, a pressure sensing system with a more prominent focus for user comfort, incorporating technologies sewn into an insole system [57]. However, Kitronyx measures only normal force and has a large purchasing price of $1400. Another example of a commercially available product is ARION, an insole product focused on speed analysis as well as slope identification and costs approximately

$270-$325, but lacks most other gait analysis features as it is centrally focused on running analysis [58]. The ARION insole system is display in Figure 9.

Fig. 9: An insole system offered by ARION. The insole system is pictured on the left, whereas the right visual demonstrates the inertial momentum unit that hangs outside the shoe when worn [58].

The last example is Stridalyzer, a smart insole gait analysis product offered by the company Retisense [59]. The system relies on pressure map distributions provided by normal force application of the user. The product also offers a mobile application that allows user to view their pressure readings. Readings incorporate inertial momentum unit data to also measure stride length, weight load, weight distribution, and imbalances. However, this system does not incorporate shear force measurements and is also offered at the minimum price of $349, but can increase to $1,999 if considering the development kit that the company offers.

Although there are some commercially available products in the field of smart insoles, they often lack numerous sensing capability, most often 3-dimensional sensing capability, and correlate to a price that is not indicative of a realistically affordable product for the end-user.

Chapter 3: Description of Methodology

For this research, methodology was broken up into the following sections: design of components and materials used for components, simulation, theoretical testing, and practical testing. Each section discusses the three designs investigated with this research.

3.1 Design and Materials

During this research, three iterations of insole systems were created. Each insole was constructed using Smooth-On Dragon Skin 10 Polydimethylsiloxane (PDMS). All central connection pieces were designed in SolidWorks using 3D Resin Printing with the material Tough 1500. Central connection pieces were printed with resign due to the increased resolution for printing of small pieces and Tough 1500 material was used primarily due to the rigidity of the material and the resistance to breaking under force. All mold designs were designed in SolidWorks and were printed with standard 3D Printing using Polylactic Acid (PLA) filament. Insole mold designs did not require the heightened resolution and were much larger than the capabilities of the resin printer.

3.1.1 Insole Design

Two insole mold designs were created and utilized for this thesis. The original design used for the first and second iteration can be seen in Figure 10 and the altered design used for the third iteration can be seen in Figure 11.

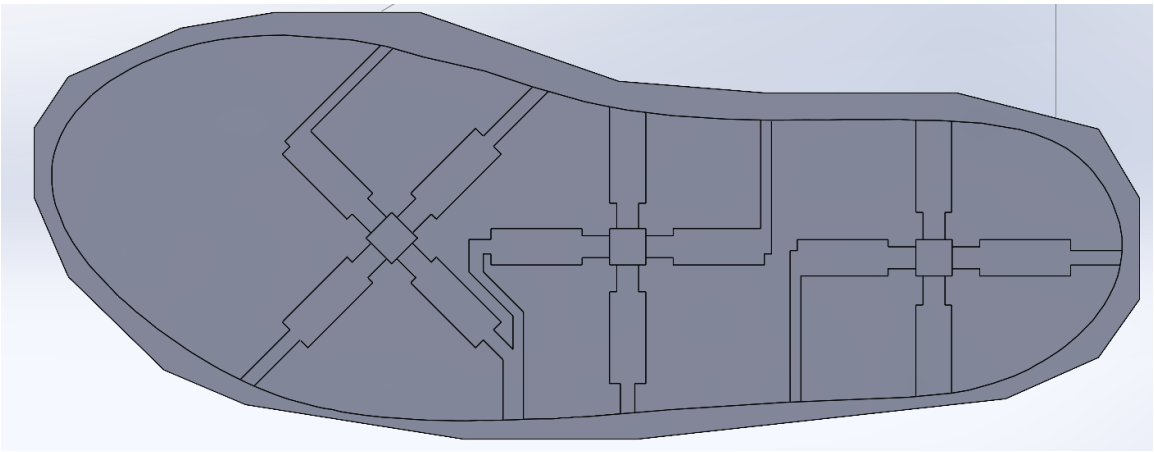

Fig. 10: The original mold design used for the research. The sensing group near the toe of the mold was turned 45° due to space limitations with relation to middle sensing group.

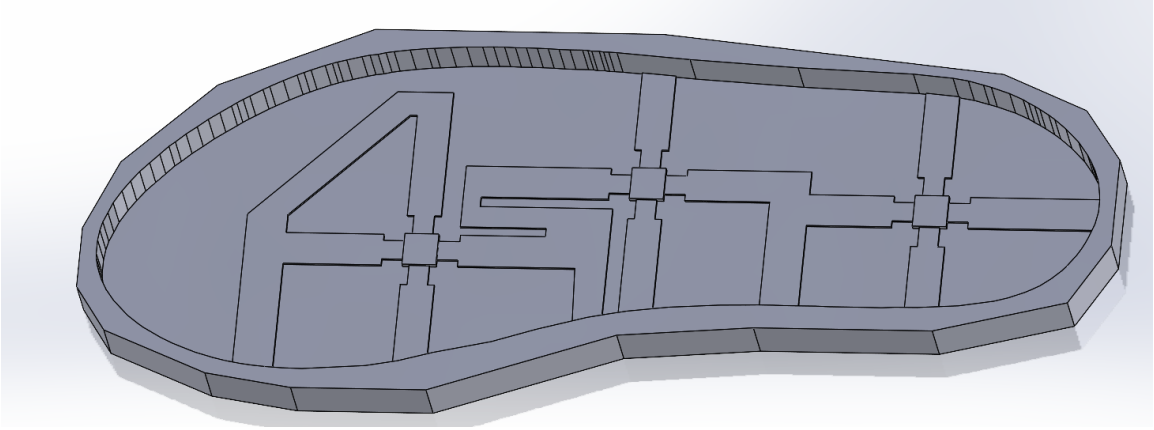

Fig. 11: The altered insole mold design for the third iteration of this research, intended to incorporate a more optimized design due to experimentation with smaller sensors.

Different amounts of PDMS were poured into each design, which created a base left insole mold once removed from the mold after approximately 5 hours. The symmetrical formation of sensors was glued directly to the gel in the three analysis locations found on the heel of the insole and referred to as the bottom group of sensors, the arch of the insole and referred to as the middle group of sensors, and the sole of the insole and referred to as the top group of sensors. After gluing, the insole system was moved to an empty mold, allowing the application of a thin layer of gel to secure the sensors in place. The approximate amounts PDMS added to each insole layer of each

design as well as the resulting hardness of each insole design, tested with a UHarbour Shore Type Hardness Tester, are summarized in Table 1.

Table 1: The resulting gel hardness measurements of each insole design tested throughout this research. Despite using the same material for each design, the hardness was slightly variable between iterations.

Design Iteration	Amount of PDMS used for base insole layer (grams)	Amount of PDMS used for top insole layer (grams)	Resultant Hardness of Insole (Shore)
Design One	250	100	13
Design Two	100	100	10
Design Three	250	100	15

With this gel molded, one example of the resulting insole design is shown in Figure 12, indicating the design one demolded insole system.

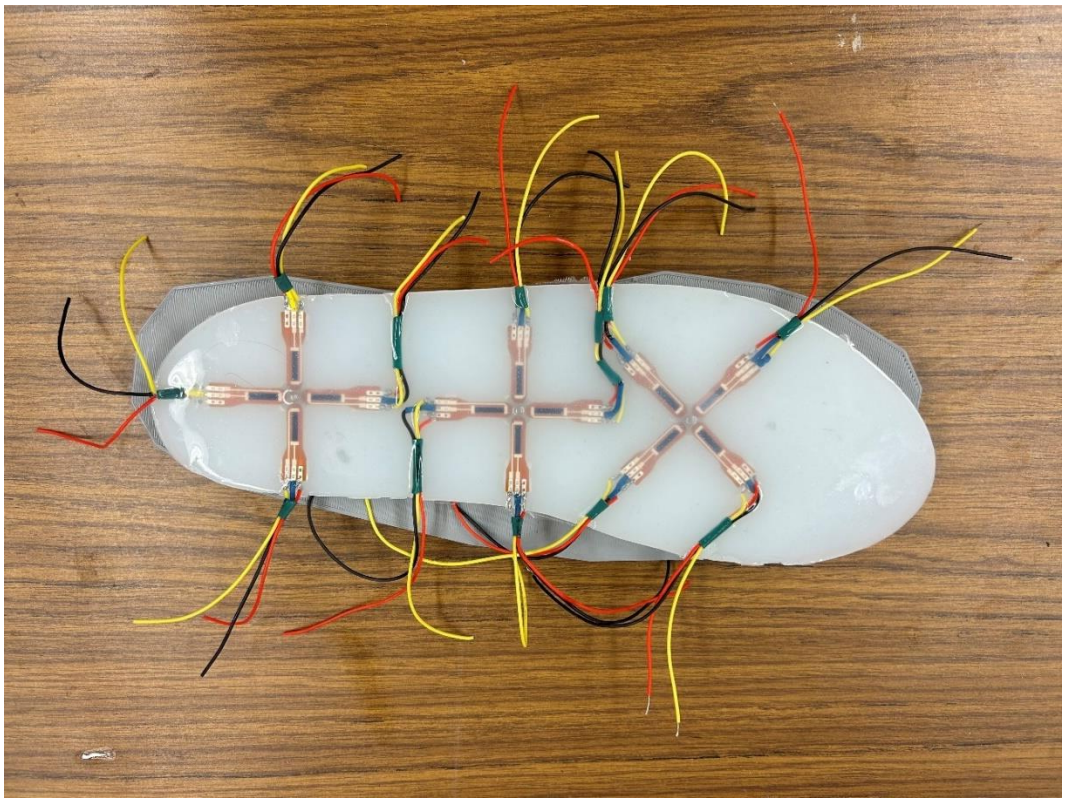

Fig. 12: The first design of the insole system. Each sensor has 1 input of 5V and 2 outputs. However, in each of the three sensing locations only 5 of the 8 outputs are used.

3.1.2 Sensor Decoupling Mechanism and Positioning

For the design of the sensors used for this experiment, there are four Flexpoint Sensor Systems bend sensors for each of the three analysis points on the foot. Each sensor is bi-directional, non-laminated, and approximately 1.3 inches in length. Each sensor's resistance can range from 200 ohms to a maximum of 500k ohms, with a neutral resistance near 2k ohms. The four sensors are arranged symmetrically, with each bend sensor across from one other, attached at a central point where the analysis point for force input will be located. Figure 13 indicates the first design iteration for the central connection point whereas Figure 14 shows the second and final design, improving upon the first iteration.

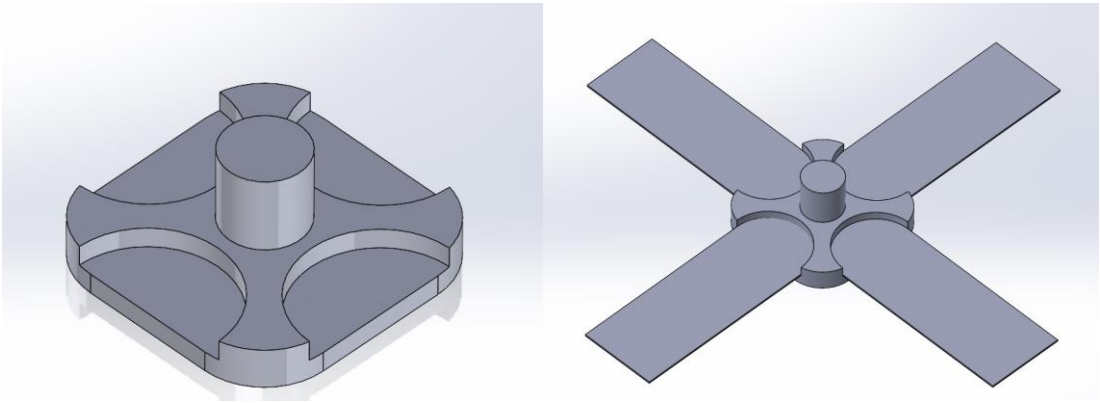

Fig. 13: The central connection points for each sensing location that the four bend sensors were attached to in the first insole system design. The left visual is the original design whereas the right visual emulates the central point with connected sensors.

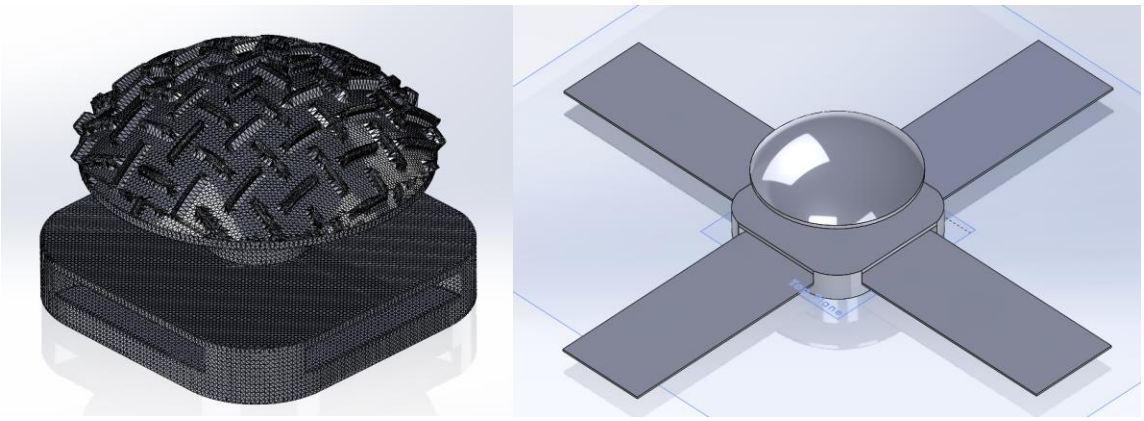

Fig. 14: The second and final design for the central connection point of the sensors. This design has grooves to protect the adhesion point of the sensors, a larger surface area in the form of a half dome to improve sensing capabilities, and a tire texture to improve collection of shear forces by increasing the friction coefficient.

In doing so, each sensor can be used in a self-decoupling manner, which relies of symmetry both mechanically and electrically, that allows for solving of each axial direction of force independently, with the X-direction correlating to the shear force perpendicular to forward movement, Y-direction correlating to the shear force parallel with forward movement, and the Z-direction correlating to normal force toward the ground while standing or moving. The relationship due to force in any direction is demonstrated in Figure 15, with the subsequent half-Wheatstone bridge compensation relationships demonstrated in Figure 16.

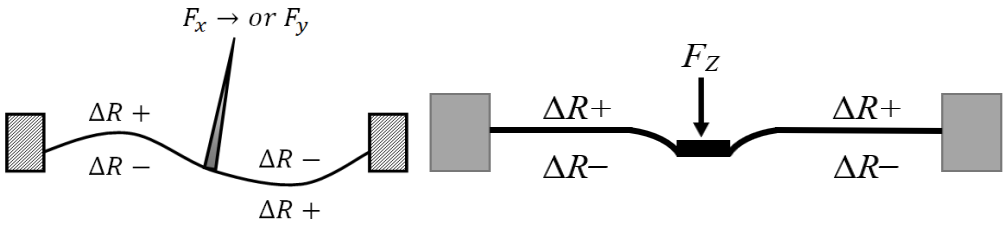

Fig. 15: The relationship between the change in resistance for each pair of resistors, dependent on the direction of force.

	F_X+	F_X-	F_Y+	F_Y-	F_Z+	F_Z-
R_{T1}	-	+	0	0	-	+
R_{B1}	+	-	0	0	+	-
R_{T2}	0	0	+	-	-	+
R_{B2}	0	0	-	+	+	-
R_{T3}	+	-	0	0	-	+
R_{B3}	-	+	0	0	+	-
R_{T4}	0	0	-	+	-	+
R_{B4}	0	0	+	-	+	-

Fig. 16: The detailed relationship for each resistance value change depending on the input force. These relationships correspond to the half-Wheatstone bridge compensation for 3-dimensional decoupling.

Considering the bilateral nature of the bend sensors used in this research, the resistors have independent resistances from the top and bottom of each sensor. Likewise, the relation between the bending of a sensor and the change in resistance between top and bottom sensors is inversely relational and changes at different rates when under small amounts of force. Because of this, a self-decoupling method utilizing one bilateral sensor not viable. By using the sensors in tandem pairs with relation to mechanical symmetry, oppositional resistors can be used as their resistances can be analyzed in relation to one another to measure force application in each direction.

However, the application of this sensor does not utilize small forces within this research. During experimentation, it was discovered that the adhesion of the sensors to the central connection point and the base of the sensors near the wiring caused the resistance of both the top and bottom resistors of each sensor to increase at the same time, but at different rates. After approximately 0.2 N of force are applied, the optimal range of motion of the system is exceeded, causing both the top resistor to bend as intended and

the bottom resistor to stretch. As both sides of the sensing film are stretching, the resistance for both sides of the sensors increases. Despite this unexpected finding, the oppositional pairs of sensors increase in resistance at the same rate with relation to one another. Additionally, considering the pair of resistors utilized to calculate change in the Z-direction, the bottom resistor increased at a slower rate than the top resistor, allowing for the decoupling mechanism equations to function properly. Design two served as an attempt to reinforce the expected relation between top and bottom resistance values.

To ensure each sensor is properly oriented with respect to the other sensors, a 3D resin printed glue mold was utilized, aiding in proper alignment and attachment to the central point for each group of sensors. Figure 17 shows the glue mold in use, with each sensor aligned at 90 degrees to adjacent sensors.

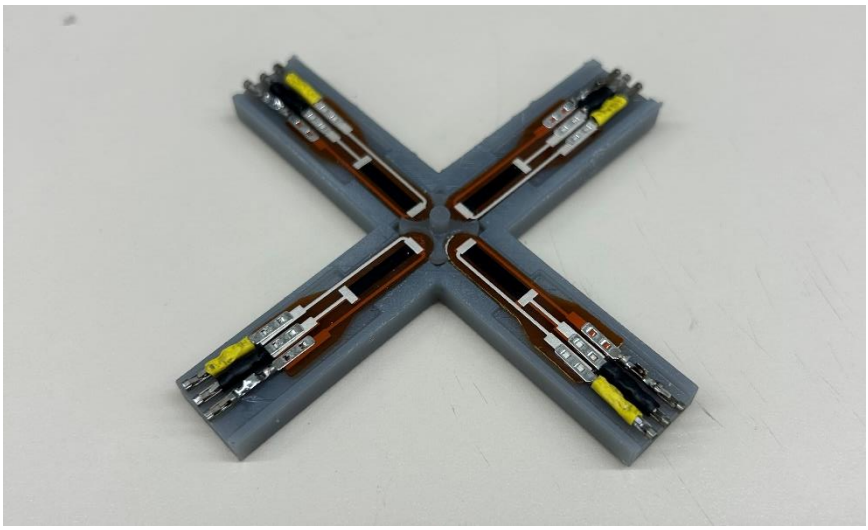

Fig. 17: The mold used to attach each sensor to the central connection point. The mold ensures symmetry of each sensor at 90° angles.

Finally, this research relies on three analysis points, placed in optimized location based on research presented in the literature review. For the purpose of this research, the analysis points will be referred to as follows: the analysis location in the forefoot nearest

the toe of the insole mold will be referred to the front sensing location, the analysis location in the midfoot near the arch of the foot will be referred to as the middle sensing location, and the analysis point in the rearfoot nearest the heel of the insole mold will be referred to as the back sensing location. For clarity, Figure 18 demonstrates the location of the analysis points found in the insole designs.

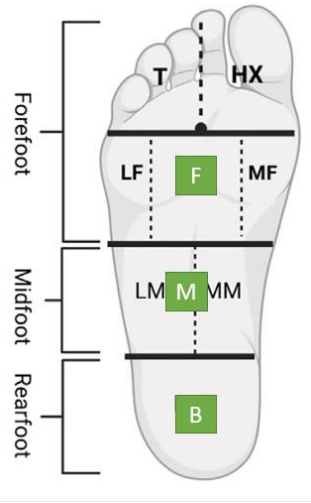

Fig. 18: The approximate positioning of each sensing location found in each insole design in this research.

3.1.3 Circuit Design

To accompany the symmetrical mechanical design of the four sensors, the half-Wheatstone bridge circuit design allows for independent sensing of each axial direction, X, Y, and Z respectively. Wheatstone bridges incorporate two parallel voltage dividers that allow researchers to measure the voltage between the two dividers, correlating any deviations to changes in the circuit, such as temperature change or, in the case of this research, a change in strain. Based on the number of active elements, or analytes of a system, different variations of Wheatstone bridges can be used. In this research, each sensor utilizes two resistance values from varying bend sensors found in the system. The resulting circuit utilized for this research incorporates half Wheatstone bridges for each

pair of resistance values, allowing for deviations in the strain of the system to be detected independently of other directions.

The resulting voltages of each pair of resistors can be separated into each axis, indicated by the below equations:

$$\begin{bmatrix} Vx \\ Vy \\ Vz \end{bmatrix} = Vs \begin{bmatrix} \frac{R_{T3}}{R_{T3}+R_C} - \frac{R_{T1}}{R_{T1}+R_C} \\ \frac{R_{B2}}{R_{B2}+R_C} - \frac{R_{B4}}{R_{B4}+R_C} \\ \frac{R_{B1}}{R_{B1}+R_C} - \frac{R_{T3}}{R_{T3}+R_C} \end{bmatrix} \quad (1)$$

When analyzing force while standing and movement has not begun or has stopped, force will only be applied in the Z-direction. For the given force resistors $R_{T1} = R_{T2} = R_{T3} = R_{T4}$ and $R_{B1} = R_{B2} = R_{B3} = R_{B4}$, the resulting equation decoupled for the Z-direction is:

$$\begin{bmatrix} Vx \\ Vy \\ Vz \end{bmatrix} = Vs\left(\frac{1}{\left(\frac{\Delta R_{B1}}{R_C}+1\right)\left(\frac{\Delta R_{T3}}{R_C}+1\right)}\right) \begin{bmatrix} 0 \\ 0 \\ \Delta R_{B1} - \Delta R_{T3} \end{bmatrix} \quad (2)$$

Likewise, if force were applied in the X-direction, such as an individual slipping or walking sideways, the normal force will result in differences in resistors R_{T1} and R_{T3}. Additionally, the other resistors are equal with relation their mechanical symmetry; this correlates to $R_{T1} = R_{B3}$**,** $R_{T2} = R_{B4}$, $R_{T3} = R_{B1}$, and $R_{T4} = R_{B2}$. This correlates to the following system of equations, indicating voltage change in the x-direction with relation to the force applied:

$$\begin{bmatrix} Vx \\ Vy \\ Vz \end{bmatrix} = Vs\left(\frac{1}{\left(\frac{\Delta R_{T1}}{R_C}+1\right)\left(\frac{\Delta R_{T3}}{R_C}+1\right)}\right) \begin{bmatrix} \Delta R_{T3} - \Delta R_{T1} \\ 0 \\ 0 \end{bmatrix} \quad (3)$$

Finally, force applied in the Y-direction, such as walking uphill or downhill, can be isolated by the decoupling method indicated with analysis of resistors R_{B2} and R_{B4}.

Once again, the other resistors in the system are equal in pairs with relation to the mechanical symmetry of the system: $R_{B2}=R_{T4}$, $R_{T2}=R_{B4}$, $R_{B1}=R_{T3}$, and $R_{B3}=R_{T1}$. The resulting system of equations for resultant voltage due to Y-directional force application is:

$$\begin{bmatrix} Vx \\ Vy \\ Vz \end{bmatrix} = Vs\left(\frac{1}{\left(\frac{\Delta R_{B2}}{R_C}+1\right)\left(\frac{\Delta R_{B4}}{R_C}+1\right)}\right)\begin{bmatrix} 0 \\ \Delta R_{B2} - \Delta R_{B4} \\ 0 \end{bmatrix} \quad (4)$$

With each individual decoupled direction, 3 directions of force can be calculated, providing normal force measurements as well as shear force measurements. This system was also tested in a simulated sense mechanically and electrically to ensure the system functions properly in a gel medium.

3.2 Simulation

In order to test the decoupling method utilized in a gel medium, the system was built in MultiSim to ensure the half-Wheatstone bridges function properly to decouple in three directions. Additionally, to ensure the sensors react properly in a gel medium, the sensing apparatuses were simulated in ANSYS at variable force input values and directions.

3.2.1 Theoretical Circuit

From a theoretical perspective, half-Wheatstone bridges will utilize two analytes and two completion resistors by measuring the voltage change between the completion resistors and the changing analysis locations. In order to simulate this, the theoretical circuit is completed and simulated in MultiSim, demonstrated below in Figure 19.

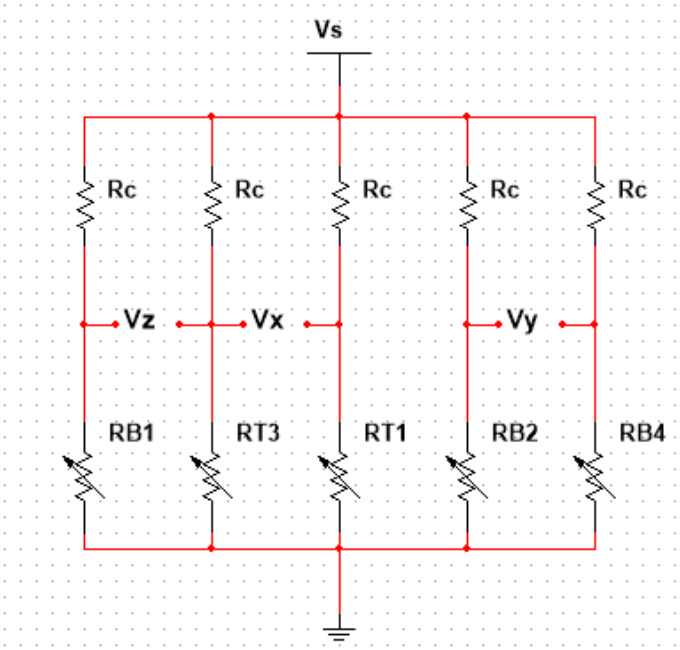

Fig. 19: The simulation of the half-Wheatstone bridges utilized to decouple the voltage outputs in three directions. The bottom half of the Figure consists of the pairs of resistors utilized from the insole system.

3.2.2 Practical Circuit

The Half-Wheatstone bridge circuit utilized for this research is shown below, represented in MultiSim. In theory, R_C is a chosen resistor that serves as completion resistors, allowing for measurement of voltage between the corresponding bend resistor resistances during force application. Typically, these resistors would remain static for testing, as the measurements between the analytes would have a static initial value between tests. However, for this circuit, there are slight variations between each resistance value from each sensor that need to be accounted for. Three of the R_C resistors are supplemented with 5k Ohm potentiometers (P502) to establish a neutral starting value from each axis and subsequently each analysis point on the insole system. These potentiometers are altered between tests to ensure that the ratio between the pairs of resistors used in the decoupling equations is the same as the ratio between the

potentiometer and the corresponding R_C completion resistor. The system was configured manually between tests to establish an output voltage of approximately 0V for each of the three axes. The practical circuit used is shown in Figure 20.

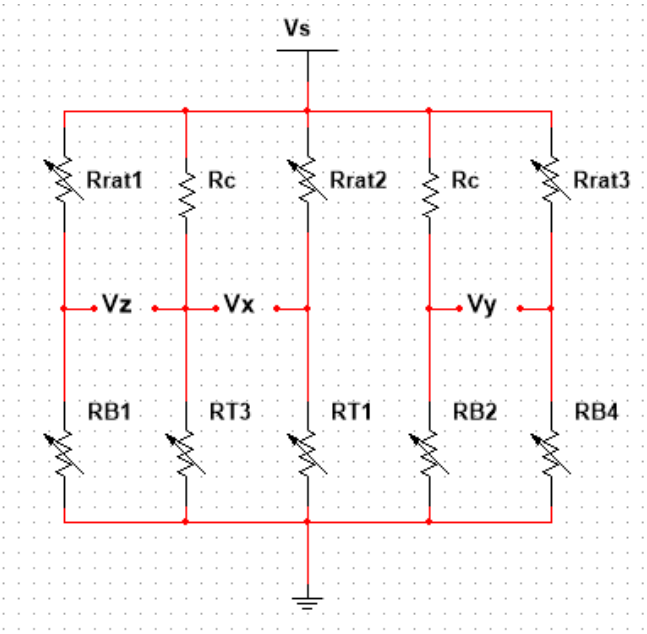

Fig. 20: MultiSim visualization of practical circuit, incorporating three potentiometers to ensure stable initial starting conditions.

Of note, although the practical half-Wheatstone bridge circuits appear to have three analytes, such as RB_1, RT_3, and $Rrat_1$ for the V_z Z-directional voltage analysis, $Rrat_1$ only changes prior to the testing beginning when establishing an initial starting voltage value of approximately 0 V. During testing, the only two analytes changing due to force inputs are the corresponding resistance values of the sensors found in the insole system, which would be RB_1 and RT_3 in the case of Z-directional force application. Functionally, $Rrat_1$, $Rrat_2$, and $Rrat_3$ perform as unique resistance values while testing occurs, only altered between tests.

While collecting each voltage correlated to each axial direction, signal amplifiers (AD620AN) were utilized to increase the voltage outputs, allowing for heightened

voltage responses due to force distribution in the system. Below in Figure 21 is each individual amplifier circuit with corresponding paired resistors as well as the overall circuit for each set of four sensors or each analyte point.

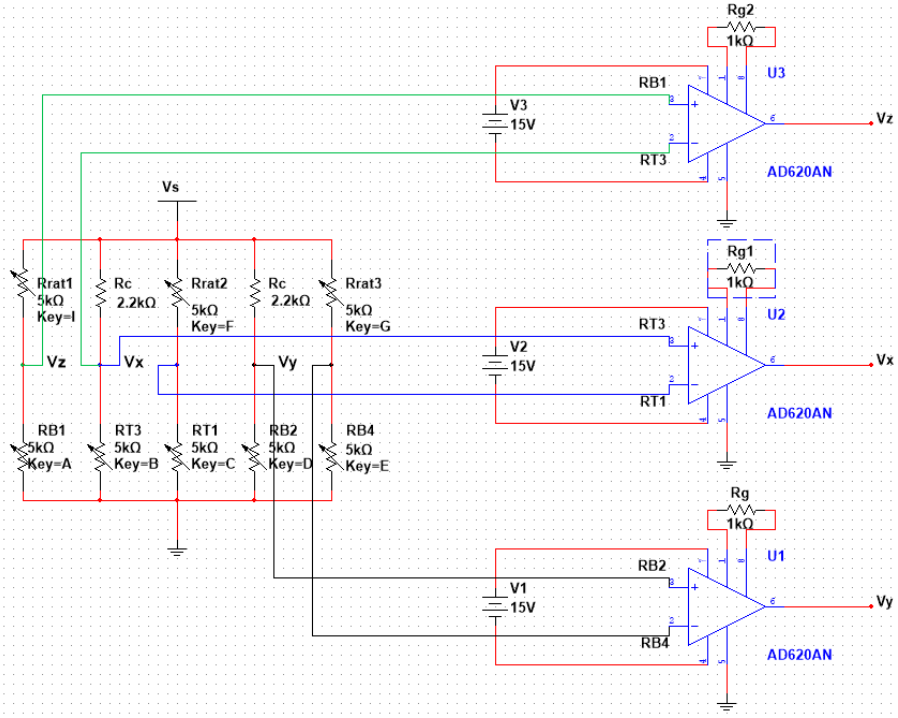

Fig. 21: The overall circuit design utilized including both the half-Wheatstone bridge circuits as well as the operation amplifiers used to analyze each directional voltage output from the circuit.

All amplifiers were powered with 15 V for power while the half-Wheatstone bridge circuit had an input voltage of 5 V. The output of each amplifier was collected in DataQ Instruments DI-1100 data acquisition units. Three data acquisition units were used concurrently, one for each set of sensors or each analyte point.

For the final circuit design, the gains for all X and Y direction amplifiers were equal and all Z direction amplifiers were equal. The gain equation for the AD620AN amplifiers is:

$$G = 1 + \left(\frac{49.4\ k\Omega}{Rg}\right) \tag{5}$$

With this equation, the following Table 2 indicates the calculated gain corresponding to each resistor used for each amplifier for the first and third design.

Table 2: The gain values used at each amplifier for insole designs 1 and 3. Front, middle, and back analysis points consisted of the same gains for each direction.

	X Direction	Y Direction	Z direction
Gain Resistor Value	20 kΩ	20 kΩ	5 kΩ
Resultant Gain Value	3.47	3.47	10.88

Design 2 incorporated shortened sensors and limited mobility, reducing their sensitivity by painting silver conductive epoxy on the conductive ink. To account for this reduced sensitivity, the following Table 3 indicates the altered gain values.

Table 3: The gain values used at each amplifier for the second insole design. The second insole system was much more varied at each analysis point, so unique gain values were adjusted accordingly.

Analysis Point		X Direction	Y Direction	Z Direction
Front	Gain Resistor Value	1 kΩ	1 kΩ	470 Ω
	Resultant Gain Value	50.4	50.4	105.1
Middle	Gain Resistor Value	5 kΩ	5 kΩ	10 kΩ
	Resultant Gain Value	10.88	10.88	5.94
Back	Gain Resistor Value	5 kΩ	5 kΩ	10 kΩ
	Resultant Gain Value	10.88	10.88	5.94

3.2.3 ANSYS Mechanical Simulations

To indicate equal values for oppositional resistors, the sensor formation was simulated in ANSYS for force analysis and bending patterns when force is being applied with different strengths and at different angles. Each sensor mounting shape was simulated to show these phenomena and are shown below. Figures 22, 23, and 24 correspond to simulation with design one of the central connection piece tested in the Z direction, X or Y only, and simultaneous X and Y testing respectively. For some visuals, the gel has been hidden in order to see the relationship between the sensors and input force.

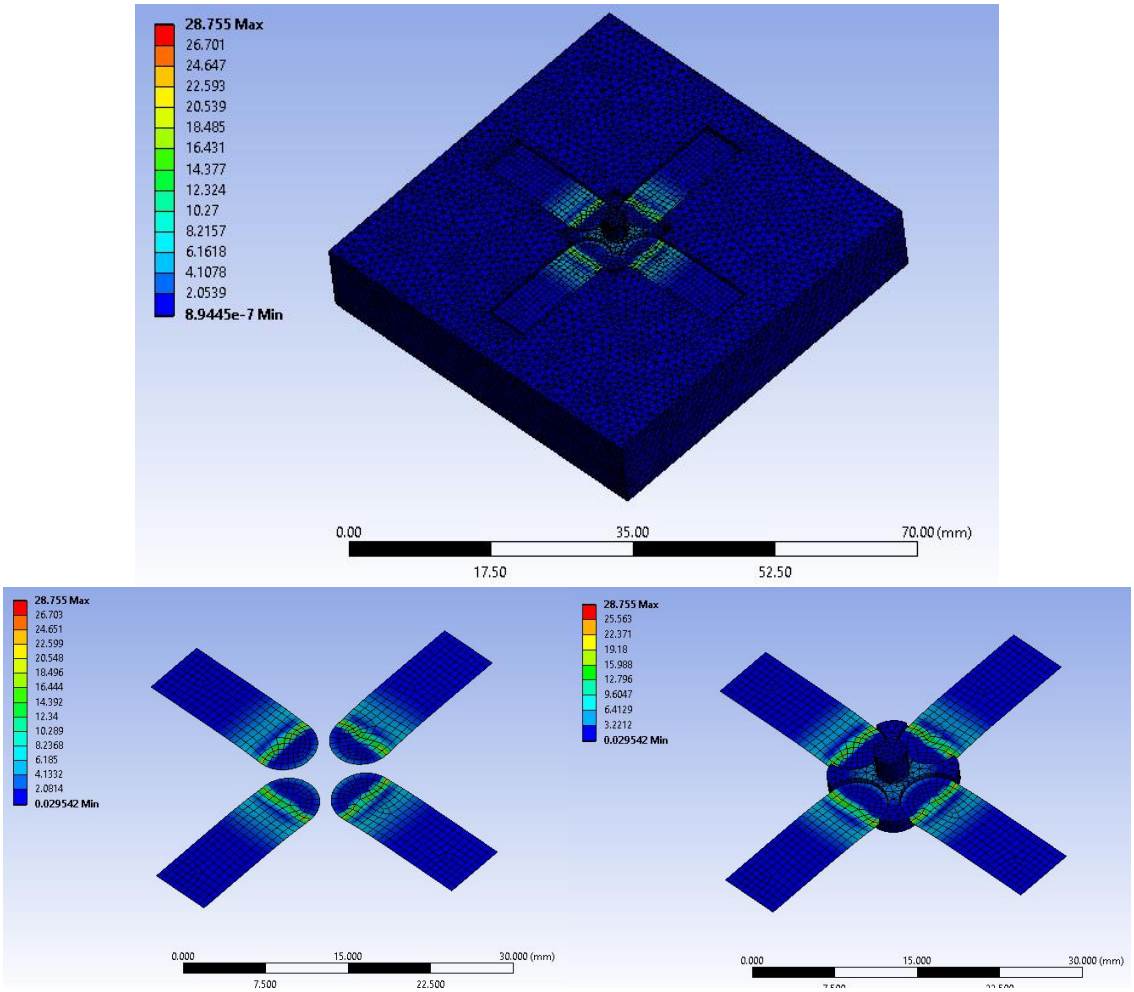

Fig. 22: The ANSYS Simulations of 10N in the Z direction with the first central connection piece design. The force indicates the stress of all sensors is equal.

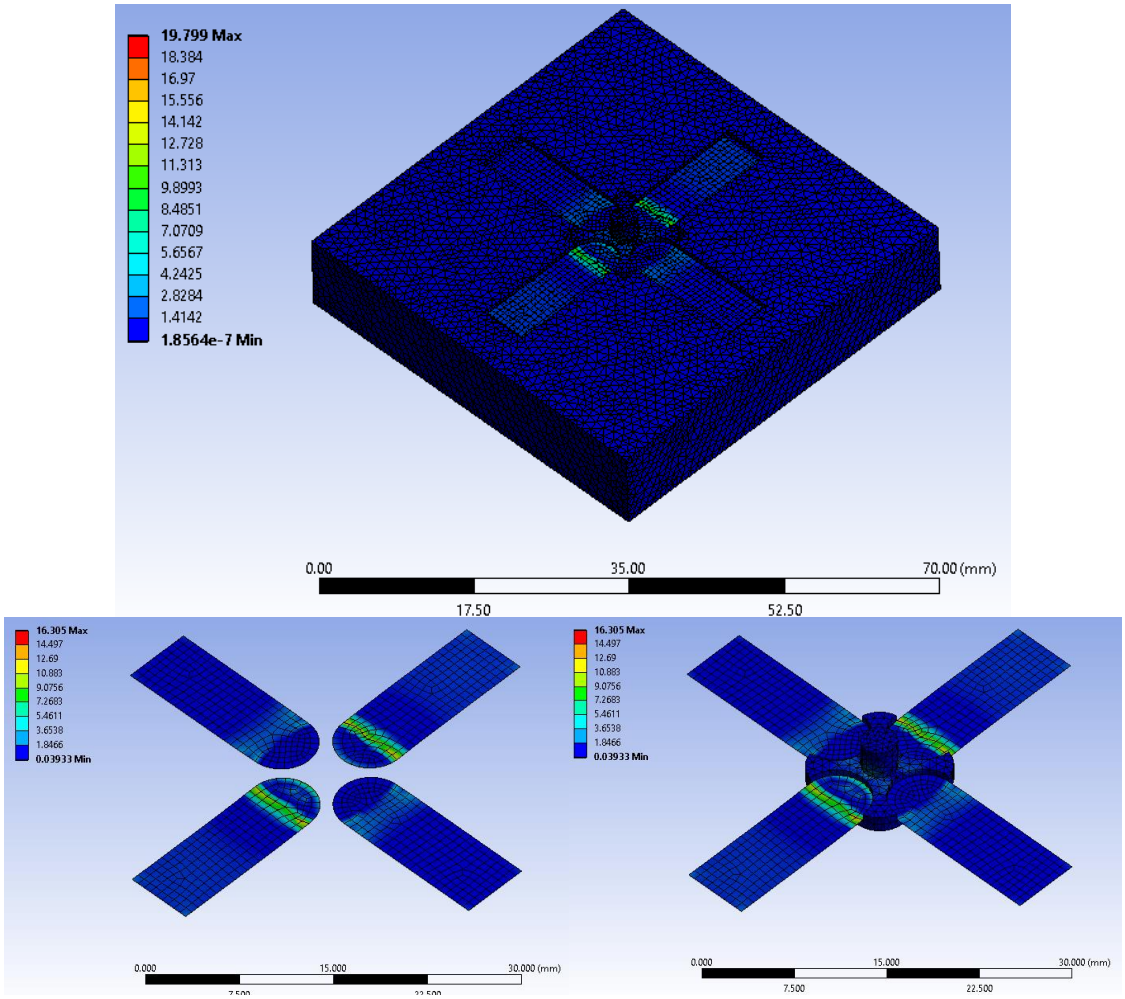

Fig. 23: The ANSYS Simulations of 3N in the X or Y direction with the first central connection piece design. The force indicates that stress of oppositional resistors is equal with respect to one another.

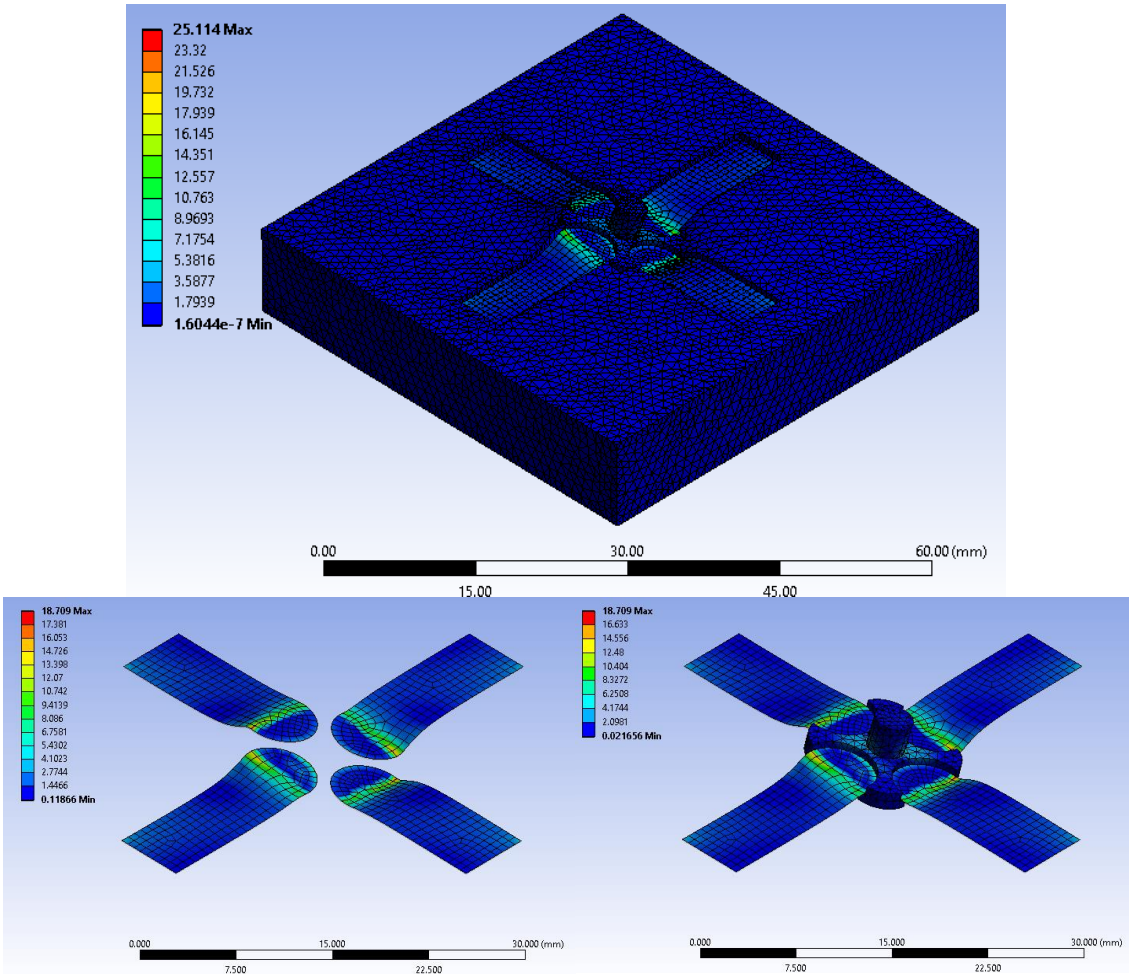

Fig. 24: The ANSYS Simulations of 3N in the X and Y direction simultaneously at a 45° angle with the first central connection piece design. The force indicates that stress of adjacent X and Y resistors are equal with respect to one another, relevant to the front sensing location of the insole system.

Additionally, figures 25, 26, and 27 correspond to simulation with design two of the central connection piece in the Z direction, X or Y direction, and simultaneous X and Y testing respectively. Once again, the gel has been hidden in order to identify the symmetrical reaction due to input force.

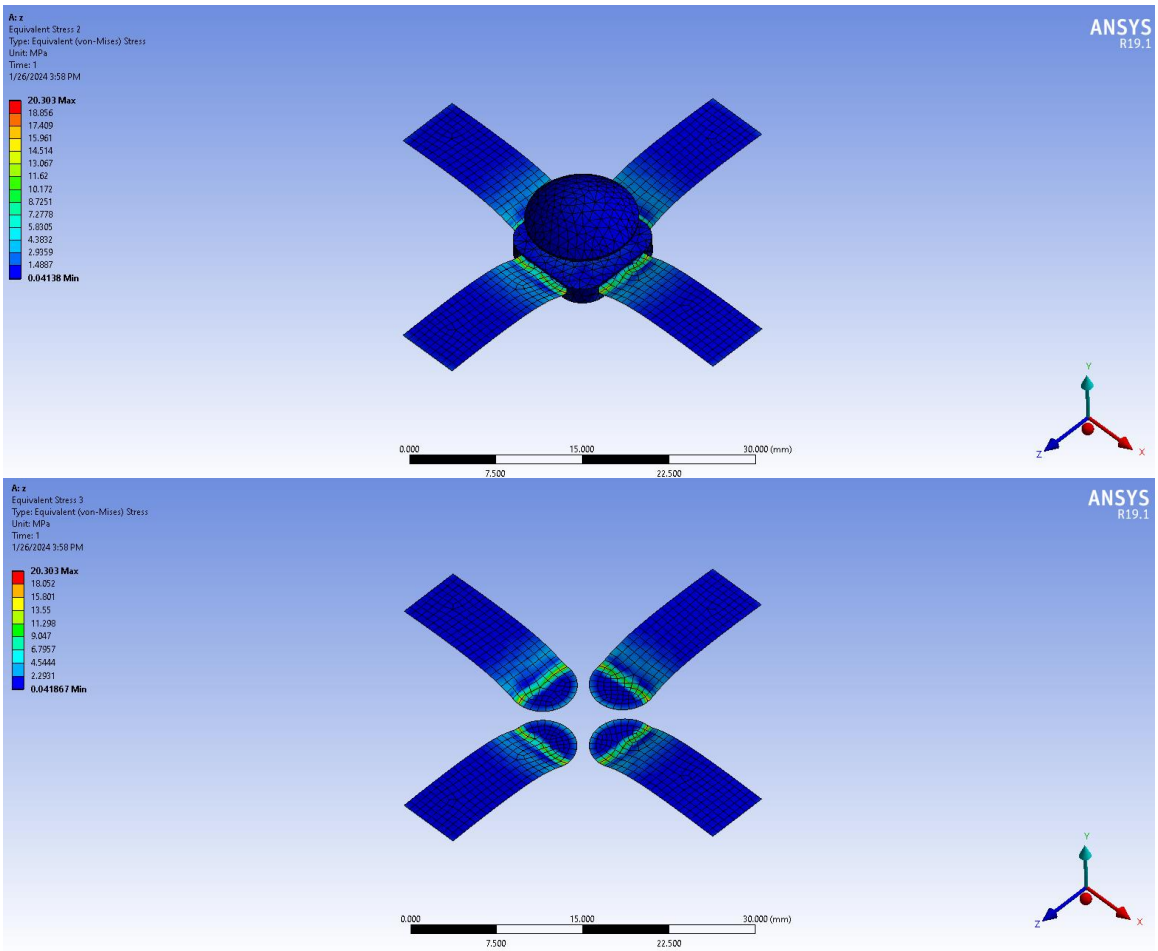

Fig. 25: The simulations of the structure with the second central connection piece. 10N of force are applied in the Z-direction and indicates equal stress values between all resistors.

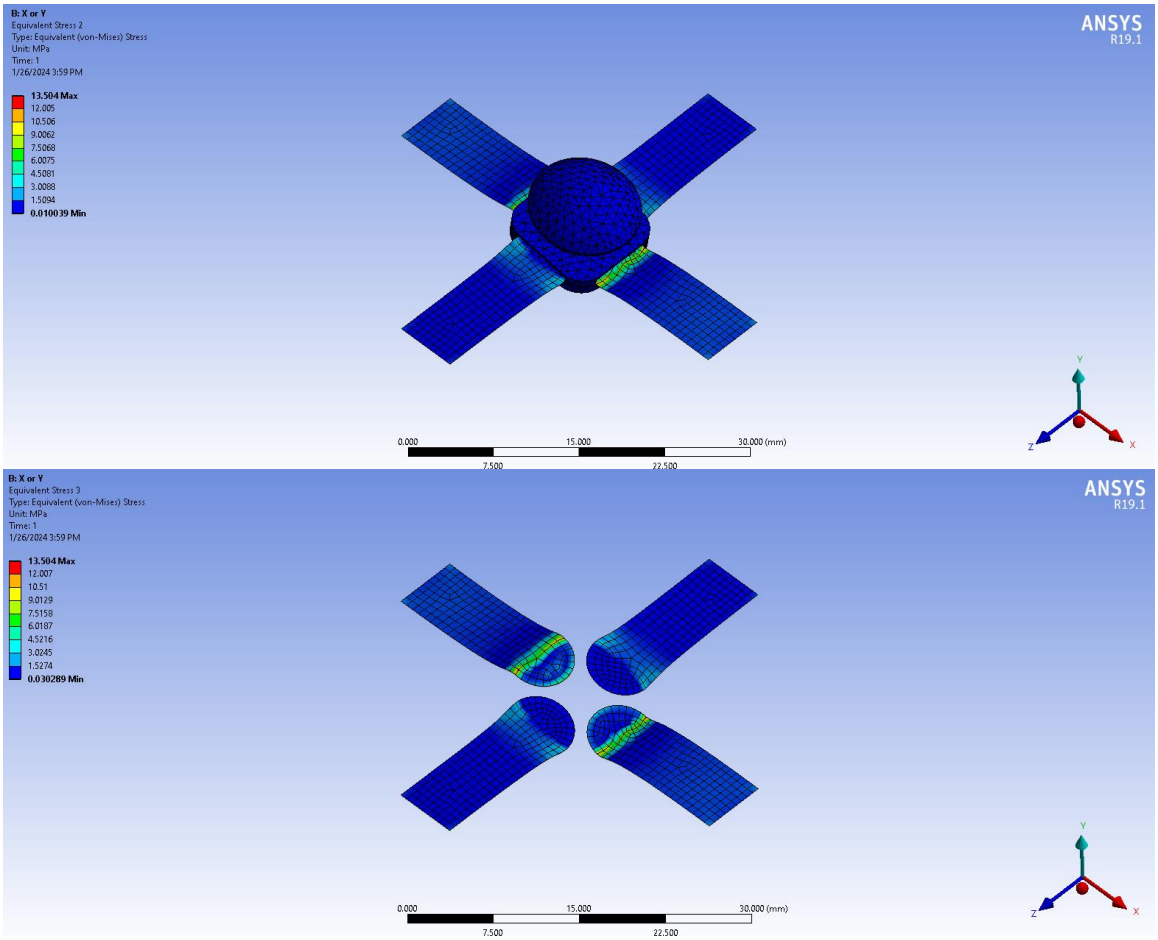

Fig. 26: The simulations of the structure with the second central connection piece. 3N of force are applied in the X or Y direction and indicates equal stress values between relevant paired resistors.

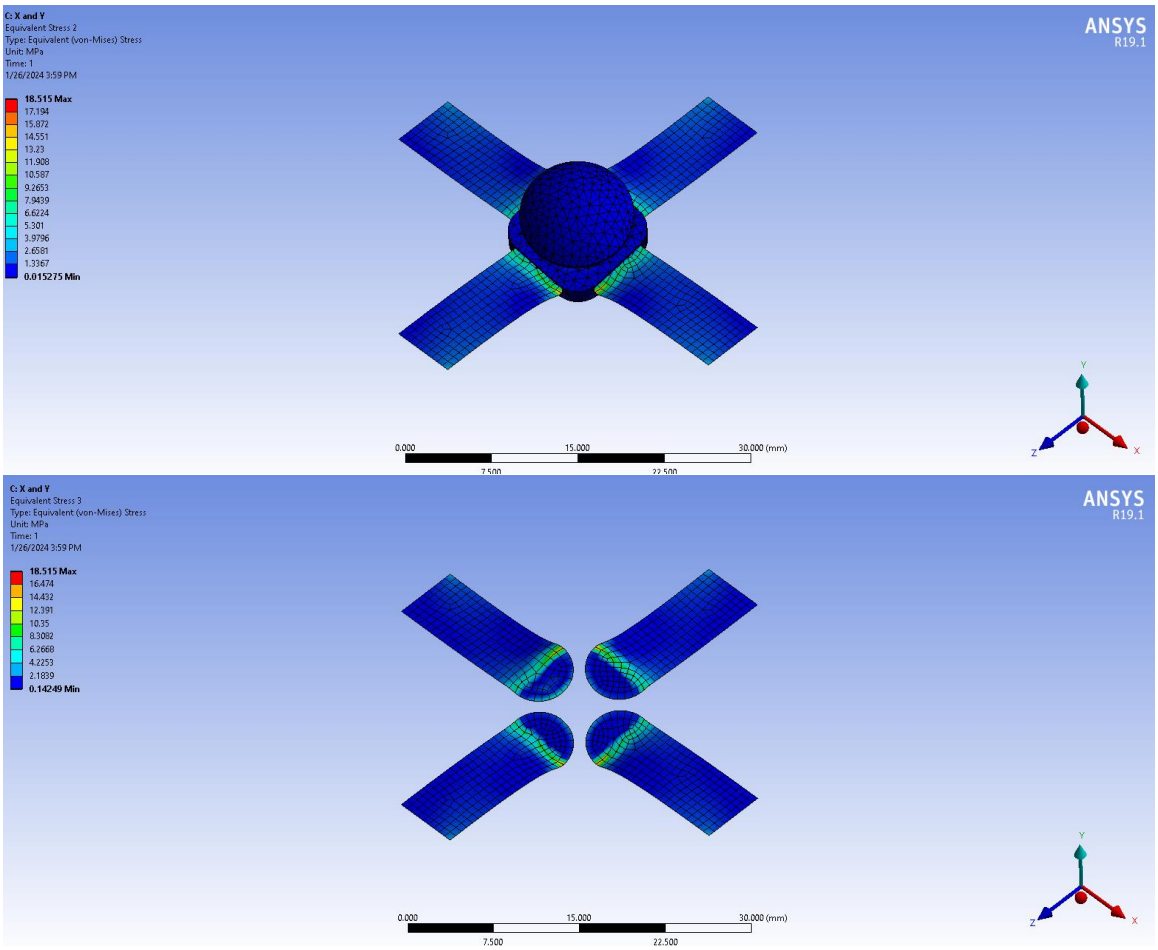

Fig. 27: The ANSYS Simulations of 3N in the X and Y direction simultaneously at a 45° angle with the second central connection piece design. The force indicates that stress of adjacent X and Y resistors are equal with respect to one another, relevant to the front sensing location of the insole system.

After confirming the self-decoupling mechanism works as intended while the analysis points are suspended in the gel insole, the experimental testing commenced.

3.3 Experimental Testing and Validation

In order to prepare for practical testing, experimental testing involved structured testing under measurable force input values. In doing so, force curve calculations could be derived and error metrics could be calculated comparing the calculated force and reference input force.

3.3.1 Experimental Verification

Experimental testing began with structured analysis incorporating specific, measurable force inputs in each direction, ensuring decoupling capability of the system after the sensors were solidified in the gel insole. Each set of four sensors were placed on a vibration isolated table and were pressed at variable force inputs, measured with a NIDEC-SHIMPO FGV-1XY digital force gauge for testing in the X and Y direction and a NIDEC-SHIMPO FG-3005 digital force gauge for testing in the Z direction. The NIDEC-SHIMPO FGV-1XY force gauge measures force applications up to 5 newtons of force with a resolution of 0.001 N and 0.2% F.S.. The NIDEC-SHIMPO FG-3005 digital force gauge measures force applications up to 50 newtons of force with a resolution of 0.01 N and 0.3% F.S.. These force gauges were attached to a Sutter Instrument MPC-285 control arm via a 3D printed mount and were controlled with a Sutter Instrument MPC-200 control system, shown in Figure 28.

Fig. 28: The Sutter Instrument Company MPC-200 series control system used for control arm movement during experimental testing and validation.

After connecting the force gauge to the control arm, the MPC-200 and associated software was used to move the control arm with 10 micrometer movements until the desired maximum force input was reached. After finding the movement distance that would correspond to the desired force input, the system was configured to move that distance in one singular movement at a set speed of 1/12 of the total distance per second. For X or Y directional tests, a maximum of 3N of force was achieved. For initial Z directional tests of the original design, a maximum of approximately 14N of force was achieved. The control arm maximum force application was found to be approximately 15 N, so the Z directional tests were reduced slightly in force applied to avoid damage to the control arm system. However, for designs two and three of this research, the NIDEC-SHIMPO 3005 force sensor battery would not hold a charge and became unusable. Due to this limitation, force values were carried on with the NIDEC-SHIMPO FGV-1XY scale, so the Z directional force was reduced to 5N. The force gauge testing setup is shown in Figure 29 and the control system software is shown in Figure 30.

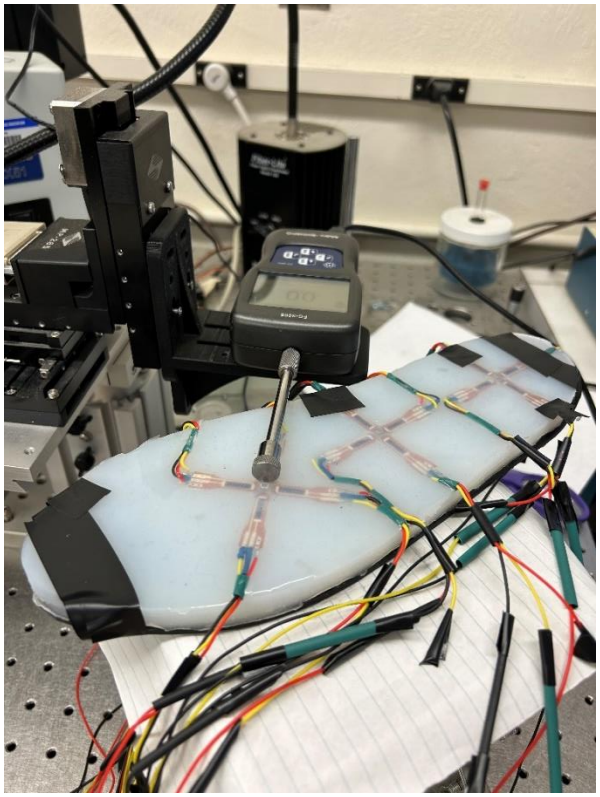

Fig. 29: The testing method of each insole design for this research. The force sensor is attached to the 3D printed arm mount on a vibration-isolated table. The arm moves along a set path to push the center connecting piece with the desired force.

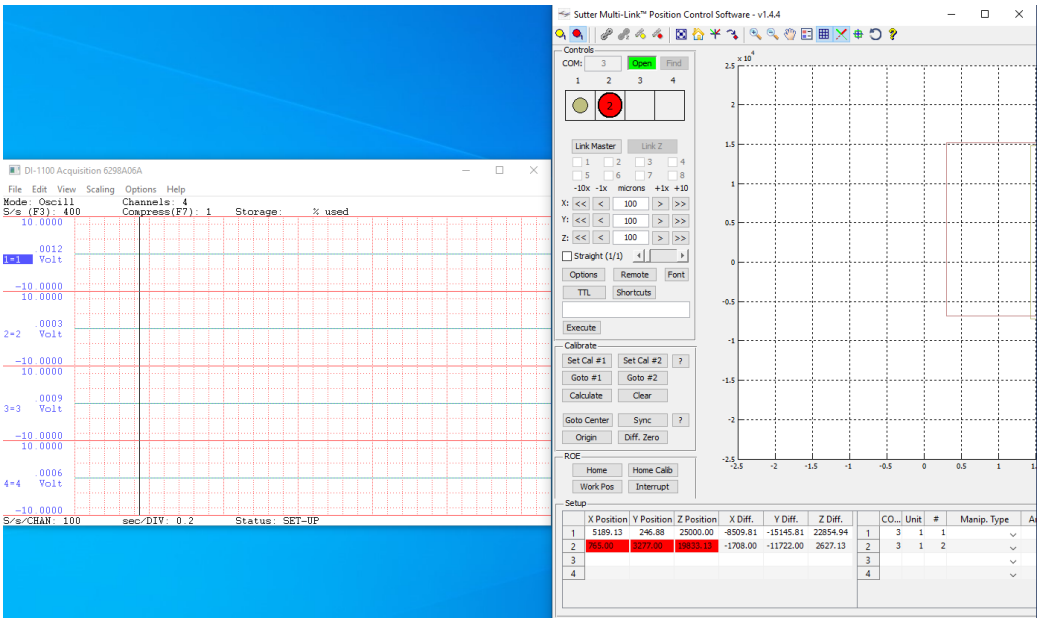

Fig. 30: The screen during testing of the insole designs. The right software is the MPC-200 microcontroller software and the left is the DAQ software for voltage analysis.

3.3.2 Sensor Modification

For designs two and three, experimentation was conducted that involved reducing the sensitivity of the sensors themselves. This entailed applying a silver conductive epoxy to the conductive ink found on the sensors themselves, functionally reducing the sensitivity of the sensors. For design 3, the sensors were further modified by cutting to reduce the size of the sensors and improve the sensor positioning in the insole system. The sensors were cut evenly using a resin printed mold shown in Figure 31. In either case, the maximum resistance of the sensors was found to be approximately 100 Ohms, or 20% of the previous maximum resistance.

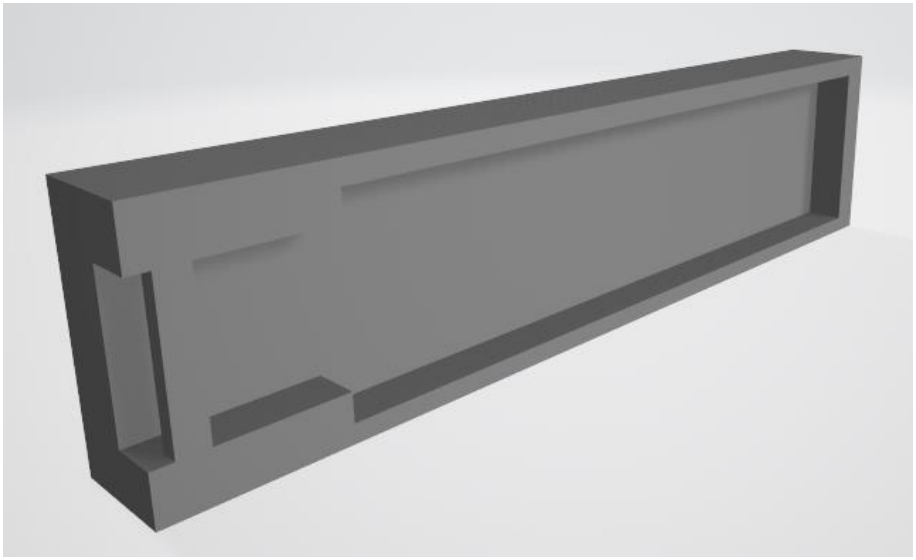

Fig. 31: The resin mold used to uniformly modify the sensors. Sensors were placed under the bar on the left and painted with silver epoxy. For design three, the sensor was cut after being painted at the edge of the mold.

3.4 Practical Testing

Once the structured validation testing was completed, the system was moved to the ground to complete practical testing. To enable easier testing, a 34-port ribbon cable was attached to connect the insole system to the half-Wheatstone bridge circuits, shown

in Figure 32. This ribbon cable also served as an extension to ensure multiple steps could be taken with the insole system.

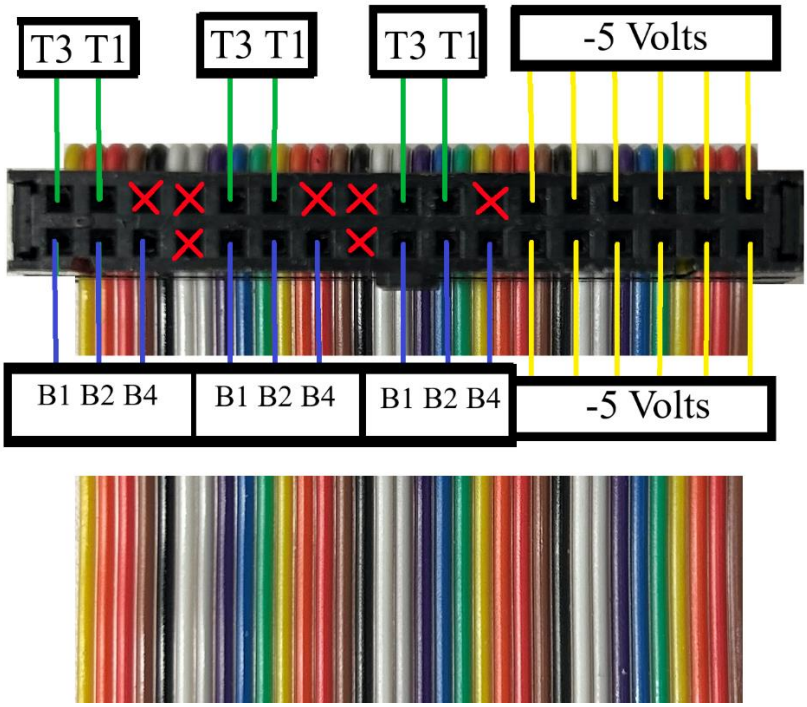

Fig. 32: The configuration for connections between the half-Wheatstone bridge circuits and the insole system components. The top and bottom resistors are labeled to the left of the Figure whereas the right -5V provides power to all sensors.

For design 1, testing began with stepping on the system for approximately 5 seconds and walking 2 steps. However, due to stress on the central piece joint attachments, practical testing quickly resulted in disconnected bend sensors from the central connection pieces. Research continued with the second design of the central connection piece, which incorporated grooves for a better adhesion between sensors and the central piece as well as a textured half dome for improved friction for shear force detection. Additionally, the large dome and grooves disallowed direct force to the connection point between the central piece and the bend sensors. The second design incorporated the reduced sensitivity by painting the sensors. Figure 33 demonstrates the

connection of the insole system with relation to the positioning of the circuits and the power supply.

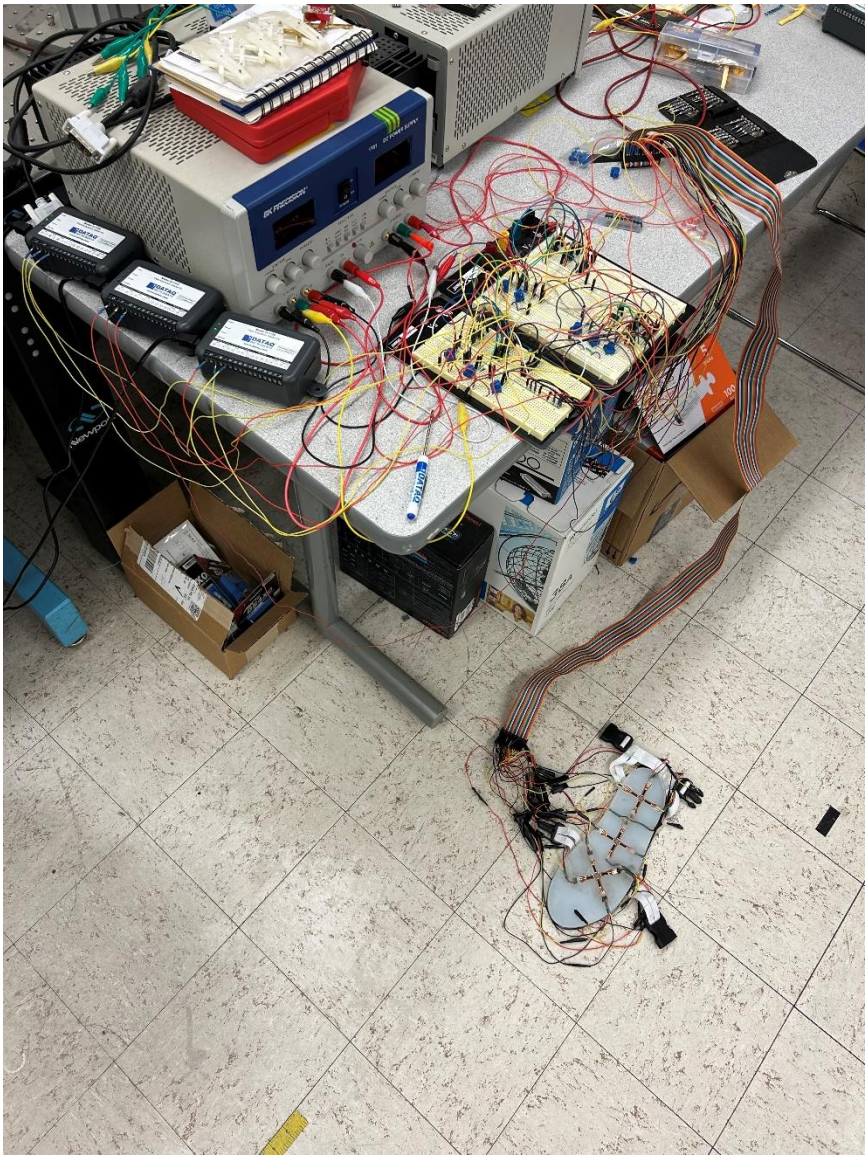

Fig. 33: The positional relationship between the insole system and the circuitry and power supply. The circuit sat on a table for the duration of testing whereas the insole system was tested on the ground adjacent to the table. Voltage outputs were collected with DATAQ data acquisition kits.

For practical testing, the insole system was attached to the foot with two elastic straps connected to the base of the insole system. One strap was located near the sole of the foot whereas the other strap wrapped around the ankle, demonstrated in Figure 34.

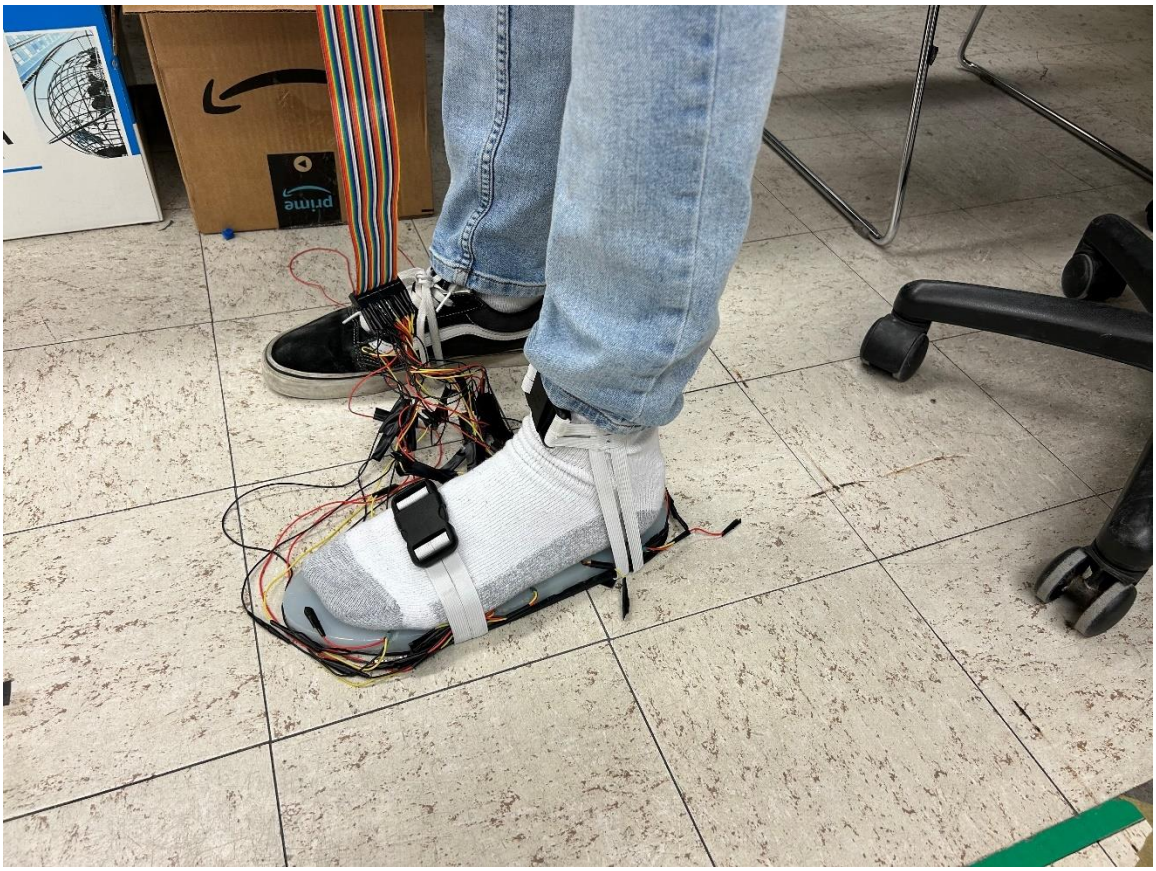

Fig. 34: The insole system attached to the foot for practical testing, attached by using elastic and buckles.

Finally, as each analysis point has three outputs during testing, readings are collected simultaneously with three DATAQ data acquisition kits. During testing, the associated software applications for the data acquisition kits collect all data simultaneously, demonstrated in Figure 35.

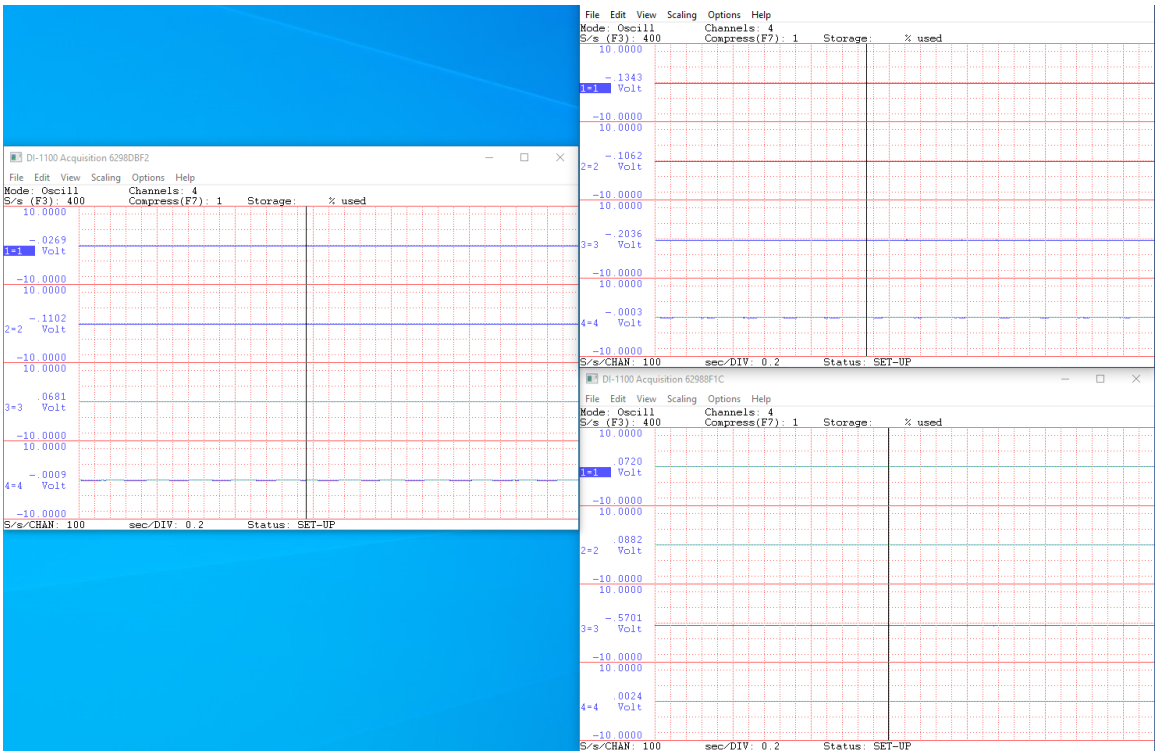

Fig. 35: The software applications of the data acquisition units collecting data for each direction and each analysis point, totaling 9 total data streams to collect. The front point would be collected by the left most program interface, the middle point would be collected by the top right program interface, and the back point would be collected by the bottom right program interface.

Chapter 4: Results

Results is broken up into each of the three designs. In each section, results will consist of the validation testing conducted with the force sensor on the vibration isolated table and the practical testing conducted while using the insole system. The validation testing served to prove the existence of a relation between the force applied and the voltage output at each sensing location.

The practical testing for the first design utilized the relation between the force and voltage to convert detected voltage outputs back to force while using the product. The second design focused on the voltage outputs, correlating the gait motions to voltage responses. This was decided after finding that the back sensing location only responded to large force values, providing no reference data or force curve equations in the experimental testing. The third design does not have practical testing as the shortened sensors proved structurally unviable currently for full body force application.

4.1 Design One

Design one served as a foundation for experimental direction. The system consisted of three analysis points, found at the heel, arch, and the sole of the foot. The sole analysis point will be referred to as the front analysis point, the arch analysis point will be referred to as the middle analysis point, and the heel analysis point will be referred to as the back analysis point. The sensors were unaltered for the first design and were connected to the first center connection point iteration. The directions of analysis are shown in Figure 36.

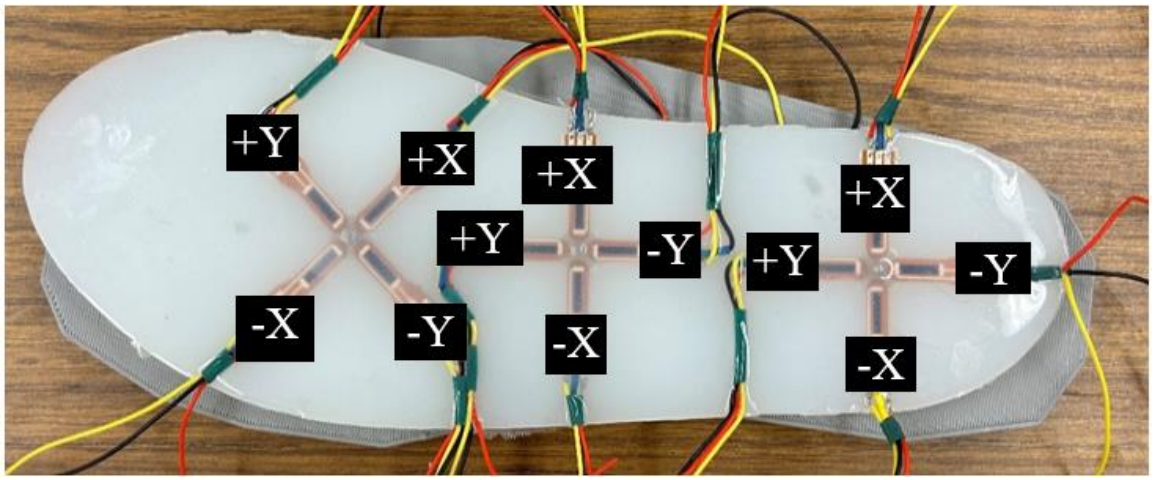

Fig. 36: The directional configurations for the first insole design.

4.1.1 Validation Results

Validation testing involves the system calibration tested on the vibration isolated table to investigate the correlation between input force and resulting output voltage between relevant resistor pairs. Results below are exemplified in the following order of visuals: voltage of relevant directions compared to the input force, analysis of the best fit line and potential delay using the Matlab system analysis toolbox, the resulting calculated force output with applied phase shift, and the hysteresis of the system after applying a time phase shift.

X-Direction Results

Front analysis point

The following Figure 37 indicates the force and decoupled voltage data collected while applying pressure to the front sole analysis point of the insole system. The red line indicates the collected reference force from the NIDEC-SHIMPO force gauge, the blue line indicates the voltage data in the X-direction, and green indicates the voltage in the Y-direction.

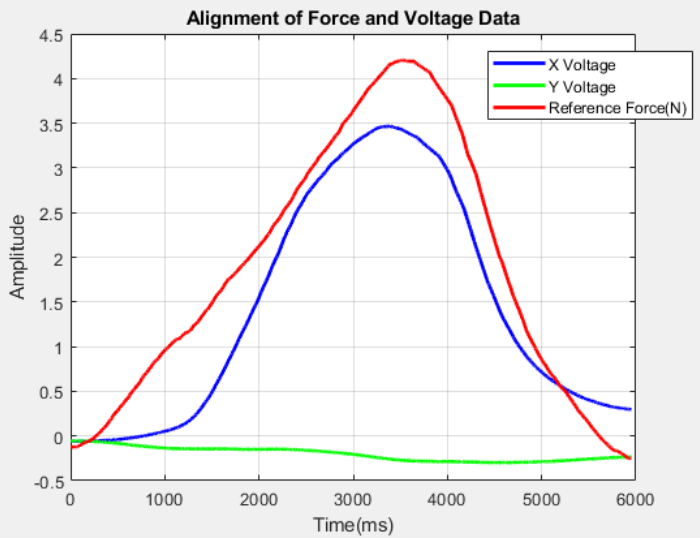

Fig. 37: The time-domain graph of the voltage response while approximately 4N of force are applied to the front analysis point of the insole system.

This data is then compared with the Matlab system analysis toolbox to establish the best fit line characteristics for the given dataset, shown in Figure 38.

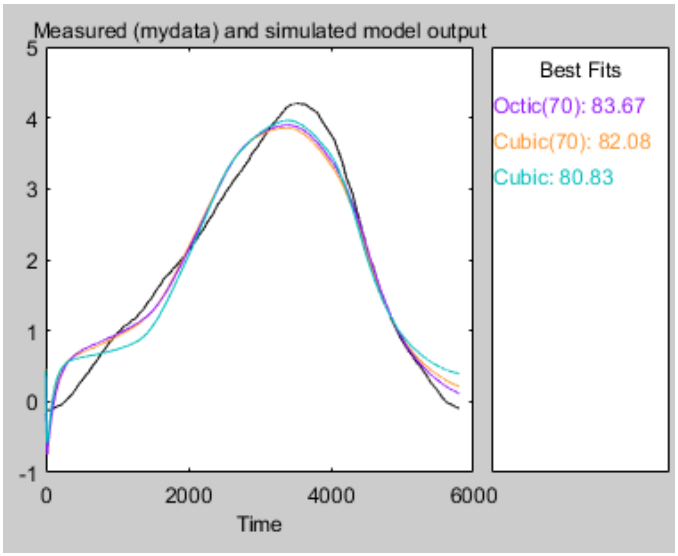

Fig. 38: The system analysis toolbox analysis of different best fit line parameters. This data resulted in a rather high order line equation, whereas most other analysis resulted in a quadratic or cubic line, often with a delay. For simplicity in comparison, the cubic line was also used for comparison to other datasets.

After finding the best fit line, the coefficients for the best fit line were calculated and used to convert the output voltage to input force to correlate between the two. Figure

39 demonstrates the cross examination between the reference force and the calculated force with the data shifted according to the system analysis best fit line.

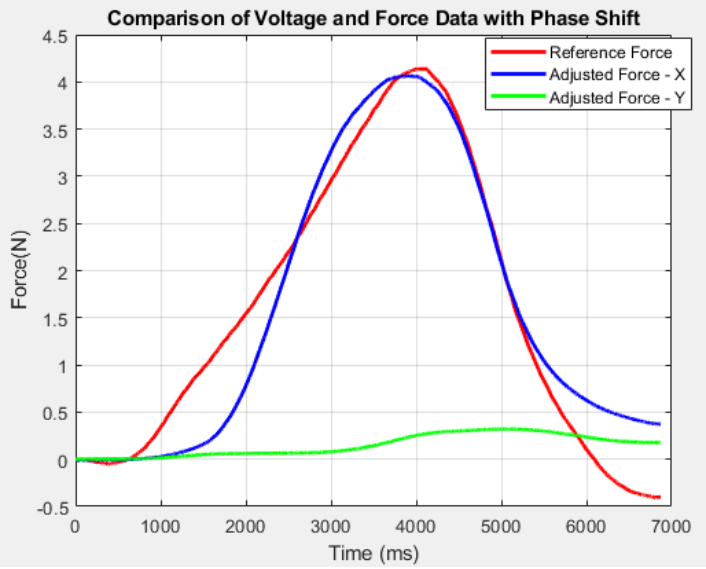

Fig. 39: The resultant force comparison between the reference force in red and the calculated X-directional force in blue. The green line indicates the Y-directional force collected simultaneously and solved for independently.

Finally, the hysteresis of the collected was analyzed, indicating the system response during pressure and release from the control arm and comparing to the equation of the line used for voltage conversion to force. Figure 40 demonstrates the force hysteresis curve while testing the system.

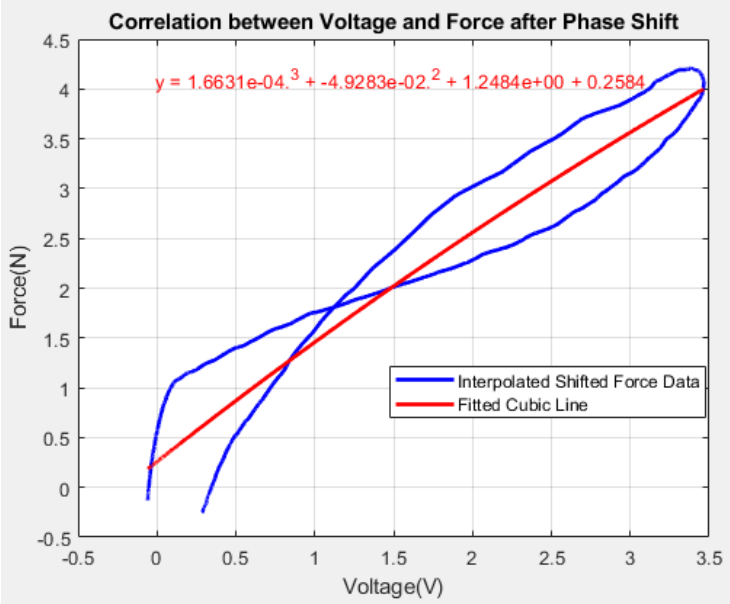

Fig. 40: The force hysteresis curve for the system during testing of the X-direction force application. The left-most blue line indicates the starting calculated force value.

The accuracy of each analysis point and applied directional force are tabulated in an error metric table found at the end of this section, comparing relative error of the system within the working range of force values greater than 0.5N, the median error, the difference in peak values between reference and calculated force, the maximum error in the working range, and the normalized maximum error of the system.

Middle analysis point

Figures 41-44 show the voltage response due to force input, the correlation between the voltage response and the force input in the Matlab system analysis toolbox for the best fit line characteristics, the comparison between the converted voltage and the reference force, and the force hysteresis curve for X-directional testing at the middle analysis point respectively.

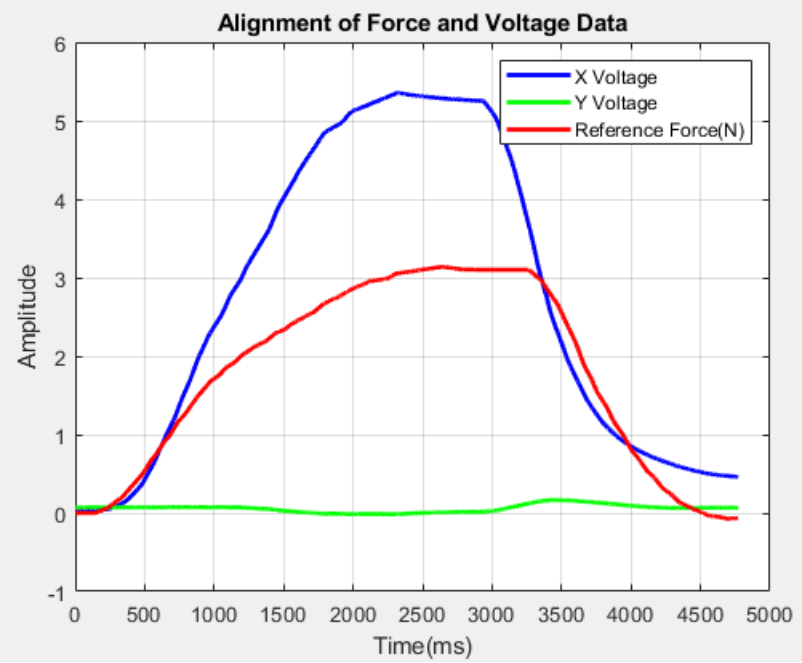

Fig. 41: The comparison between reference force and resultant voltage at the middle analysis point during an X-directional force of 3N.

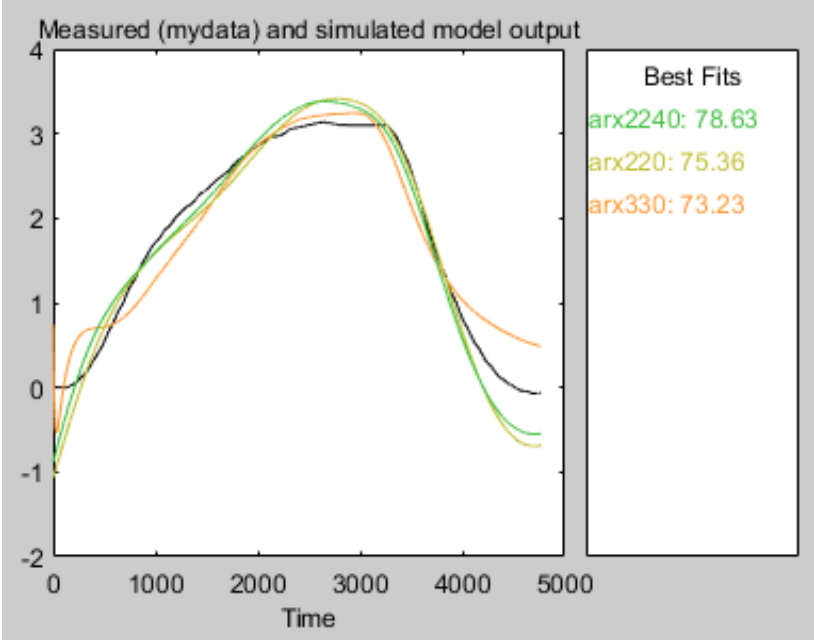

Fig. 42: The system analysis toolbox data report for the best fit line parameters. The resulting best fit line parameters were a quadratic line with a delay of 40.

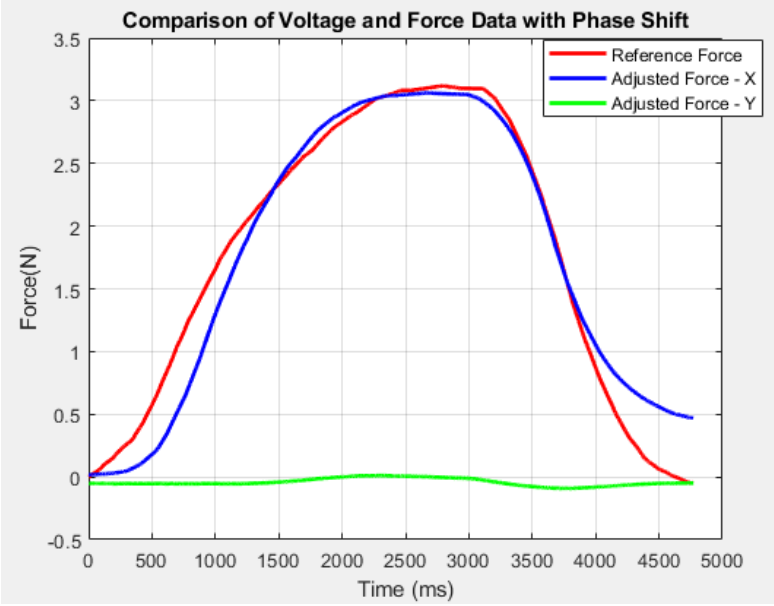

Fig. 43: The visualization of the voltage converted back to force and compared to the reference force. The red is the reference force, the blue is the X-direction calculated force response, and green is the Y-directional force calculated independently.

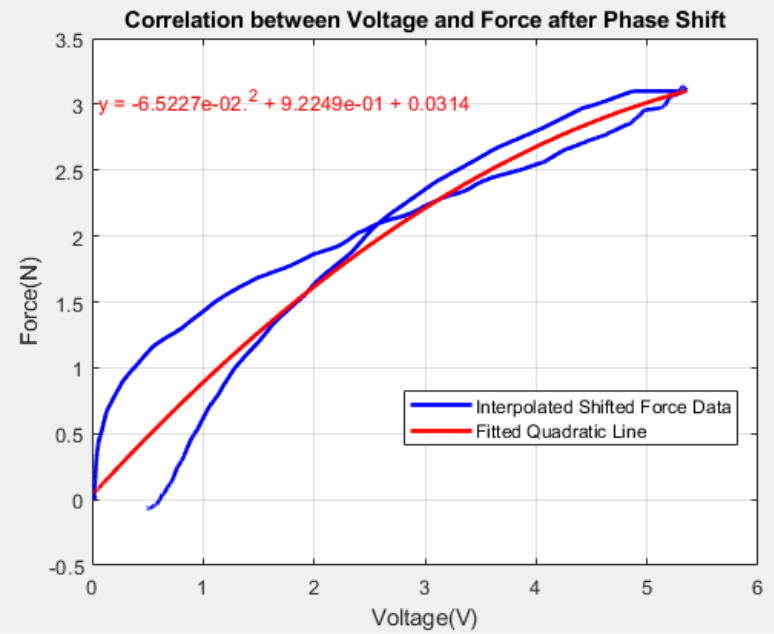

Fig. 44: The hysteresis curve visualizing the comparison between the calculated force and the best fit line used for the conversion during the pressing and releasing of the force sensor. The left most blue line indicates the resting position.

Back analysis point

Figures 45-48 show the voltage response due to force input, the correlation between the voltage response and the force input in the Matlab system analysis toolbox for the best fit line characteristics, the comparison between the converted voltage and the reference force, and the force hysteresis curve for X-directional testing at the back analysis point respectively.

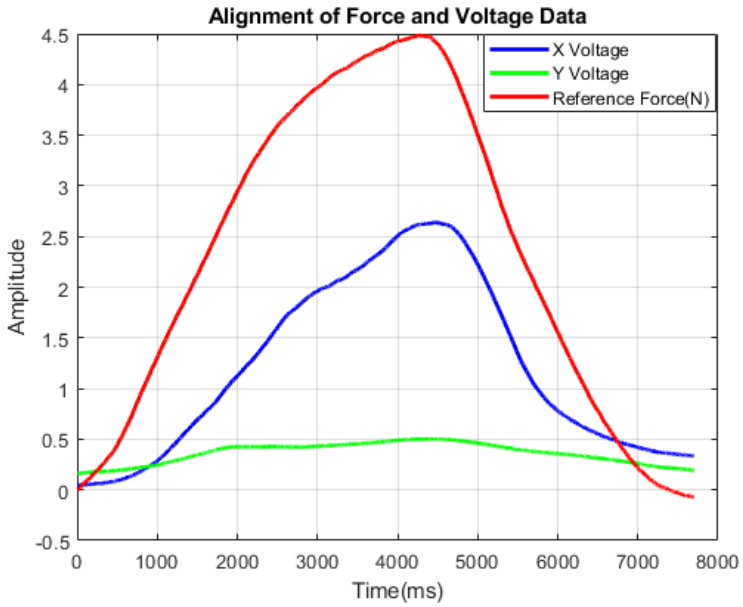

Fig. 45: The comparison between the resultant voltage in the X and Y direction due to an input reference force applied in the X-direction.

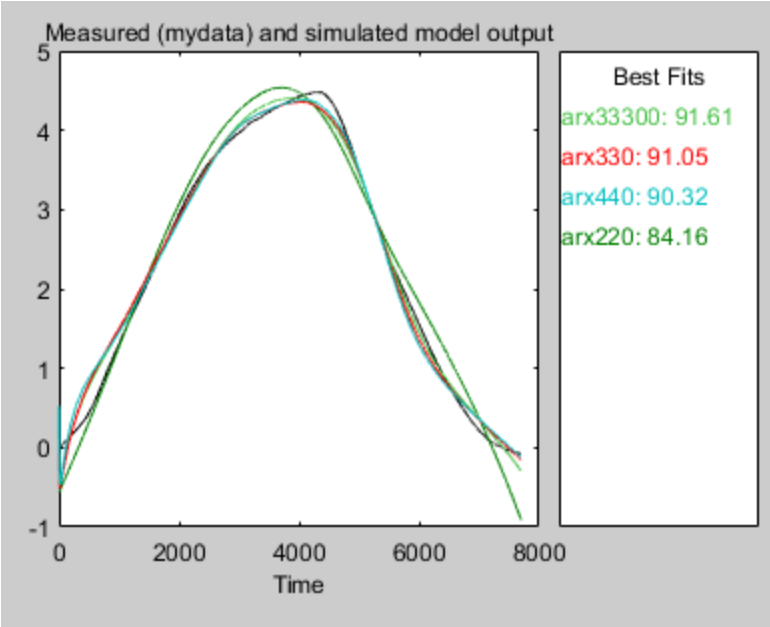

Fig. 46: The system analysis toolbox output for the best fit line parameters for the back analysis point in the X-direction. The best fit line for this analyte was found to be a cubic line with a delay of 300.

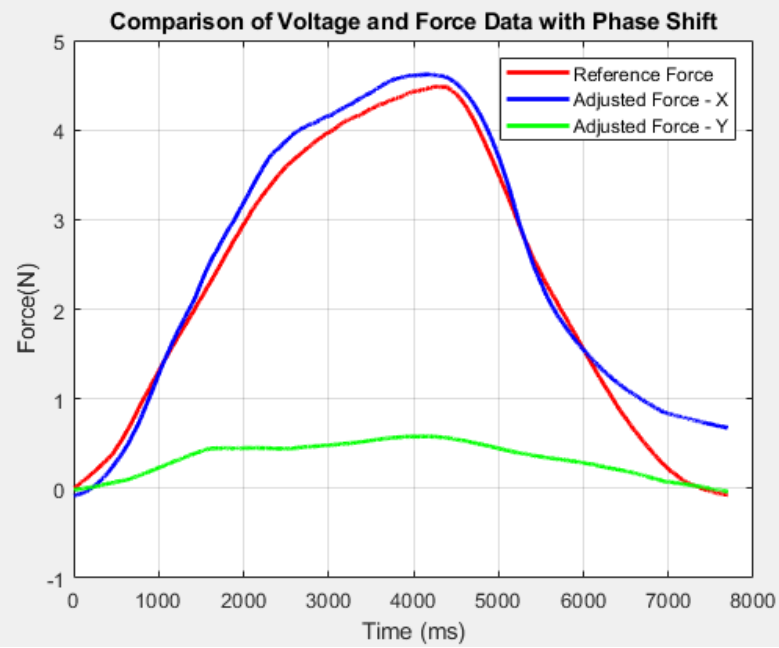

Fig. 47: The comparison between the reference force in red and the calculated forces for the X and Y directions. The blue line indicates the calculated X-directional force and the green line indicates the Y-directional force.

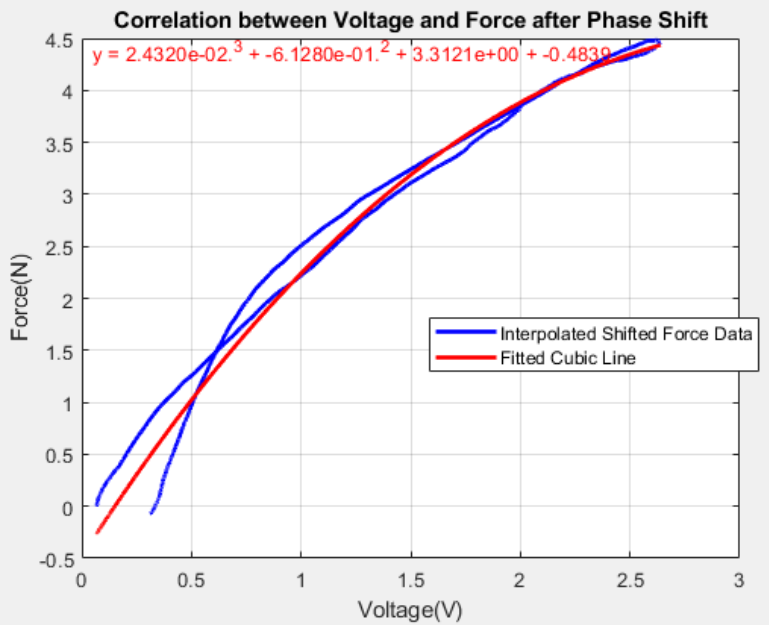

Fig. 48: The hysteresis curve visualizing the comparison between the calculated force and the best fit line used for the conversion during the pressing and releasing of the force sensor. The left most blue line indicates the resting position.

Y-Direction Results

Front analysis point

Figures 49-52 show the voltage response due to force input, the correlation between the voltage response and the force input in the Matlab system analysis toolbox for the best fit line characteristics, the comparison between the converted voltage and the reference force, and the force hysteresis curve for Y-directional testing at the front analysis point respectively.

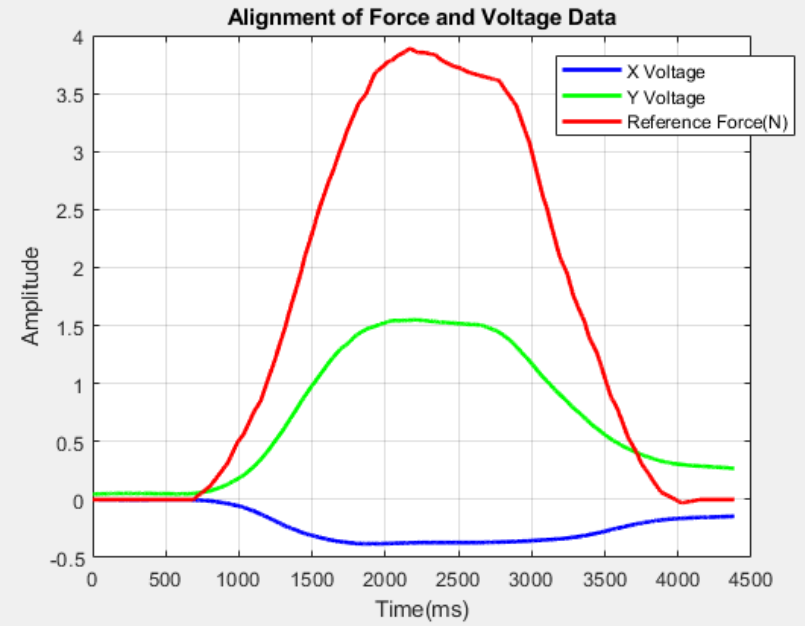

Fig. 49: The comparison between the reference force in red and the output voltages in the X and Y directions. The green line indicates the Y resultant voltage and the blue line indicates the X resultant voltage.

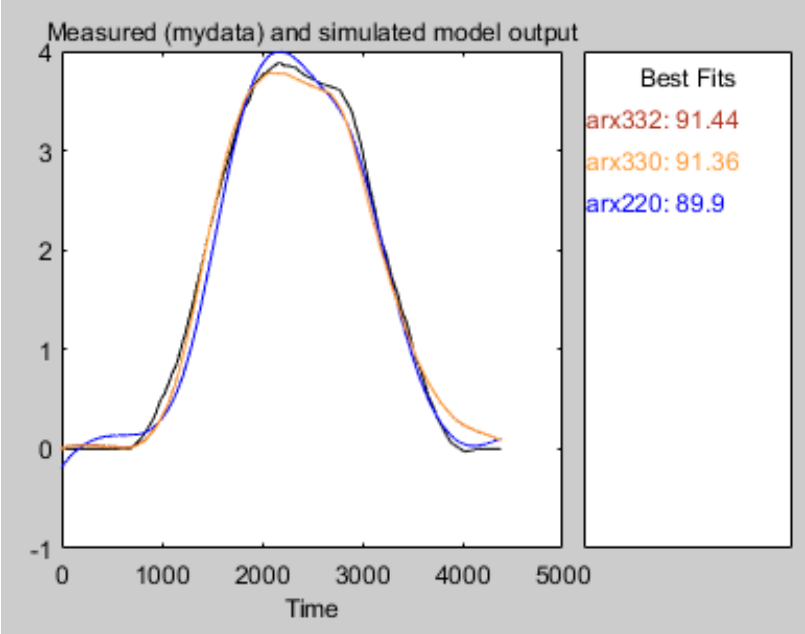

Fig. 50: The system analysis toolbox output for the best fit line parameters. For this dataset, the best fit line parameters found for this dataset was a cubic line with a small delay of 2.

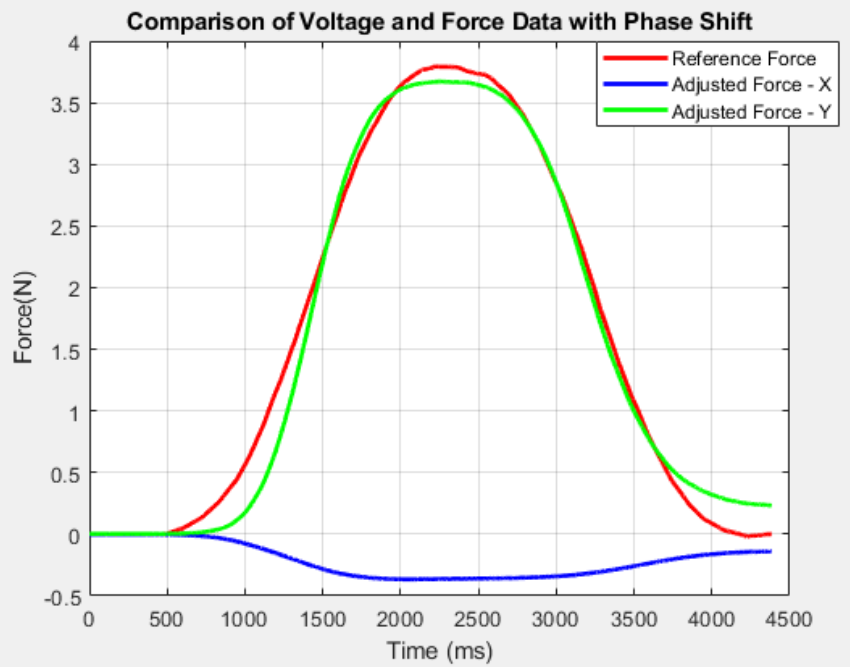

Fig. 51: The comparison of the converted voltage of both the X and Y direction and the reference input force. The Y force is shown in green and the blue line demonstrates the X force.

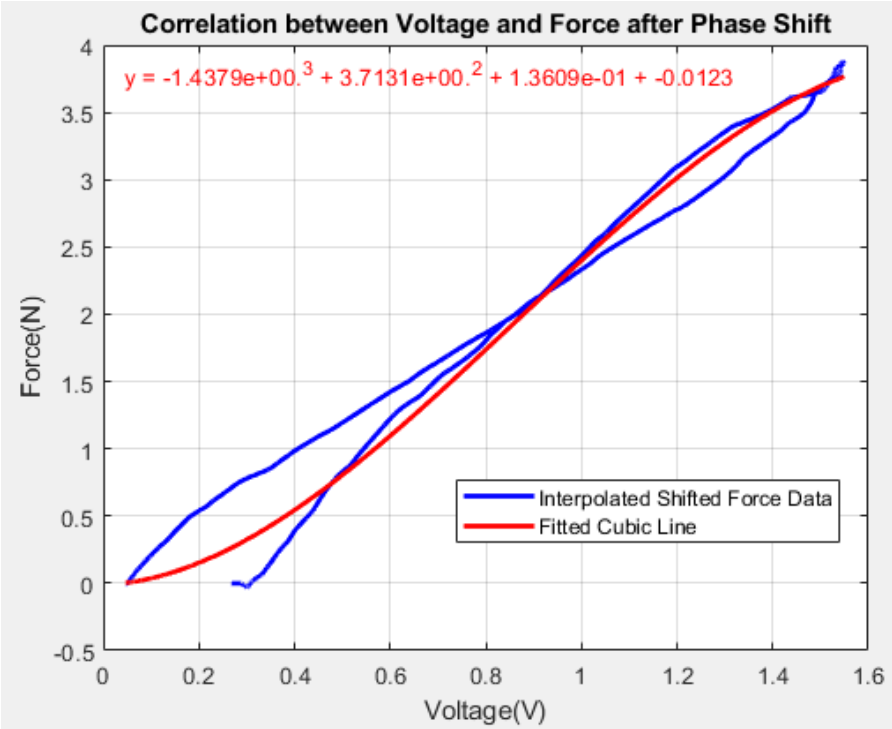

Fig. 52: The hysteresis curve visualizing the comparison between the calculated force and the best fit line used for the conversion during the pressing and releasing of the force sensor. The left most blue line indicates the resting position.

Middle analysis point

Figures 53-56 show the voltage response due to force input, the correlation between the voltage response and the force input in the Matlab system analysis toolbox for the best fit line characteristics, the comparison between the converted voltage and the reference force, and the force hysteresis curve for Y-directional testing at the middle analysis point respectively.

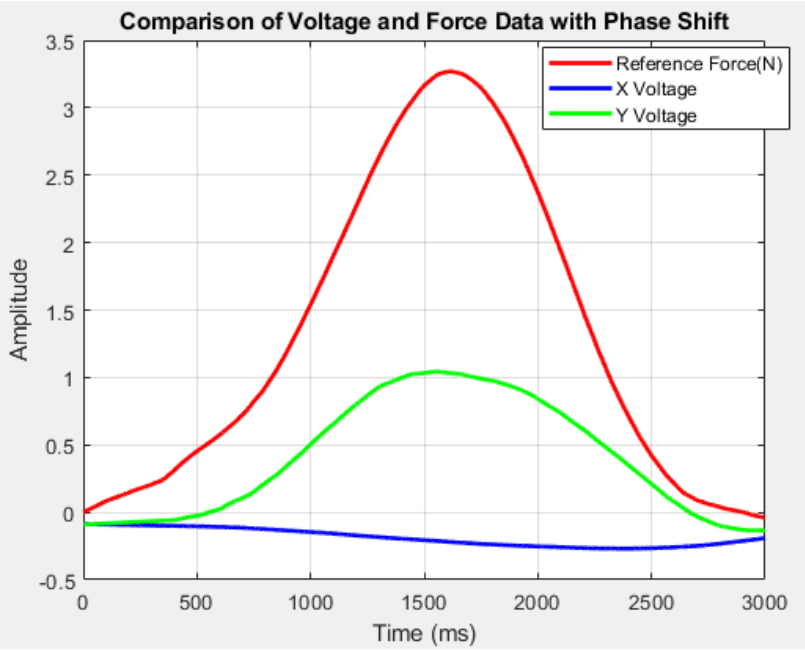

Fig. 53: The comparison between the reference force in red and the output voltages in the X and Y directions. The green line indicates the Y resultant voltage and the blue line indicates the X resultant voltage.

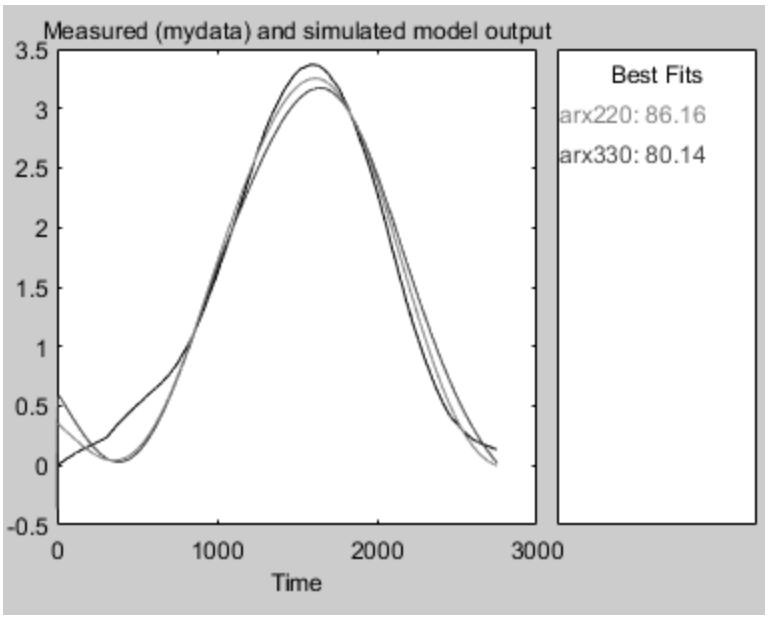

Fig. 54: The system analysis toolbox data report for the best fit line parameters. The resulting best fit line parameters were a quadratic line with no delay.

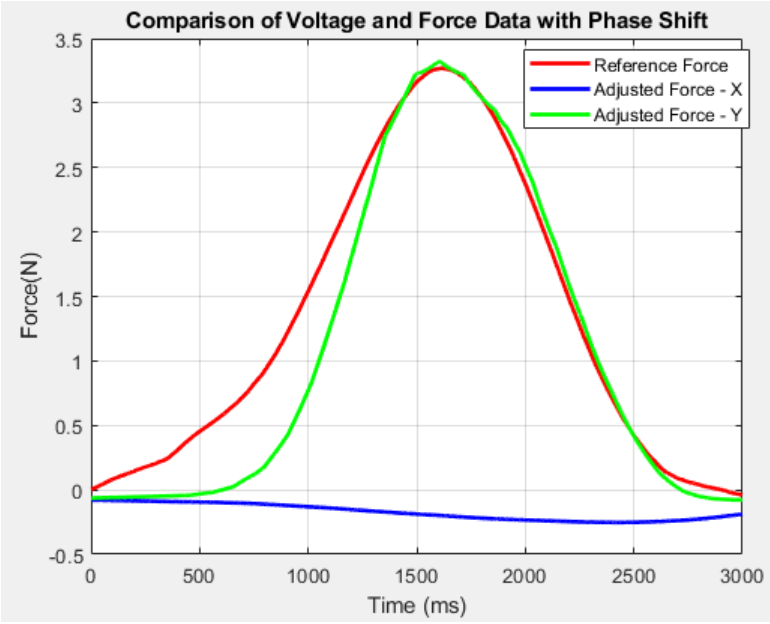

Fig. 55: The visualization of the voltage converted back to force and compared to the reference force. The red is the reference force, the green is the Y-direction calculated force response, and blue is the X-directional force calculated independently.

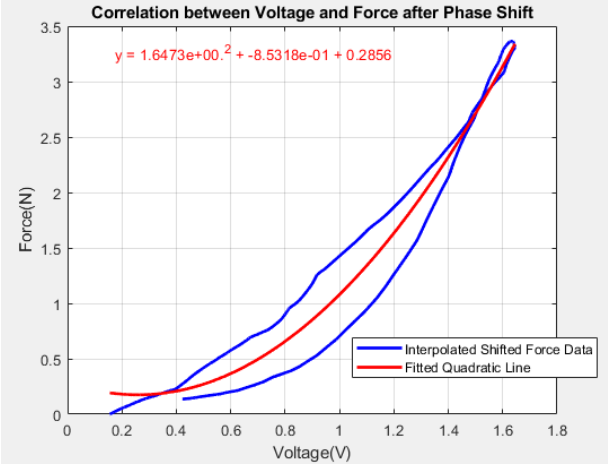

Fig. 56: The hysteresis curve visualizing the comparison between the calculated force and the best fit line used for the conversion during the pressing and releasing of the force sensor. The left most blue line indicates the resting position.

Back analysis point

Figures 57-60 show the voltage response due to force input, the correlation between the voltage response and the force input in the Matlab system analysis toolbox for the best fit line characteristics, the comparison between the converted voltage and the reference force, and the force hysteresis curve for Y-directional testing at the back analysis point respectively.

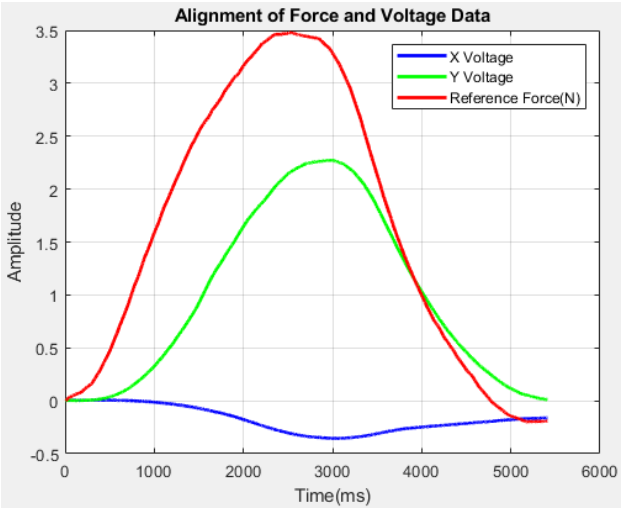

Fig. 57: The comparison between the reference force in red and the output voltages in the X and Y directions. The green line indicates the Y resultant voltage and the blue line indicates the X resultant voltage.

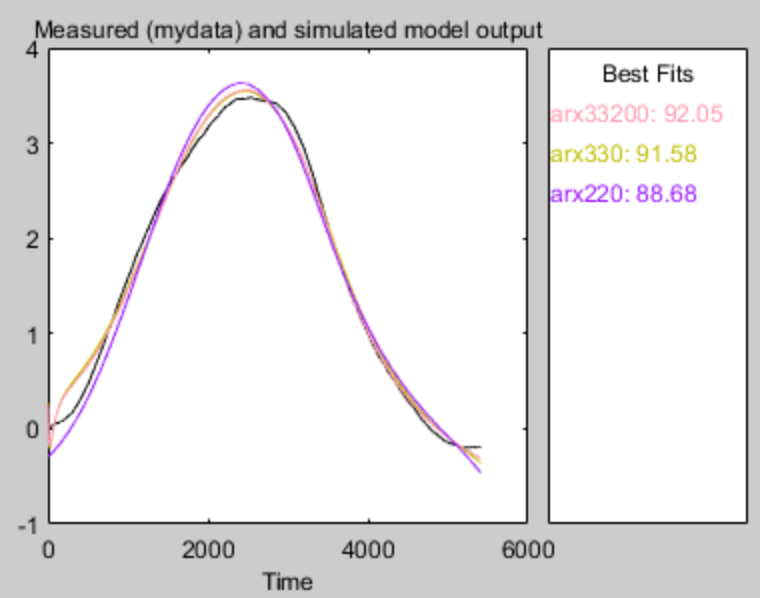

Fig. 58: The system analysis toolbox data report for the best fit line parameters. The resulting best fit line parameters were a cubic line with a delay of 200.

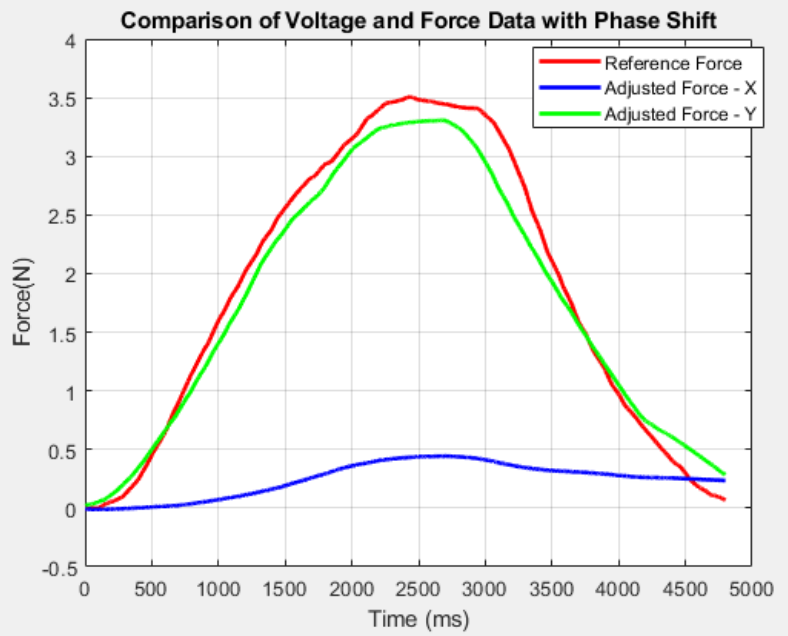

Fig. 59: The visualization of the voltage converted back to force and compared to the reference force. The red is the reference force, the green is the Y-direction calculated force response, and blue is the X-directional force calculated independently.

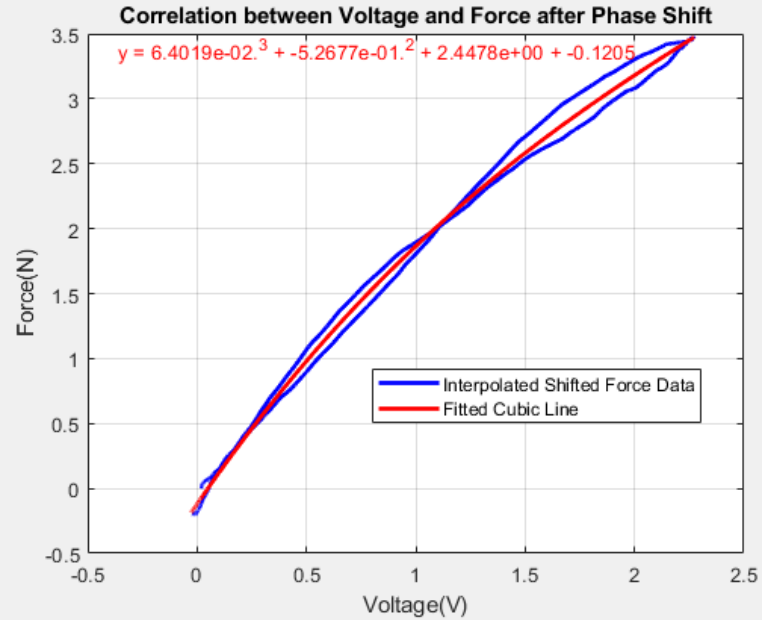

Fig. 60: The hysteresis curve visualizing the comparison between the calculated force and the best fit line used for the conversion during the pressing and releasing of the force sensor. The left most blue line indicates the resting position.

Z-Direction Results

Front analysis point

Figures 61-64 show the voltage response due to force input, the correlation between the voltage response and the force input in the Matlab system analysis toolbox for the best fit line characteristics, the comparison between the converted voltage and the reference force, and the force hysteresis curve for Z-directional testing at the front analysis point respectively.

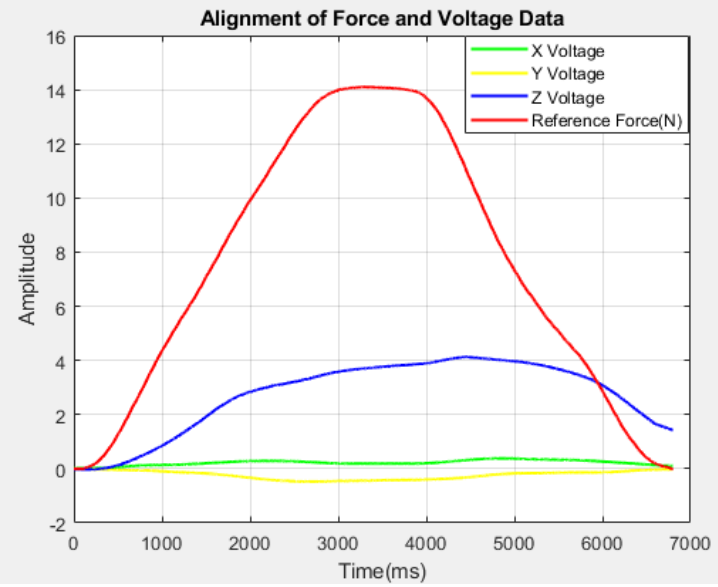

Fig. 61: The comparison between the reference force in red and the output voltages in the X, Y, and Z directions. The green line indicates the X resultant voltage, the yellow line indicates the Y resultant voltage, and the blue line indicates the Z resultant voltage.

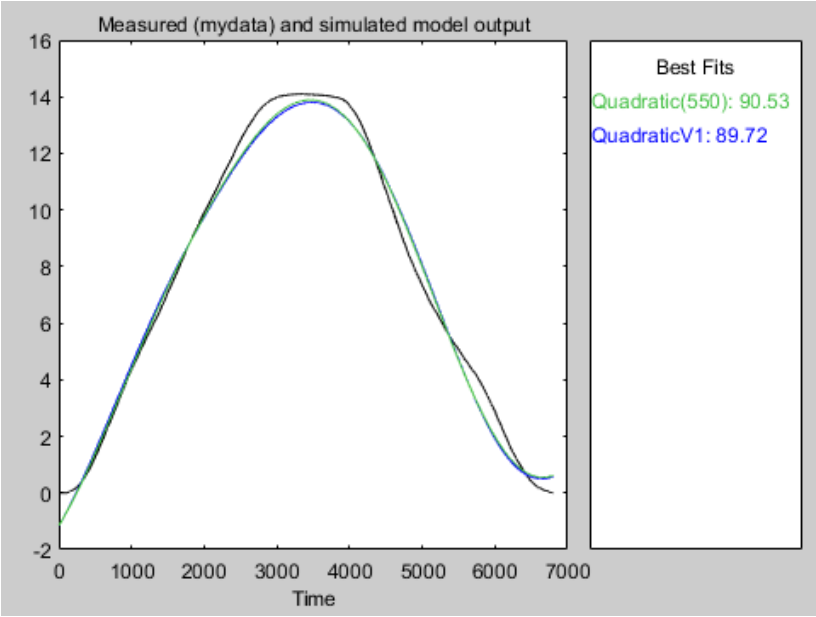

Fig. 62: The system analysis toolbox data report for the best fit line parameters. The resulting best fit line parameters were a quadratic line with a delay of 550.

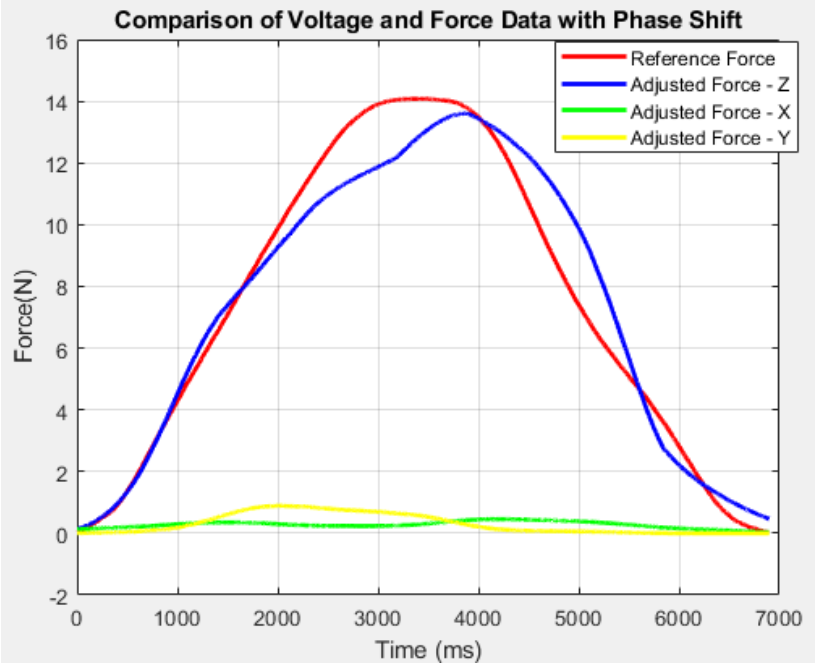

Fig. 63: The visualization of the voltage converted back to force and compared to the reference force. The red is the reference force, the green is the X-direction calculated force response, the yellow is the Y-direction calculated force response, and blue is the Z-directional calculated force response.

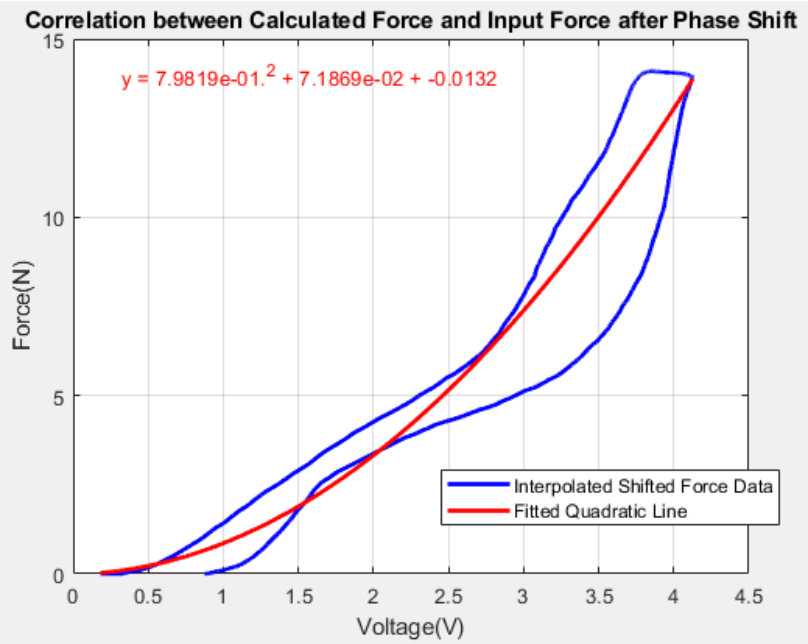

Fig. 64: The hysteresis curve visualizing the comparison between the calculated force and the best fit line used for the conversion during the pressing and releasing of the force sensor. The left most blue line indicates the resting position.

Middle analysis point

Figures 65-68 show the voltage response due to force input, the correlation between the voltage response and the force input in the Matlab system analysis toolbox for the best fit line characteristics, the comparison between the converted voltage and the reference force, and the force hysteresis curve for Z-directional testing at the middle analysis point respectively.

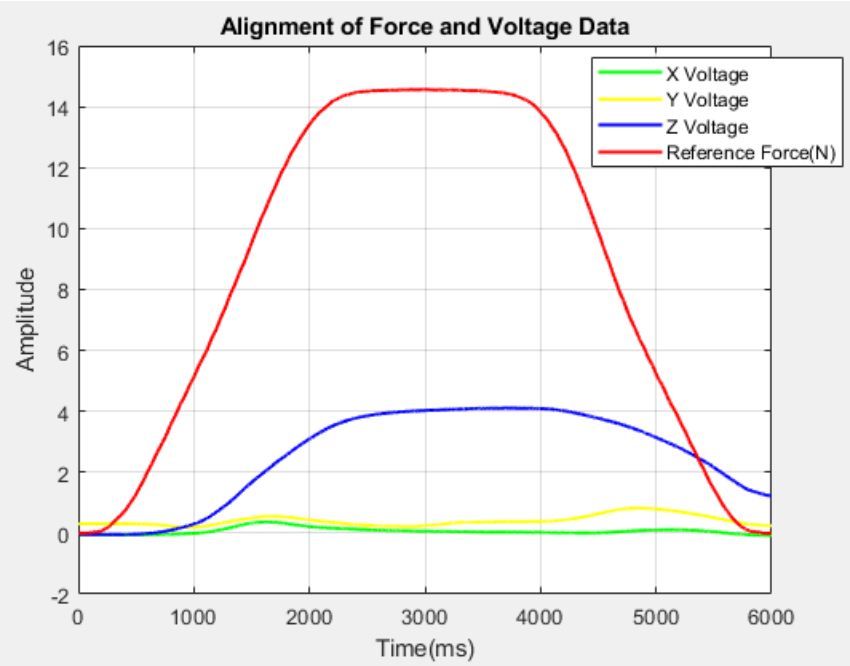

Fig. 65: The comparison between the reference force in red and the output voltages in the X, Y, and Z directions. The green line indicates the X resultant voltage, the yellow line indicates the Y resultant voltage, and the blue line indicates the Z resultant voltage.

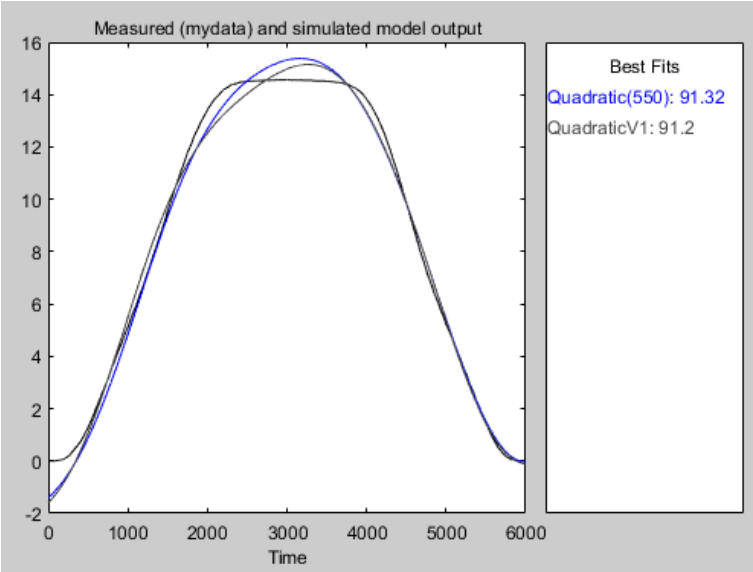

Fig. 66: The system analysis toolbox data report for the best fit line parameters. The resulting best fit line parameters were a quadratic line with a delay of 550.

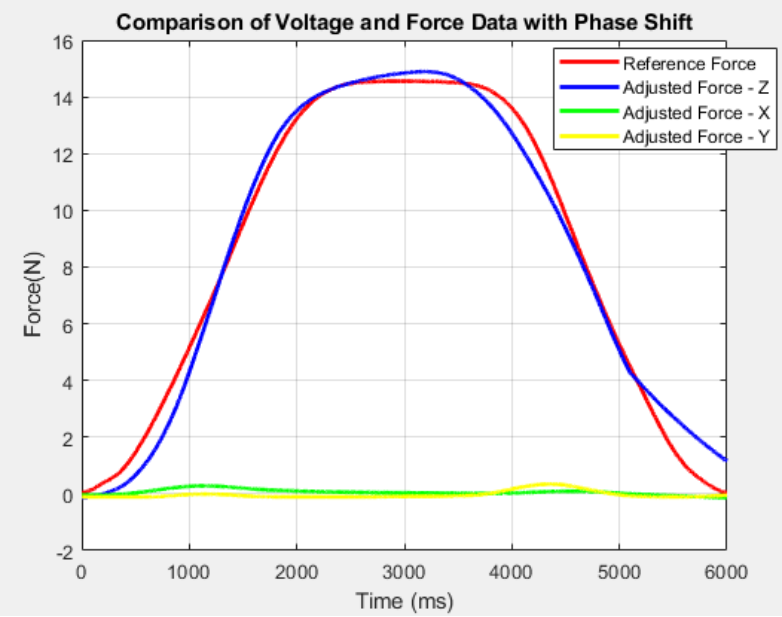

Fig. 67: The visualization of the voltage converted back to force and compared to the reference force. The red is the reference force, the green is the X-direction calculated force response, the yellow is the Y-direction calculated force response, and blue is the Z-directional calculated force response.

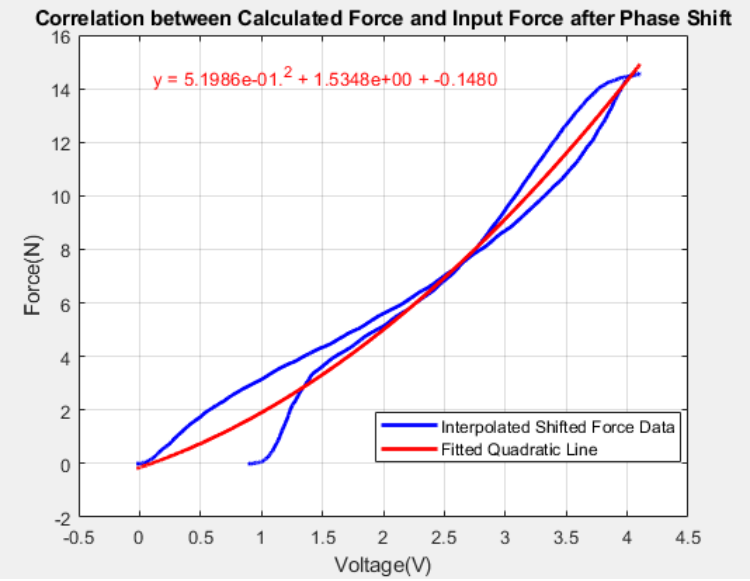

Fig. 68: The hysteresis curve visualizing the comparison between the calculated force and the best fit line used for the conversion during the pressing and releasing of the force sensor. The left most blue line indicates the resting position.

Back analysis point

Figures 69-72 show the voltage response due to force input, the correlation between the voltage response and the force input in the Matlab system analysis toolbox for the best fit line characteristics, the comparison between the converted voltage and the reference force, and the force hysteresis curve for Z-directional testing at the back analysis point respectively.

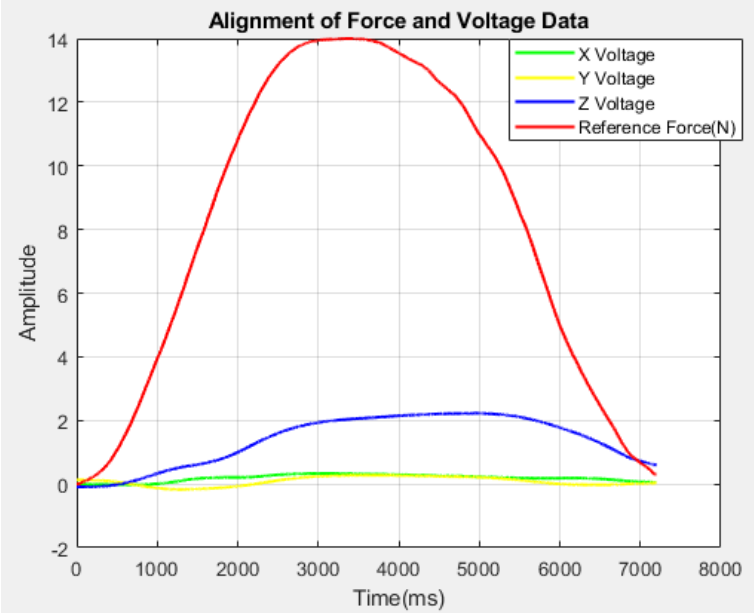

Fig. 69: The comparison between the reference force in red and the output voltages in the X, Y, and Z directions. The green line indicates the X resultant voltage, the yellow line indicates the Y resultant voltage, and the blue line indicates the Z resultant voltage.

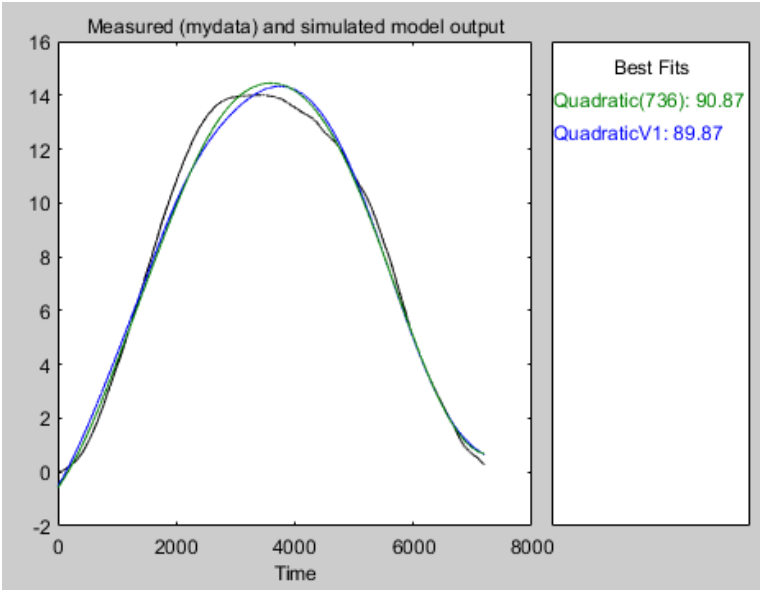

Fig. 70: The system analysis toolbox data report for the best fit line parameters. The resulting best fit line parameters were a quadratic line with a delay of 736.

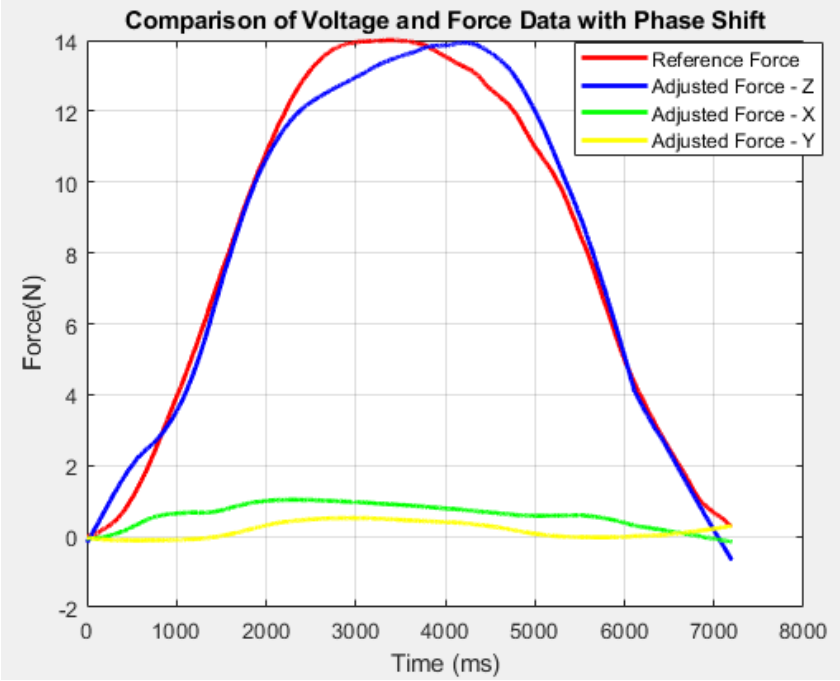

Fig. 71: The visualization of the voltage converted back to force and compared to the reference force. The red is the reference force, the green is the X-direction calculated force response, the yellow is the Y-direction calculated force response, and blue is the Z-directional calculated force response.

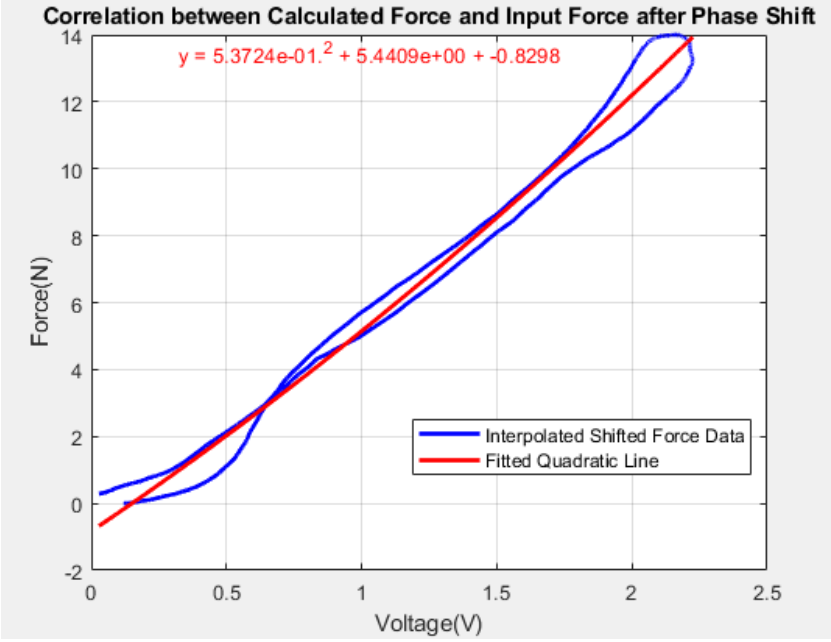

Fig. 72: The hysteresis curve visualizing the comparison between the calculated force and the best fit line used for the conversion during the pressing and releasing of the force sensor. The left most blue line indicates the resting position.

Data Summary

Summarizing this data, Table 4 demonstrates the equations used to convert the collected voltage back to force application for practical testing.

Table 4: The equations of each directional analyte collected during the theoretical testing of the first design to convert the output voltage back to force when testing practically. Y indicates the force calculated while X refers to the voltage collected from the pair of resistors that correlate to that direction.

Group of Sensors	Direction of Analysis	Equation
Front	X	$Y = 0.00016631 * X^3 – 0.0049283 * X^2 + 1.2484 * X + 0.2584$
	Y	$Y = -1.4379 * X^3 + 3.7131 * X^2 + 0.13609 * X + 0.0123$
	Z	$Y = 0.79819 * X^2 + 7.1869 * X – 0.0132$
Middle	X	$Y = -0.065227 * X^2 + 0.92249 * X + 0.0314$
	Y	$Y = 1.6473 * X^2 – 0.85318 * X + 0.2856$
	Z	$Y = 0.51986 * X^2 + 1.5348 * X – 0.148$
Back	X	$Y = 0.02432 * X^3 – 0.6128 * X^2 + 3.3121 * X – 0.483$
	Y	$Y = 0.15096 * X^3 – 0.70229 * X^2 +2.2686 * X + 0.0744$
	Z	$Y = 0.53724 * X^2 + 5.4409 * X – 0.8298$

Additionally, the error is tabulated in Table 5, summarizing the average error percentage over the working range of each force reading, the median error percentage of the dataset, the difference in maximum values between the calculated force and the reference force, the maximum error within the working range, and the maximum error value normalized across the dataset by dividing by the range of the dataset to indicate the variability of the data.

Table 5: The errors found at each analysis point in the insole system. The "modified" indication corresponds to analyzing the working range rather than the entirety of the dataset, as minimal force values between 0-0.5N proved to increase error of the system drastically.

Sensor Location	Average Error Percent (Modified)	Median Error Percent	Peak Difference Error Percent	Maximum Error Percent (Modified)	Maximum Error Percent (Normalized)
Front X	14.4559	31.7588	1.7994	76.6489	21.8897
Middle X	12.6048	3.2754	1.8179	113.6838	21.4498
Back X	7.241	5.7975	2.9877	41.7648	9.2811
Front Y	14.9224	3.5318	3.2083	87.9293	23.1393
Middle Y	8.4226	20.8717	1.6555	49.8107	15.3264
Back Y	12.7795	8.4389	5.7186	151.8581	43.3880
Front Z	10.9867	9.597	3.3581	34.3426	2.4530
Middle Z	5.112	4.4739	2.2981	73.2182	4.9808
Back Z	7.8559	5.9166	0.47967	81.5747	5.8268
Average	10.49	10.41	2.59	78.98	16.41

4.1.2 Practical Testing Results

For practical testing of design 1, the system was initially attached to the foot and tested by stepping and walking for two monitored steps: one short step and one large stride. However, the system was ultimately attached to the shoe, enabling consistent results and inspiring changes to the insole system used for designs two and three. Additionally, the structural integrity of the first design allowed for a shortened timeframe of practical testing, also contributing to changes to the second and third iteration of this research.

Stepping Results

Figures 73, 74, and 75 demonstrate the voltage responses from the front, middle, and back analysis locations while stepping on the insole system.

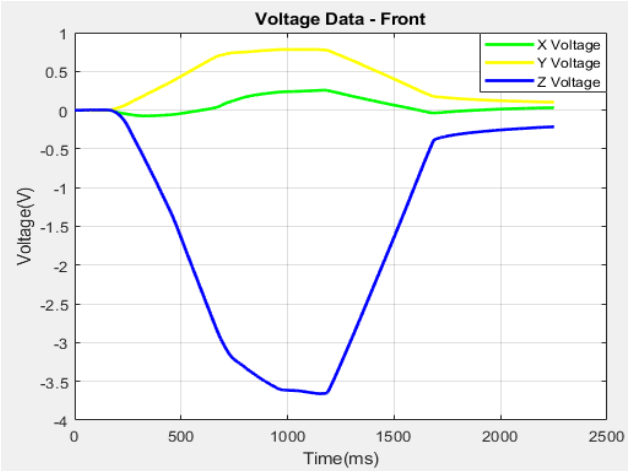

Fig. 73: The voltage output of each directional voltage collected at the front sensing location for the first insole design.

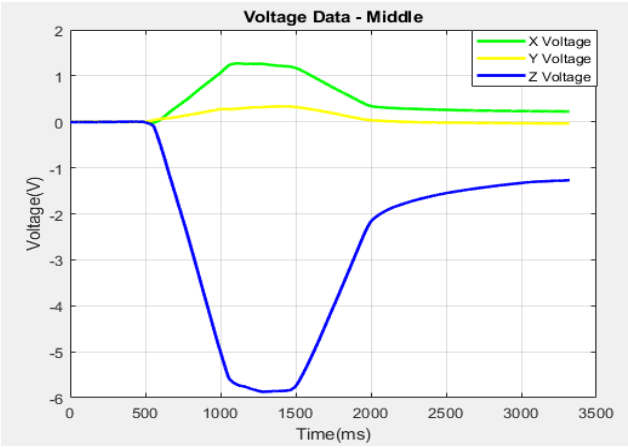

Fig. 74: The voltage output of each directional voltage collected at the middle sensing location for the first insole design.

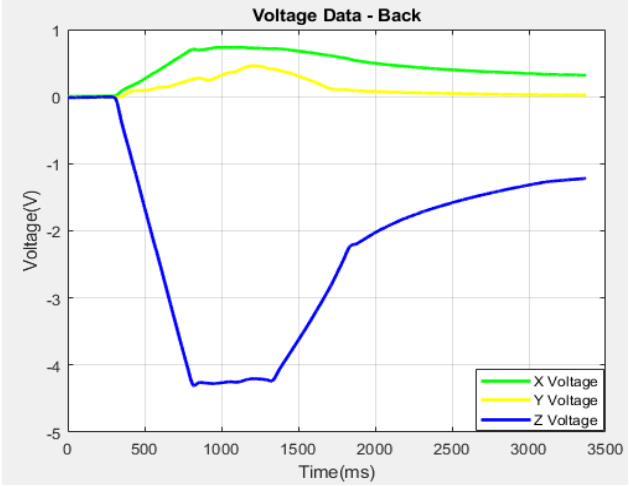

Fig. 75: The voltage output of each directional voltage collected at the back sensing location for the first insole design.

With these voltages, the respective line equations collected from experimental testing were used to convert the voltage values to force values at each analysis point, displayed in Figures 76, 77, and 78.

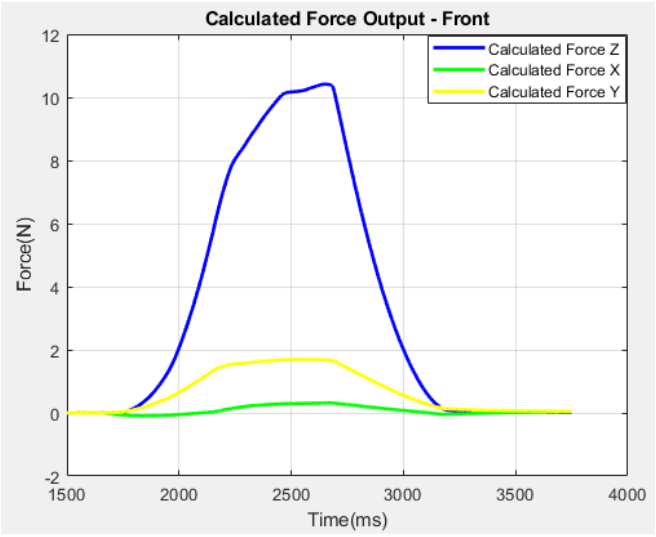

Fig. 76: The voltage data from the front sensing location converted back to force using the force curve calculations from experimental testing.

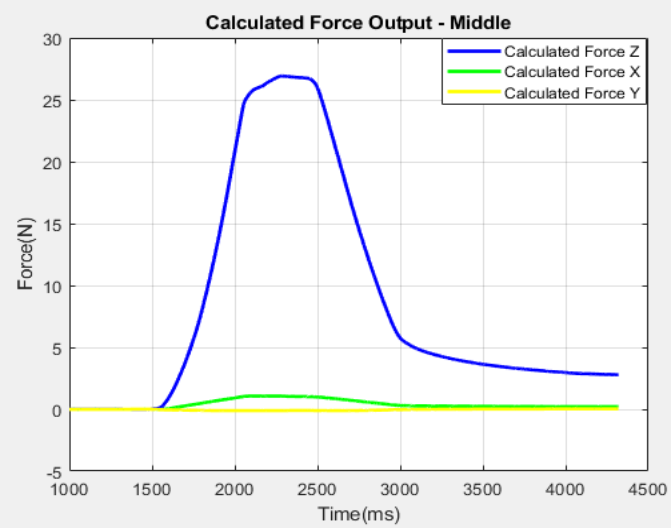

Fig. 77: The voltage data from the middle sensing location converted back to force using the force curve calculations from experimental testing.

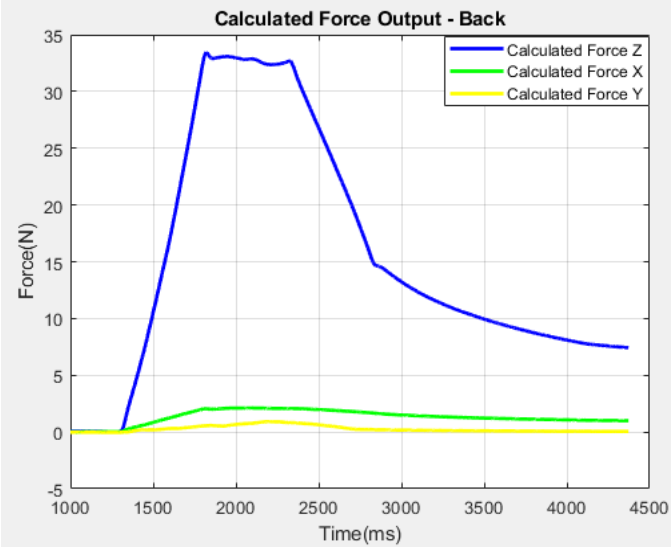

Fig. 78: This is the voltage data from the back sensing location converted back to force using the force curve calculations from experimental testing.

Walking Results

The system was then tested by starting the data collection, attaching the insole system to the shoe, and taking two variably distanced steps. Figures 79, 80, and 81 demonstrate the voltage responses from each analysis point throughout the two steps.

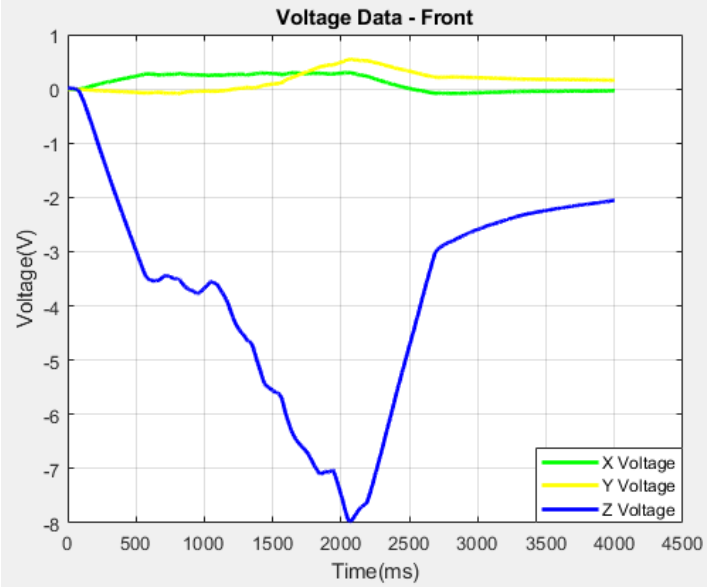

Fig. 79: The voltage output of each directional voltage collected at the front sensing location for the first insole design while walking with the device worn.

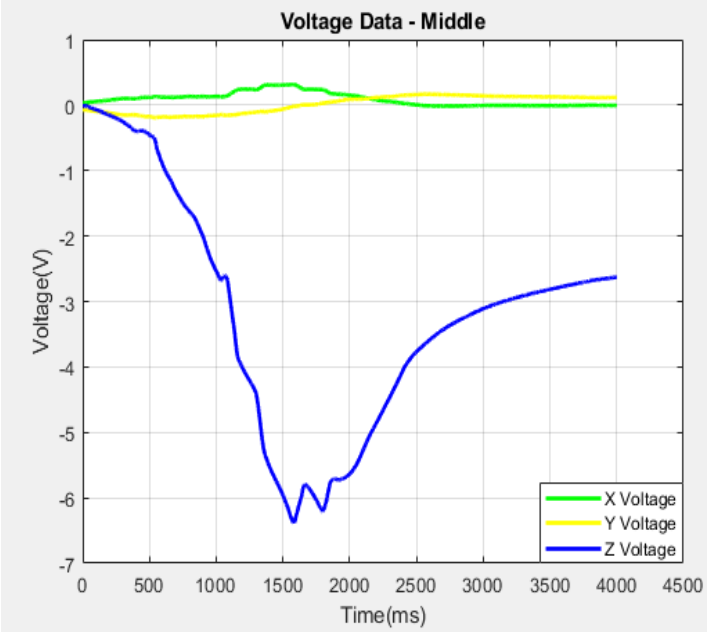

Fig. 80: The voltage output of each directional voltage collected at the middle sensing location for the first insole design while walking with the device worn.

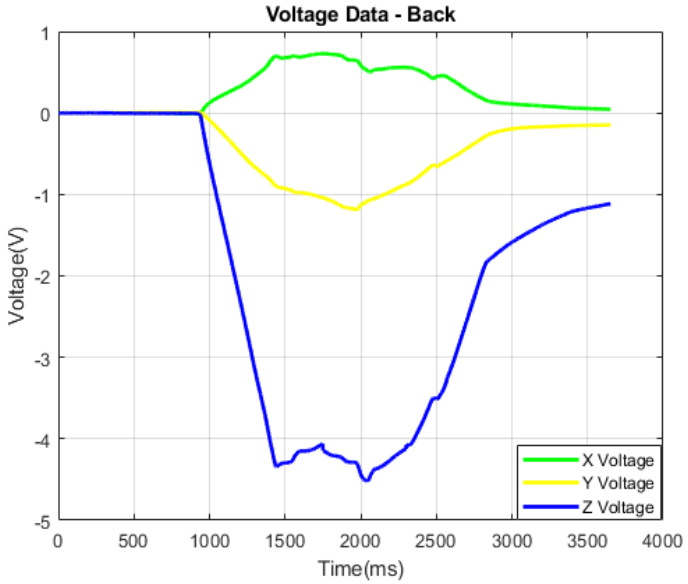

Fig. 81: The voltage output of each directional voltage collected at the back sensing location for the first insole design while walking with the device worn.

Once again, the collected voltage conversion equations collected during the experimental testing were applied to the voltage to convert back to force values. Figures 82, 83, and 84 indicate the force values collected at each analysis point while walking on the insole system.

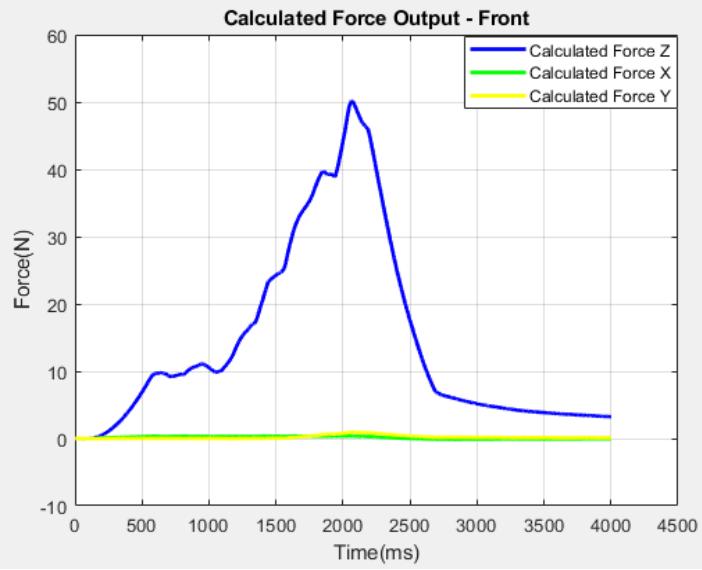

Fig. 82: The voltage data from the front sensing location converted back to force using the force curve calculations from experimental testing during practical testing while walking with the device worn.

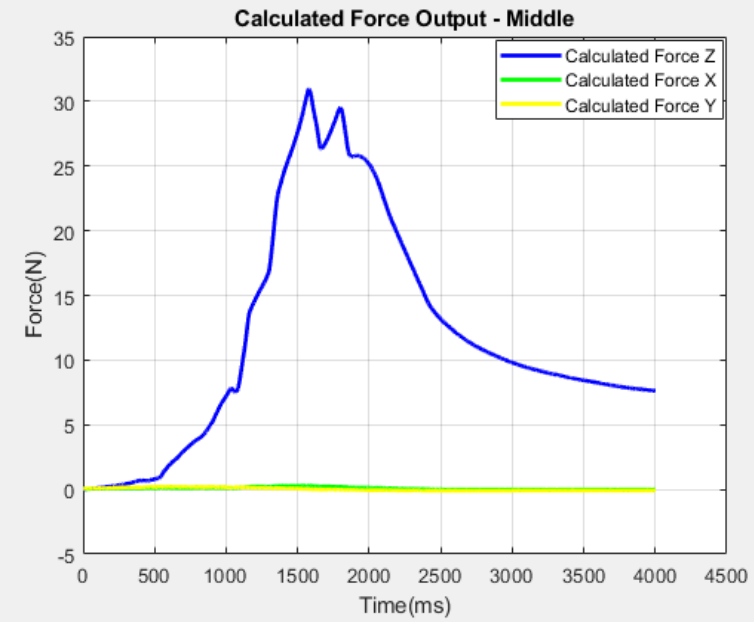

Fig. 83: The voltage data from the middle sensing location converted back to force using the force curve calculations from experimental testing during practical testing while walking with the device worn.

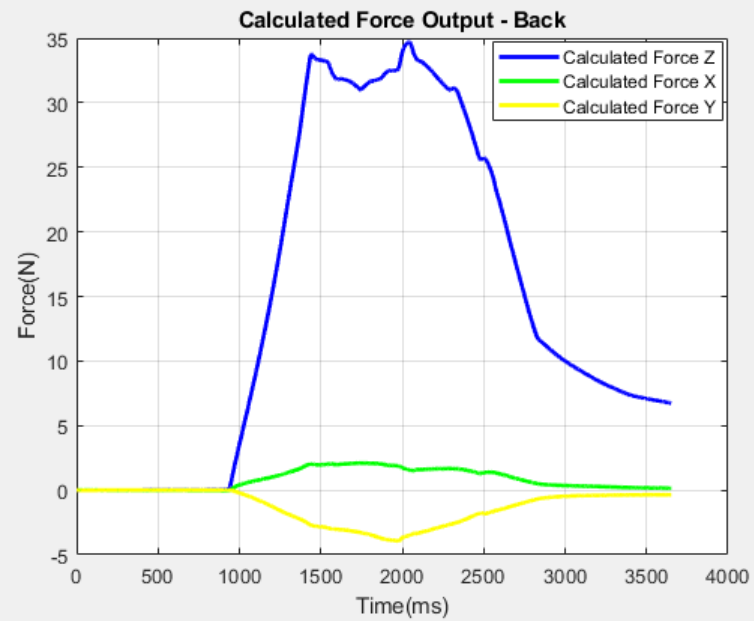

Fig. 84: The voltage data from the back sensing location converted back to force using the force curve calculations from experimental testing during practical testing while walking with the device worn.

From here, the second insole design was tested, first experimentally like the first design and then practically.

4.2 Design Two

Design two implemented sensors that were manually reduced in sensitivity by applying a thin film of silver conductive epoxy adhesive directly to the conductive ink found on the sensors. In doing so, the functional range and sensitivity of the bend sensors were reduced, but ensured that Z-direction force resulted in an increase in top sensor resistance and a decrease in bottom sensor resistance. The second design is displayed in Figure 85.

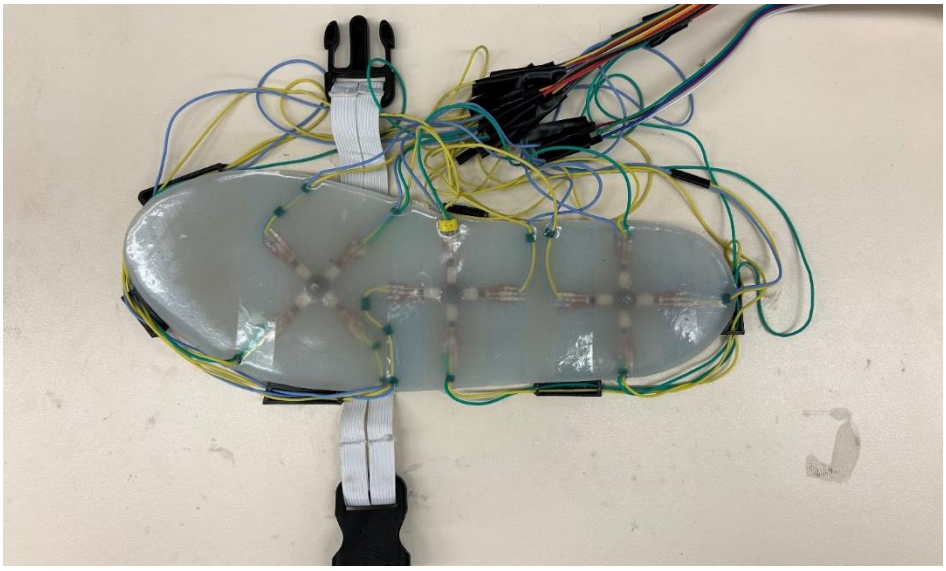

Fig. 85: The second insole design utilized for this research, incorporating sensors with reduced sensitivity.

The following sections will provide visual aids in the following order: the voltage response of relevant directions while application of force, the system analysis toolbox best fit line parameter analysis, the converted force calculation from the relevant voltage response directions compared to the reference force, and the hysteresis curve comparing the calculated force and the deviation from the best fit line.

Of note, the back sensor location results did not exhibit any change in voltage at values less than 5N for the experimental testing. However, the back sensor location did exhibit voltage response when practically tested.

4.2.1 Validation Results

X-Direction Results

Front analysis point

Figures 86-89 show the voltage response due to force input, the correlation between the voltage response and the force input in the Matlab system analysis toolbox for the best fit line characteristics, the comparison between the converted voltage and the reference force, and the force hysteresis curve for X-directional testing at the front analysis point respectively.

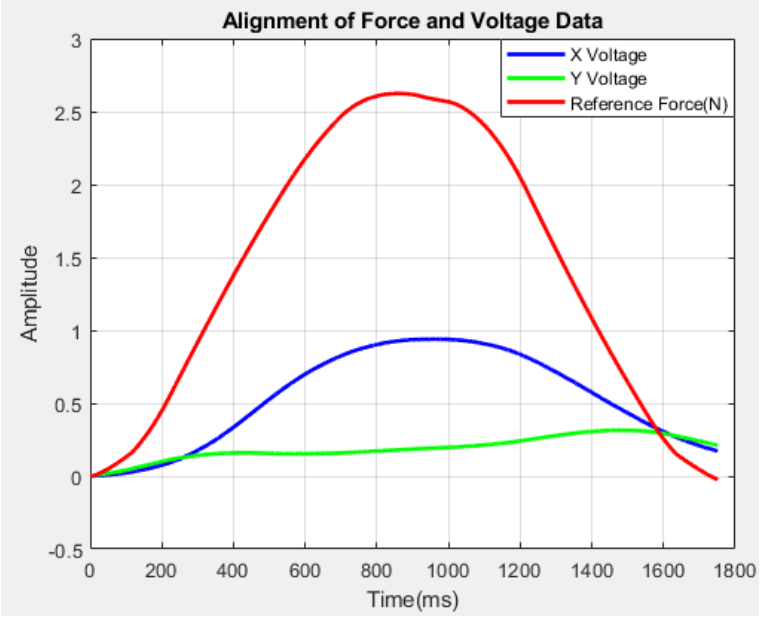

Fig. 86: The comparison between the reference force in red and the output voltages in the X and Y directions. The green line indicates the Y resultant voltage and the blue line indicates the X resultant voltage.

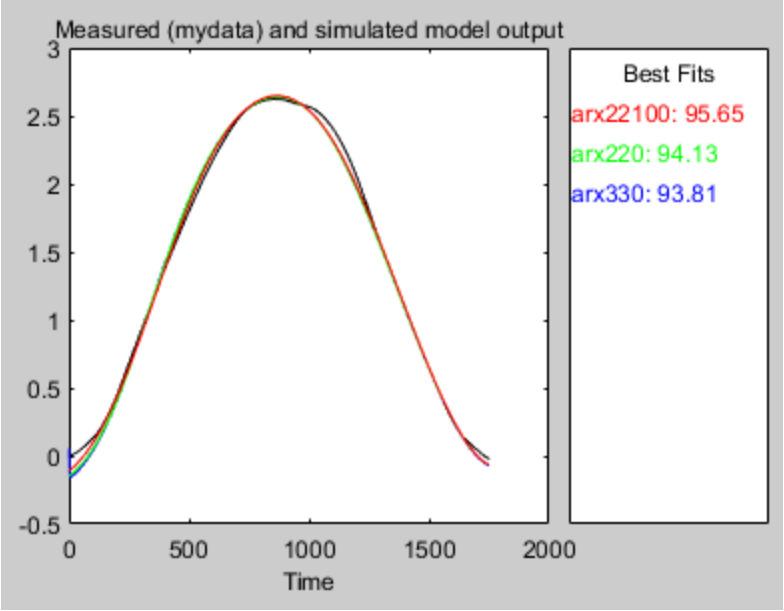

Fig. 87: The system analysis toolbox data report for the best fit line parameters. The resulting best fit line parameters were a quadratic line with a delay of 100.

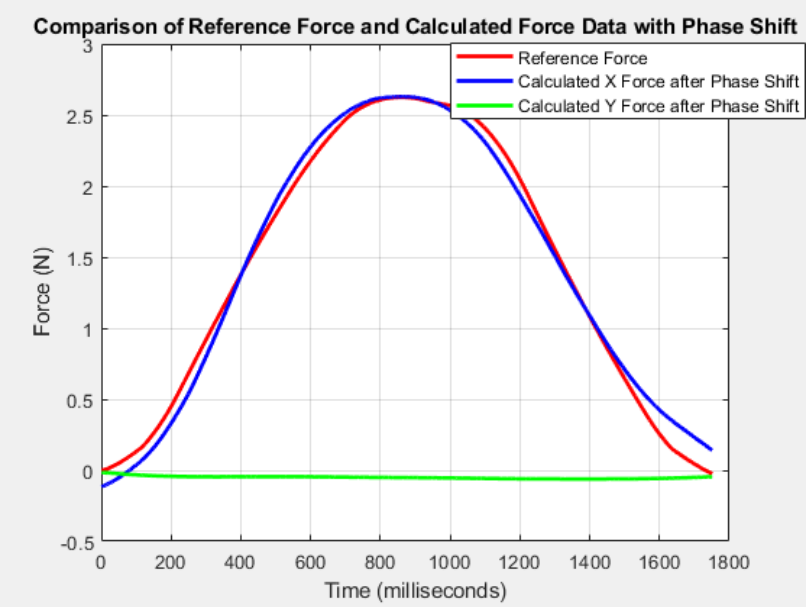

Fig. 88: The comparison between the reference force in red and the calculated forces for the X and Y directions. The blue line indicates the calculated X-directional force and the green line indicates the Y-directional force.

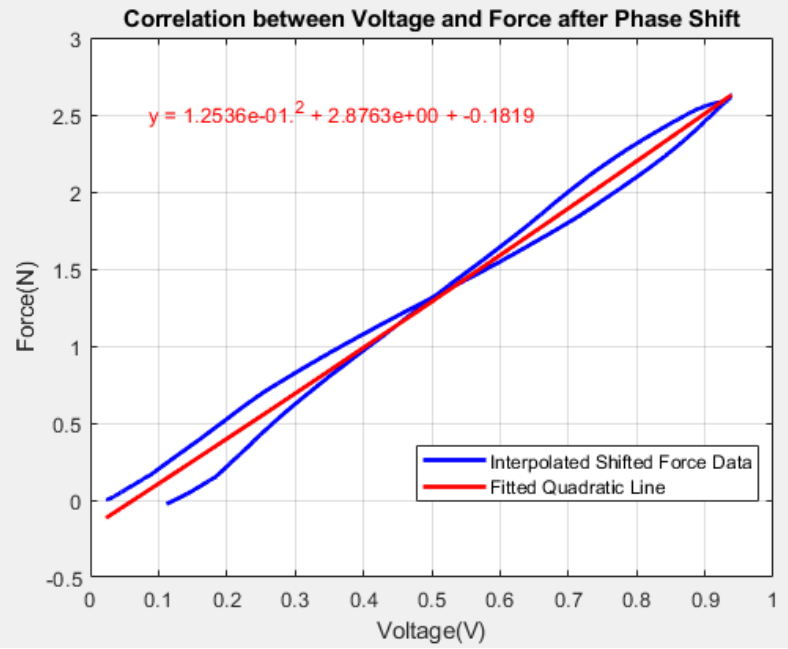

Fig. 89: The hysteresis curve visualizing the comparison between the calculated force and the best fit line used for the conversion during the pressing and releasing of the force sensor. The left most blue line indicates the resting position.

Middle analysis point

Figures 90-93 show the voltage response due to force input, the correlation between the voltage response and the force input in the Matlab system analysis toolbox for the best fit line characteristics, the comparison between the converted voltage and the reference force, and the force hysteresis curve for X-directional testing at the middle analysis point respectively.

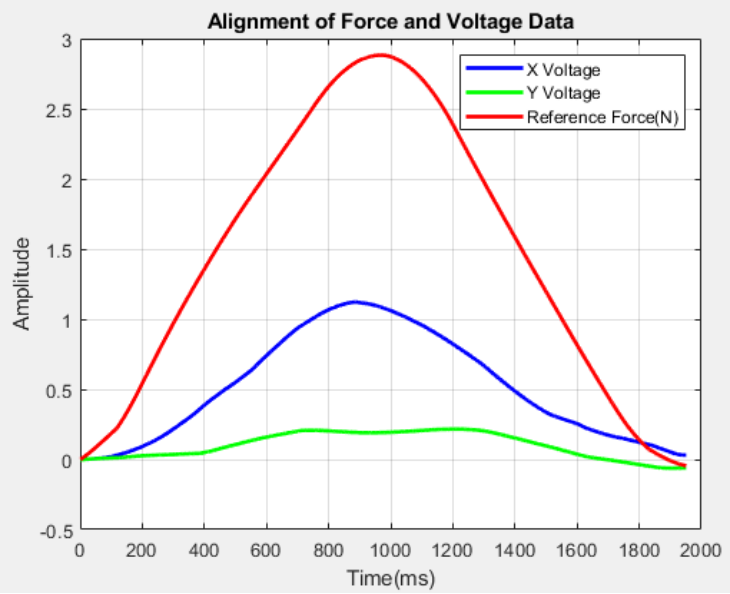

Fig. 90: The comparison between the reference force in red and the output voltages in the X and Y directions. The green line indicates the Y resultant voltage and the blue line indicates the X resultant voltage.

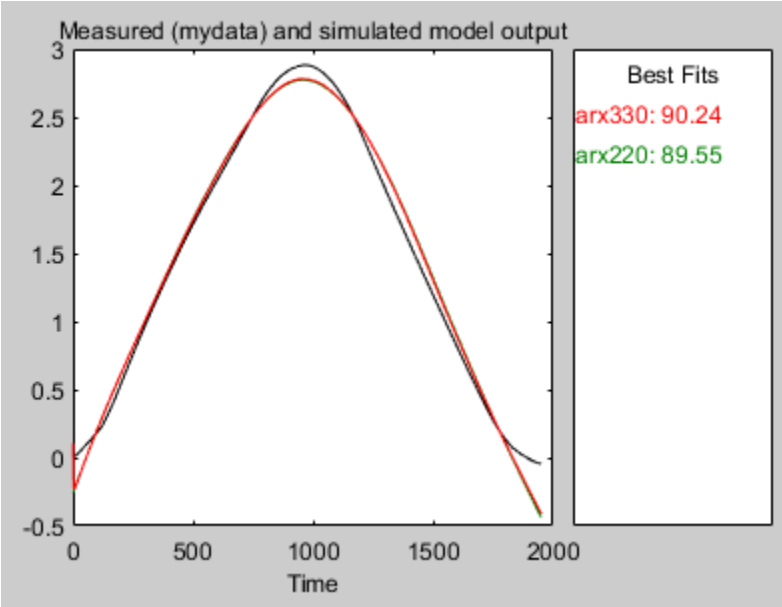

Fig. 91: The system analysis toolbox data report for the best fit line parameters. The resulting best fit line parameters were a cubic line with no delay.

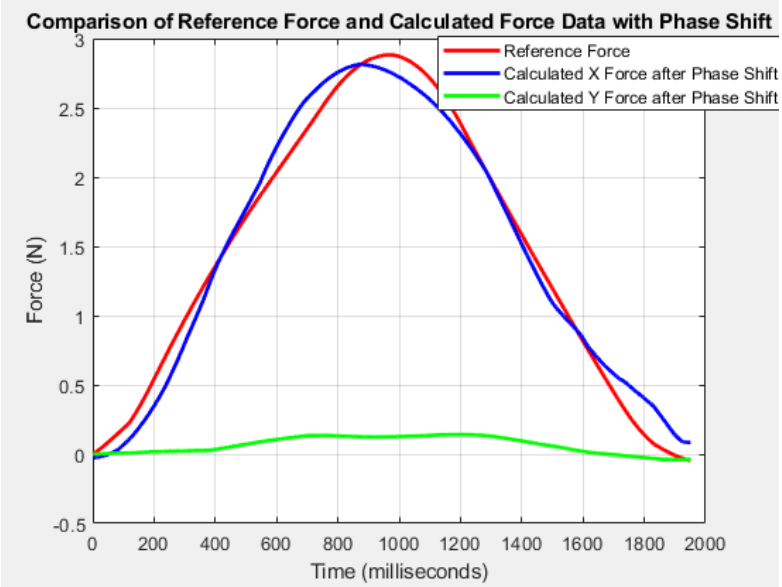

Fig. 92: The comparison between the reference force in red and the calculated forces for the X and Y directions. The blue line indicates the calculated X-directional force and the green line indicates the Y-directional force.

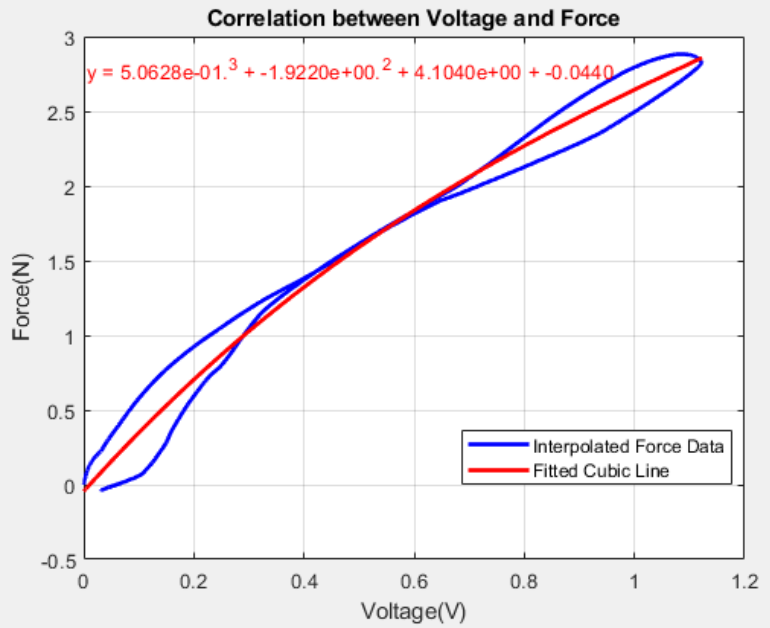

Fig. 93: The hysteresis curve visualizing the comparison between the calculated force and the best fit line used for the conversion during the pressing and releasing of the force sensor. The left most blue line indicates the resting position.

Y-Direction Results

Front analysis point

Figures 94-97 show the voltage response due to force input, the correlation between the voltage response and the force input in the Matlab system analysis toolbox for the best fit line characteristics, the comparison between the converted voltage and the reference force, and the force hysteresis curve for Y-directional testing at the front analysis point respectively.

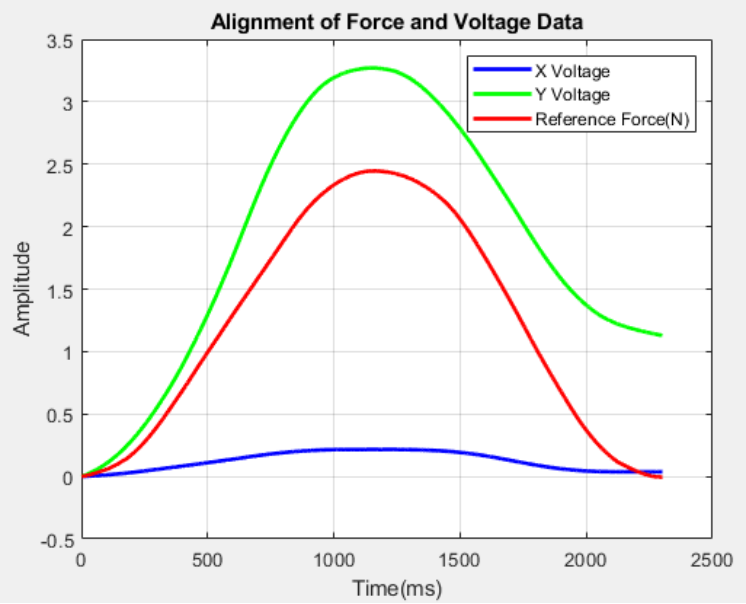

Fig. 94: The comparison between the reference force in red and the output voltages in the X and Y directions. The green line indicates the Y resultant voltage and the blue line indicates the X resultant voltage.

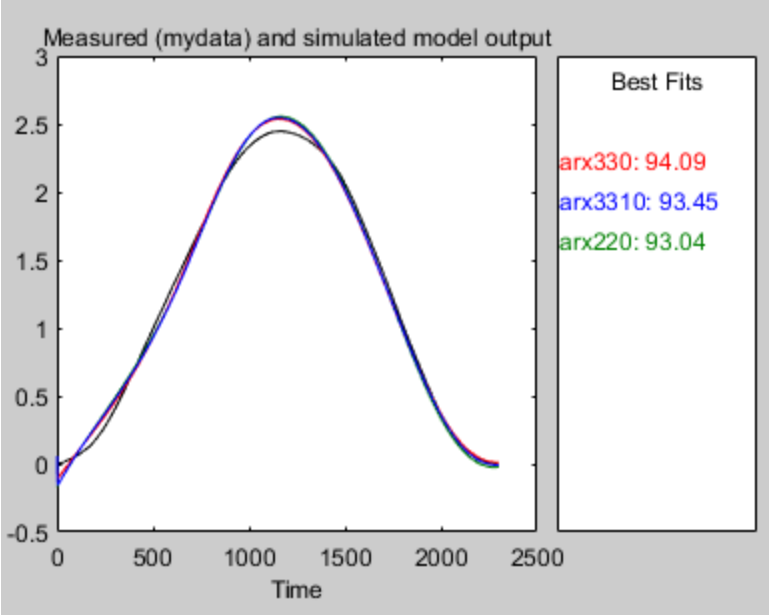

Fig. 95: The system analysis toolbox data report for the best fit line parameters. The resulting best fit line parameters were a cubic line with no delay.

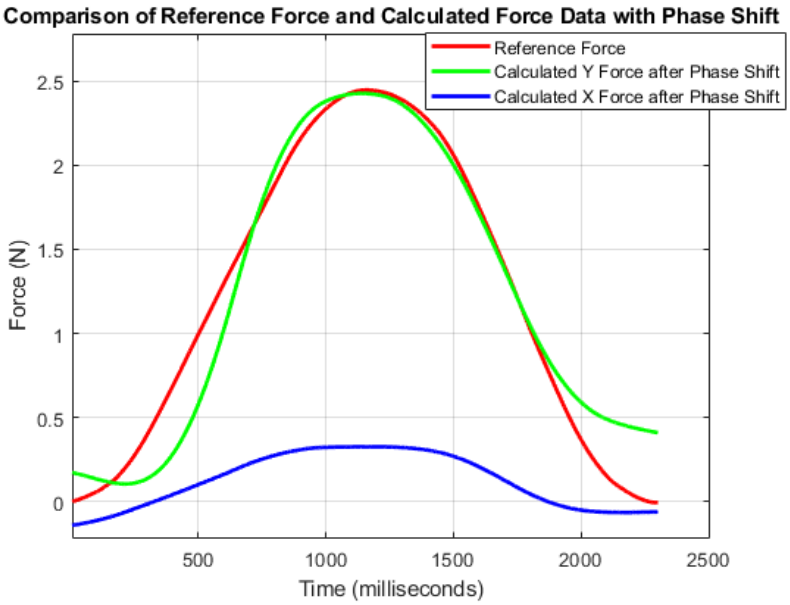

Fig. 96: The comparison between the reference force in red and the calculated forces for the X and Y directions. The green line indicates the calculated Y-directional force and the blue line indicates the X-directional force.

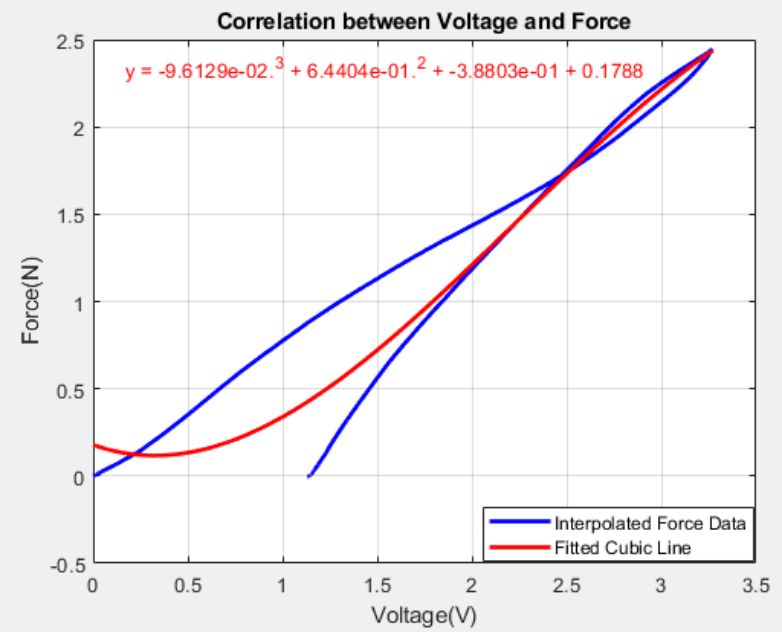

Fig. 97: The hysteresis curve visualizing the comparison between the calculated force and the best fit line used for the conversion during the pressing and releasing of the force sensor. The left most blue line indicates the resting position.

Middle analysis point

Figures 98-101 show the voltage response due to force input, the correlation between the voltage response and the force input in the Matlab system analysis toolbox for the best fit line characteristics, the comparison between the converted voltage and the reference force, and the force hysteresis curve for Y-directional testing at the middle analysis point respectively.

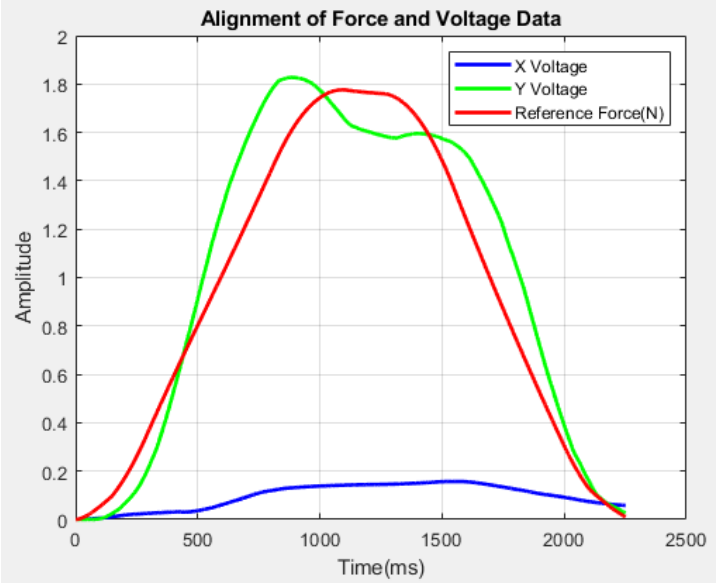

Fig. 98: The comparison between the reference force in red and the output voltages in the X and Y directions. The green line indicates the Y resultant voltage and the blue line indicates the X resultant voltage.

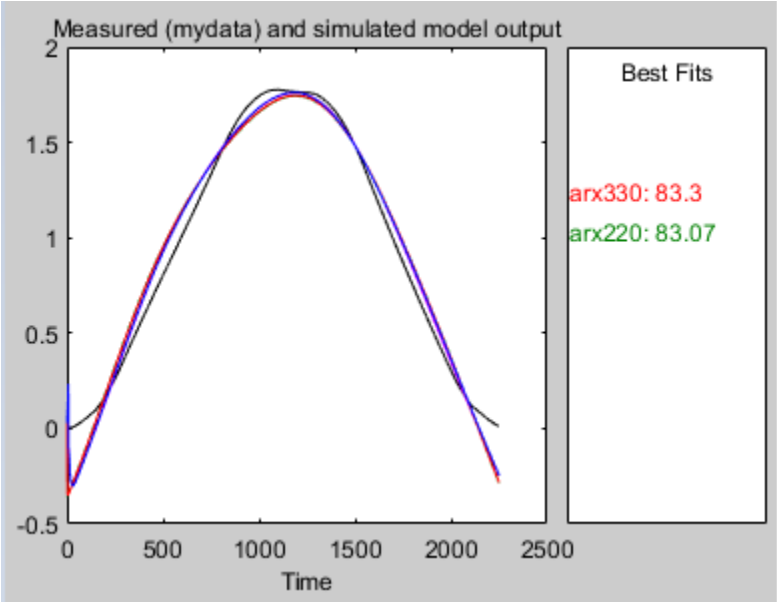

Fig. 99: The system analysis toolbox data report for the best fit line parameters. The resulting best fit line parameters were a cubic line with no delay.

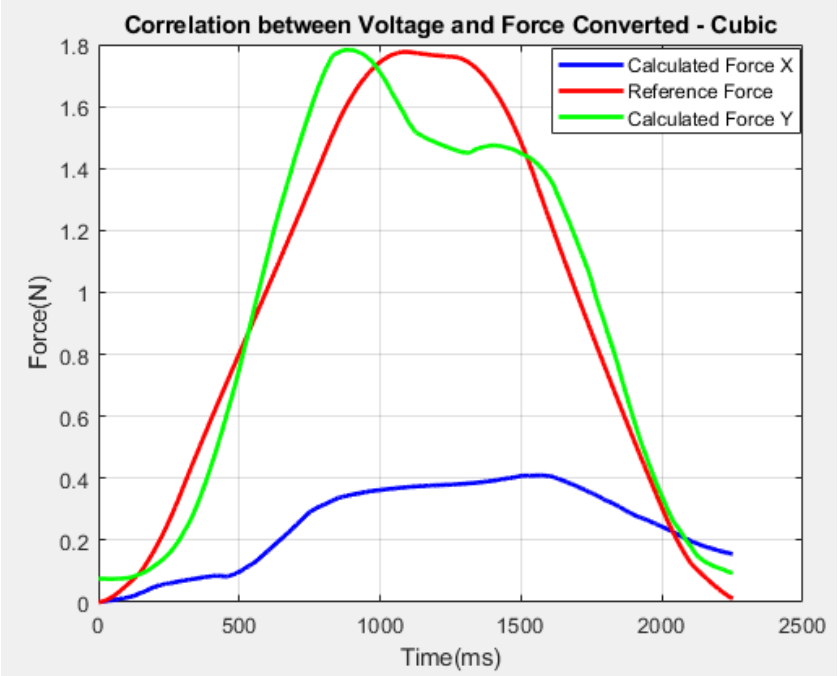

Fig. 100: The comparison between the reference force in red and the calculated forces for the X and Y directions. The green line indicates the calculated Y-directional force and the blue line indicates the X-directional force.

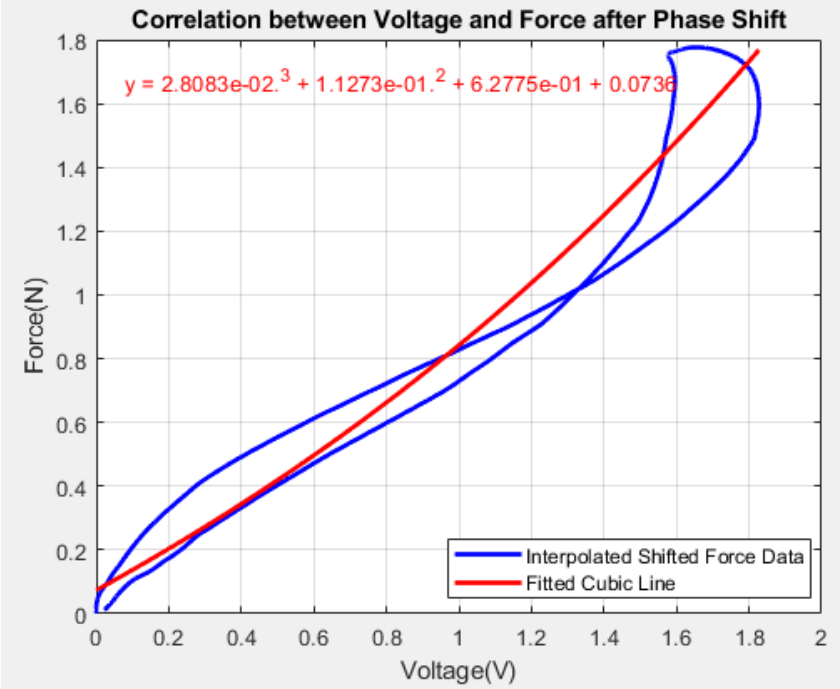

Fig. 101: The hysteresis curve visualizing the comparison between the calculated force and the best fit line used for the conversion during the pressing and releasing of the force sensor. The left most blue line indicates the resting position.

Z-Direction Results

Front analysis point

Figures 102-105 show the voltage response due to force input, the correlation between the voltage response and the force input in the Matlab system analysis toolbox for the best fit line characteristics, the comparison between the converted voltage and the reference force, and the force hysteresis curve for Z-directional testing at the front analysis point respectively.

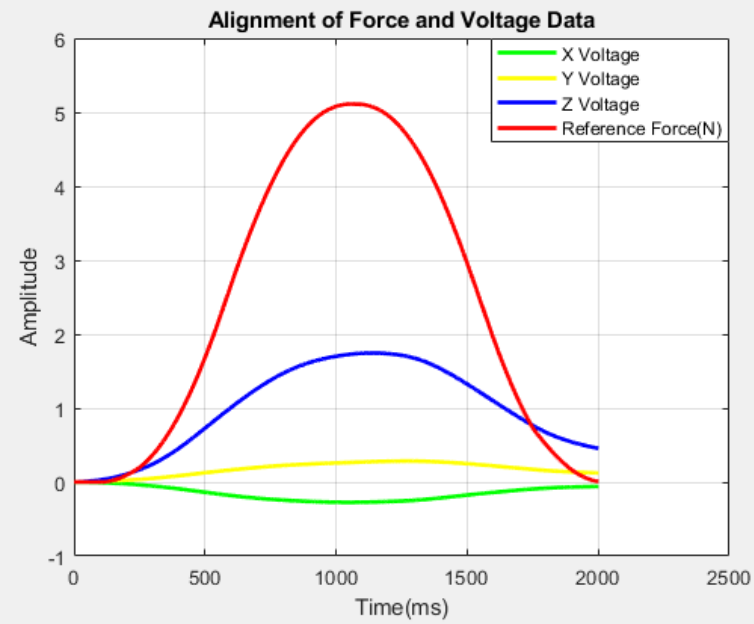

Fig. 102: The comparison between the reference force in red and the output voltages in the X, Y, and Z directions. The green line indicates the X resultant voltage, the yellow line indicates the Y resultant voltage, and the blue line indicates the Z resultant voltage.

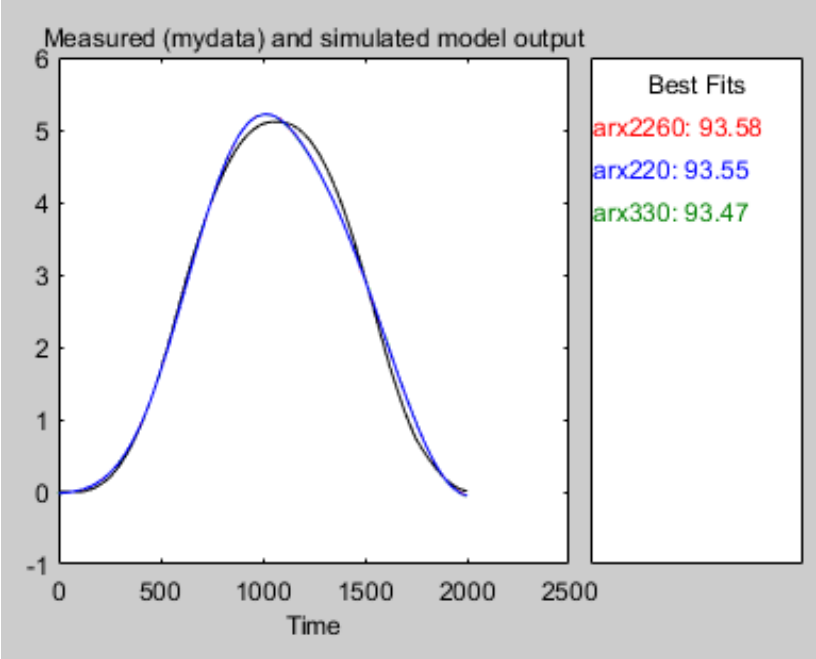

Fig. 103: The system analysis toolbox data report for the best fit line parameters. The resulting best fit line parameters were a quadratic line with a delay of 60.

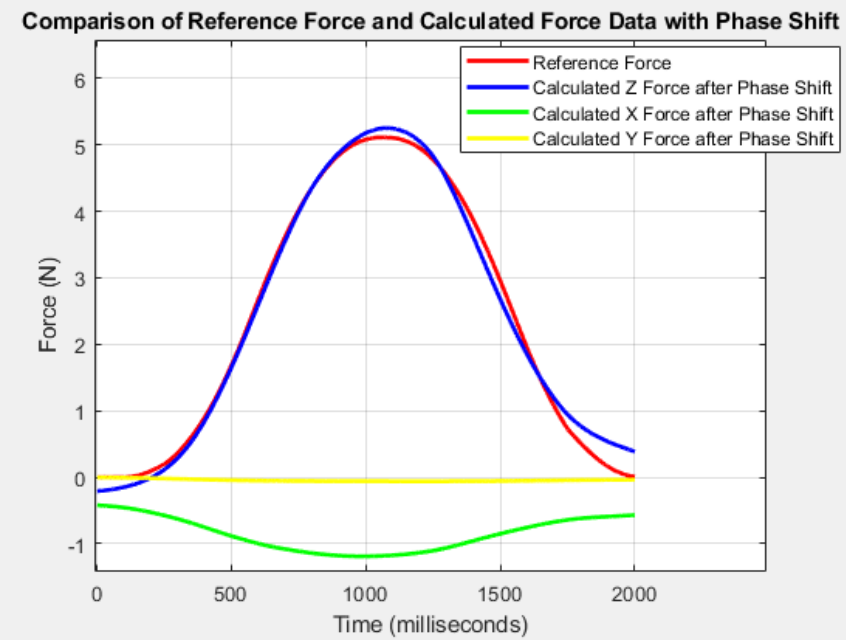

Fig. 104: The visualization of the voltage converted back to force and compared to the reference force. The red is the reference force, the green is the X-direction calculated force response, the yellow is the Y-direction calculated force response, and blue is the Z-directional calculated force response.

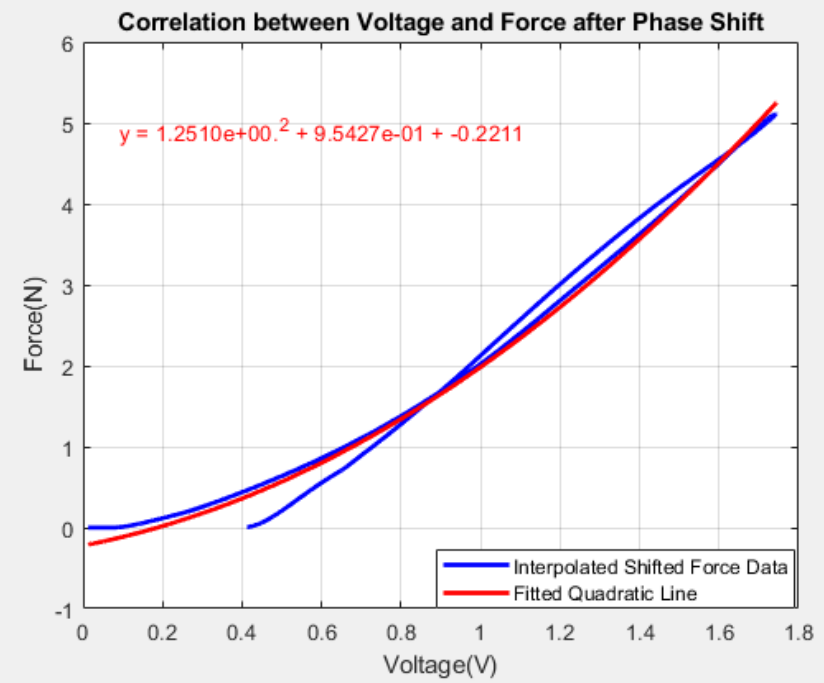

Fig. 105: The hysteresis curve visualizing the comparison between the calculated force and the best fit line used for the conversion during the pressing and releasing of the force sensor. The left most blue line indicates the resting position.

Middle analysis point

Figures 106-109 show the voltage response due to force input, the correlation between the voltage response and the force input in the Matlab system analysis toolbox for the best fit line characteristics, the comparison between the converted voltage and the reference force, and the force hysteresis curve for Z-directional testing at the middle analysis point respectively.

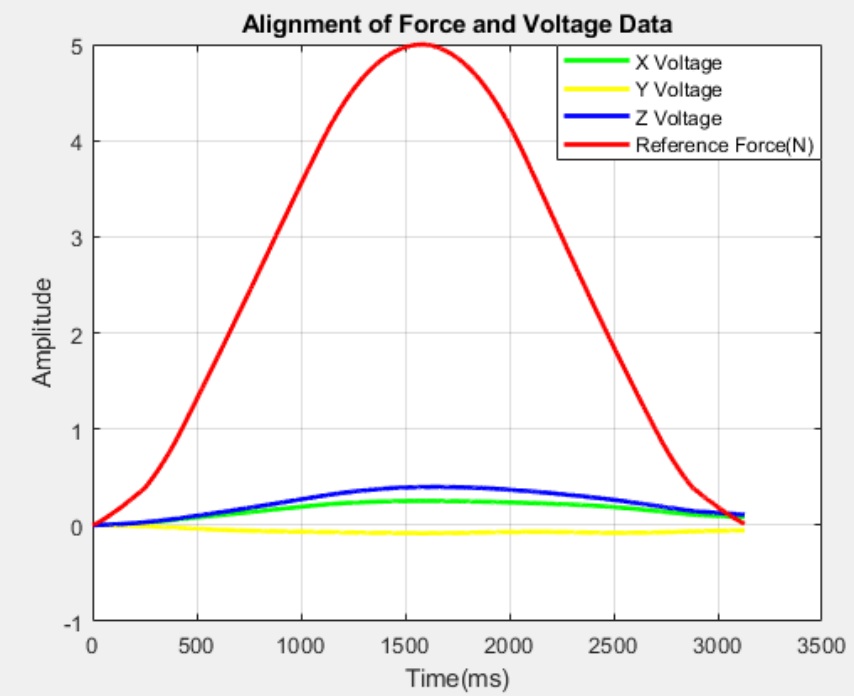

Fig. 106: The comparison between the reference force in red and the output voltages in the X, Y, and Z directions. The green line indicates the X resultant voltage, the yellow line indicates the Y resultant voltage, and the blue line indicates the Z resultant voltage.

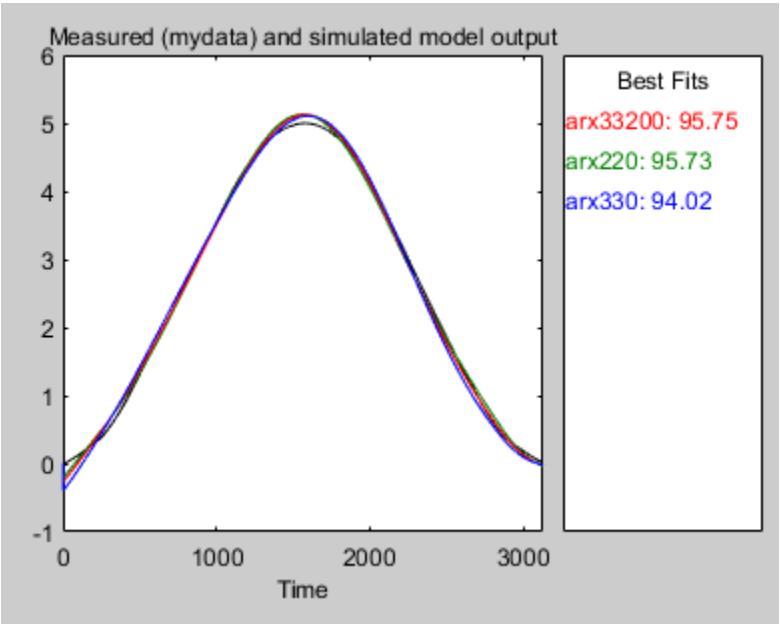

Fig. 107: The system analysis toolbox data report for the best fit line parameters. The resulting best fit line parameters were a cubic line with a delay of 200.

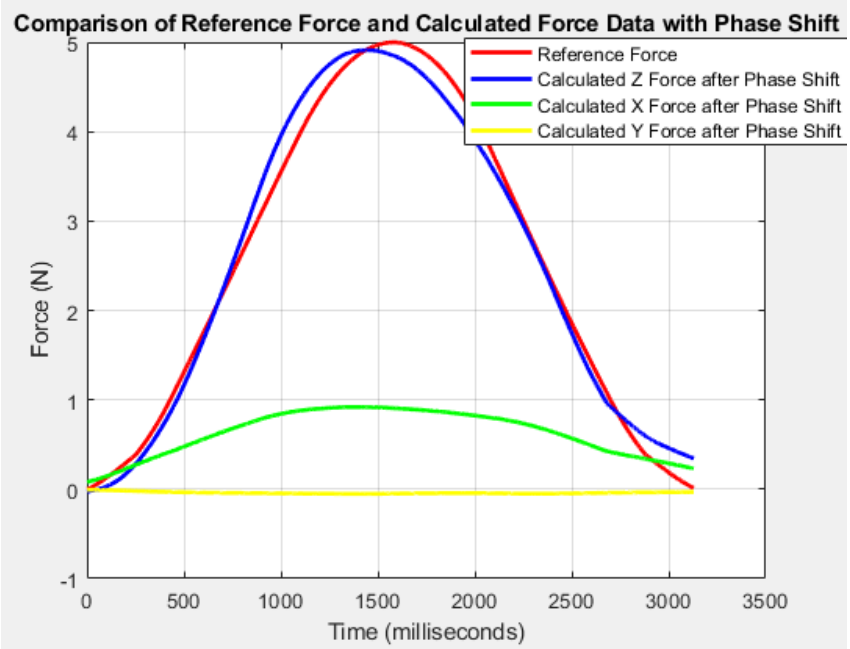

Fig. 108: The visualization of the voltage converted back to force and compared to the reference force. The red is the reference force, the green is the X-direction calculated force response, the yellow is the Y-direction calculated force response, and blue is the Z-directional calculated force response.

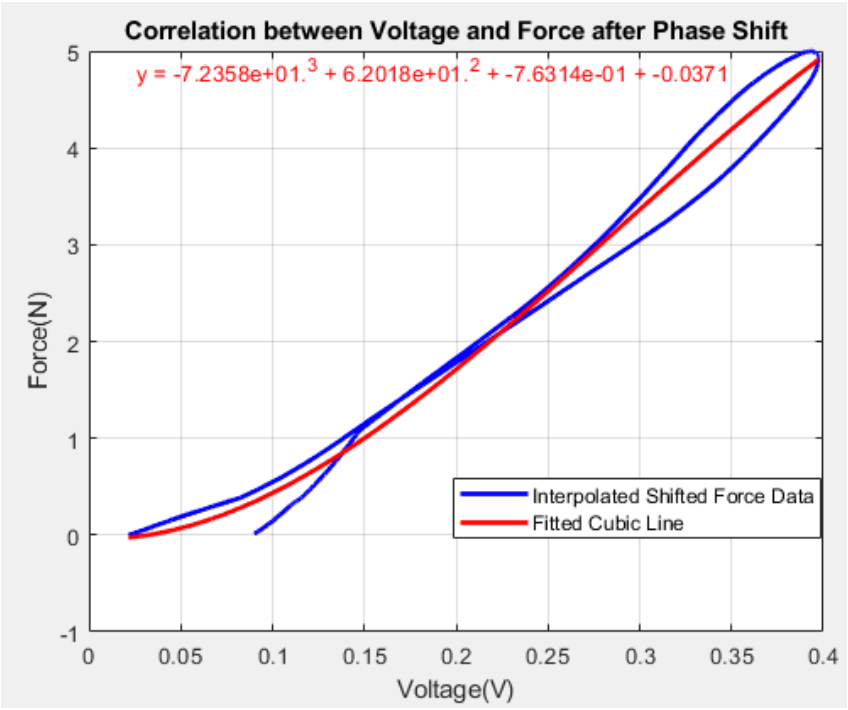

Fig. 109: The hysteresis curve visualizing the comparison between the calculated force and the best fit line used for the conversion during the pressing and releasing of the force sensor. The left most blue line indicates the resting position.

Data Summary

The error is tabulated in Table 6, summarizing the average error percentage over the working range of each force reading, the median error percentage of the dataset, the difference in maximum values between the calculated force and the reference force, the maximum error within the working range, and the maximum error value normalized across the dataset by dividing by the range of the dataset to indicate the variability of the data.

Table 6: The error metrics comparing the calculated force from the voltage output and the reference force input. The "modified" indication correlates to the calculations within the working range of the system for values greater than 0.5 N. The back analysis location did not exhibit change within the experimental testing range.

	Average Error Percent (Modified)	Median Percent Error	Peak Difference Error Percent	Maximum Error Percent (Modified)	Max Error Percent (Normalized)
Front X	5.246	4.6545	0.19005	47.0057	17.7526
Middle X	5.0603	5.3291	0.87577	37.4172	12.7819
Back X	N/A	N/A	N/A	N/A	N/A
Front Y	9.481	8.6059	3.56	35.8582	14.6281
Middle Y	11.6642	15.2347	4.3305	20.5689	11.5801
Back Y	N/A	N/A	N/A	N/A	N/A
Front Z	5.3142	3.0729	0.34974	57.2436	11.1982
Middle Z	6.5225	6.4552	1.7386	26.7658	5.3535
Back Z	N/A	N/A	N/A	N/A	N/A
Average	7.21	7.23	1.84	37.48	12.22

4.2.2 Practical Testing Results

After experimental testing to find the best fit line equations for each direction at each analysis point, the insole system was tested practically by attaching directly to the foot. Once attached, the system was tested with multiple gait methods, including

standing, walking on a flat surface, walking uphill, walking downhill, sidestepping left to right, and sidestepping right to left. All tests were conducted multiple times to research repeatability of output trends.

Concurrently, the gait methods were also tested visually with marker analysis. Visual analysis allowed for identification of different phases during each gait method utilized during the practical testing.

Standing

First, the system was tested by attaching the insole to the foot while seated. Then, from a seated position, the user stood up for several second, and sat back down, demonstrated in Figure 110.

Fig. 110: A demonstration of the user wearing the device from a seated position and standing on the device, collecting resultant voltage at all analysis points.

The resulting voltage was collected, displayed in Figures 111-113 for the front analysis point tests, Figures 114-116 for the middle analysis point tests, and Figures 117-119 for the back analysis point tests.

Front analysis point

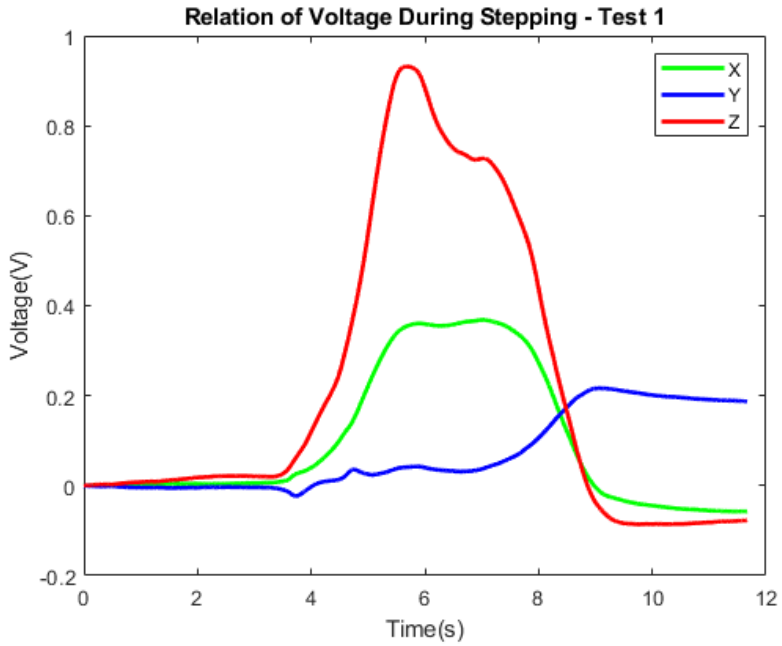

Fig. 111: The resulting voltages of the front system analysis point during practical testing during the first test of standing with the insole system.

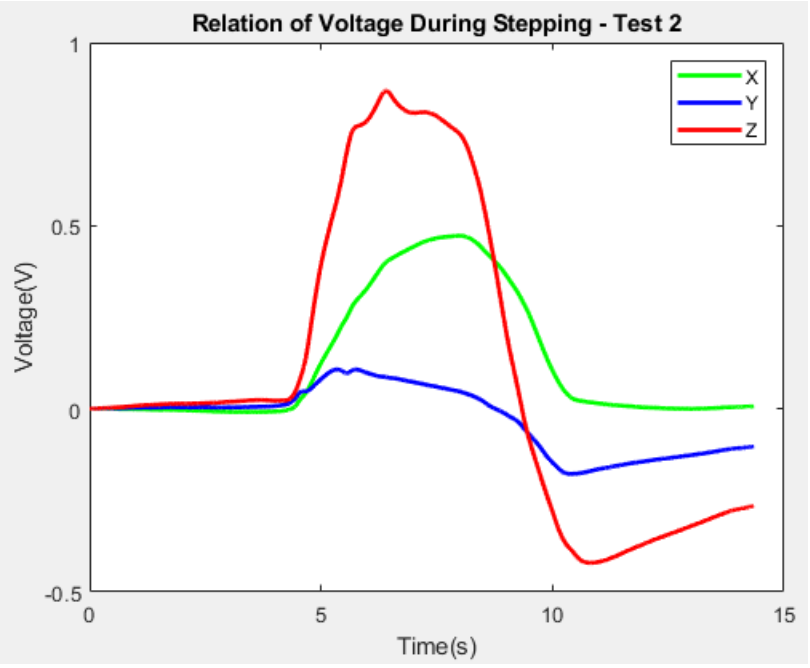

Fig. 112: The resulting voltages of the front system analysis point during practical testing during the second test of standing with the insole system.

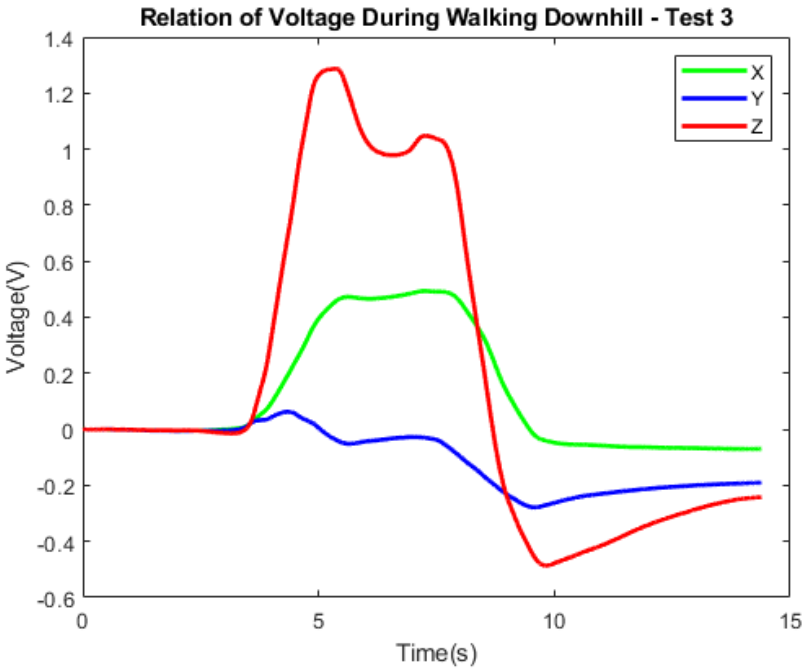

Fig. 113: The resulting voltages of the front system analysis point during practical testing during the first test of standing with the insole system.

Middle analysis point

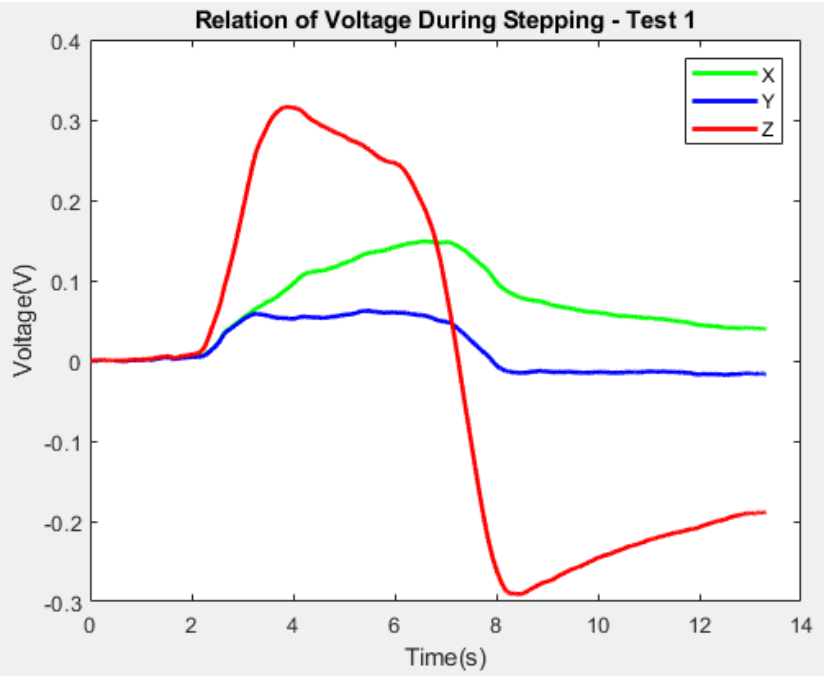

Fig. 114: The resulting voltages of the middle system analysis point during practical testing during the first test of standing with the insole system.

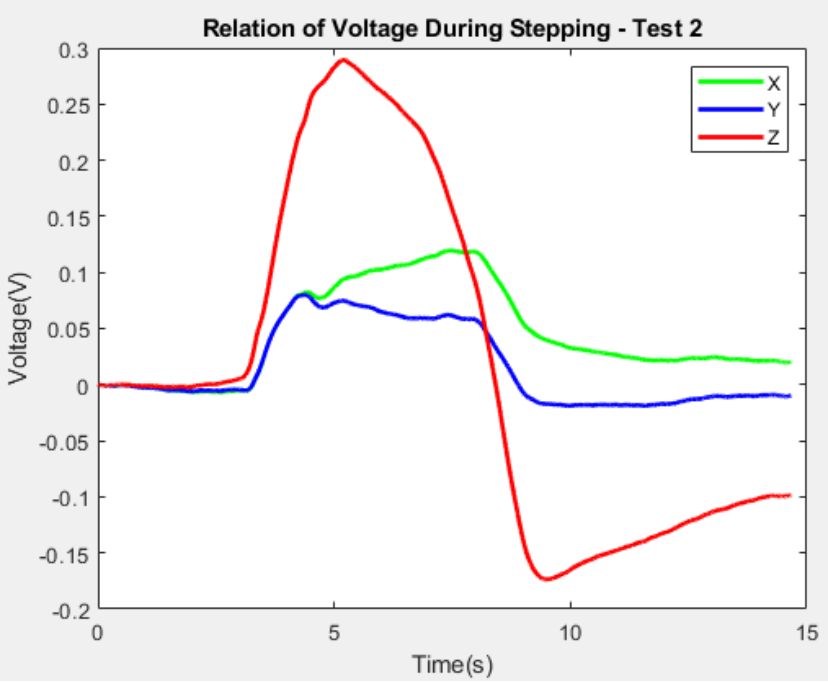

Fig. 115: The resulting voltages of the middle system analysis point during practical testing during the second test of standing with the insole system.

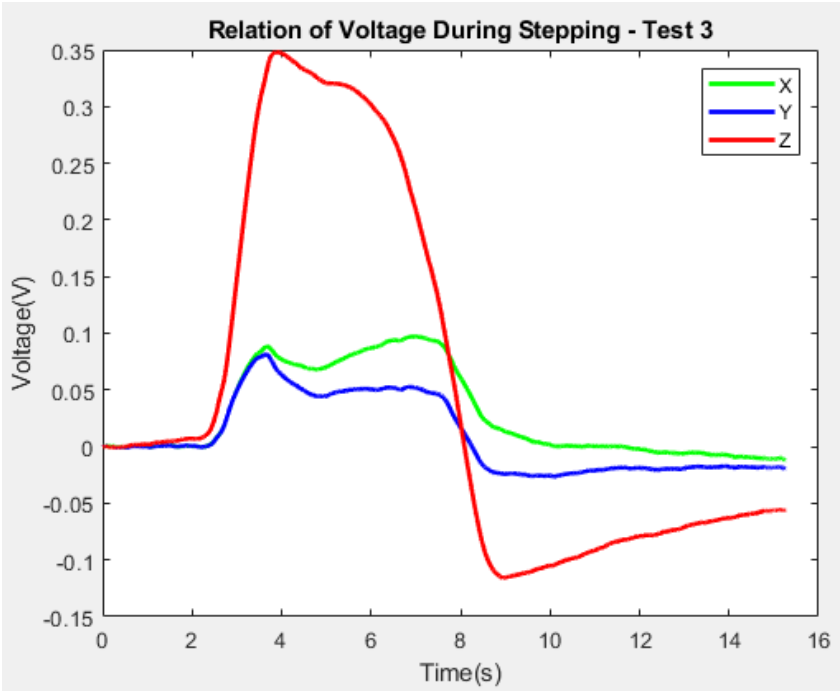

Fig. 116: The resulting voltages of the middle system analysis point during practical testing during the third test of standing with the insole system.

Back analysis point

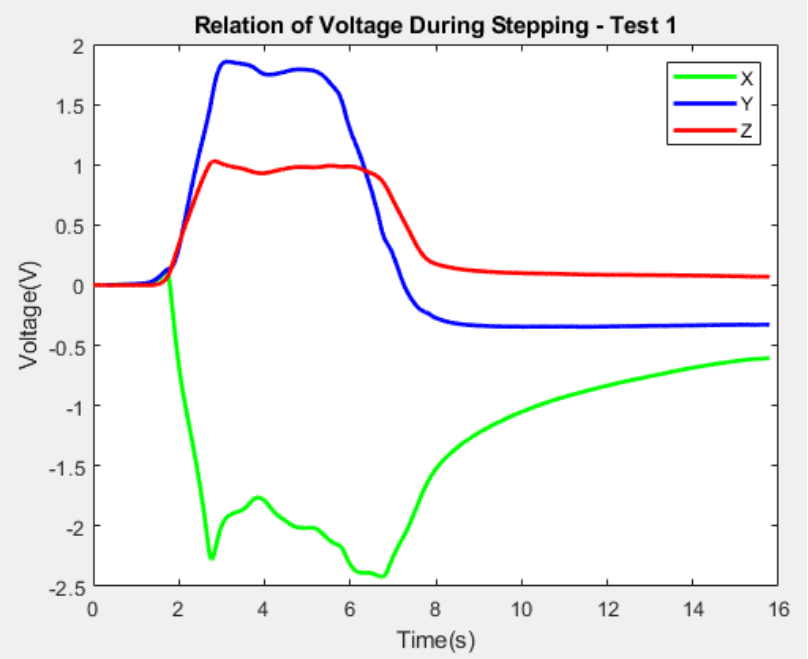

Fig. 117: The resulting voltages of the back system analysis point during practical testing during the first test of standing with the insole system.

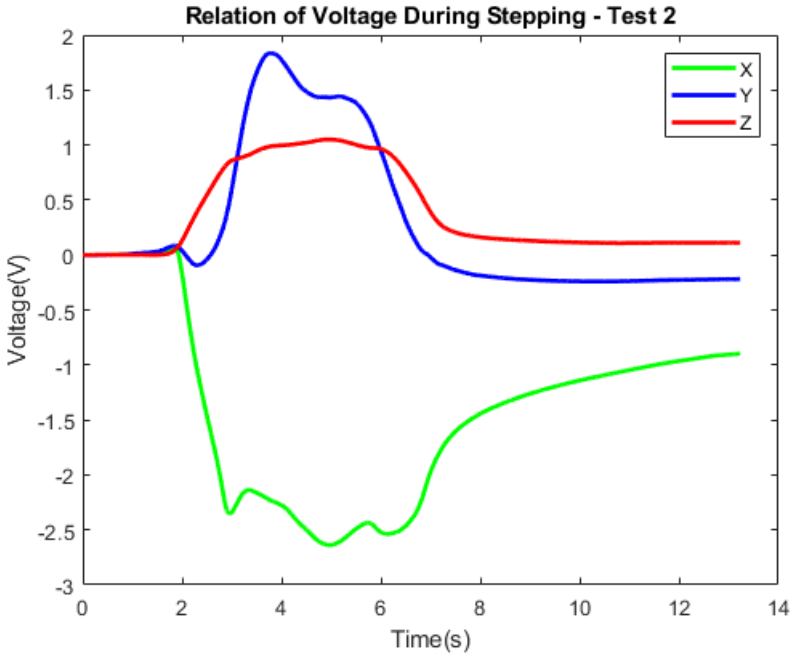

Fig. 118: The resulting voltages of the back system analysis point during practical testing during the second test of standing with the insole system.

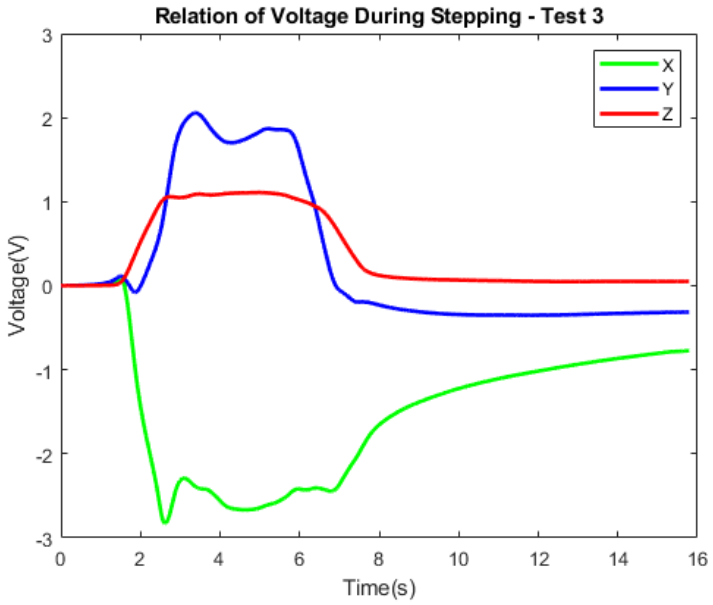

Fig. 119: The resulting voltages of the back system analysis point during practical testing during the third test of standing with the insole system.

Walking – Flat Surface

Next, the system was attached to the foot and was used to walk on a flat surface. The walking method was analyzed visually and processed in Matlab to identify different walking phases, demonstrated in Figure 120.

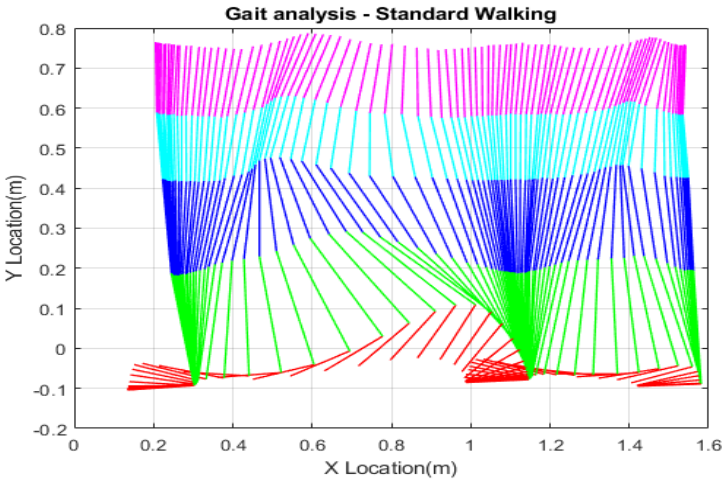

Fig. 120: The Matlab visualization of the marker analysis data collected during testing to identify different walking phases for the gait motion of walking on a flat surface.

The results from the front, middle, and back sensing locations are displayed in Figures 121-123, 124-126, and 127-129 respectively.

Front analysis point

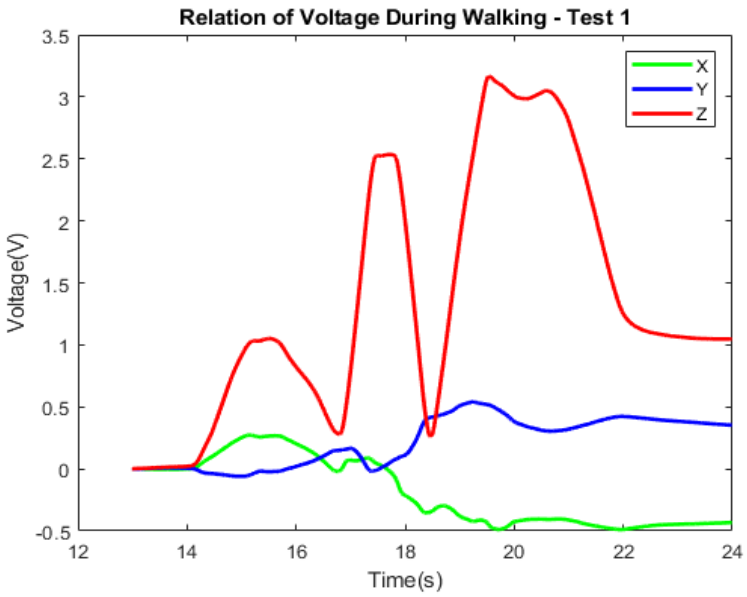

Fig. 121: The resulting voltages of the front system analysis point during practical testing during the first test of walking with the insole system.

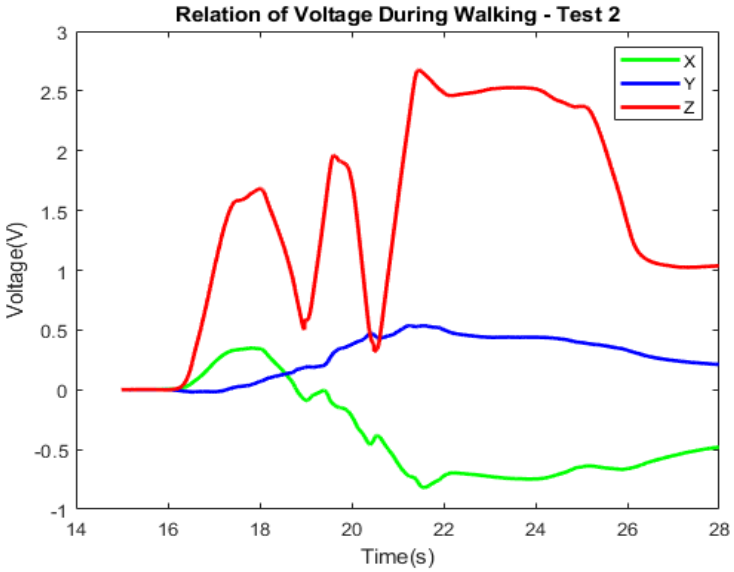

Fig. 122: The resulting voltages of the front system analysis point during practical testing during the second test of walking with the insole system.

Fig. 123: The resulting voltages of the front system analysis point during practical testing during the third test of walking with the insole system.

Middle analysis point

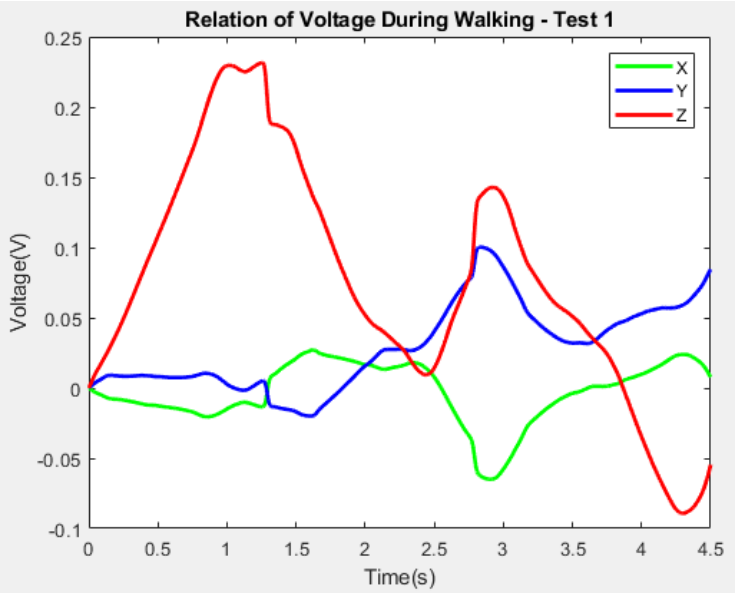

Fig. 124: The resulting voltages of the middle system analysis point during practical testing during the first test of walking with the insole system.

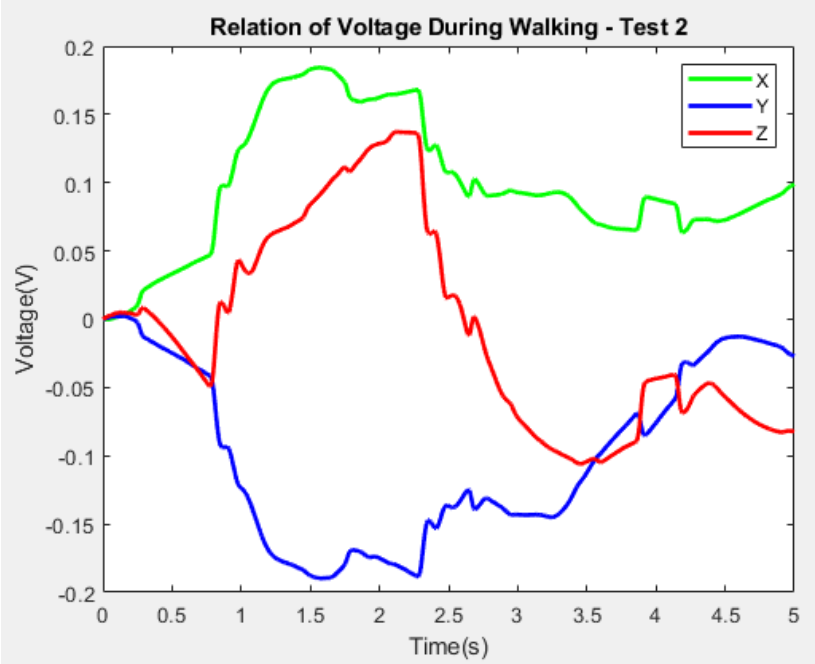

Fig. 125: The resulting voltages of the middle system analysis point during practical testing during the second test of walking with the insole system.

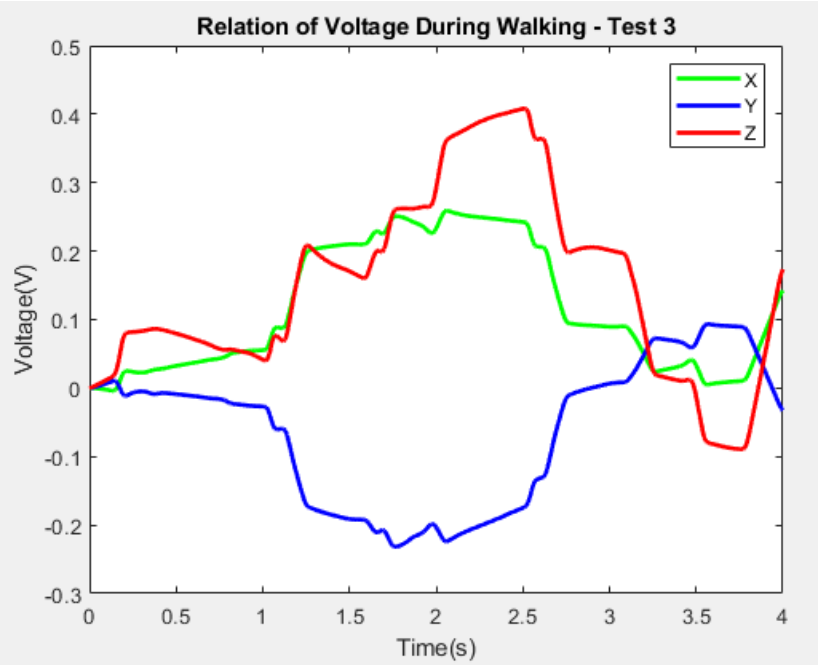

Fig. 126: The resulting voltages of the middle system analysis point during practical testing during the third test of walking with the insole system.

Back analysis point

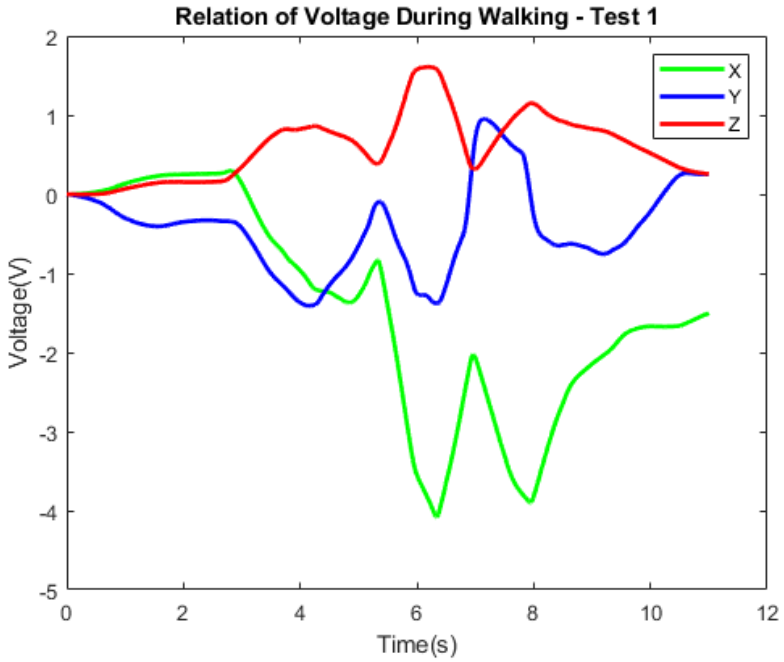

Fig. 127: The resulting voltages of the back system analysis point during practical testing during the first test of walking with the insole system.

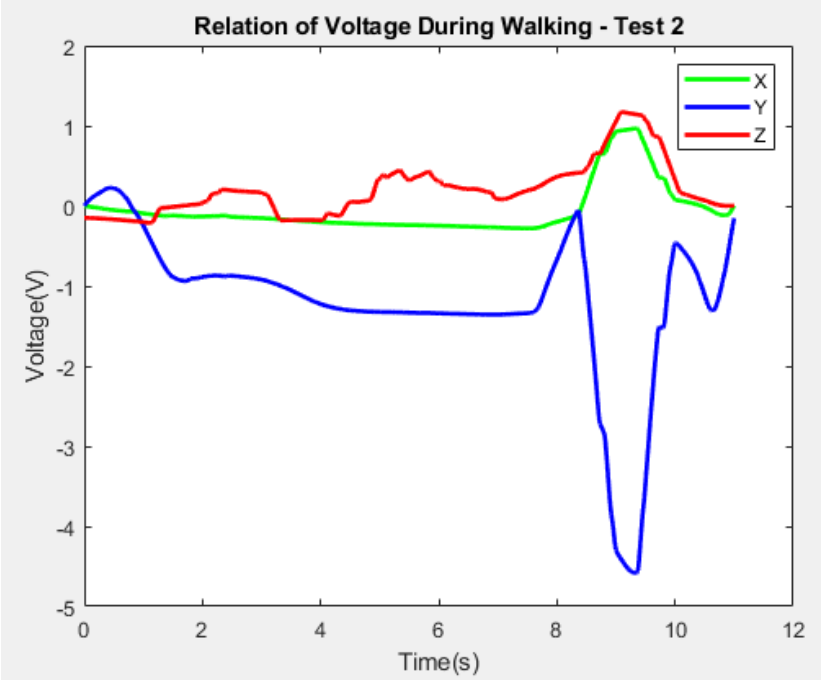

Fig. 128: The resulting voltages of the back system analysis point during practical testing during the second test of walking with the insole system.

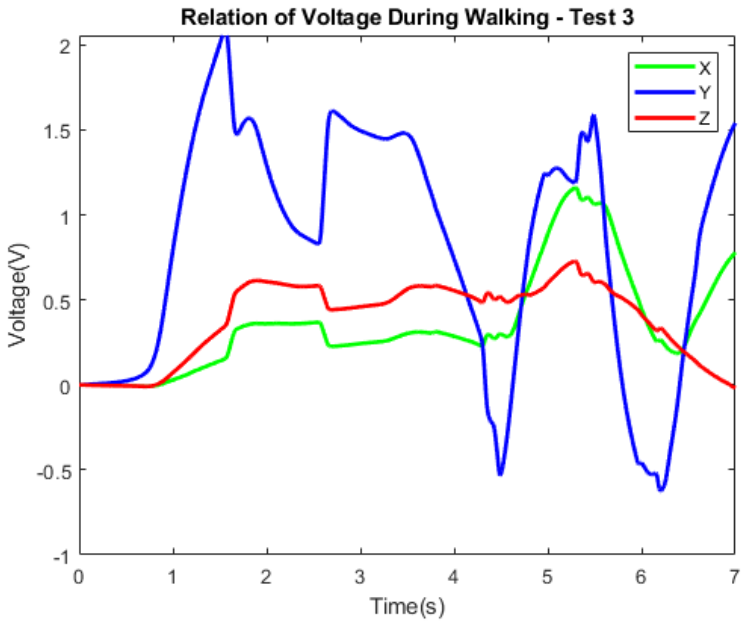

Fig. 129: The resulting voltages of the back system analysis point during practical testing during the third test of walking with the insole system.

Walking – Uphill

The system was then used to walk on an uphill surface. Once again, the gait motion was analyzed visually and processed in Matlab to identify walking phases during motion, demonstrated in Figure 130.

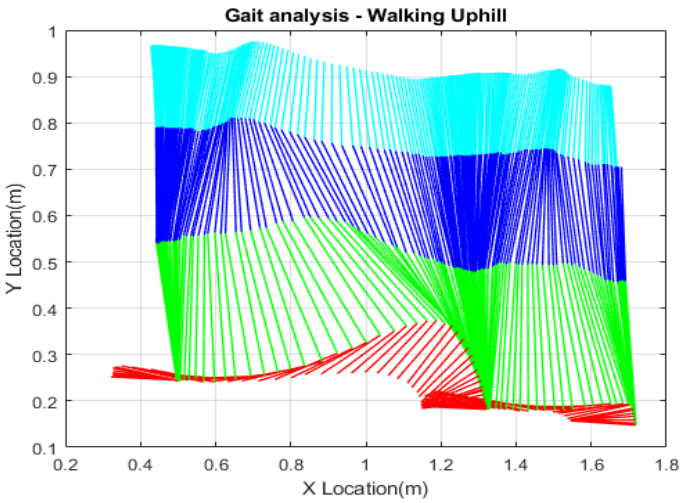

Fig. 130: The Matlab visualization of the marker analysis data collected during testing to identify different walking phases for the gait motion of walking uphill on a sloped surface.

The results from each analysis point are displayed in Figures 131-133, 134-136, and 137-139 respectively.

Front analysis point

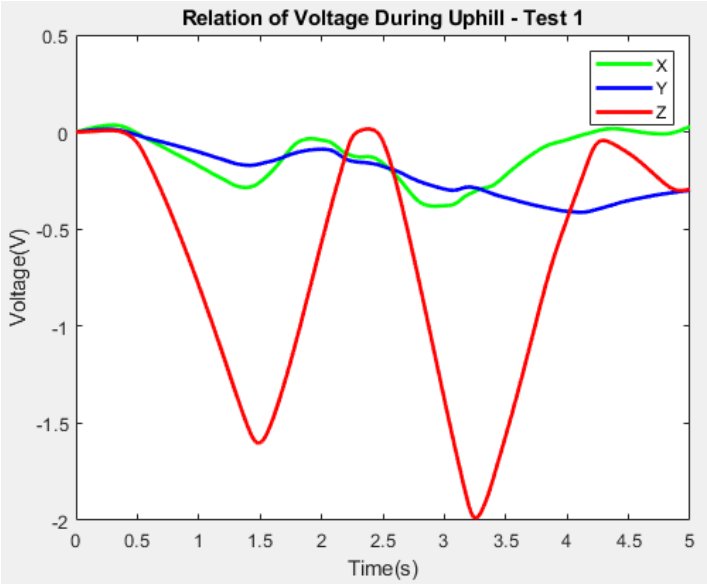

Fig. 131: The resulting voltages of the front system analysis point during practical testing during the first test of walking uphill with the insole system.

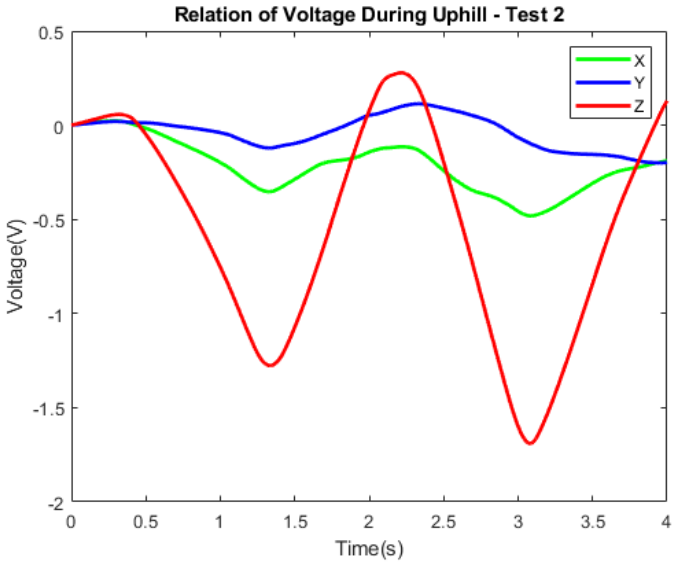

Fig. 132: The resulting voltages of the front system analysis point during practical testing during the second test of walking uphill with the insole system.

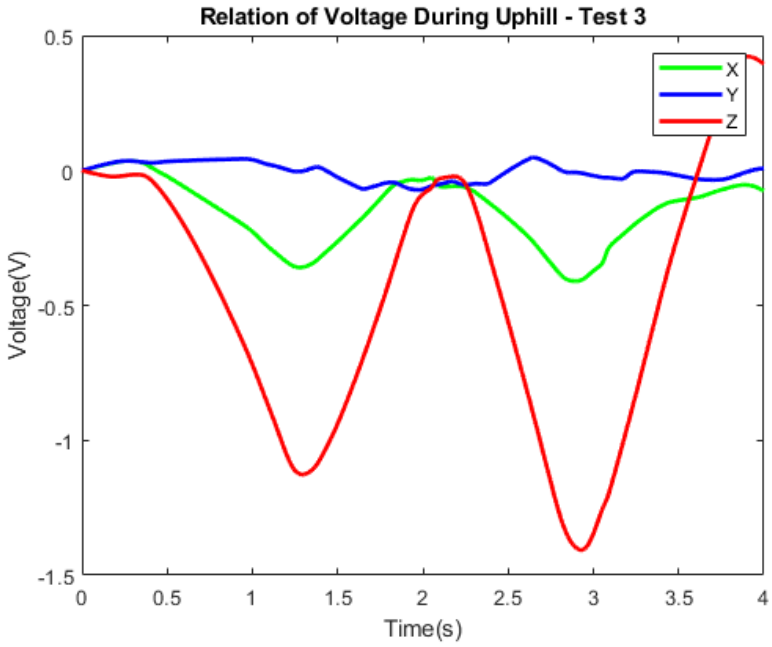

Fig. 133: The resulting voltages of the front system analysis point during practical testing during the third test of walking uphill with the insole system.

Middle analysis point

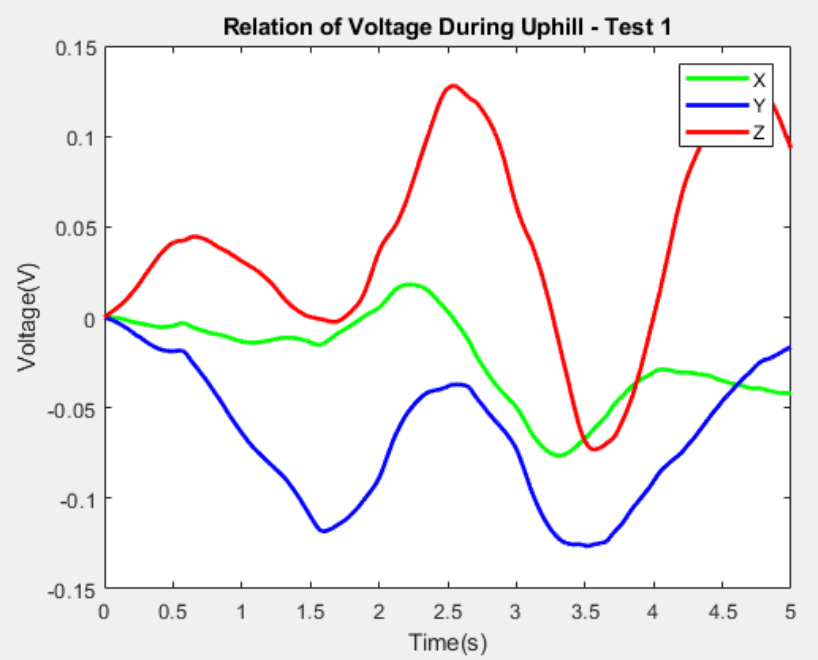

Fig. 134: The resulting voltages of the middle system analysis point during practical testing during the first test of walking uphill with the insole system.

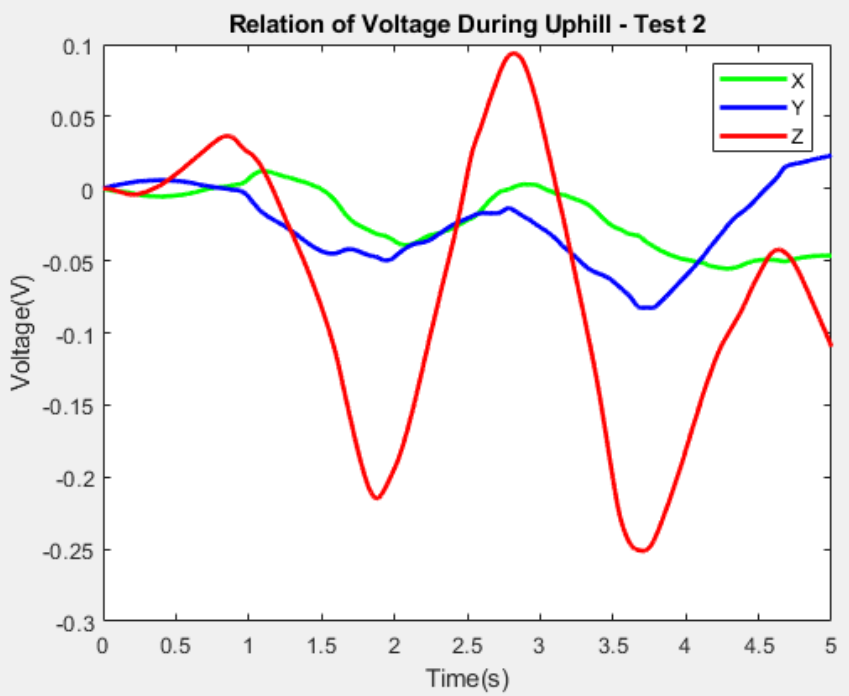

Fig. 135: The resulting voltages of the middle system analysis point during practical testing during the second test of walking uphill with the insole system.

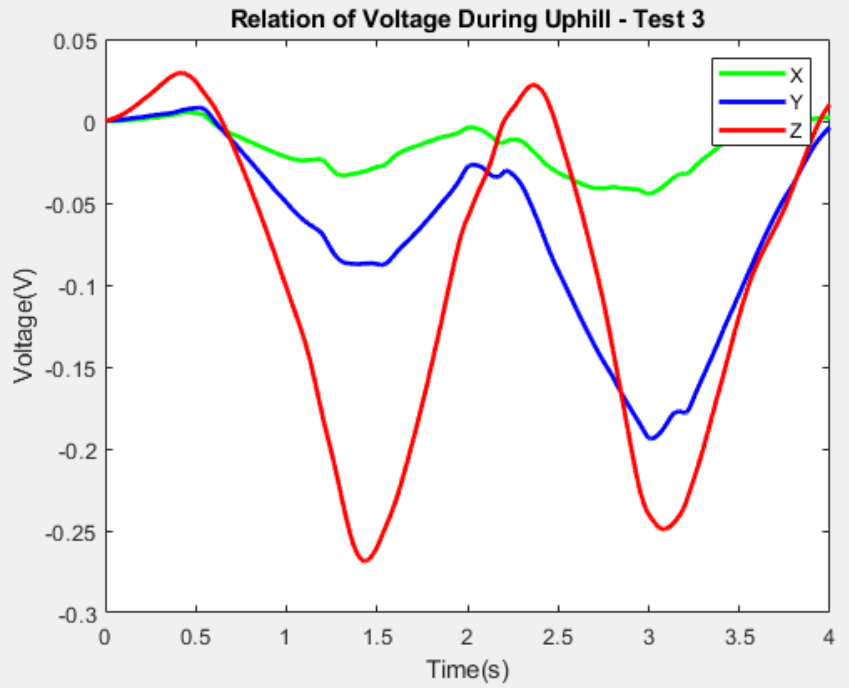

Fig. 136: The resulting voltages of the middle system analysis point during practical testing during the third test of walking uphill with the insole system.

Back analysis point

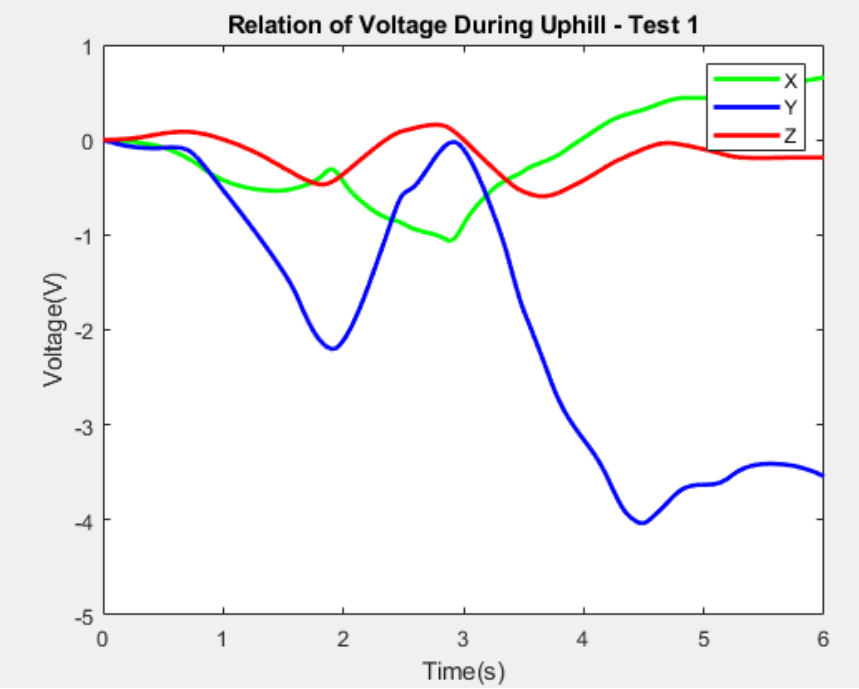

Fig. 137: The resulting voltages of the back system analysis point during practical testing during the first test of walking uphill with the insole system.

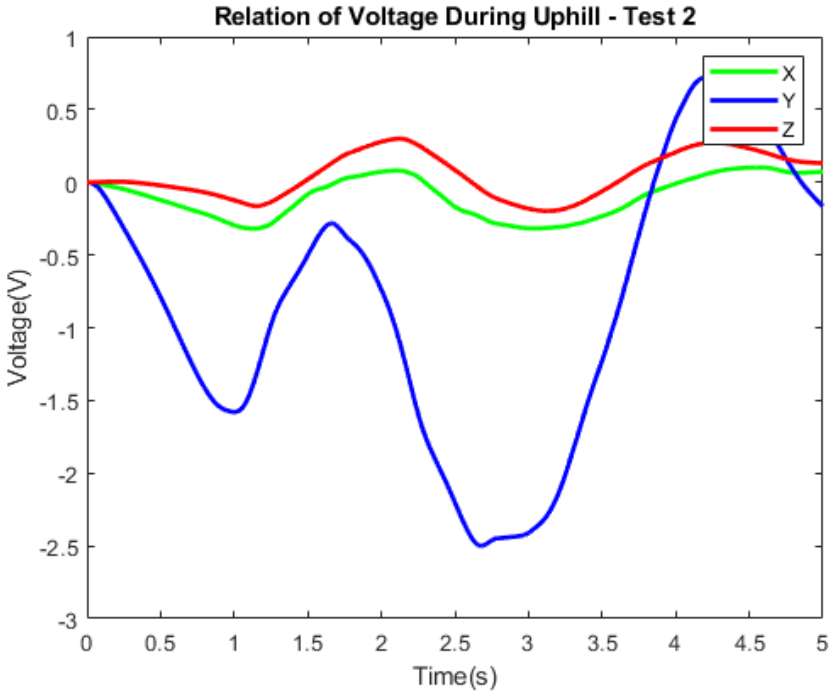

Fig. 138: The resulting voltages of the back system analysis point during practical testing during the second test of walking uphill with the insole system.

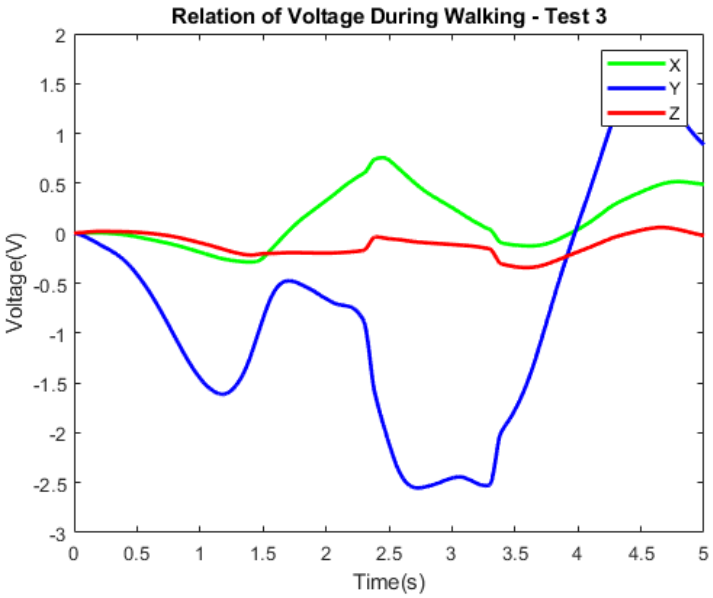

Fig. 139: The resulting voltages of the back system analysis point during practical testing during the first test of walking uphill with the insole system.

Walking – Downhill

Next, the insole system was tested walking down a slope. The gait motion was analyzed visually and processed in Matlab to identify walking phases during the gait motion, displayed in Figure 140.

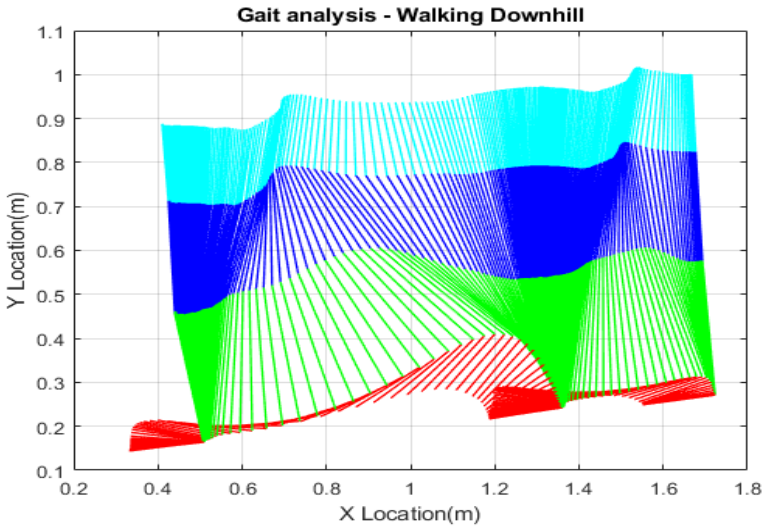

Fig. 140: The Matlab visualization of the marker analysis data collected during testing to identify different walking phases for the gait motion of walking downhill on a sloped surface.

The results for each analysis point are displayed in Figures 141-143, 144-146, and 147-149.

Front analysis point

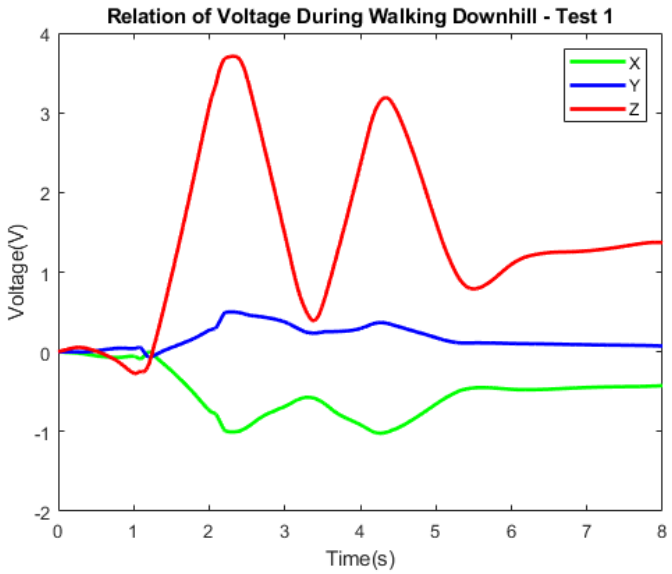

Fig. 141: The resulting voltages of the front system analysis point during practical testing during the first test of walking downhill with the insole system.

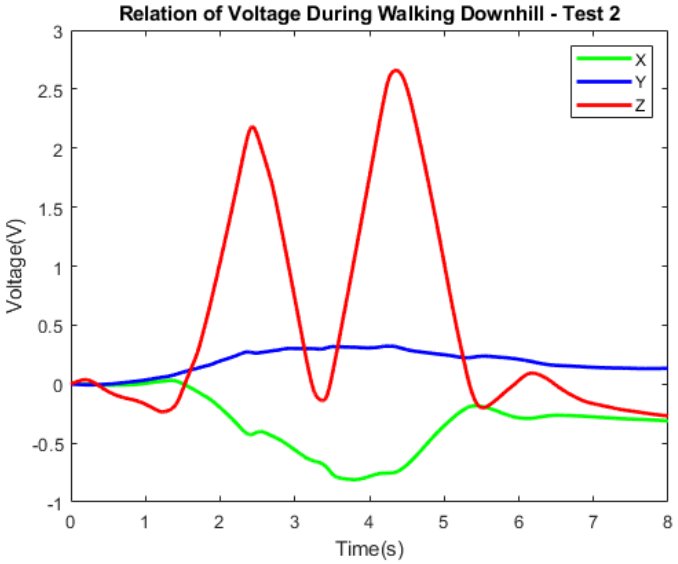

Fig. 142: The resulting voltages of the front system analysis point during practical testing during the second test of walking downhill with the insole system.

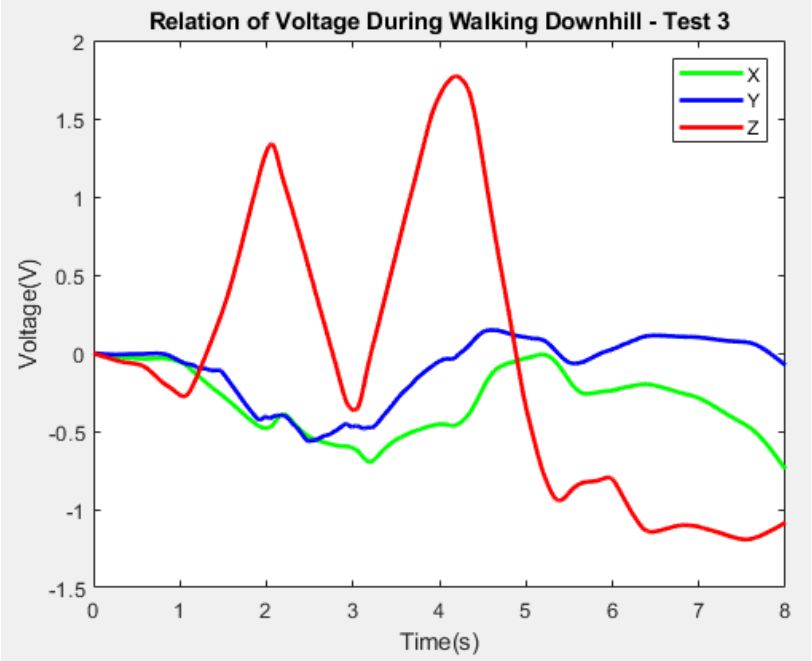

Fig. 143: The resulting voltages of the front system analysis point during practical testing during the third test of walking downhill with the insole system.

Middle analysis point

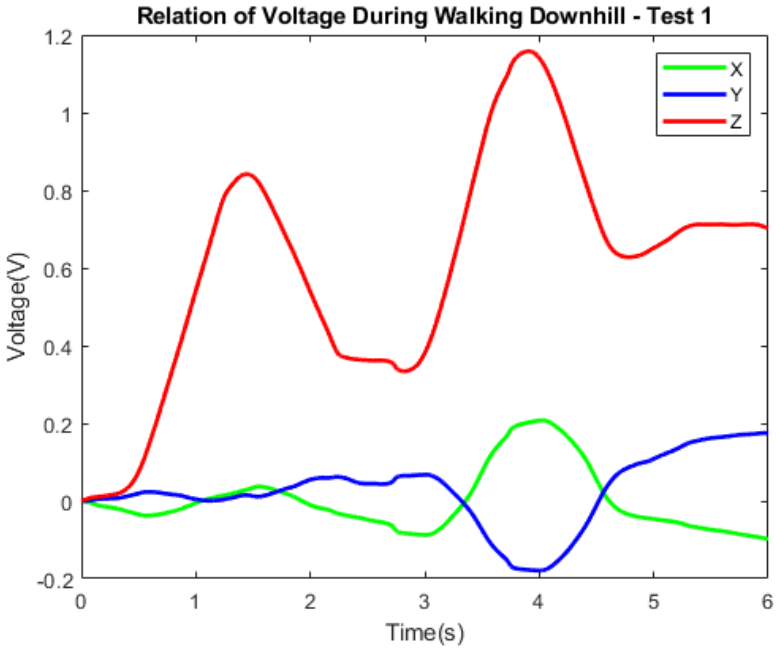

Fig. 144: The resulting voltages of the middle system analysis point during practical testing during the first test of walking downhill with the insole system.

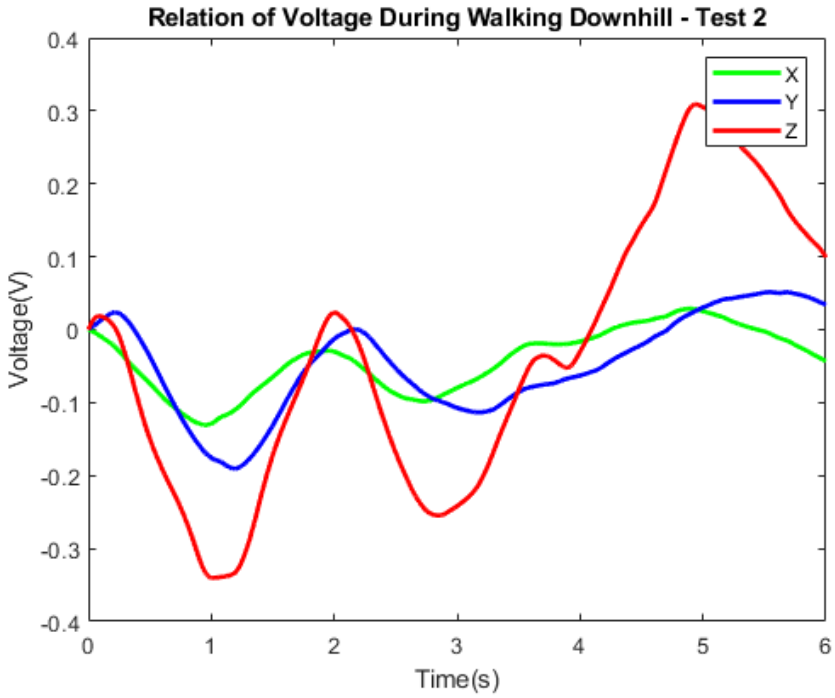

Fig. 145: The resulting voltages of the middle system analysis point during practical testing during the second test of walking downhill with the insole system.

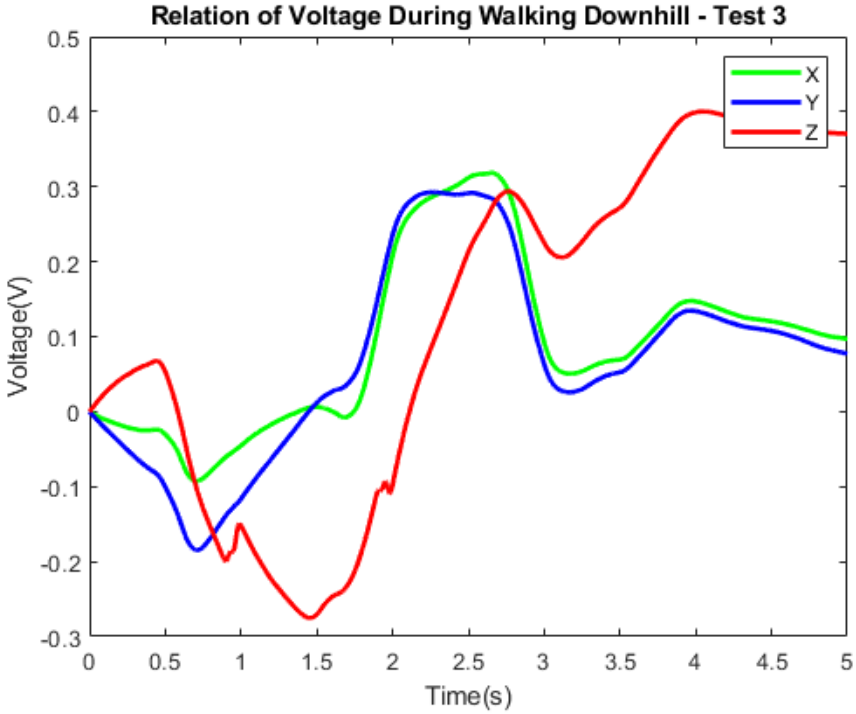

Fig. 146: The resulting voltages of the middle system analysis point during practical testing during the third test of walking downhill with the insole system.

Back analysis point

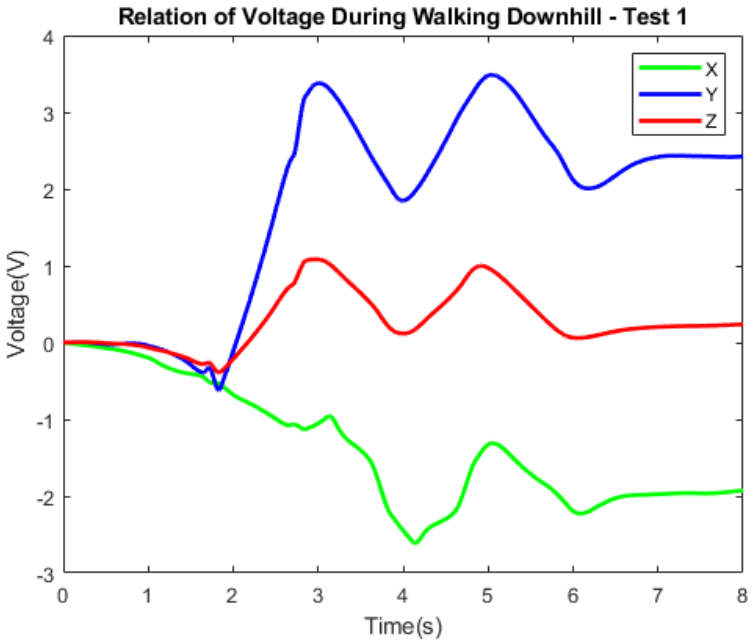

Fig. 147: The resulting voltages of the back system analysis point during practical testing during the first test of walking downhill with the insole system.

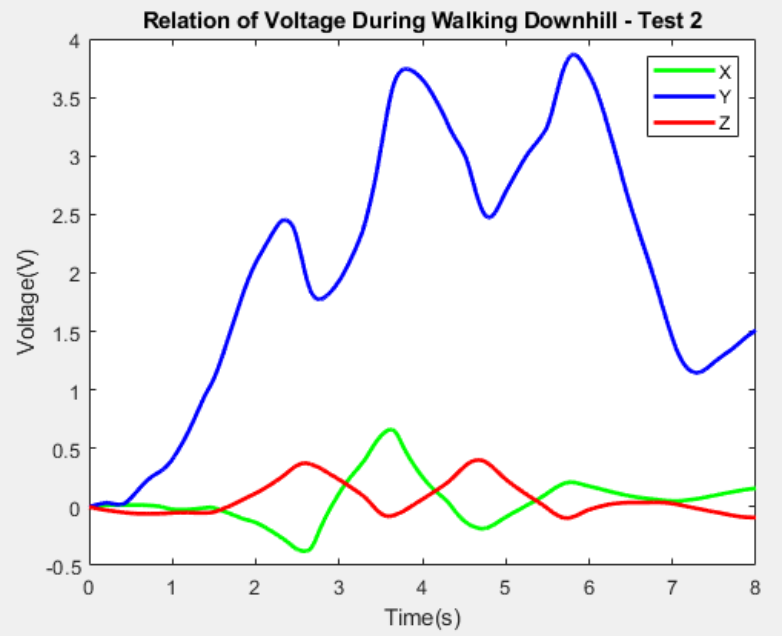

Fig. 148: The resulting voltages of the back system analysis point during practical testing during the second test of walking downhill with the insole system.

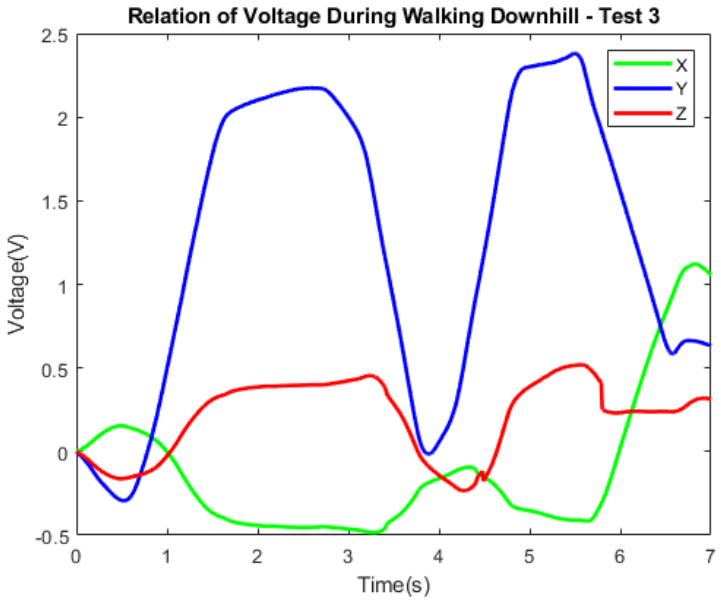

Fig. 149: The resulting voltages of the back system analysis point during practical testing during the third test of walking downhill with the insole system.

Sidestepping – Left to Right

To analyze shear forces, gait motion involved sidestepping from the left to the right. The sidestepping motion was analyzed visually and processed in Matlab to identify walking phases during the motion, displayed in Figure 150.

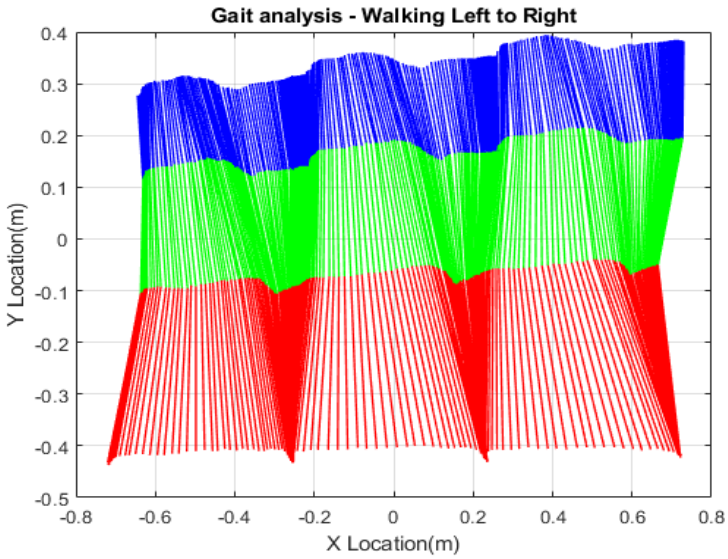

Fig. 150: The Matlab visualization of the marker analysis data collected during testing to identify different walking phases for the gait motion of sidestepping from left to right.

All datasets collected at each analysis point are displayed in Figures 151-153, 154-156, and 157-159.

Front analysis point

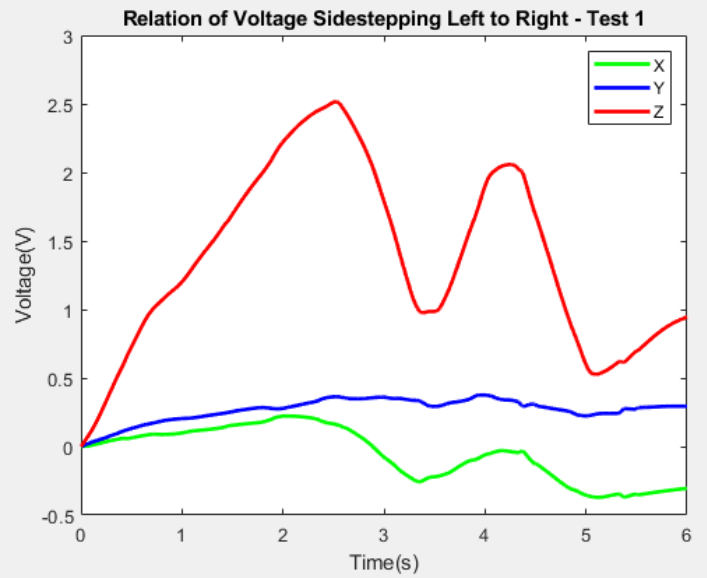

Fig. 151: The resulting voltages of the front system analysis point during practical testing during the first test of sidestepping from left to right with the insole system.

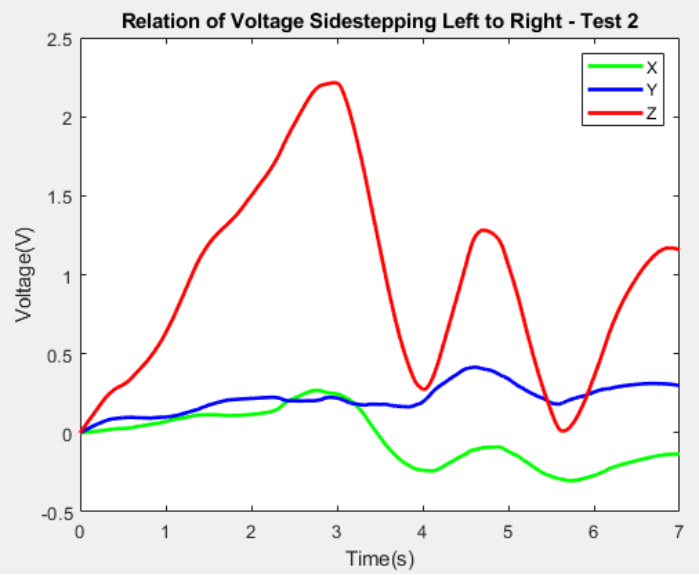

Fig. 152: The resulting voltages of the front system analysis point during practical testing during the second test of sidestepping from left to right with the insole system.

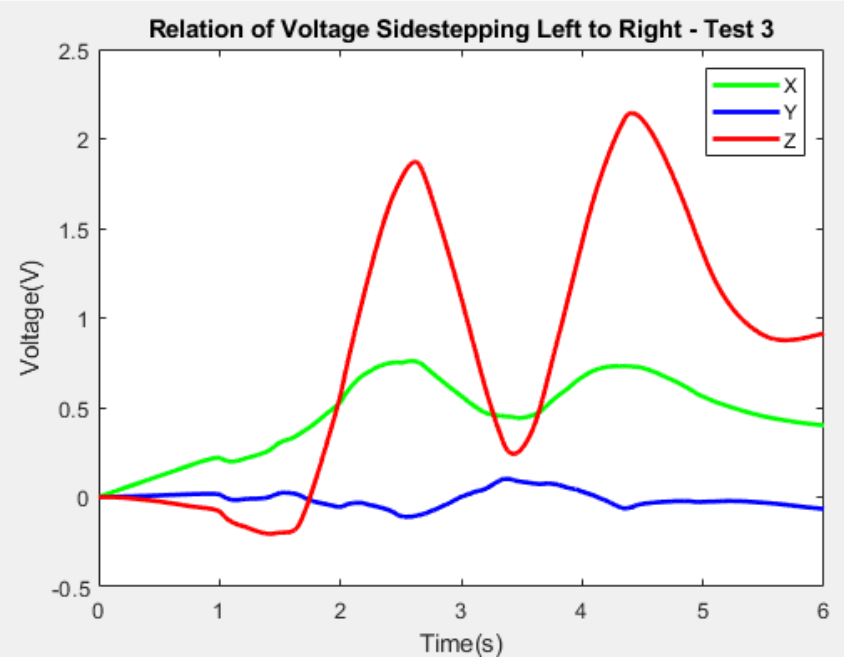

Fig. 153: The resulting voltages of the front system analysis point during practical testing during the third test of sidestepping from left to right with the insole system.

Middle analysis point

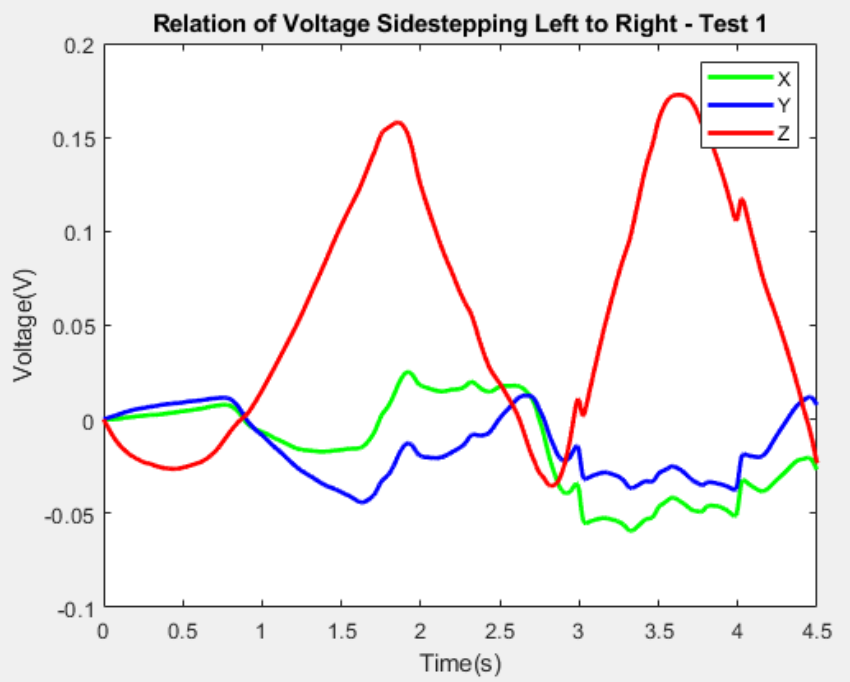

Fig. 154: The resulting voltages of the middle system analysis point during practical testing during the first test of sidestepping from left to right with the insole system.

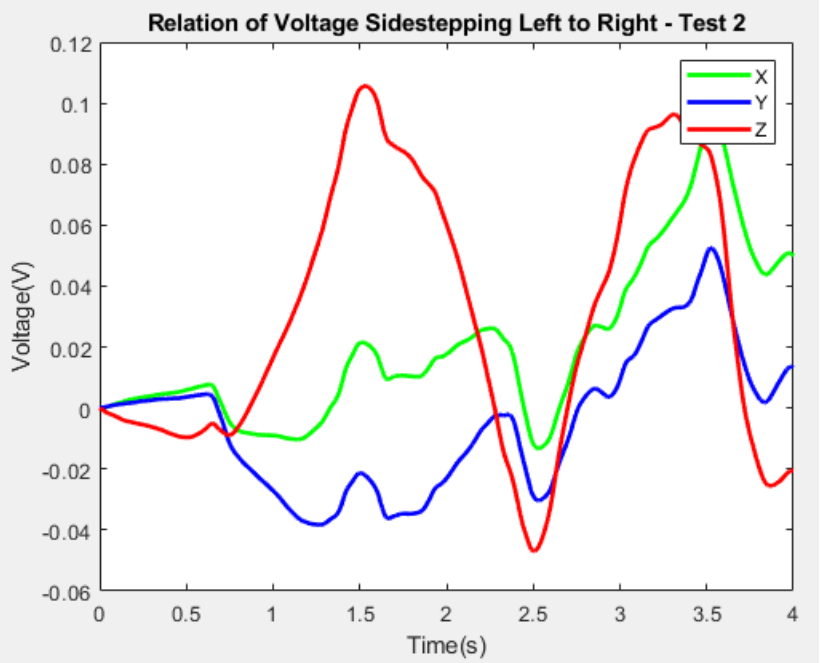

Fig. 155: The resulting voltages of the middle system analysis point during practical testing during the second test of sidestepping from left to right with the insole system.

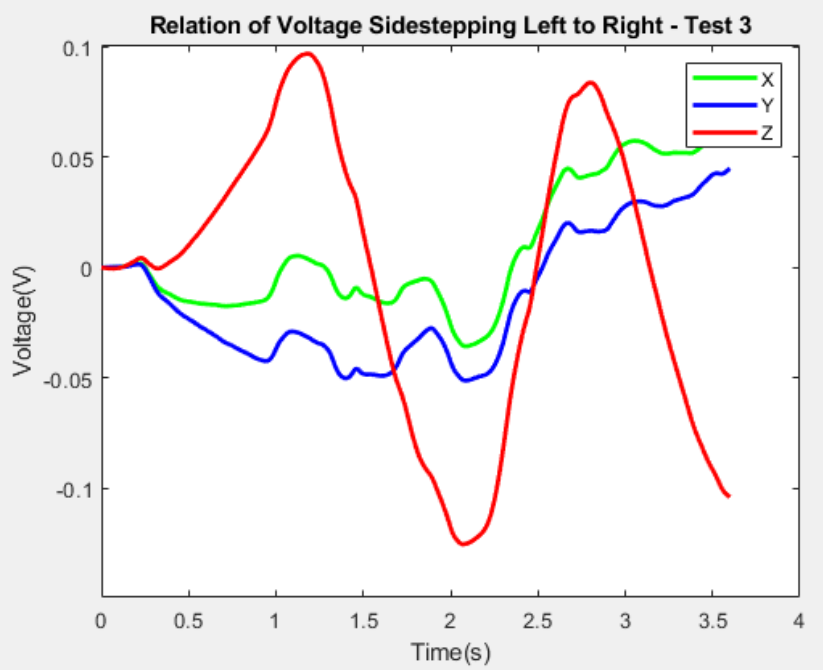

Fig. 156: The resulting voltages of the middle system analysis point during practical testing during the third test of sidestepping from left to right with the insole system.

Back analysis point

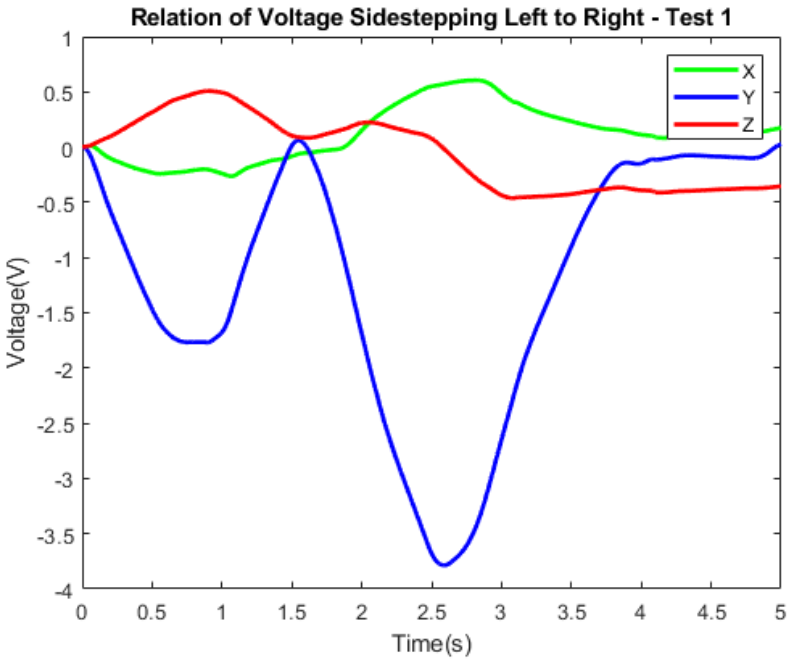

Fig. 157: The resulting voltages of the back system analysis point during practical testing during the first test of sidestepping from left to right with the insole system.

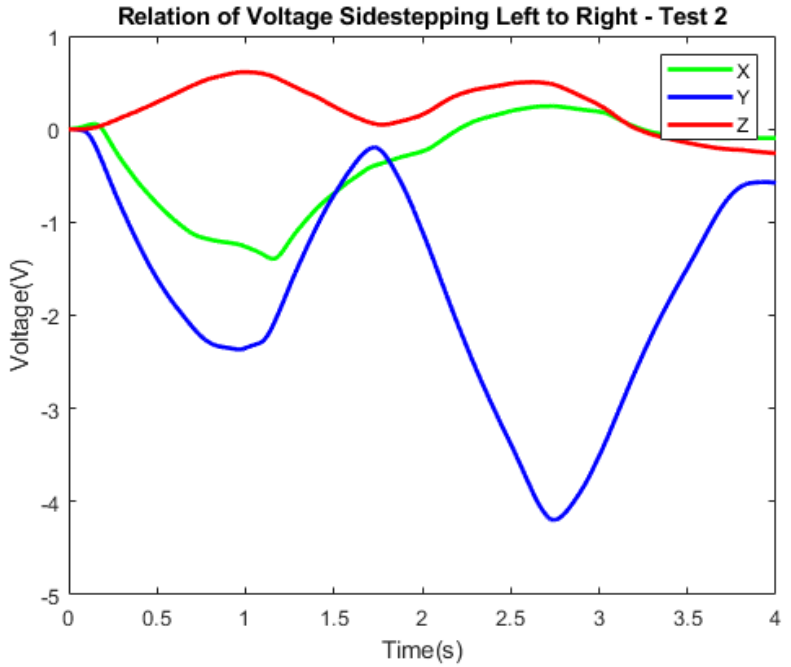

Fig. 158: The resulting voltages of the back system analysis point during practical testing during the second test of sidestepping from left to right with the insole system.

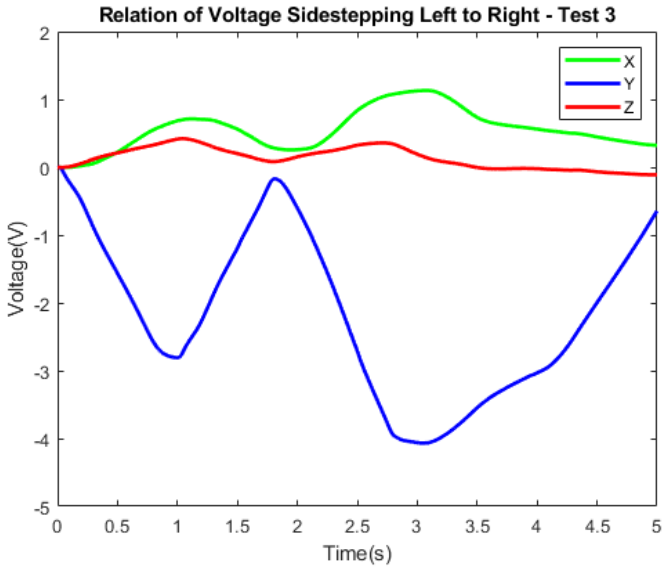

Fig. 159: The resulting voltages of the back system analysis point during practical testing during the third test of sidestepping from left to right with the insole system.

Sidestepping – Right to Left

Finally, shear force identification was tested in the opposite direction sidestepping from right to left. The motion was analyzed visually and processed in Matlab for walking phases identification, displayed in Figure 160.

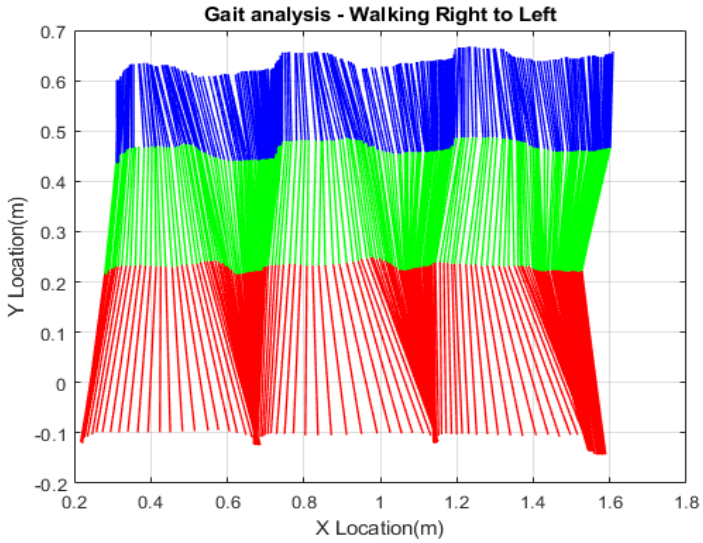

Fig. 160: The Matlab visualization of the marker analysis data collected during testing to identify different walking phases for the gait motion of sidestepping from right to left.

The final datasets from each analysis point are displayed in Figures 161-163, 164-166, and 167-169.

Front analysis point

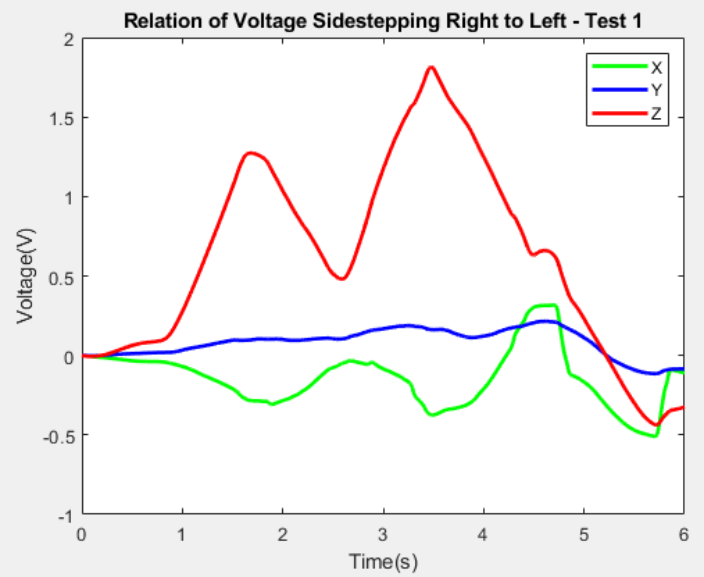

Fig. 161: The resulting voltages of the front system analysis point during practical testing during the first test of sidestepping from right to left with the insole system.

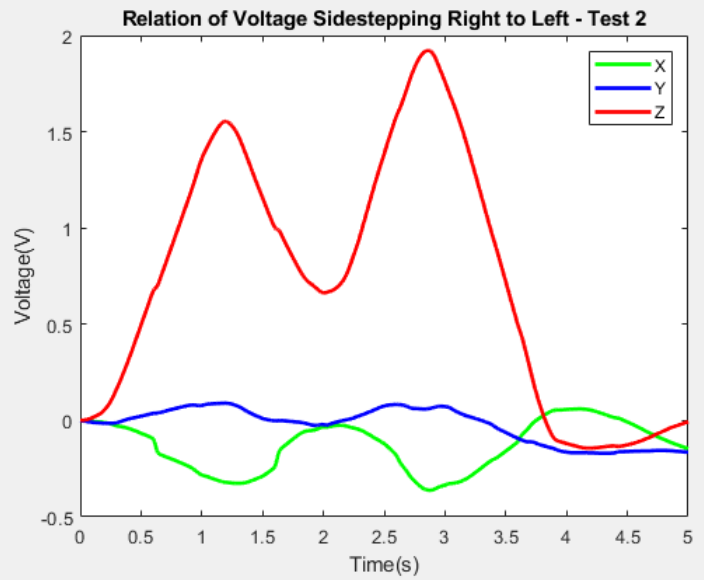

Fig. 162: The resulting voltages of the front system analysis point during practical testing during the second test of sidestepping from right to left with the insole system.

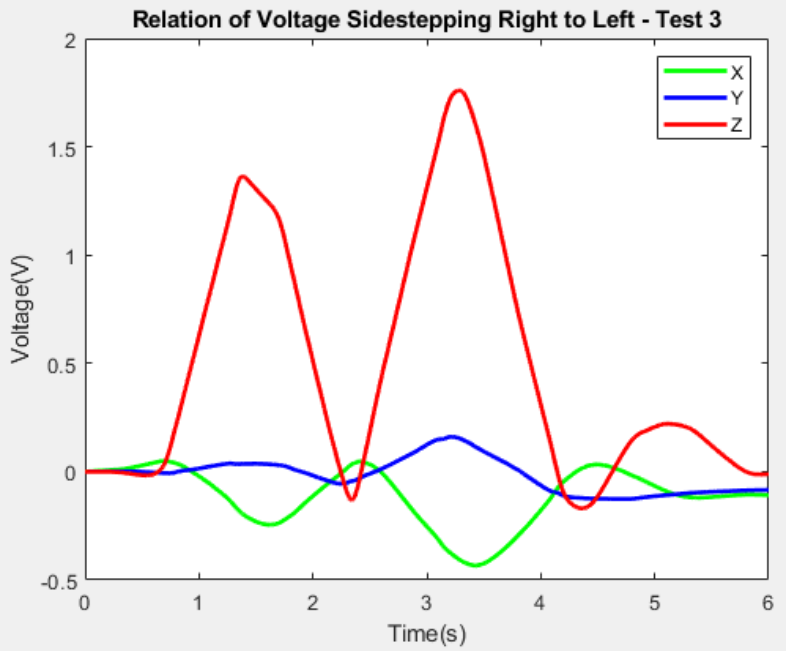

Fig. 163: The resulting voltages of the front system analysis point during practical testing during the third test of sidestepping from right to left with the insole system.

Middle analysis point

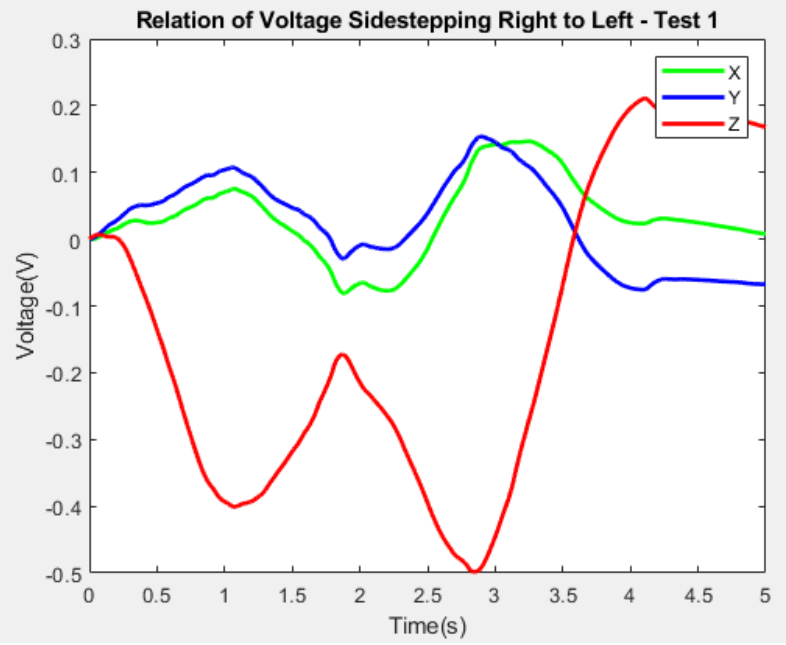

Fig. 164: The resulting voltages of the middle system analysis point during practical testing during the first test of sidestepping from right to left with the insole system.

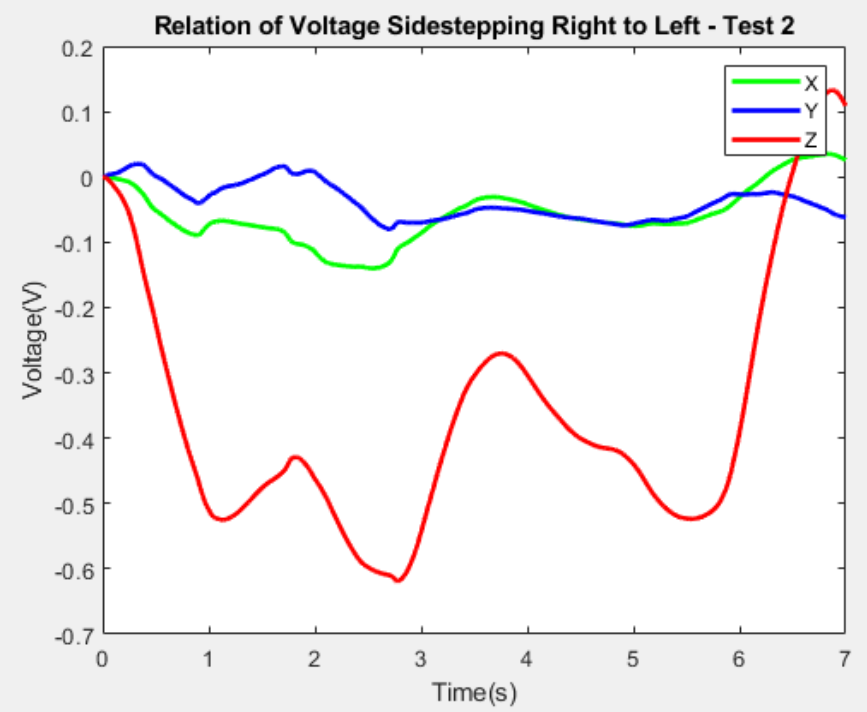

Fig. 165: The resulting voltages of the middle system analysis point during practical testing during the second test of sidestepping from right to left with the insole system.

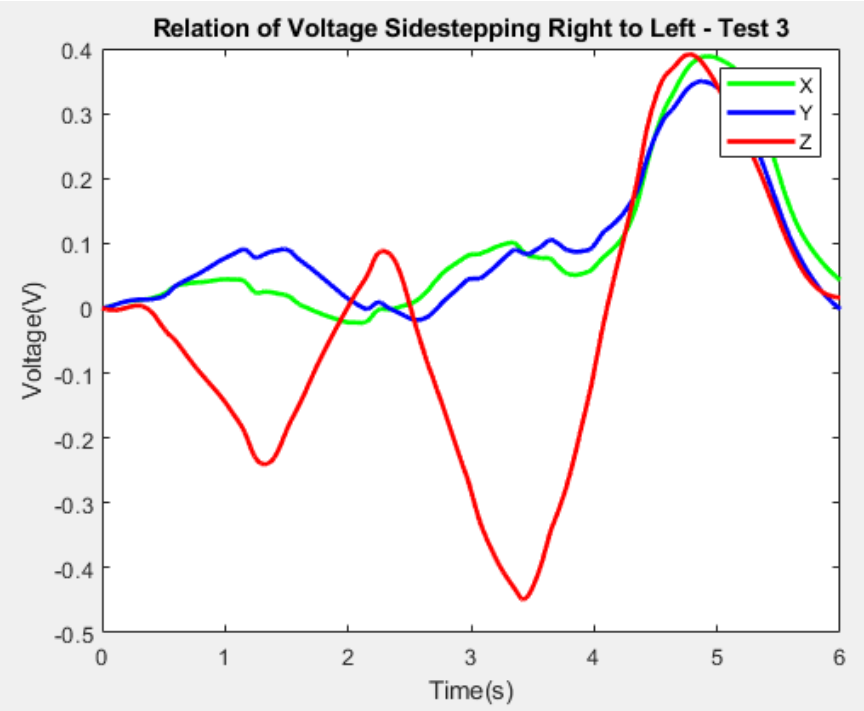

Fig. 166: The resulting voltages of the middle system analysis point during practical testing during the third test of sidestepping from right to left with the insole system.

Back analysis point

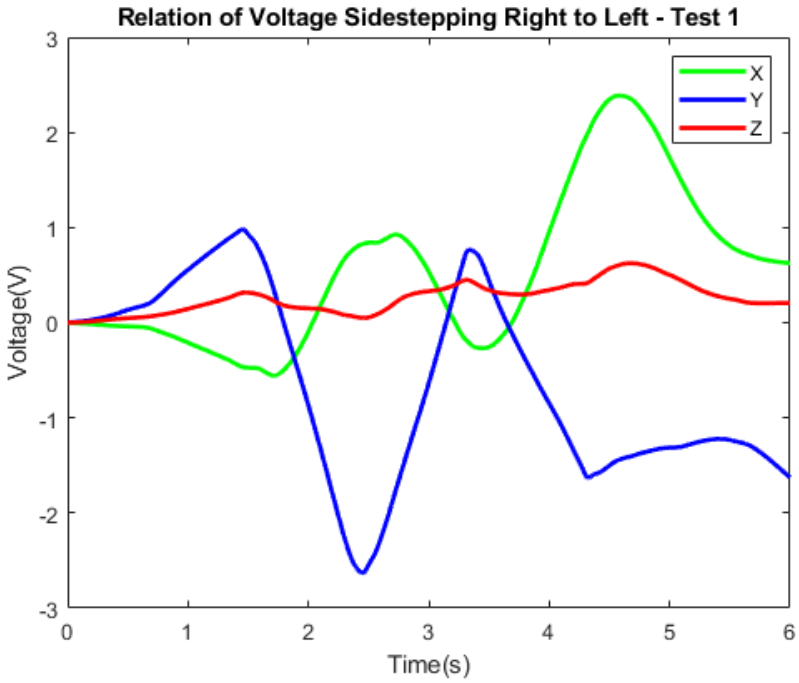

Fig. 167: The resulting voltages of the back system analysis point during practical testing during the first test of sidestepping from right to left with the insole system.

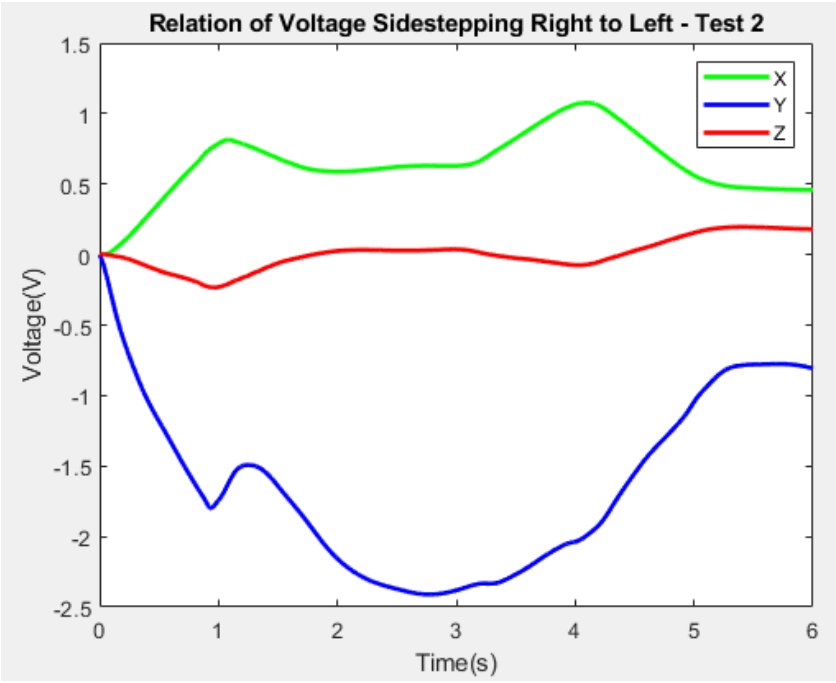

Fig. 168: The resulting voltages of the back system analysis point during practical testing during the second test of sidestepping from right to left with the insole system.

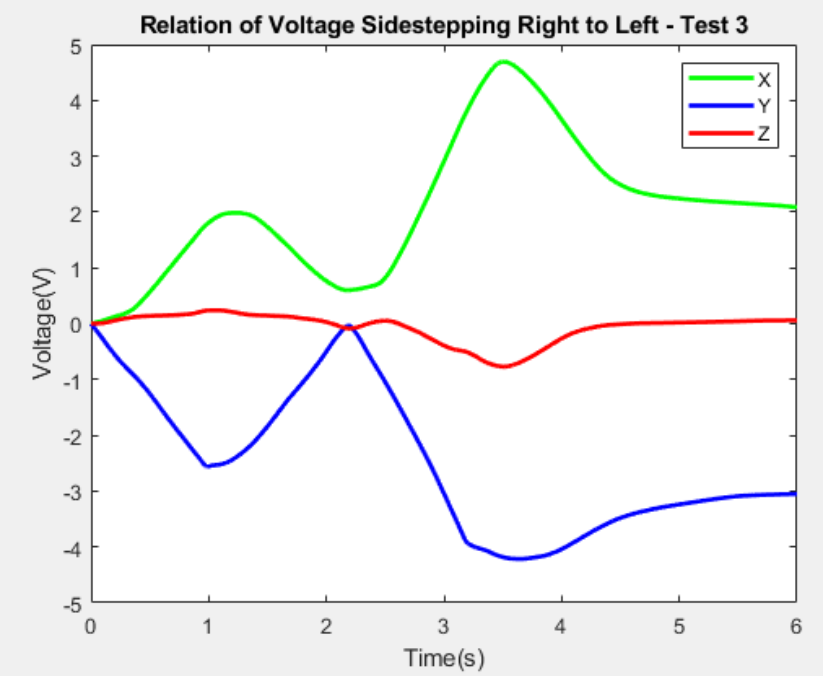

Fig. 169: The resulting voltages of the back system analysis point during practical testing during the third test of sidestepping from right to left with the insole system.

Preliminary Pattern Identification Checklist

After collecting data from each gait method test, the results were compared visually to one another. Table 7 indicates the identifiable trends from the gait testing methods.

Table 7: The preliminary pattern identification checklist for each gait motion tested practically.

Sensing Location	**Stepping**	**Walking – Flat**	**Walking – Uphill**	**Walking – Downhill**	**Sidestepping – Left to Right**	**Sidestepping – Right to Left**	**Identification Percentage**
Front	Yes	Yes	Yes	Yes	Yes	Yes	100%
Middle	Yes	No	Yes	No	No	No	33%
Back	Yes	No	Yes	Yes	No	No	50%
Whole Sensing	Yes	No	Yes	Yes	No	No	50%/61%

4.3 Design Three

Design three incorporated the most modified sensors, including sensors that were painted with silver epoxy to reduce the sensitivity as well as cut uniformly to reduce the size of the analysis point. In doing so, the sensors were placed in more optimal locations for data collection. Figure 170 displays the third insole design for this research.

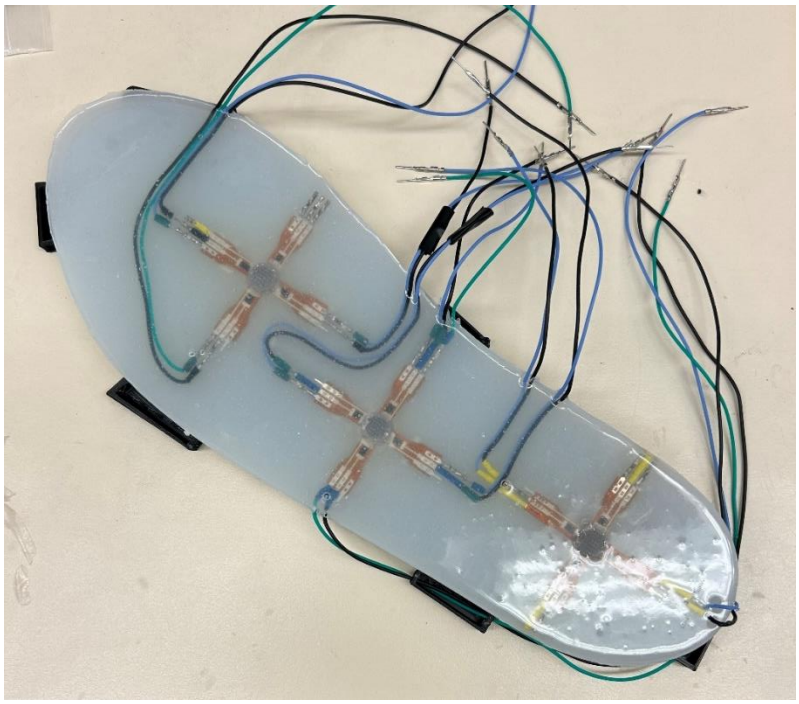

Fig. 170: The third and final insole design used for this research, utilizing shortened sensors for more optimal placement.

4.3.1 Validation Results

The following sections will display results for each direction in the following order: voltage of relevant directions compared to the input force, analysis of the best fit line and potential delay using the Matlab system analysis toolbox, the resulting calculated force output with applied phase shift, and the hysteresis of the system after applying a time phase shift.

X-Direction Results

Front analysis point

Figures 171-174 show the voltage response due to force input, the correlation between the voltage response and the force input in the Matlab system analysis toolbox for the best fit line characteristics, the comparison between the converted voltage and the reference force, and the force hysteresis curve for X-directional testing at the front analysis point respectively.

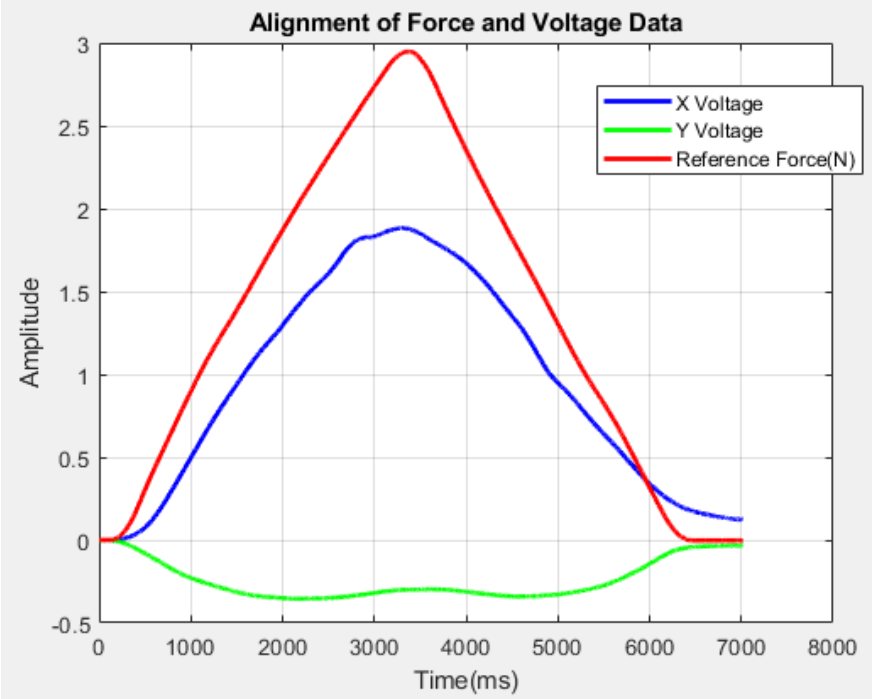

Fig. 171: The comparison between the reference force in red and the output voltages in the X and Y directions. The blue line indicates the X resultant voltage and the green line indicates the Y resultant voltage.

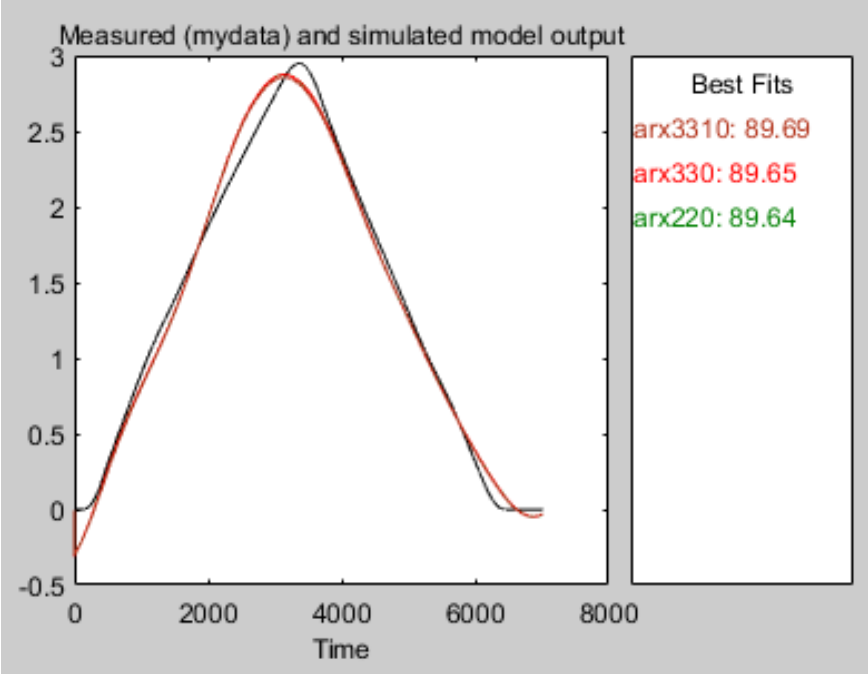

Fig. 172: The system analysis toolbox data report for the best fit line parameters. The resulting best fit line parameters were a cubic line with a delay of 10.

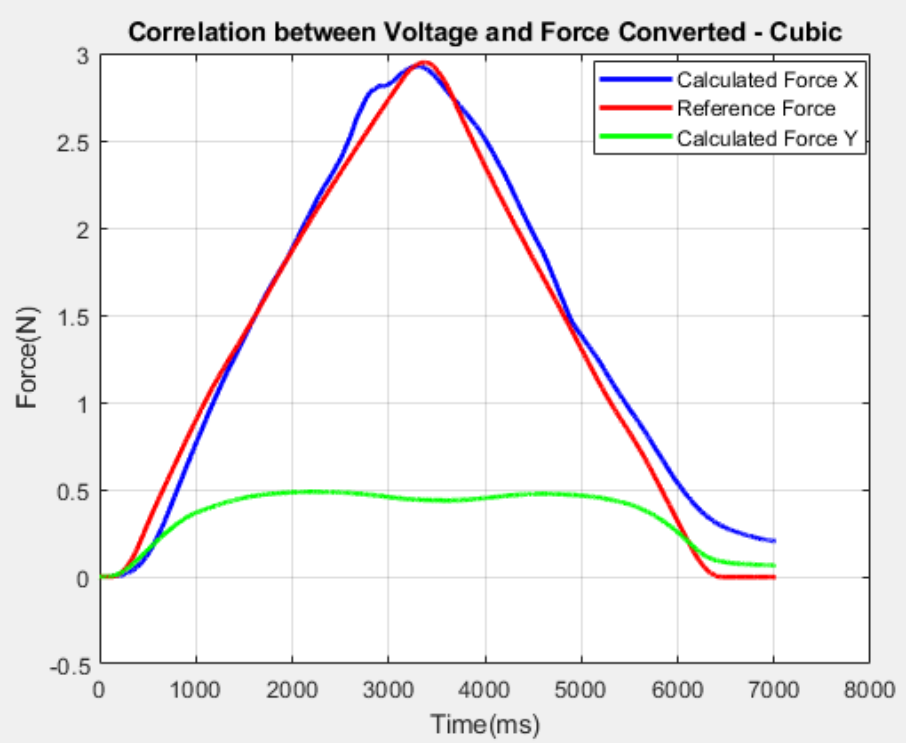

Fig. 173: The comparison between the reference force in red and the calculated forces for the X and Y directions. The blue line indicates the calculated X-directional force and the green line indicates the Y-directional force.

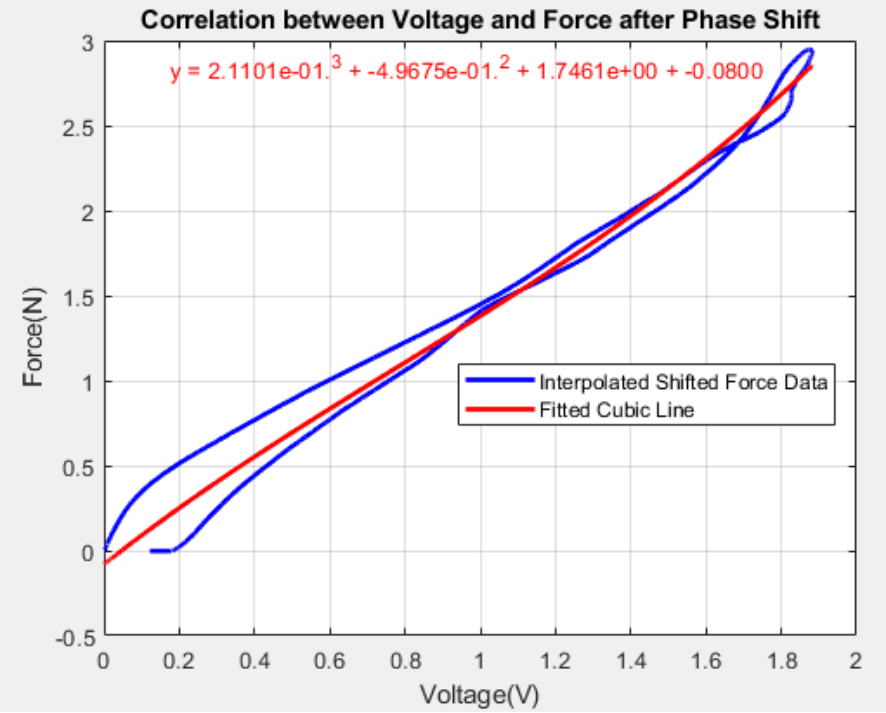

Fig. 174: The hysteresis curve visualizing the comparison between the calculated force and the best fit line used for the conversion during the pressing and releasing of the force sensor. The left most blue line indicates the resting position.

Middle analysis point

Figures 175-178 show the voltage response due to force input, the correlation between the voltage response and the force input in the Matlab system analysis toolbox for the best fit line characteristics, the comparison between the converted voltage and the reference force, and the force hysteresis curve for X-directional testing at the middle analysis point respectively.

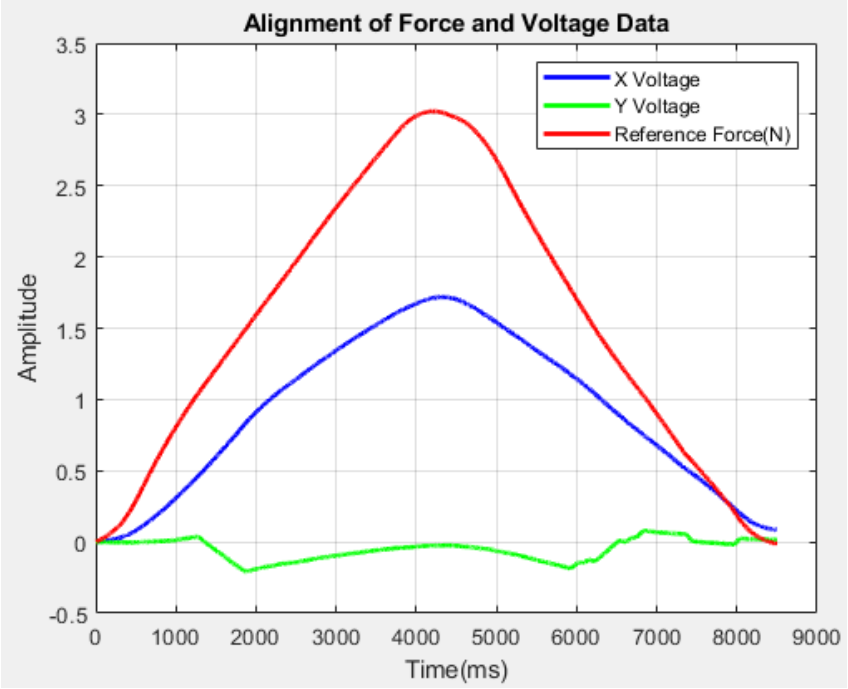

Fig. 175: The comparison between the reference force in red and the output voltages in the X and Y directions. The blue line indicates the X resultant voltage and the green line indicates the Y resultant voltage.

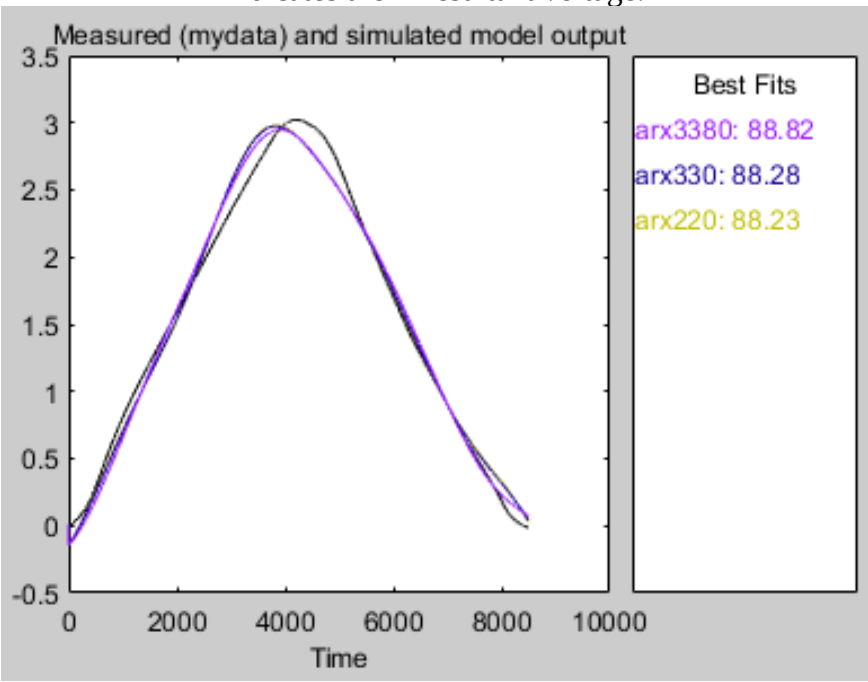

Fig. 176: The system analysis toolbox data report for the best fit line parameters. The resulting best fit line parameters were a cubic line with a delay of 80.

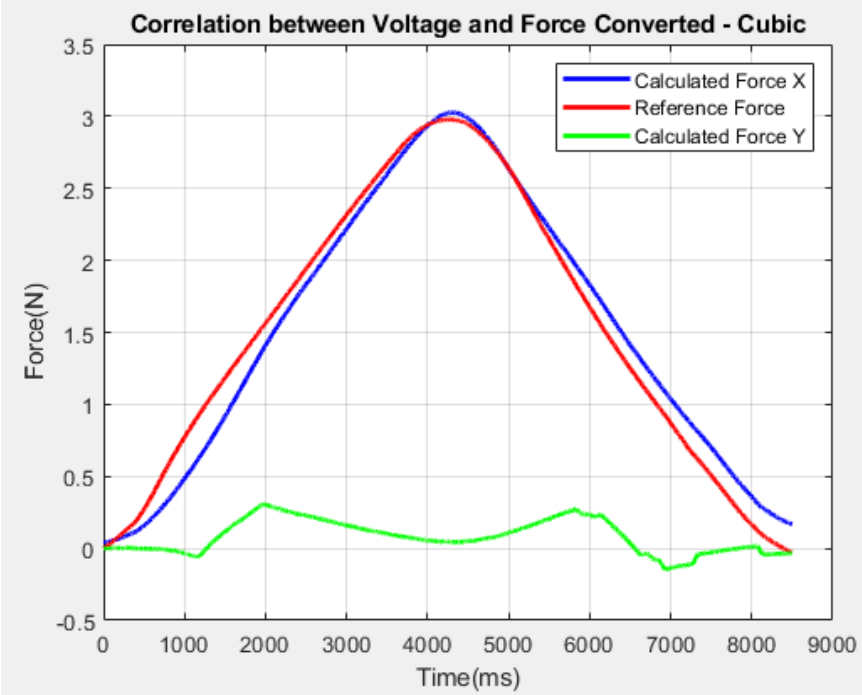

Fig. 177: The comparison between the reference force in red and the calculated forces for the X and Y directions. The blue line indicates the calculated X-directional force and the green line indicates the Y-directional force.

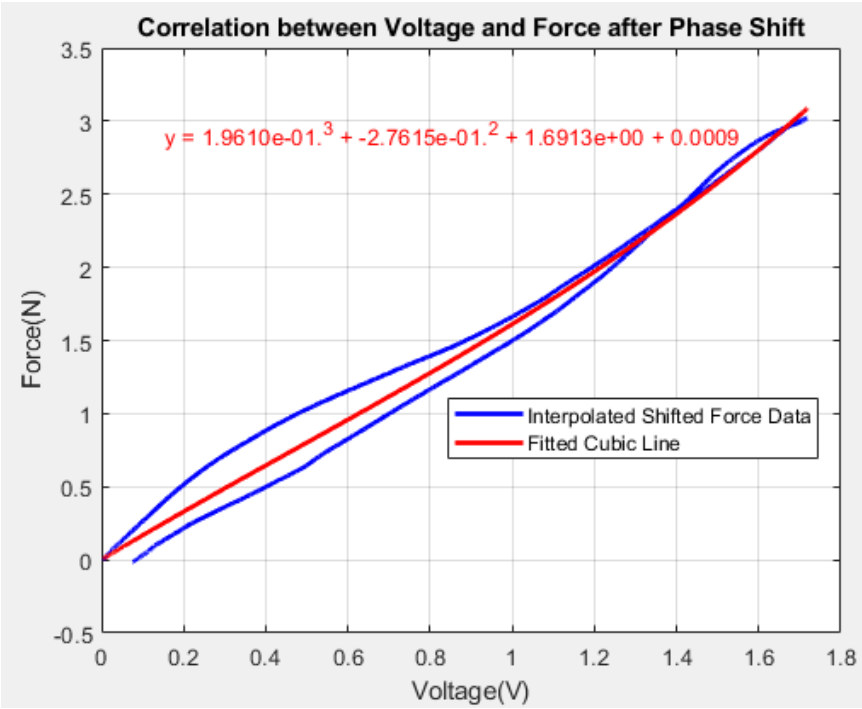

Fig. 178: The hysteresis curve visualizing the comparison between the calculated force and the best fit line used for the conversion during the pressing and releasing of the force sensor. The left most blue line indicates the resting position.

Back analysis point

Figures 179-182 show the voltage response due to force input, the correlation between the voltage response and the force input in the Matlab system analysis toolbox for the best fit line characteristics, the comparison between the converted voltage and the reference force, and the force hysteresis curve for X-directional testing at the back analysis point respectively.

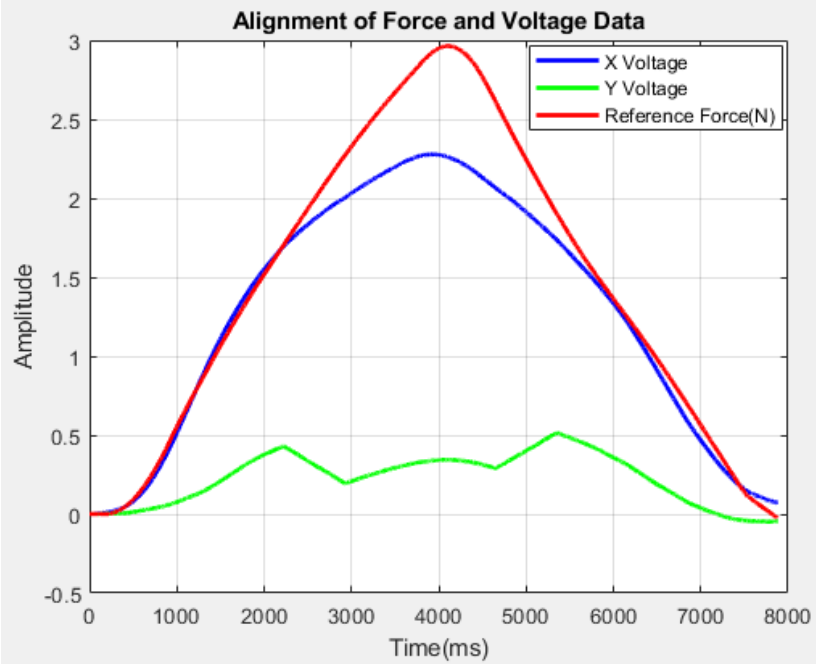

Fig. 179: The comparison between the reference force in red and the output voltages in the X and Y directions. The blue line indicates the X resultant voltage and the green line indicates the Y resultant voltage.

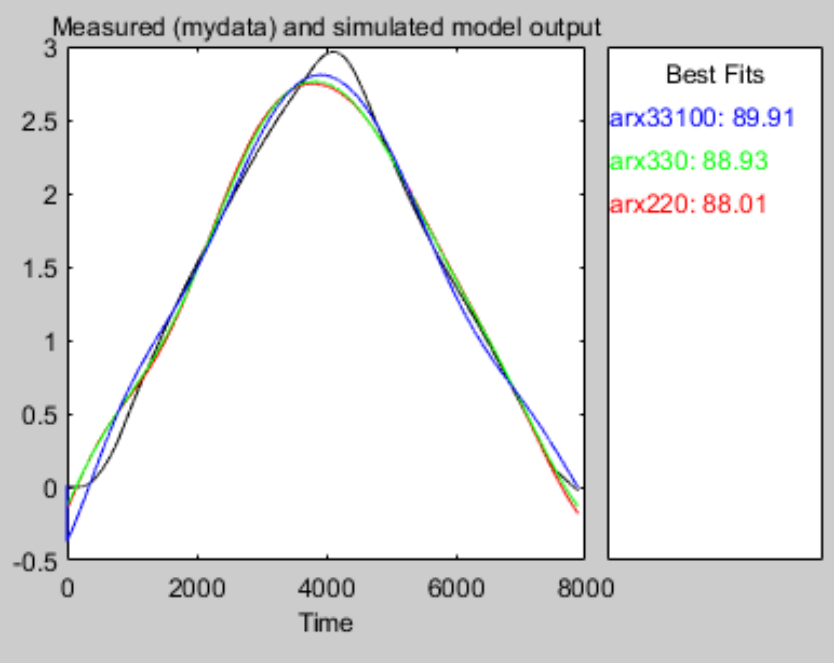

Fig. 180: The system analysis toolbox data report for the best fit line parameters. The resulting best fit line parameters were a cubic line with a delay of 100.

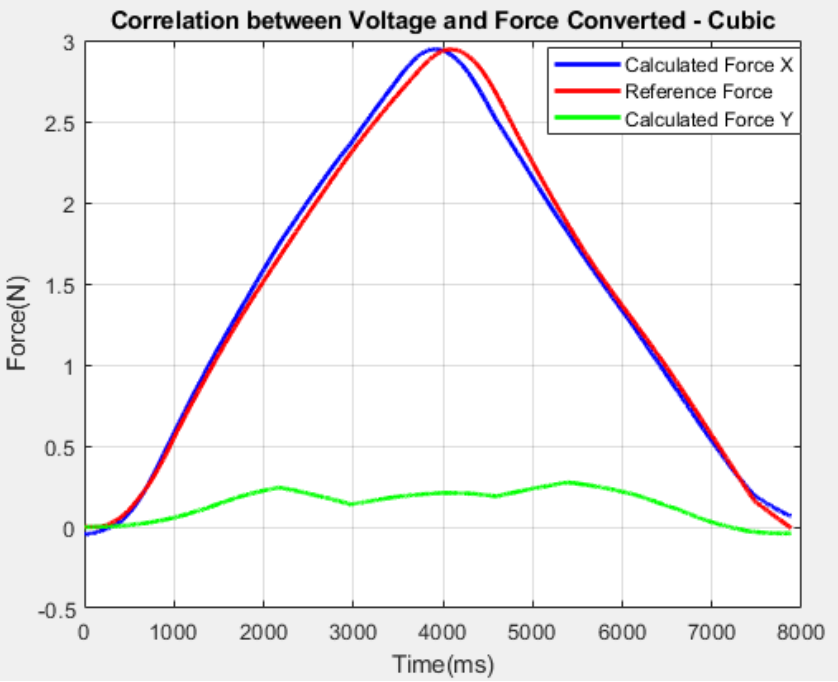

Fig. 181: The comparison between the reference force in red and the calculated forces for the X and Y directions. The blue line indicates the calculated X-directional force and the green line indicates the Y-directional force.

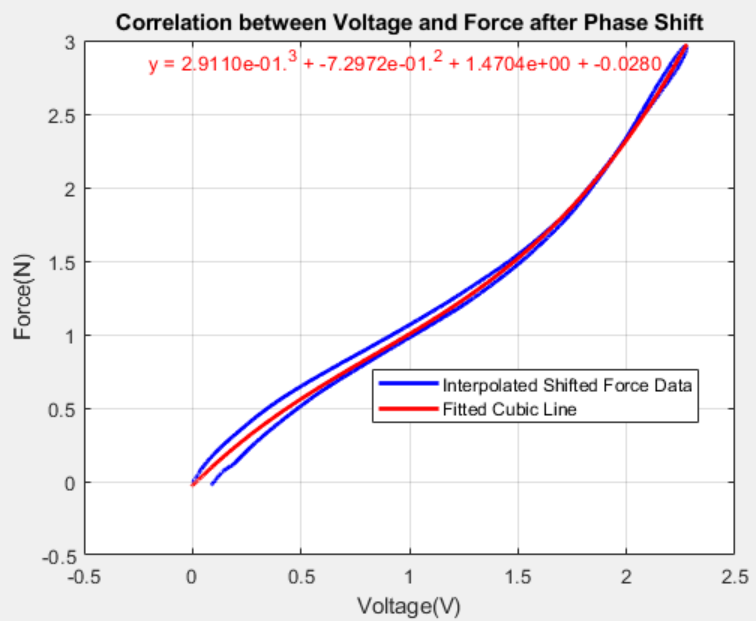

Fig. 182: The hysteresis curve visualizing the comparison between the calculated force and the best fit line used for the conversion during the pressing and releasing of the force sensor. The left most blue line indicates the resting position.

Y-Direction Results

Front analysis point

Figures 183-186 show the voltage response due to force input, the correlation between the voltage response and the force input in the Matlab system analysis toolbox for the best fit line characteristics, the comparison between the converted voltage and the reference force, and the force hysteresis curve for Y-directional testing at the front analysis point respectively.

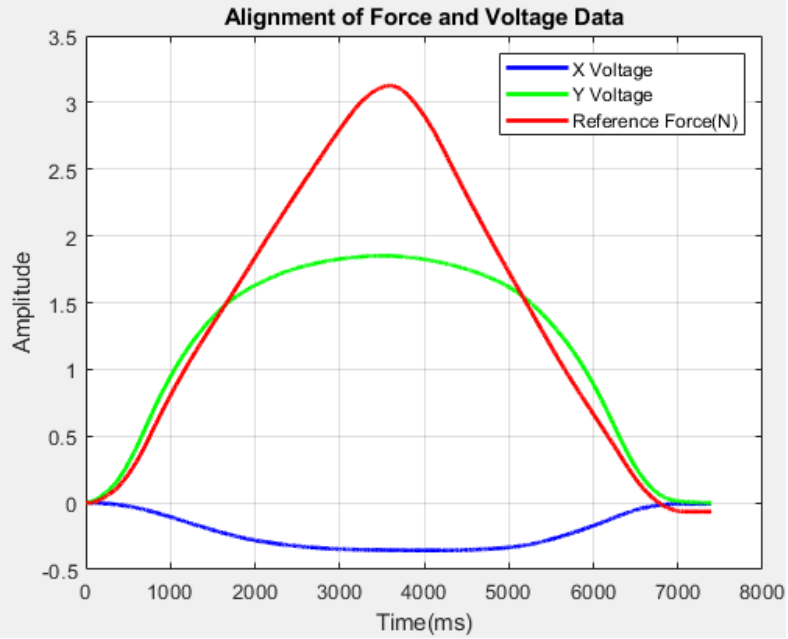

Fig. 183: The comparison between the reference force in red and the output voltages in the X and Y directions. The green line indicates the Y resultant voltage and the blue line indicates the X resultant voltage.

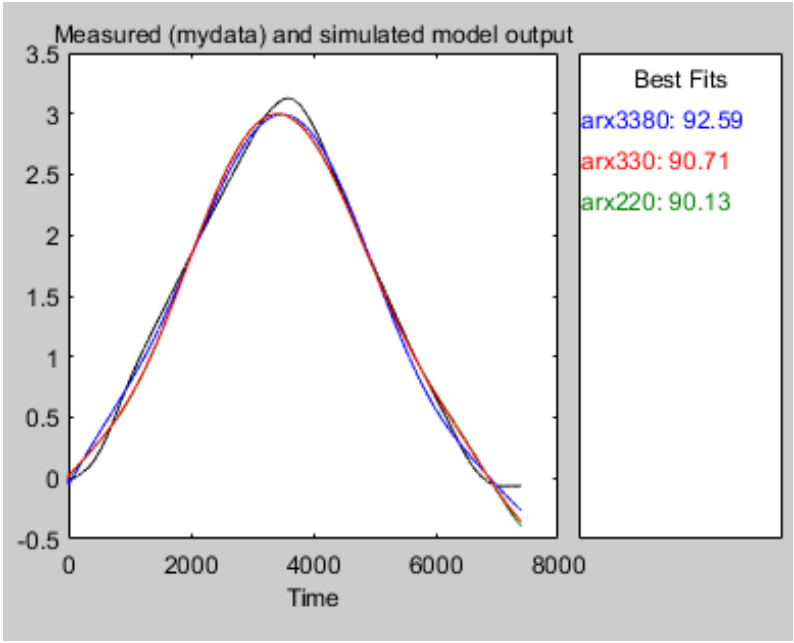

Fig. 184: The system analysis toolbox data report for the best fit line parameters. The resulting best fit line parameters were a cubic line with a delay of 80.

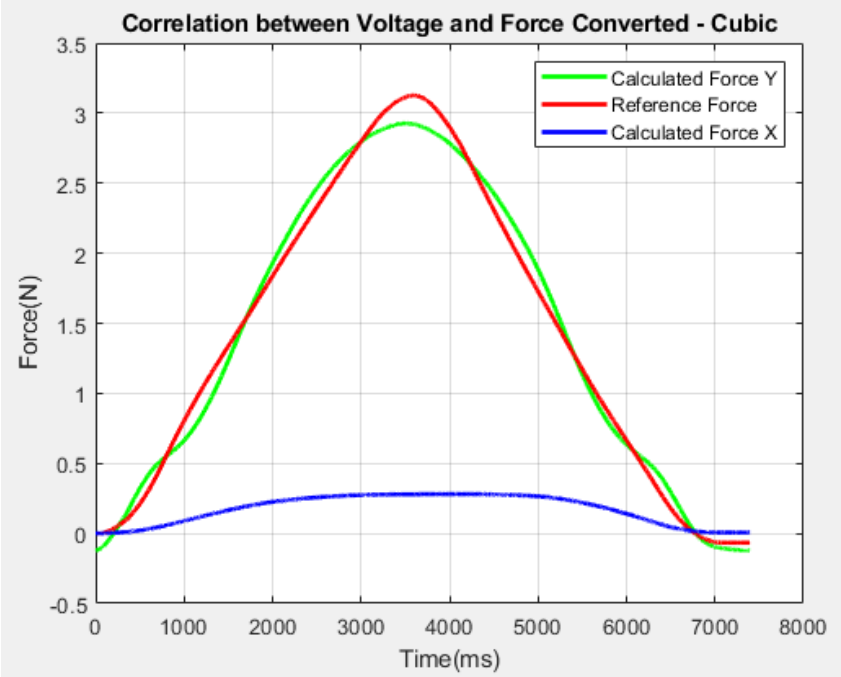

Fig. 185: The comparison between the reference force in red and the calculated forces for the X and Y directions. The green line indicates the calculated Y-directional force and the blue line indicates the X-directional force.

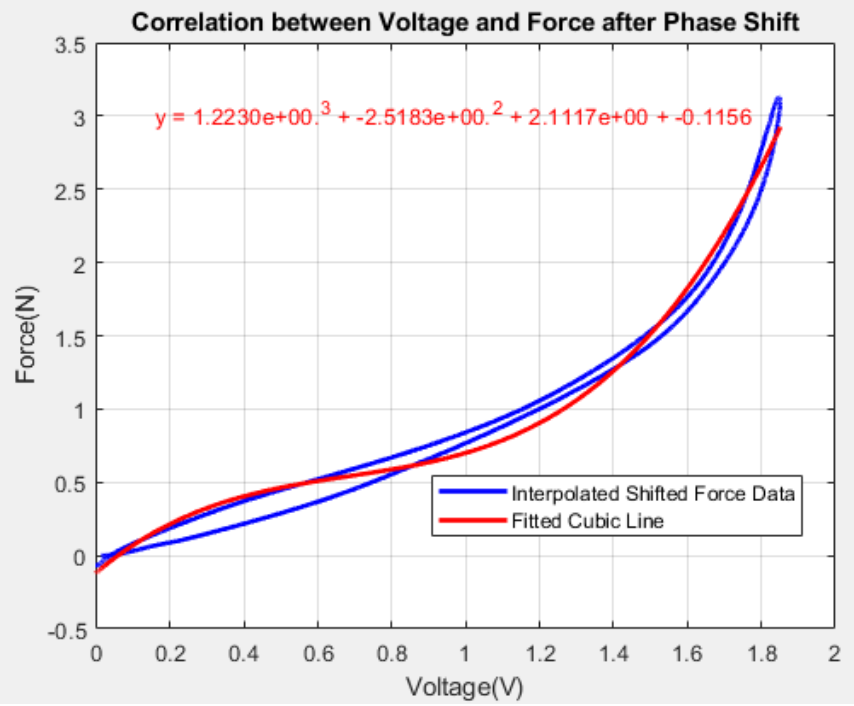

Fig. 186: The hysteresis curve visualizing the comparison between the calculated force and the best fit line used for the conversion during the pressing and releasing of the force sensor. The left most blue line indicates the resting position.

Middle analysis point

Figures 187-190 show the voltage response due to force input, the correlation between the voltage response and the force input in the Matlab system analysis toolbox for the best fit line characteristics, the comparison between the converted voltage and the reference force, and the force hysteresis curve for Y-directional testing at the middle analysis point respectively.

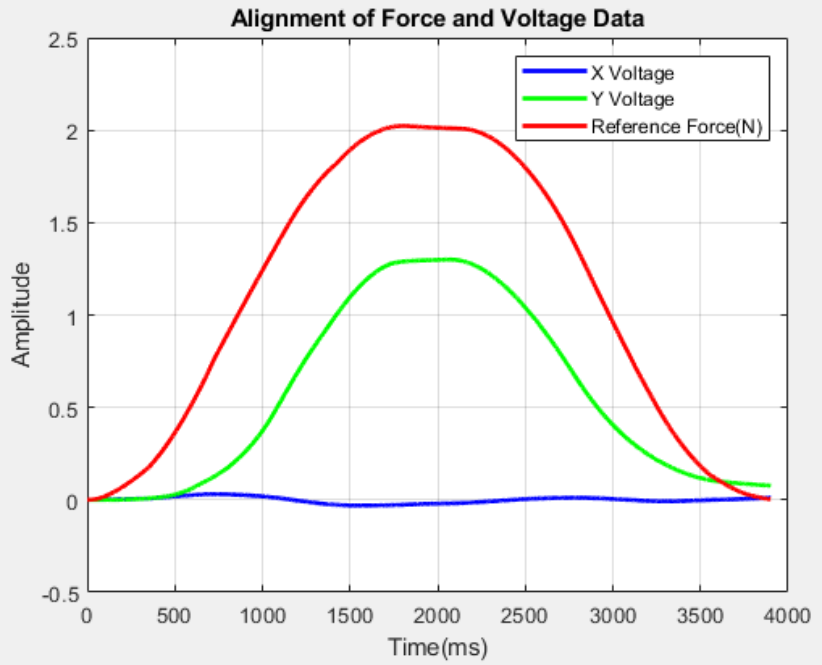

Fig. 187: The comparison between the reference force in red and the output voltages in the X and Y directions. The green line indicates the Y resultant voltage and the blue line indicates the X resultant voltage.

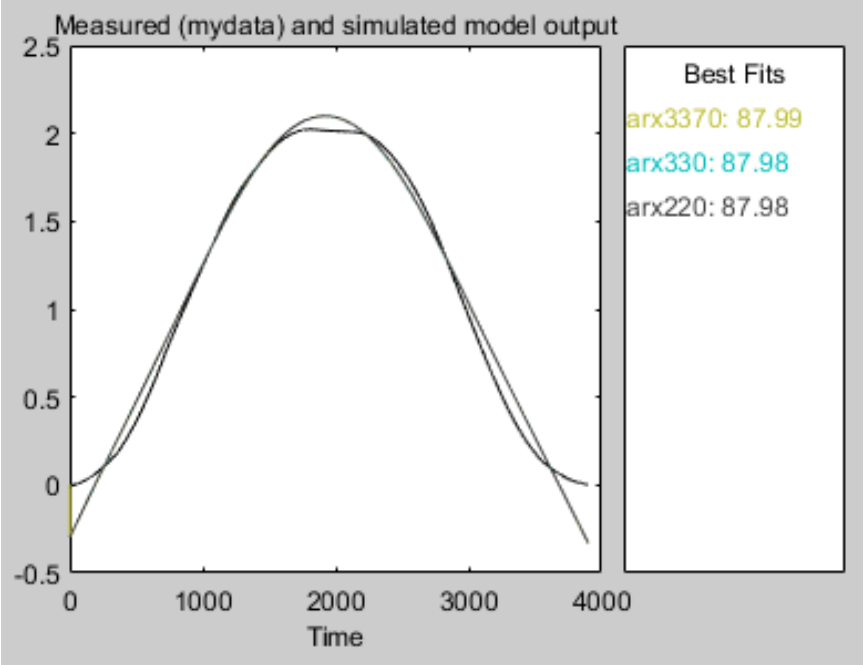

Fig. 188: The system analysis toolbox data report for the best fit line parameters. The resulting best fit line parameters were a cubic line with a delay of 70.

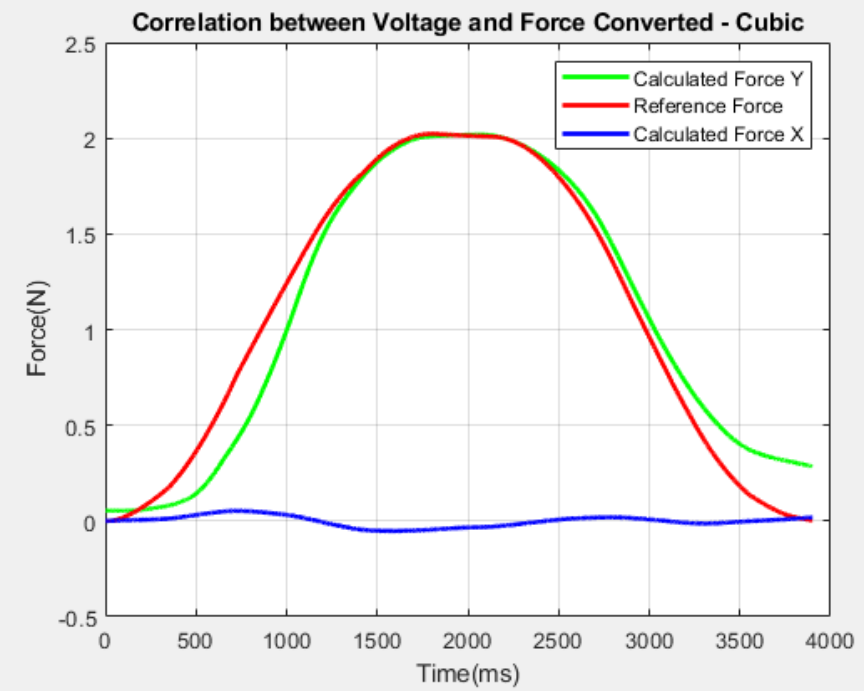

Fig. 189: The comparison between the reference force in red and the calculated forces for the X and Y directions. The green line indicates the calculated Y-directional force and the blue line indicates the X-directional force.

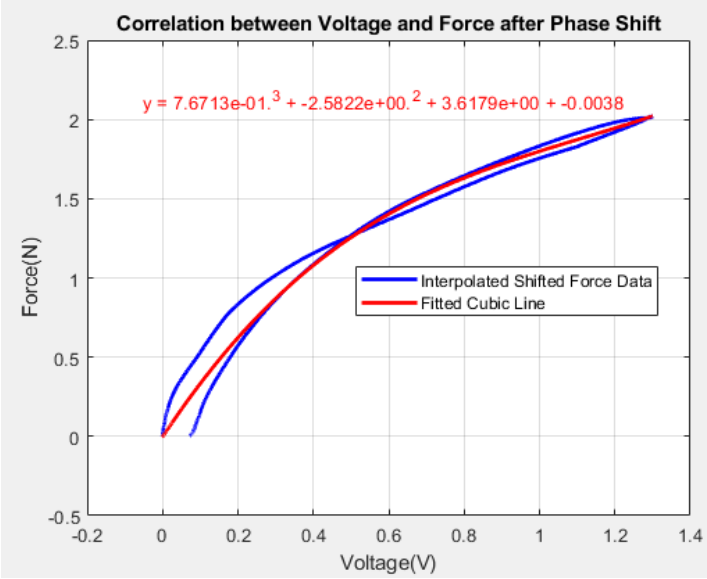

Fig. 190: The hysteresis curve visualizing the comparison between the calculated force and the best fit line used for the conversion during the pressing and releasing of the force sensor. The left most blue line indicates the resting position.

Back analysis point

Figures 191-194 show the voltage response due to force input, the correlation between the voltage response and the force input in the Matlab system analysis toolbox for the best fit line characteristics, the comparison between the converted voltage and the reference force, and the force hysteresis curve for Y-directional testing at the back analysis point respectively.

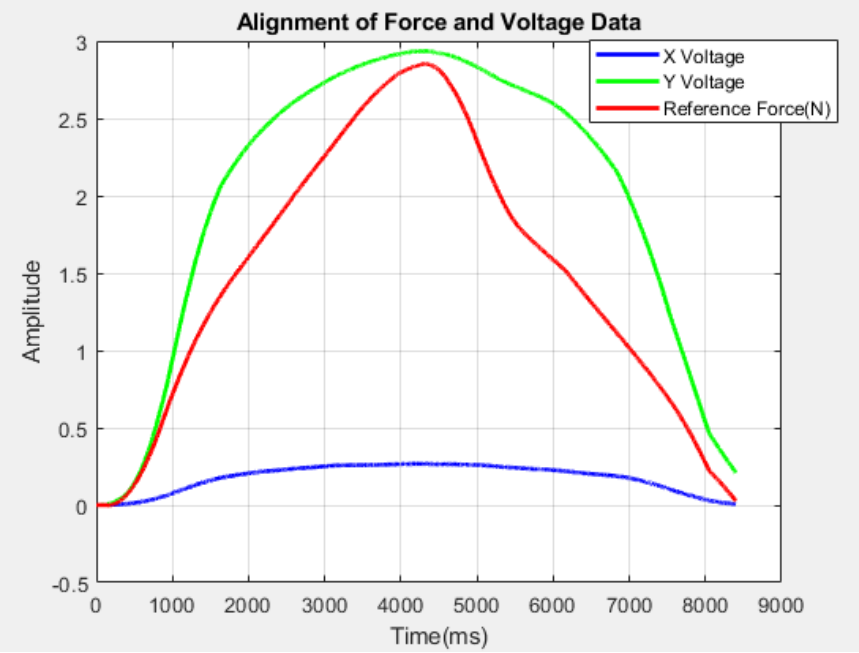

Fig. 191: The comparison between the reference force in red and the output voltages in the X and Y directions. The green line indicates the Y resultant voltage and the blue line indicates the X resultant voltage.

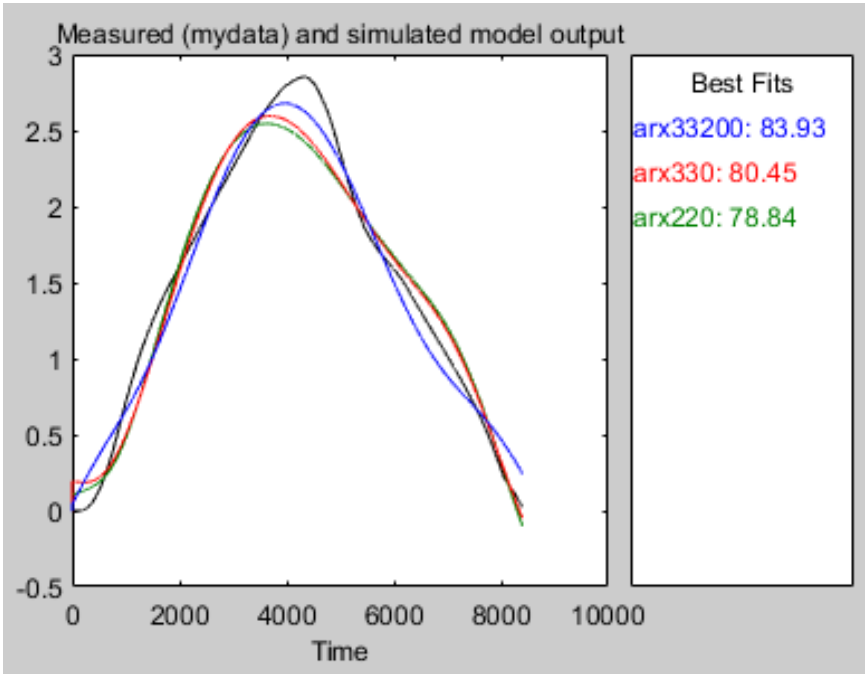

Fig. 192: The system analysis toolbox data report for the best fit line parameters. The resulting best fit line parameters were a cubic line with a delay of 200.

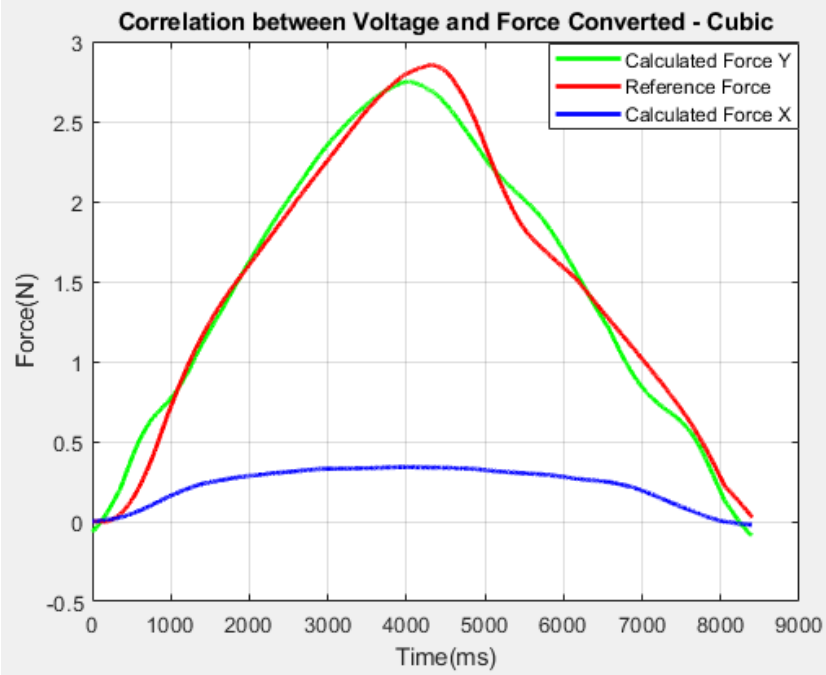

Fig. 193: The comparison between the reference force in red and the calculated forces for the X and Y directions. The green line indicates the calculated Y-directional force and the blue line indicates the X-directional force.

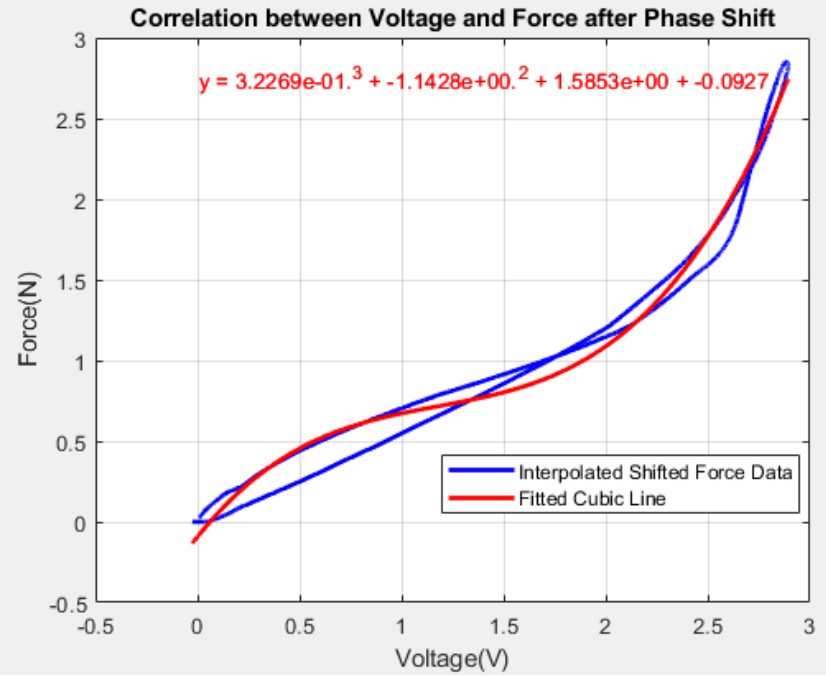

Fig. 194: The hysteresis curve visualizing the comparison between the calculated force and the best fit line used for the conversion during the pressing and releasing of the force sensor. The left most blue line indicates the resting position.

Z-Direction Results

Front analysis point

Figures 195-198 show the voltage response due to force input, the correlation between the voltage response and the force input in the Matlab system analysis toolbox for the best fit line characteristics, the comparison between the converted voltage and the reference force, and the force hysteresis curve for Z-directional testing at the front analysis point respectively.

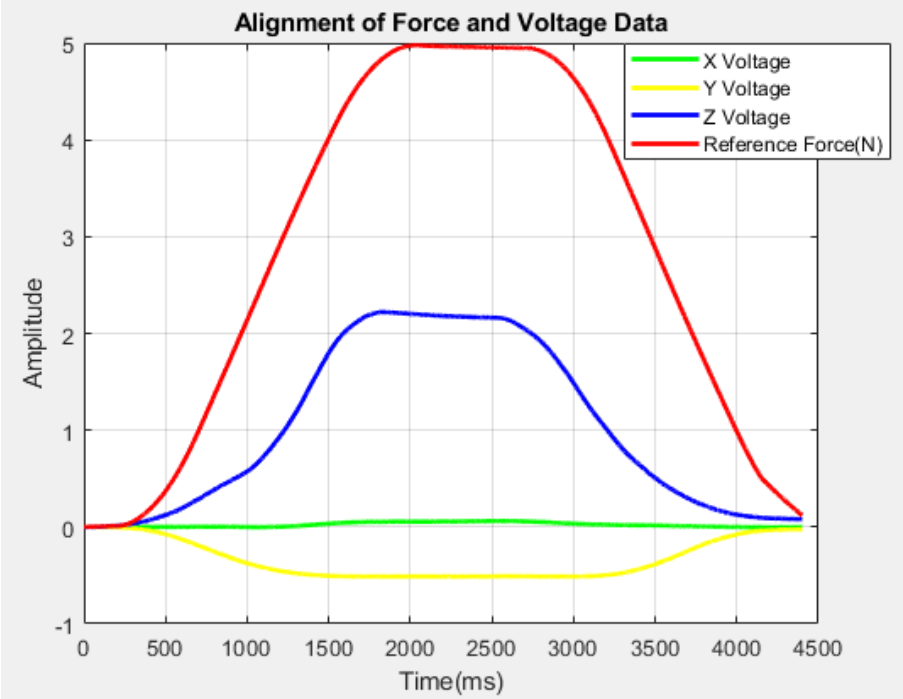

Fig. 195: The comparison between the reference force in red and the output voltages in the X, Y, and Z directions. The green line indicates the X resultant voltage, the yellow line indicates the Y resultant voltage, and the blue line indicates the Z resultant voltage.

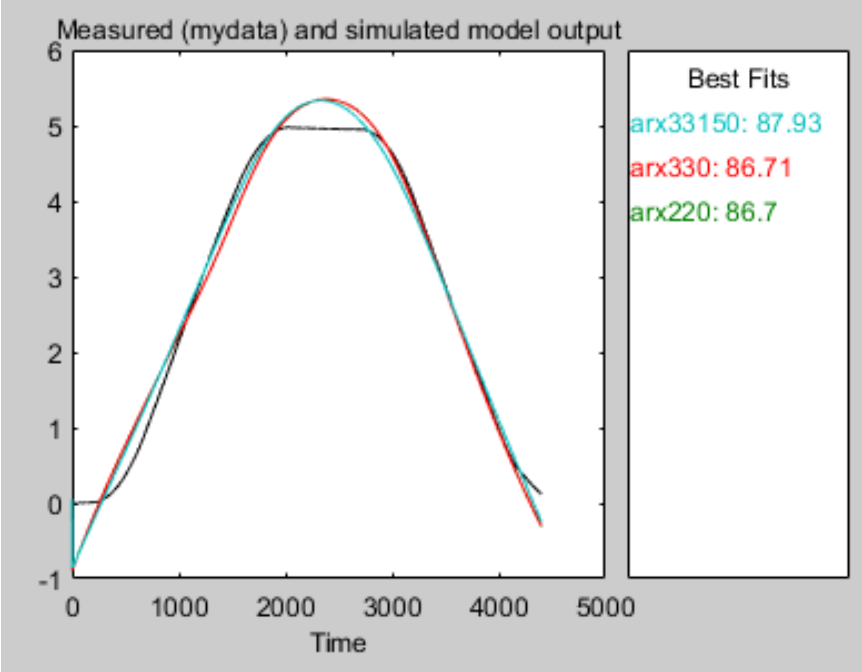

Fig. 196: The system analysis toolbox data report for the best fit line parameters. The resulting best fit line parameters were a cubic line with a delay of 150.

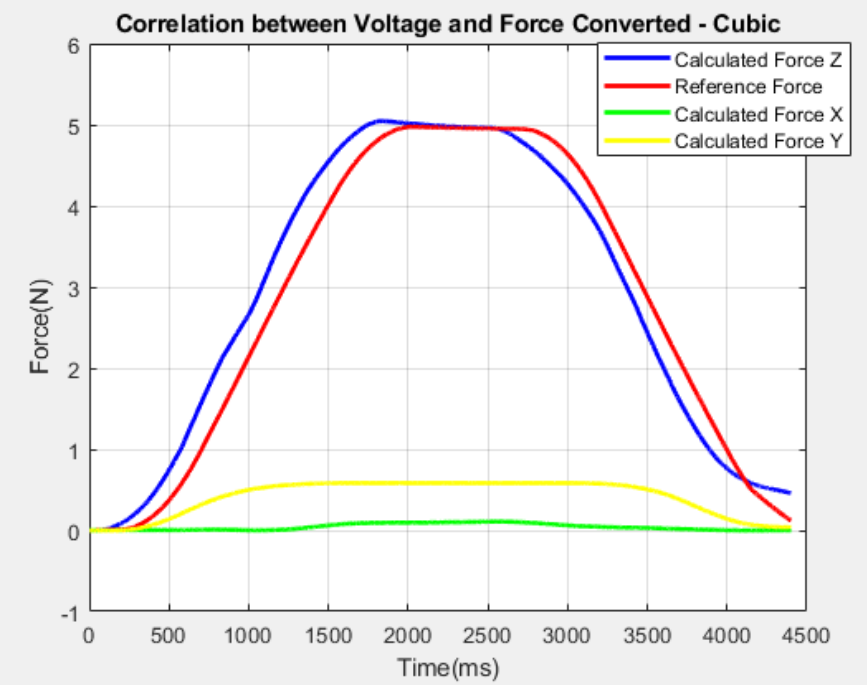

Fig. 197: The visualization of the voltage converted back to force and compared to the reference force. The red is the reference force, the green is the X-direction calculated force response, the yellow is the Y-direction calculated force response, and blue is the Z-directional calculated force response.

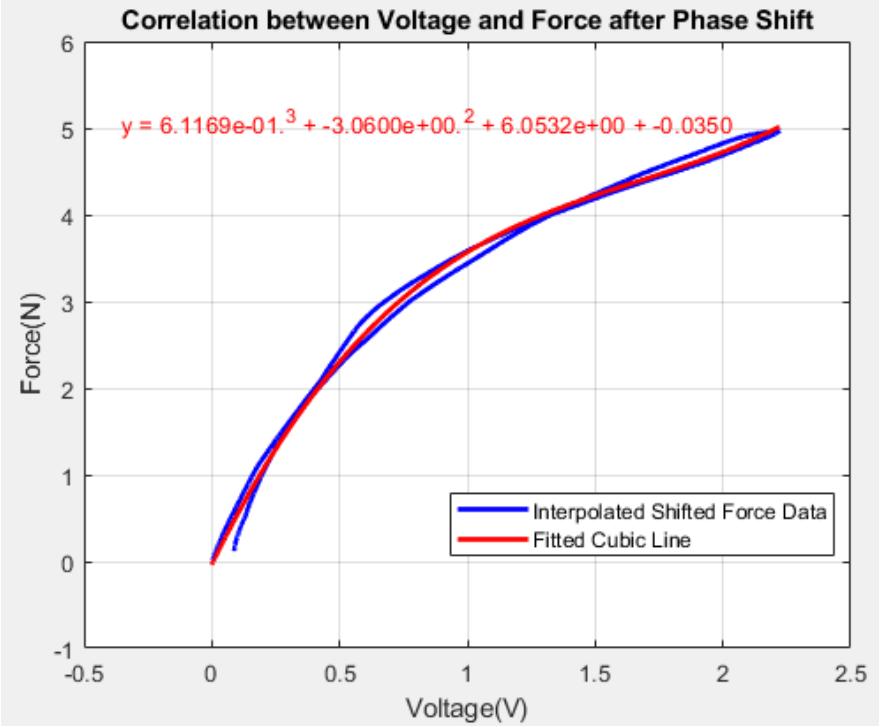

Fig. 198: The hysteresis curve visualizing the comparison between the calculated force and the best fit line used for the conversion during the pressing and releasing of the force sensor. The left most blue line indicates the resting position.

Middle analysis point

Figures 199-202 show the voltage response due to force input, the correlation between the voltage response and the force input in the Matlab system analysis toolbox for the best fit line characteristics, the comparison between the converted voltage and the reference force, and the force hysteresis curve for Z-directional testing at the middle analysis point respectively.

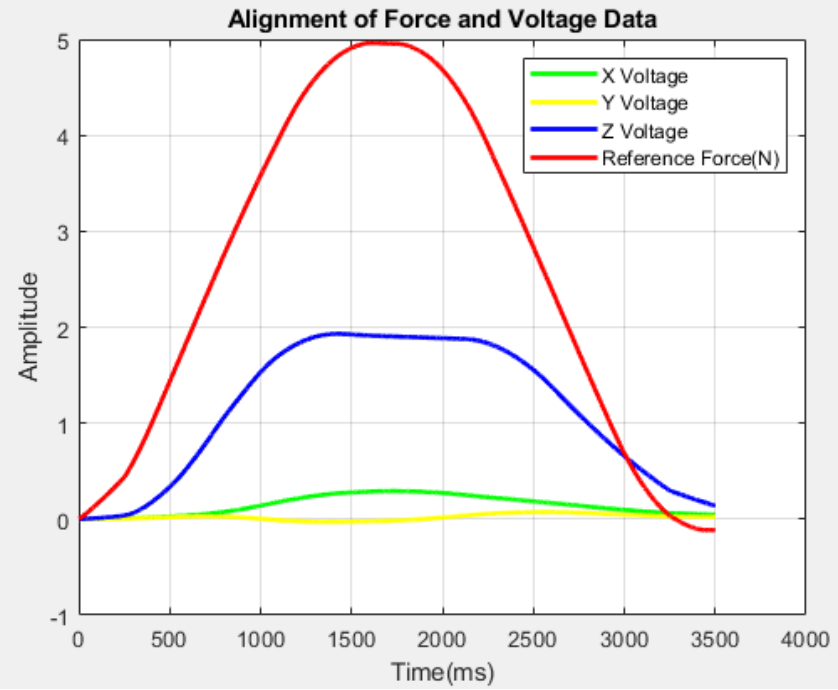

Fig. 199: The comparison between the reference force in red and the output voltages in the X, Y, and Z directions. The green line indicates the X resultant voltage, the yellow line indicates the Y resultant voltage, and the blue line indicates the Z resultant voltage.

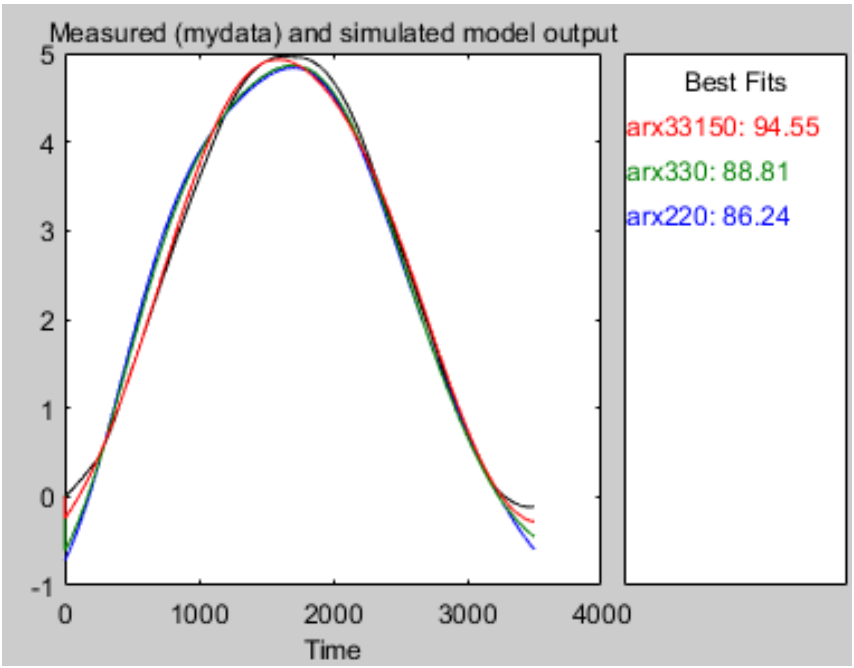

Fig. 200: The system analysis toolbox data report for the best fit line parameters. The resulting best fit line parameters were a cubic line with a delay of 150.

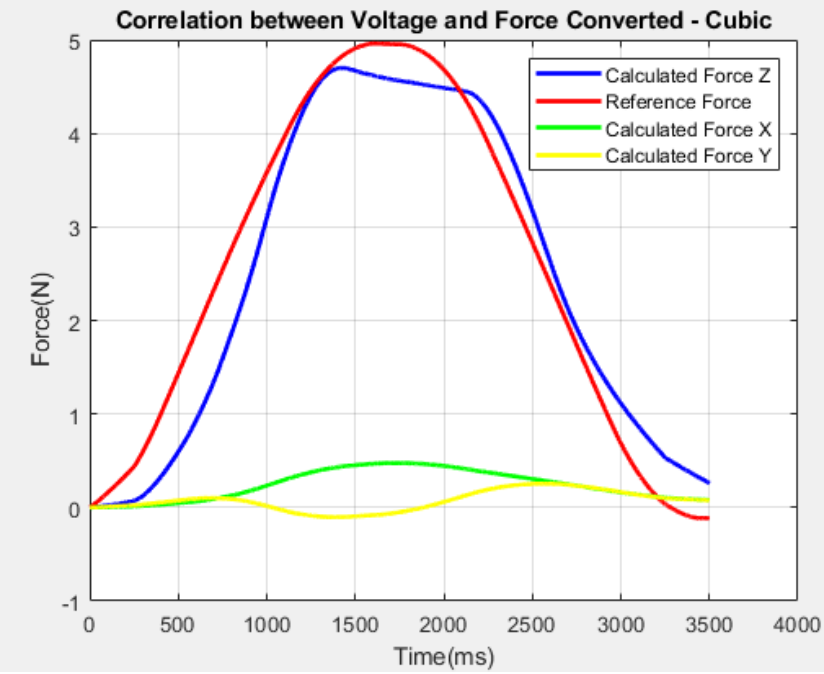

Fig. 201: The visualization of the voltage converted back to force and compared to the reference force. The red is the reference force, the green is the X-direction calculated force response, the yellow is the Y-direction calculated force response, and blue is the Z-directional calculated force response.

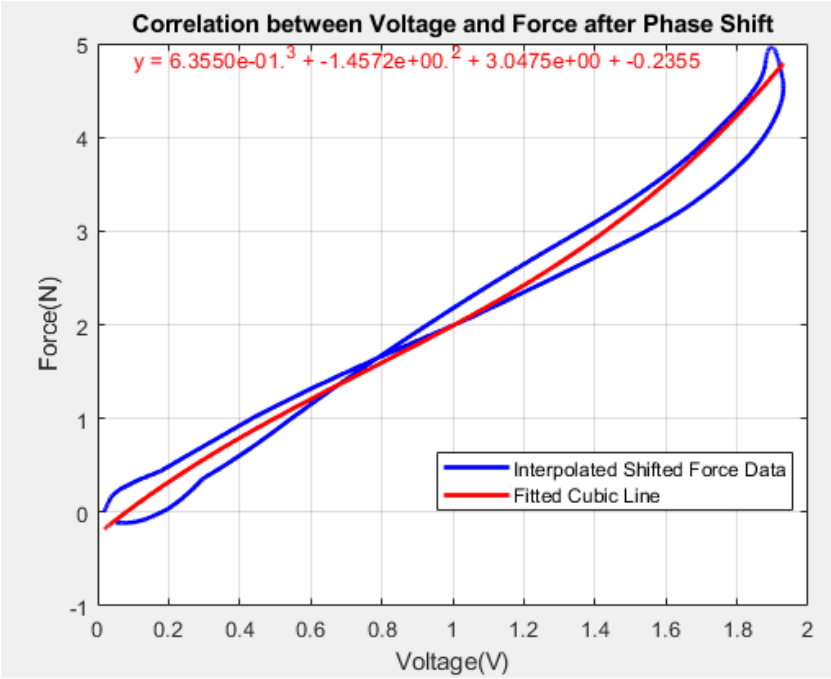

Fig. 202: The hysteresis curve visualizing the comparison between the calculated force and the best fit line used for the conversion during the pressing and releasing of the force sensor. The left most blue line indicates the resting position.

Back analysis point

Figures 203-206 show the voltage response due to force input, the correlation between the voltage response and the force input in the Matlab system analysis toolbox for the best fit line characteristics, the comparison between the converted voltage and the reference force, and the force hysteresis curve for Z-directional testing at the back analysis point respectively.

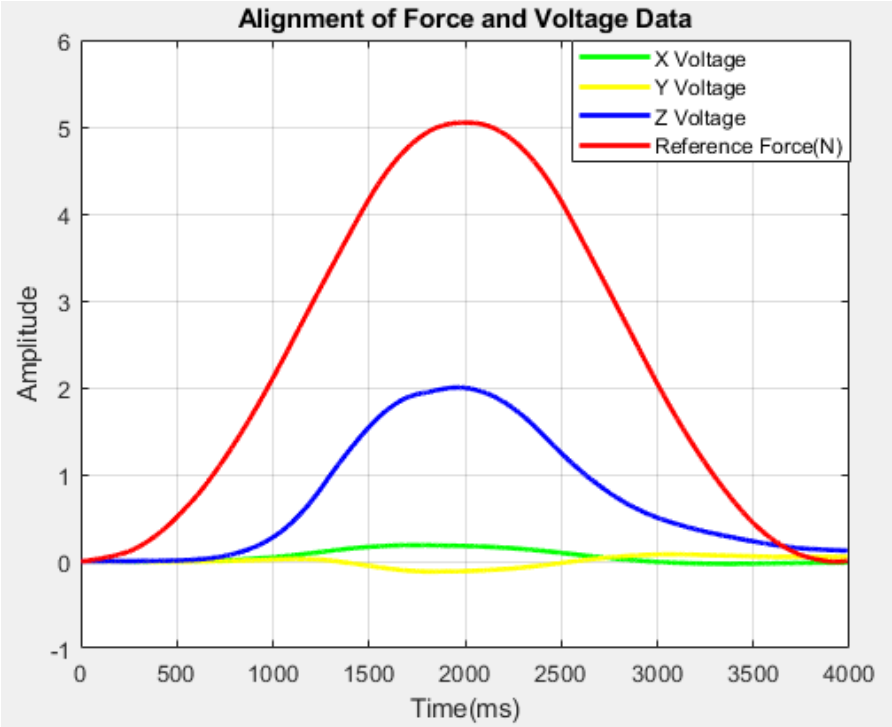

Fig. 203: The comparison between the reference force in red and the output voltages in the X, Y, and Z directions. The green line indicates the X resultant voltage, the yellow line indicates the Y resultant voltage, and the blue line indicates the Z resultant voltage.

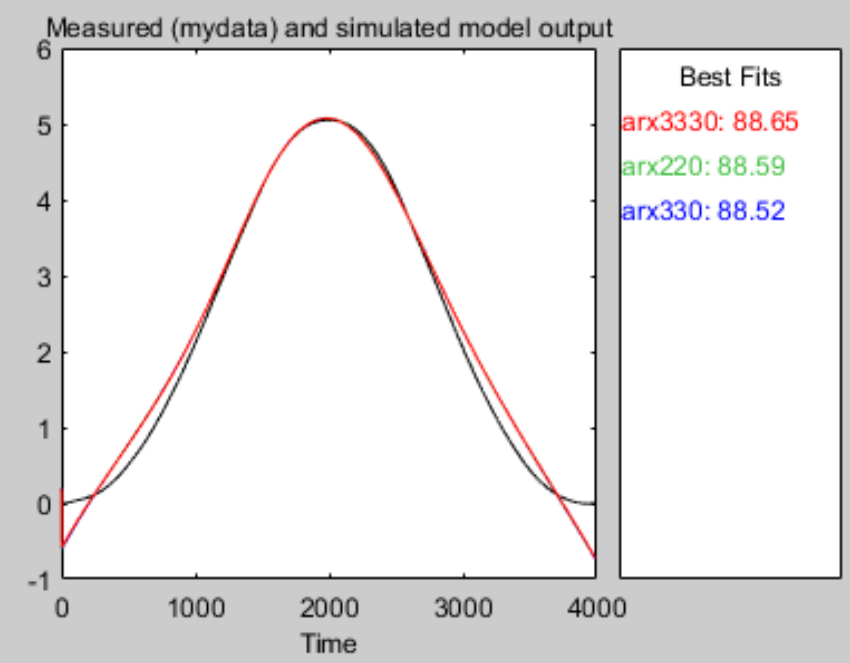

Fig. 204: The system analysis toolbox data report for the best fit line parameters. The resulting best fit line parameters were a cubic line with a delay of 30.

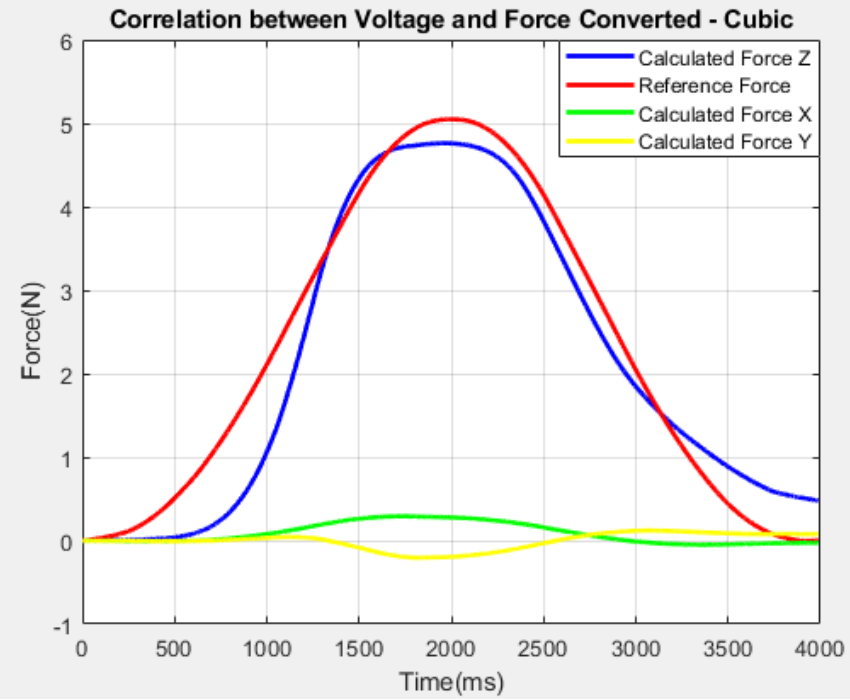

Fig. 205: The visualization of the voltage converted back to force and compared to the reference force. The red is the reference force, the green is the X-direction calculated force response, the yellow is the Y-direction calculated force response, and blue is the Z-directional calculated force response.

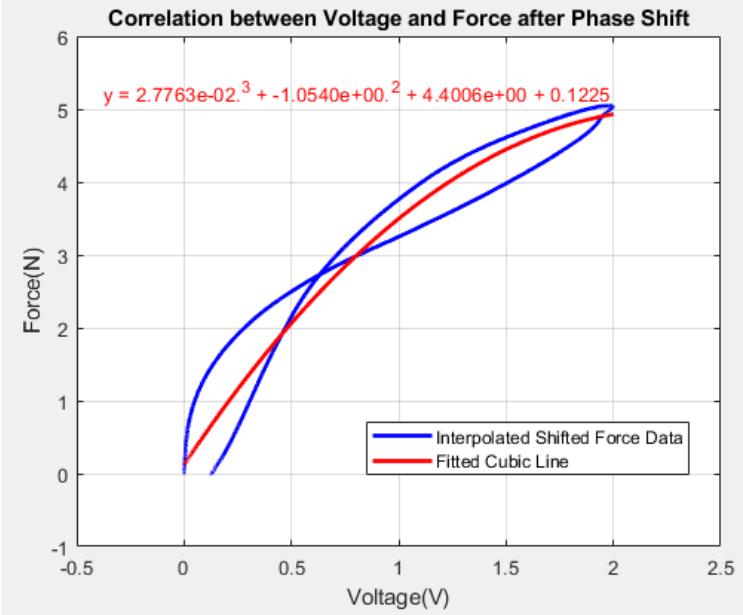

Fig. 206: The hysteresis curve visualizing the comparison between the calculated force and the best fit line used for the conversion during the pressing and releasing of the force sensor. The left most blue line indicates the resting position.

Data Summary

From the collected data, Table 8 indicates each directional equation that would convert output voltage into force application for practical testing.

Table 8: The equations of each directional analyte collected during the theoretical testing of the third design to convert the output voltage back to force when testing practically. Y indicates the force calculated while X refers to the voltage collected from the pair of resistors that correlate to that direction.

Group of Sensors	Direction of Analysis	Equation
Front	X	$Y = 0.20339 * X^3 – 0.46934 * X^2 + 1.7177 * X – 0.07$
	Y	$Y = 1.223 * X^3 – 2.5183 * X^2 + 2.1117 * X – 0.1156$
	Z	$Y = 0.61169 * X^3 – 3.06 * X^2 + 6.0532 * X – 0.035$
Middle	X	$Y = 0.1961 * X^3 – 0.27615 * X^2 + 1.6913 * X + 0.0009$
	Y	$Y = 0.76713 * X^3 – 2.5822 * X^2 + 3.6179 * X – 0.0038$
	Z	$Y = 0.6355 * X^3 – 1.4572 * X^2 + 3.0475 * X – 0.2355$
Back	X	$Y = 0.2911 * X^3 – 0.72972 * X^2 + 1.4704 * X – 0.028$
	Y	$Y = 0.32269 * X^3 – 1.1428 * X^2 + 1.5853 * X – 0.0927$
	Z	$Y = 0.027763 * X^3 – 1.054 * X^2 + 4.4006 * X + 0.1225$

Finally, the error of this system is tabulated in Table 9. In this table, the average error percentage for values within the working range of the system, the median percent error, the difference in maximum values for the reference force and the calculated force, the maximum percent error of the working range, and the maximum error of the working range normalized across the range of the system.

Table 9: The tabulated percent error results collected during testing of the insole system. The "modified" indication pertains to analysis of the system within the working range of values above 0.5 N. Values between 0-0.5 N drastically increased the overall error values of the system.

Analysis Location	Average Error Percent (Modified)	Median Error Percent	Peak Difference Error Percent	Maximum Error Percent (Modified)	Maximum Error Percent (Normalized)
Front X	6.6494	7.8282	0.47378	32.8333	11.1259
Middle X	5.6333	6.6102	1.6875	29.6746	9.8401
Back X	2.428	2.5774	0.28751	15.1296	5.1279
Front Y	6.4562	7.7811	6.5472	16.7097	5.2335
Middle Y	2.193	2.9811	0.12141	21.5355	10.6427
Back Y	5.1732	5.2829	3.7308	13.4994	4.7315
Front Z	2.9336	2.0538	0.81025	25.8683	5.1979
Middle Z	6.3115	7.3393	3.4899	25.5607	5.0354
Back Z	13.1031	13.1031	4.7702	66.4583	13.1539
Average	5.65	6.17	2.44	27.47	7.71

The system at this point was moved to begin practical testing by stepping and walking with the insole system. However, the third design lacked the structural integrity between the cut sensors and the central connection piece required for practical testing, leading to the system breaking prior to practical testing.

Chapter 5: Discussion

For the purpose of diversifying the different datasets that were collected during testing for research development, discussion will be separated into three sections: experimental testing for each insole design, practical testing for each insole design, and general issues experienced during research.

Experimental Testing

The experimental testing conducted under structured force inputs yielded error analysis that provided insight into the improvement efforts between insole design iterations. In the first iteration, all error metric categories yielded the largest values, indicating an unoptimized design in several categories. The second insole design yielded better results in each category in comparison to design one. However, despite the system improving in all metric categories, it is still important to realize the limitations of the sensing positions due to the size limitations of the sensors. Design three served to functionally improve this, successfully providing improved positioning of the modified sensors in more optimal locations. Additionally, design three continued to improve in most error metric categories, with the lowest average working range error of 5.65% and a maximum normalized percent error of 7.71%. However, the peak difference error was 2.44%, slightly worse than the second insole design of 1.84%.

Practical Testing

Practical testing was conducted for designs one and two. Focusing on design one, several design characteristics proved beneficial to analyze for future design optimization. Firstly, as the force application from the foot is much larger in surface area and less

optimized in location, the system was extremely erratic for practical testing. However, testing the system while wearing a shoe improved response at all analysis locations, leading to design improvements to the central connection piece utilized for designs two and three. The increased surface area of the central connection piece improved the response from the insole system while testing practically. Additionally, the adhesion location of the sensors to the central connection piece proved to be a limiting factor for the first insole design, consistently resulting in disconnected sensors and therefore a nonfunctional insole system. However, the central connection piece used for design two protected the adhesion point, improving the durability of the insole system tremendously.

Focusing on the gait pattern identification of design two, each system analysis point provided varied accuracy with reference to the outputs due to different gait methods. The front analysis point consistently provided clear, repeatable, and expected outputs for each movement method. Likely, this correlates to the proximity of the front sensor location and the optimized sensor location used for the third insole design. Alternatively, the middle sensing location proved to be much more erratic with outputs during practical testing.

The back sensing location provided a unique scenario comparatively with relation to positioning. Despite the similarity between the back sensing location used for design two and the optimal sensing location used for design three, the back sensing location of design two still provided erratic results for certain gait analysis tests, namely walking and sidestepping in both directions. This may be due to direct force being applied to the sensing film of the sensors rather than isolated force applied to the central connection

piece. In addition to this, the back sensing location most likely experience the greatest variety for force positioning, due to the nature of the heel during movement.

Although the practical testing for design three yielded promising results with regard to error metrics and sensor location optimization, the connection points between the sensors and the central connection piece proved unstable in a practical sense. Research is ongoing to improve the adhesion of the sensors to the central connection piece in design three.

General Discussion

Several design flaws were discovered throughout the creation of each insole design. Most notably, the current insole designs are not conducive for repairs. Once the sensing units are molded into the insole system, repair options for broken sensors results in further issues. If a sensor disconnects from the central connection piece, the gel must be dismantled to remove the sensing units, reattach the sensor, and replaced. However, considering the design reliance on a symmetrical system, repaired sensing units typically resulted in asymmetrical gel remolding after repairs.

Despite this difficulty, the utilization of a gel as the main material in an insole system improved comfortability and size of an insole system without reducing the durability or viability of the system overall. The insole design incorporated an end-user friendly design, iteratively prioritizing improved results without the cost of alternative factors such as comfort or cost. Regardless of design iteration, system remained viable for experimental testing for all sensing locations and directional testing. By modifying the sensors in house, overall research costs were able to remain minimal, resulting in a system less than $100 in cost. Overall, optimizations were made in terms of reduced

rigidity, size, comfortability, cost, and directional analysis capability and optimized sensing locations.

Back Matter

Future Work

During this research, there were several limiting factors that were established throughout the progression of this research. One of the initial difficulties planned around when designing the system was the size of the sensing system itself. Each sensor is approximately 1.3” including the metal mounting pins and center system point designed to connect the four sensor is approximately 0.4”. After connecting each sensor to the center point, the total length across including both sensors and the center point accumulates to approximately 2.8”, providing a minimum size requirement for the system to fit into a shoe. The smallest width of a shoe is found in the heel, so the original design incorporated a mold design that was at least 3” wide with relation to the heel. This design correlated approximately to a US size 11 shoe.

Although design efforts were made and significantly decreased the minimum size required to incorporate this system into a shoe, these efforts should continue to be investigated and further improved to ensure this system can be utilized by all individuals, regardless of shoe size. Modifications to the sensor were only capable at the bending end of the sensor, the sensors could be reduced in size even further if modifications near the metal pins was viable as well.

Considering the differences between the structured experimental testing results and practical testing results, it is clear to see that the increased area of force from the pressure of a foot and the body weight of an individual causes the system to behave differently. Utilizing the promising results from design 3 consisting of reduced sensitivity

and shortened sensor length, another design should be investigated that utilizes a shortened sensitivity but orients the conductive ink further away from the location of force. As mentioned, the smallest width of the system will consistently be located at the heel of any system design, so this would also ideally be the first limiting factor with regard to sensor placement.

The width of the heel section of the insole system is approximately 75 mm and the shortened conductive ink for each modified sensor from design 3 was 4 mm. Seeing as each analysis point requires two oppositional sensors, excluding the size of the sensor itself, this would account for 8 mm of the available space, resulting in 67 mm remaining in the heel region of the insole system. However, if the conductive ink section of the sensors were located at the edges of the insole system at the heel, this would disallow direct force to the conductive ink of sensor. Theoretically, this would result in uniform responses with respect to the experimental testing conducted with the force sensor and the practical testing by using the system.

One large limiting factor with relation to the size of the system is the minimized population size of viable users for the product. As mentioned, this system is estimated to be a size 11 in US men's sizing. With the current design, the insole system cannot fit into any sizes smaller. Therefore, further investigation is required to reduce the size of the system to increase the viable candidates of this system. This would incorporate the potential alternative size discussed previously as well as alternative sensor locations.

In tandem with this comes the implementation of a wireless system that can operate in shoes without an external power supply unit such as the one used in this research. This would require the implementation of a battery system as well as a wireless

sensing function for the voltage during use of the insole system. For safety of the user, the voltage running through the system could be investigated and potentially lowered. In either case, this would likely result in digital amplification instead of the physical amplification of the signal amplifiers used in this research for preliminary results.

The most likely next research involving this insole system should work to improve the system identification, namely correlating the voltage responses of the system with certain gait methods. The initial results demonstrated in this paper certainly indicate patterns in response, but further research should involve identification and demonstration of potentially dangerous force distributions. This could include pronating, supinating, walking on uneven terrain, or even less dangerous distributions such as analysis as individuals use the system while sidestepping as tested in this research.

With this in mind, it should also be a focus to improve the end-user's quality of interaction with the system readings. This could incorporate something such as a mobile application that allows the user to see live updates on their walking patterns or general patterns over a set period of time. The system would ideally indicate gait trends and, in more serious cases, could recommend seeing a physician for treatment or implementation of orthopedic inserts to counteract the unhealthy gait. Assuming efforts can be made in reducing the size of the system, ideally alternative designs could be placed within orthopedic inserts as well to measure their progress in improving their walking patterns. The system could also be implemented with less essential functions, such as monitoring weight, blood pressure, and temperature of the user.

Additionally, this research focused solely on the production of an initial insole system design with relation to limited participants. Although the research indicates

consistent results for preliminary analysis, this system should be tested in a user study with a diverse population for varied and valuable analysis. Potential populations that should be present for future analysis should include individuals with diabetic foot ulcers as similar research tends to focus on, elderly populations, package delivery employees, weight lifters, as well as healthy individuals.

References

[1] I. Almuteb, R. Hua, and Y. Wang, “Smart Insoles Review (2008-2021): Applications, potentials, and future,” *Smart Health*, vol. 25, p. 100301, Jul. 2022. doi:10.1016/j.smhl.2022.100301

[2] J. Kymissis, C. Kendall, J. Paradiso and N. Gershenfeld, "Parasitic power harvesting in shoes," *Digest of Papers. Second International Symposium on Wearable Computers (Cat. No.98EX215)*, Pittsburgh, PA, USA, 1998, pp. 132-139, doi: 10.1109/ISWC.1998.729539.

[3] Pappas, I. P. I., Keller, T., Mangold, S., Popovic, M. R., Dietz, V., & Morari, M. (2004). A reliable gyroscope-based gait-phase detection sensor embedded in a shoe insole. *IEEE Sensors Journal*, *4*(2), 268–274. https://doi.org/10.1109/JSEN.2004.823671

[4] Parikesit, E., Mengko, T. L. R., & Zakaria, H. (2011). Wearable gait measurement system based on accelerometer and pressure sensor. *2011 2nd International Conference on Instrumentation, Communications, Information Technology, and Biomedical Engineering*, 395–398. https://doi.org/10.1109/ICICI-BME.2011.6108634

[5] Chen, J., Zhang, M., Dai, Y., Xie, Y., Tian, W., Xu, L., & Gao, S. (2020). A force–voltage responsivity stabilization method for piezoelectric-based insole gait analysis for high detection accuracy in health monitoring. *International Journal of Distributed Sensor Networks*, *16*(3), 155014772090544-. https://doi.org/10.1177/1550147720905441

[6] Dai, Y., Xie, Y., Chen, J., Kang, S., Xu, L., & Gao, S. (2020). A lamination-based piezoelectric insole gait analysis system for massive production for Internet-of-health things. *International Journal of Distributed Sensor Networks*, *16*(3), 155014772090543-. https://doi.org/10.1177/1550147720905431

[7] Deng, C., Tang, W., Liu, L., Chen, B., Li, M., & Wang, Z. L. (2018). Self -Powered Insole Plantar Pressure Mapping System. *Advanced Functional Materials*, *28*(29). https://doi.org/10.1002/adfm.201801606

[8] Masum, H., Chattopadhyay, S., Bhaumik, S., & Ray, R. (2016). Utilisation of skewness of wavelet-based approximate coefficient in walking speed assessment. *IET Science, Measurement & Technology*, *10*(8), 977–982. https://doi.org/10.1049/iet-smt.2016.0263

[9] Howell, A. M., Kobayashi, T., Hayes, H. A., Foreman, K. B., & Bamberg, S. J. M. (2013). Kinetic Gait Analysis Using a Low-Cost Insole. *IEEE Transactions on Biomedical Engineering*, *60*(12), 3284–3290. https://doi.org/10.1109/TBME.2013.2250972

[10] Keatsamarn, T., Visitsattapongse, S., Aoyama, H., & Pintavirooj, C. (2021). Optical-Based Foot Plantar Pressure Measurement System for Potential Application in Human Postural Control Measurement and Person Identification. *Sensors (Basel, Switzerland)*, *21*(13), 4437-. https://doi.org/10.3390/s21134437

[11] Safarloo, S., Núñez-Cascajero, A., Sanchez-Gomez, R., & Vázquez, C. (2022). Polymer Optical Fiber Plantar Pressure Sensors: Design and Validation. *Sensors (Basel, Switzerland), 22*(10), 3883-. https://doi.org/10.3390/s22103883

[12] Gabriele Rescio, Alessandro Leone, Luca Francioso, & Pietro Siciliano. (2018). Sensorized Insole for Diabetic Foot Monitoring. *Proceedings*, *2*(13), 860-. https://doi.org/10.3390/proceedings2130860

[13] L. Wang et al., "A portable insole system to simultaneously measure plantar pressure and shear stress," IEEE Sensors Journal, vol. 22, no. 9, pp. 9104–9113, 2022. doi:10.1109/jsen.2022.3162713

[14] L. Du, X. Zhu, and J. Zhe, "An Inductive Sensor for Real-Time Measurement of Plantar Normal and Shear Forces Distribution," *IEEE transactions on bio-medical engineering/IEEE transactions on biomedical engineering*, vol. 62, no. 5, pp. 1316–1323, May 2015, doi: https://doi.org/10.1109/tbme.2014.2386136.

[15] Cha, Y., Kim, H., & Kim, D. (2018). Flexible Piezoelectric Sensor-Based Gait Recognition. *Sensors (Basel, Switzerland), 18*(2), 468-. https://doi.org/10.3390/s18020468

[16] Lind, R. F., Love, L. J., Rowe, J. C., & Pin, F. G. (2009). Multi-axis foot reaction force/torque sensor for biomedical applications. *2009 IEEE/RSJ International Conference on Intelligent Robots and Systems*, 2575–2579. https://doi.org/10.1109/IROS.2009.5353917

[17] Mori, T., Hamatani, M., Noguchi, H., Oe, M., & Sanada, H. (2012). Insole-Type Simultaneous Measurement System of Plantar Pressure and Shear Force During Gait for Diabetic Patients. *Journal of Robotics and Mechatronics*, *24*(5), 766–772. https://doi.org/10.20965/jrm.2012.p0766

[18] Hu, S., Li, H., Lu, W., Han, T., Xu, Y., Shi, X., Peng, Z., & Cao, X. (2024). Triboelectric Insoles with Normal-Shear Plantar Stress Perception. *Advanced Functional Materials*, *34*(16). https://doi.org/10.1002/adfm.202313458

[19] Sorrentino, I., Chavez, F. J. A., Latella, C., Fiorio, L., Traversaro, S., Rapetti, L., Tirupachuri, Y., Guedelha, N., Maggiali, M., Dussoni, S., Metta, G., & Pucci, D. (2020). A Novel Sensorised Insole for Sensing Feet Pressure Distributions. *Sensors (Basel, Switzerland), 20*(3), 747-. https://doi.org/10.3390/s20030747

[20] Mustufa, Y. S. A., Barton, J., O'Flynn, B., Davies, R., McCullagh, P., & Zheng, H. (2015). Design of a smart insole for ambulatory assessment of gait. *The Institute of Electrical and Electronics Engineers, Inc. (IEEE) Conference Proceedings*, 1-.

[21] Hu, F.-L., Jiang, D.-L., Xuan, X.-W., Li, H.-J., & Li, M.-J. (2024). High-Sensitivity Plantar Pressure Antenna Sensor Based on EBG Array for Gait Monitoring. *IEEE Sensors Journal*, *24*(8), 1–1. https://doi.org/10.1109/JSEN.2024.3372947

[22] A. Ohnishi, T. Terada, and M. Tsukamoto, “A Method for Recognizing Postures and Gestures Using Foot Pressure Sensors,” *Journal of Information Processing*, vol. 27, no. 0, pp. 348–358, 2019, doi: https://doi.org/10.2197/ipsjjip.27.348.

[23] Sazonov, E. S., Hegde, N., & Wenlong Tang. (2013). Development of SmartStep: An insole-based physical activity monitor. *2013 35TH ANNUAL INTERNATIONAL CONFERENCE OF THE IEEE ENGINEERING IN MEDICINE AND BIOLOGY SOCIETY (EMBC)*, *2013*, 7209–7212. https://doi.org/10.1109/EMBC.2013.6611221

[24] Roden, T., LeGrand, R., Fernandez, R., Brown, J., Deaton, J., & Ross, J. (2014). Development of a smart insole tracking system for physical therapy and athletics. *Proceedings of the 7th International Conference on Pervasive Technologies Related to Assistive Environments*, 1–6. https://doi.org/10.1145/2674396.2674415

[25] J. Jo and H. Park, “RFInsole: Batteryless Gait-Monitoring Smart Insole Based on Passive RFID Tags,” Sep. 2021, doi: https://doi.org/10.1145/3460421.3478810.

[26] Doriot, N., & Cheze, L. (2004). A three-dimensional kinematic and dynamic study of the lower limb during the stance phase of gait using an homogeneous matrix approach. *IEEE Transactions on Biomedical Engineering*, *51*(1), 21–27. https://doi.org/10.1109/TBME.2003.820357

[27] Moro, M., Marchesi, G., Hesse, F., Odone, F., & Casadio, M. (2022). Markerless vs. Marker-Based Gait Analysis: A Proof of Concept Study. *Sensors (Basel, Switzerland)*, *22*(5), 2011-. https://doi.org/10.3390/s22052011

[28] Ceseracciu, E., Sawacha, Z., & Cobelli, C. (2014). Comparison of Markerless and Marker-Based Motion Capture Technologies through Simultaneous Data Collection during Gait: Proof of Concept. *PloS One*, *9*(3), e87640–e87640. https://doi.org/10.1371/journal.pone.0087640

[29] Lonini, L., Moon, Y., Embry, K., Cotton, R. J., McKenzie, K., Jenz, S., & Jayaraman, A. (2022). Video-Based Pose Estimation for Gait Analysis in Stroke Survivors during Clinical Assessments: A Proof-of-Concept Study. *Digital Biomarkers*, *6*(1), 9–18. https://doi.org/10.1159/000520732

[30] Hu, F.-L., Jiang, D.-L., Xuan, X.-W., Li, H.-J., & Li, M.-J. (2024). High-Sensitivity Plantar Pressure Antenna Sensor Based on EBG Array for Gait Monitoring. *IEEE Sensors Journal*, *24*(8), 1–1. https://doi.org/10.1109/JSEN.2024.3372947

[31] Rajala, S. (née K., & Lekkala, J. (2014). Plantar shear stress measurements — A review. *Clinical Biomechanics (Bristol)*, *29*(5), 475–483. https://doi.org/10.1016/j.clinbiomech.2014.04.009

[32] Tavares C, Domingues MF, Frizera-Neto A, Leite T, Leitão C, Alberto N, Marques C, Radwan A, Rocon E, André P, Antunes P. Gait Shear and Plantar Pressure Monitoring: A Non-Invasive OFS Based Solution for e-Health Architectures. Sensors (Basel). 2018 Apr 25;18(5):1334. doi: 10.3390/s18051334. PMID: 29693624; PMCID: PMC5982155.

[33] Mertodikromo, J., Zorin, F., & Lee, C. J. (2020). A Low-Profile Shear Force Sensor for Wearable Applications. *IEEE Sensors Journal*, *20*(18), 10453–10459. https://doi.org/10.1109/JSEN.2020.2985396

[34] I. Mohammad and H. Huang, "Shear sensing based on a microstrip patch antenna," *Measurement Science and Technology*, vol. 23, no. 10, p. 105705, Sep. 2012, doi: https://doi.org/10.1088/0957-0233/23/10/105705.

[35] Guo, Y., Wang, L., & Xue, R. (2012). Design and Development on Piezoelectric Ceramic Type Insole 3D Force Measurement System Based on LabVIEW. *MANUFACTURING SCIENCE AND TECHNOLOGY, PTS 1-8*, *383–390*, 774-. https://doi.org/10.4028/www.scientific.net/AMR.383-390.774

[36] Zhao, J., Guo, Y., & Wang, L. (2013). An Insole Plantar Pressure Measurement System Based on 3D Forces Piezoelectric Sensor. *Sensors & Transducers*, *160*(12), 49–49.

[37] Eguchi, R., & Takahashi, M. (2023). Estimation of Three-Dimensional Ground Reaction Forces During Walking and Turning Using Insole Pressure Sensors Based on Gait Pattern Recognition. *IEEE Sensors Journal*, *23*(24), 31278–31286. https://doi.org/10.1109/JSEN.2023.3330633

[38] Zhao, N., Luo, Y., & Shen, Y. (2023). Design and Development of a Highly Performant 3-D Flexible Microforce Sensor for Miniature Biomedical Applications. *IEEE Sensors Journal*, *23*(4), 1–1. https://doi.org/10.1109/JSEN.2022.3233451

[39] Meena, K. V., Mathew, R., Leelavathi, J., & Ravi Sankar, A. (2017). Performance comparison of a single element piezoresistor with a half-active Wheatstone bridge for miniaturized pressure sensors. *Measurement : Journal of the International Measurement Confederation*, *111*, 340–350. https://doi.org/10.1016/j.measurement.2017.07.052

[40] G. Saggio and G. Orengo, "Flex sensor characterization against shape and curvature changes," *Sensors and Actuators A: Physical*, vol. 273, pp. 221–231, Apr. 2018, doi: https://doi.org/10.1016/j.sna.2018.02.035.

[41] G. Gerboni, A. Diodato, G. Ciuti, M. Cianchetti, and A. Menciassi, "Feedback Control of Soft Robot Actuators via Commercial Flex Bend Sensors," *IEEE/ASME Transactions on Mechatronics*, vol. 22, no. 4, pp. 1881–1888, Aug. 2017, doi: https://doi.org/10.1109/tmech.2017.2699677.

[42] Y. Zheng, Y. Peng, G. Wang, X. Liu, X. Dong, and J. Wang, "Development and evaluation of a sensor glove for hand function assessment and preliminary attempts at assessing hand coordination," *Measurement*, vol. 93, pp. 1–12, Nov. 2016, doi: https://doi.org/10.1016/j.measurement.2016.06.059.

[43] Ling, E., Lepow, B., Zhou, H., Enriquez, A., Mullen, A., & Najafi, B. (2020). The impact of diabetic foot ulcers and unilateral offloading footwear on gait in people with diabetes. *Clinical Biomechanics (Bristol)*, *73*, 157–161. https://doi.org/10.1016/j.clinbiomech.2020.01.014

[44] Scarton, A., Guiotto, A., Malaquias, T., Spolaor, F., Sinigaglia, G., Cobelli, C., Jonkers, I., & Sawacha, Z. (2018). A methodological framework for detecting ulcers' risk in diabetic foot subjects by combining gait analysis, a new musculoskeletal foot model and a foot finite element model. *Gait & Posture*, *60*, 279–285. https://doi.org/10.1016/j.gaitpost.2017.08.036

[45] Gnanasundaram, S., Ramalingam, P., Das, B. N., & Viswanathan, V. (2020). Gait changes in persons with diabetes: Early risk marker for diabetic foot ulcer. *Foot and Ankle Surgery*, *26*(2), 163–168. https://doi.org/10.1016/j.fas.2019.01.005

[46] Bacarin, T. A., Sacco, I. C. N., & Hennig, E. M. (2009). Plantar Pressure Distribution Patterns During Gait in Diabetic Neuropathy Patients with a History of Foot Ulcers. *Clinics (São Paulo, Brazil)*, *64*(2), 113–120. https://doi.org/10.1590/S1807-59322009000200008

[47] Giacomozzi, C. (2014). Preservation of gait biomechanics during offloading treatment of diabetic foot ulcers. *Journal of Foot and Ankle Research*, *7*(S1), 1-n/a. https://doi.org/10.1186/1757-1146-7-S1-A26

[48] Fernando, M. E., Crowther, R. G., Lazzarini, P. A., Sangla, K. S., Buttner, P., & Golledge, J. (2016). Gait parameters of people with diabetes-related neuropathic plantar foot ulcers. *Clinical Biomechanics (Bristol)*, *37*, 98–107. https://doi.org/10.1016/j.clinbiomech.2016.06.006

[49] Ebrahim Abdi, Mansour Eslami, & Mohand Taghipour. (2017). Effect of medial and lateral heel wedge changes On mechanical parameters of diabetic foot ulcers during gait. *Biyumikānīk-i varzishī*, *3*(3), 3–4.

[50] Tsakanikas, V., Ntanis, A., Rigas, G., Androutsos, C., Boucharas, D., Tachos, N., Skaramagkas, V., Chatzaki, C., Kefalopoulou, Z., Tsiknakis, M., & Fotiadis, D. (2023). Evaluating Gait Impairment in Parkinson's Disease from Instrumented Insole and IMU Sensor Data. *Sensors (Basel, Switzerland)*, *23*(8), 3902-. https://doi.org/10.3390/s23083902

[51] Chatzaki, C., Skaramagkas, V., Tachos, N., Christodoulakis, G., Maniadi, E., Kefalopoulou, Z., Fotiadis, D. I., & Tsiknakis, M. (2021). The Smart-Insole Dataset: Gait Analysis Using Wearable Sensors with a Focus on Elderly and Parkinson's Patients. *Sensors (Basel, Switzerland)*, *21*(8), 2821-. https://doi.org/10.3390/s21082821

[52] Mazumder, O., Khandelwal, P., Gavas, R., & Sinha, A. (2018). Assessment of insole based gait feature variation with progression of Parkinson's disease. *2018 IEEE SENSORS*, 486–489.

[53] Parati, M., Gallotta, M., Muletti, M., Pirola, A., Bellafa, A., De Maria, B., & Ferrante, S. (2022). Validation of Pressure-Sensing Insoles in Patients with Parkinson's Disease during Overground Walking in Single and Cognitive Dual-Task Conditions. *Sensors (Basel, Switzerland)*, *22*(17), 6392-. https://doi.org/10.3390/s22176392

[54] Tinazzi, M., Pilotto, A., Morgante, F., Marcuzzo, E., Cuoco, S., Ceravolo, R., Mazzucchi, S., Padovani, A., Romito, L. M., Eleopra, R., Nicoletti, A., Dallocchio, C., Arbasino, C., Bono, F., Magro, G., Demartini, B., Gambini, O., Modugno, N., Olivola, E., … Geroin, C. (2021). Functional gait disorders: Demographic and clinical correlations. *Parkinsonism & Related Disorders*, *91*, 32–36. https://doi.org/10.1016/j.parkreldis.2021.08.012

[55] Lipsitz, L. A., Lough, M., Niemi, J., Travison, T., Howlett, H., & Manor, B. (2015). A Shoe Insole Delivering Subsensory Vibratory Noise Improves Balance and Gait in Healthy Elderly People. *Archives of Physical Medicine and Rehabilitation*, *96*(3), 432–439. https://doi.org/10.1016/j.apmr.2014.10.004

[56] Unger, E. W., Histing, T., Rollmann, M. F., Orth, M., Herath, E., Menger, M., Herath, S. C., Grimm, B., Pohlemann, T., & Braun, B. J. (2021). Development of a dynamic fall risk profile in elderly nursing home residents: A free field gait analysis based study. *Archives of Gerontology and Geriatrics*, *93*, 104294–104294. https://doi.org/10.1016/j.archger.2020.104294

[57] E. T. Kim and S. Kim, “Development of smart insole for cycle time measurement in sewing process,” *Fashion and Textiles*, vol. 8, no. 1, Jan. 2021, doi: https://doi.org/10.1186/s40691-020-00234-5.

[58] Bas Van Hooren, P. Willems, G. Plasqui, and K. Meijer, “The accuracy of commercially available instrumented insoles (ARION) for measuring spatiotemporal running metrics,” *Scandinavian Journal of Medicine & Science in Sports*, vol. 33, no. 9, pp. 1703–1715, Jun. 2023, doi: https://doi.org/10.1111/sms.14424.

[59] R. Shaji and A. Singh, "Stridalyzer Insight Smart Insoles: a Clinical Grade Gait Analysis System," 2019 4th International Conference on Internet of Things: Smart Innovation and Usages (IoT-SIU), Ghaziabad, India, 2019, pp. 1-6, doi: 10.1109/IoT-SIU.2019.8777489.

Appendix

Force Curve Calculations Code

```
clc;
close all;
clear;

% Load voltage data from DAQ
voltageData = readtable('VoltageFilename.xlsx', 'ReadRowName', false);

% Load reference force data from Shimpo
forceData = readtable('ForceFileName.csv', 'ReadRowName', false);

% Extract relevant columns
% Make negative if tested in negative direction
voltageColumnx = -voltageData.Volt;  % Replace 'Volt' with the actual
column name

% Make negative if tested in negative direction
voltageColumny = voltageData.Volt_1;

% Force shimpo data
forceColumn = forceData.Var2;

% If force data collected is 0.1 resolution time scale (ideal 0.01)
% Original time vector
timeRes = 0.1;
desiredlength = length(forceColumn) * 10;
originalTimeVector_F = (0:length(forceColumn)-1) * timeRes;
originalTimeVector_F = originalTimeVector_F';
originalTimeVector = 1:length(voltageColumnx);

% Smooth data daq data
windowsize = length(voltageColumnx) .* 0.1;
xx = movmean(voltageColumnx, windowsize);
yy = movmean(voltageColumny, windowsize);

% Create a new time vector with the desired resolution (0.01 seconds)
% New time vector with number of cells is voltagecol
newTimeVector = linspace(originalTimeVector_F(1),
originalTimeVector_F(end), desiredlength);
interpForceColumn = interp1(originalTimeVector_F, forceColumn,
newTimeVector, 'linear', 'extrap');

% Crop force data (forcecolumn longer) or check same length (change length
% of voltage column before)
newForce = interpForceColumn(1:length(xx));
```

```
% Smooth shimpo force data
force_smooth = movmean(newForce, windowsize);

% Check if force/voltage collection begins at zero
% Otherwise, fix all values in force_smooth dataset
if force_smooth(1,1) ~= 0
    force_smooth = force_smooth - force_smooth(1,1);
end

if xx(1,1) ~= 0
    xx = xx - xx(1,1);
end

if yy(1,1) ~= 0
    yy = yy - yy(1,1);
end

% Find cross-correlation between force and voltage data
[correlation, lag] = xcorr(yy, force_smooth);

% Find the lag (time shift) at which the cross-correlation is maximum
[~, maxIndex] = max(correlation);
timeShift = lag(maxIndex);

% Perform quadratic regression to get the conversion equation
coefficients_quadratic_x = polyfit(xx, force_smooth, 2);
coefficients_quadratic_y = polyfit(yy, force_smooth, 2);

% Calculate the y values of the fitted quadratic line
fittedLine_quadratic_x = polyval(coefficients_quadratic_x, xx);
fittedLine_quadratic_y = polyval(coefficients_quadratic_y, yy);

% Perform cubic regression to get the conversion equation
coefficients_cubic_x = polyfit(xx, force_smooth, 3);
coefficients_cubic_y = polyfit(yy, force_smooth, 3);

% Calculate the y values of the fitted cubic line
fittedLine_cubic_x = polyval(coefficients_cubic_x, xx);
fittedLine_cubic_y = polyval(coefficients_cubic_y, yy);

% Display the time shift and linear regression coefficients
fprintf('Time shift: %.2f milliseconds\n', timeShift);
fprintf('Quadratic Regression Coefficients: %.4f (a2), %.4f (a1), %.4f
(a0)\n', coefficients_quadratic_y(1), coefficients_quadratic_y(2),
coefficients_quadratic_y(3));
fprintf('Cubic Regression Coefficients: %.4f (a3), %.4f (a2), %.4f (a1),
%.4f (a0)\n', coefficients_cubic_y(1), coefficients_cubic_y(2),
coefficients_cubic_y(3), coefficients_cubic_y(4));

% Create a plot of the aligned data
```

```
figure;
plot(xx, 'b-', 'LineWidth', 2, 'DisplayName', 'Aligned Y Voltage');
hold on;
plot(yy, 'g-', 'LineWidth', 2, 'DisplayName', 'Aligned X Voltage');
plot(force_smooth, 'r-', 'LineWidth', 2, 'DisplayName', 'Force Data');
xlabel('Time(ms)');
ylabel('Amplitude');
title('Alignment of Force and Voltage Data');
legend('X Voltage', 'Y Voltage', 'Reference Force(N)');
grid on;

% Convert back to force-quadratic
force_x_quadratic =
((xx.^2).*(coefficients_quadratic_x(1)))+(xx.*coefficients_quadratic_x(2))
;
force_y_quadratic = ((yy.^2).*-1.4788)+(yy.*3.4099);
figure;
plot(originalTimeVector, force_x_quadratic, 'b-', originalTimeVector,
force_smooth, 'r-', 'LineWidth', 2, 'DisplayName', 'Interpolated Force
Data');
hold on;
plot(originalTimeVector, force_y_quadratic, 'g-', 'LineWidth', 2,
'DisplayName', 'Interpolated Force Data');
xlabel('Time(ms)');
ylabel('Force(N)');
title('Correlation between Force and Voltage Converted - Quadratic');
legend('Calculated Force X', 'Reference Force', 'Calculated Force Y');
% equationText_quad = sprintf('y = %.4x.^2 + %.4x + %.4f',
coefficients_quadratic_y(1), coefficients_quadratic_y(2),
coefficients_quadratic_y(3));
% text(min(force_y_quadratic) + 1, max(force_smooth) - 0.1,
equationText_quad, 'Color', 'r');
grid on;

% Convert back to force-cubic
force_x_cubic =
((xx.^3).*(coefficients_cubic_x(1)))+(xx.^2).*(coefficients_cubic_x(2))+(x
x.*coefficients_cubic_x(3))+coefficients_cubic_x(4);
% force_y_cubic =
((yy.^3).*(coefficients_cubic_y(1)))+(yy.^2).*(coefficients_cubic_y(2))+(y
y.*coefficients_cubic_y(3))+coefficients_cubic_y(4);
figure;
plot(originalTimeVector, force_x_cubic, 'b-', originalTimeVector,
force_smooth, 'r-', 'LineWidth', 2, 'DisplayName', 'Interpolated Force
Data');
hold on;
xlabel('Time(ms)');
ylabel('Force(N)');
title('Correlation between Voltage and Force Converted - Cubic');
legend('Calculated Force', 'Reference Force');
```

```
equationText_cubic = sprintf('y = %.4x.^3 + %.4x.^2 + %.4x + %.4f',
coefficients_cubic_x(1), coefficients_cubic_x(2), coefficients_cubic_x(3),
coefficients_cubic_x(4));
text(min(force_x_cubic) + 1, max(force_smooth) - 0.1, equationText_cubic,
'Color', 'r');
grid on;

% Line hysteresis graph
% Create a plot of the aligned data with interpolated force data
figure;
plot(xx, force_smooth, 'b-', 'LineWidth', 2, 'DisplayName', 'Interpolated
Force Data');
hold on;
plot(xx, fittedLine_cubic_x, 'r-', 'LineWidth', 2, 'DisplayName', 'Fitted
Linear Line');
xlabel('Voltage(V)');
ylabel('Force(N)');
title('Correlation between Voltage and Force');
legend('Interpolated Force Data', 'Fitted Cubic Line');

% Show quadratic line
equationText_quad = sprintf('y = %.4x.^2 + %.4x + %.4f',
coefficients_quadratic_x(1), coefficients_quadratic_x(2),
coefficients_quadratic_x(3));
text(min(force_x_quadratic), max(force_smooth) + 0.2, equationText_quad,
'Color', 'r');

% Show Cubic Line
% equationText_cubic = sprintf('y = %.4x.^3 + %.4x.^2 + %.4x + %.4f',
coefficients_cubic_x(1), coefficients_cubic_x(2), coefficients_cubic_x(3),
coefficients_cubic_x(4));
% text(min(force_x_cubic) - 0.5, max(force_smooth) - 0.1,
equationText_cubic, 'Color', 'r');
grid on;

% Corrected hysteresis graph
% Add phase shift and redo visuals
phase_shift = 20;
shiftedTimeVector = originalTimeVector - phase_shift;
shiftedVoltageData_x = interp1(shiftedTimeVector, xx, originalTimeVector,
'linear', 'extrap');
shiftedVoltageData_y = interp1(shiftedTimeVector, yy, originalTimeVector,
'linear', 'extrap');

% Solve for new correlation
shifted_coefficients_quadratic_x = polyfit(shiftedVoltageData_x,
force_smooth, 2);
shifted_fittedLine_quadratic_x = polyval(shifted_coefficients_quadratic_x,
shiftedVoltageData_x);
```

```
shifted_coefficients_quadratic_y = polyfit(shiftedVoltageData_y,
force_smooth, 2);
shifted_fittedLine_quadratic_y = polyval(shifted_coefficients_quadratic_y,
shiftedVoltageData_y);

shifted_coefficients_cubic_x = polyfit(shiftedVoltageData_x, force_smooth,
3);
shifted_fittedLine_cubic_x = polyval(shifted_coefficients_cubic_x,
shiftedVoltageData_x);

shifted_coefficients_cubic_y = polyfit(shiftedVoltageData_y, force_smooth,
3);
shifted_fittedLine_cubic_y = polyval(shifted_coefficients_cubic_y,
shiftedVoltageData_y);

% Corrected visuals
% Voltage Visuals
figure;
plot(shiftedVoltageData_x, 'g-', 'LineWidth', 2, 'DisplayName', 'Aligned Y
Voltage');
hold on;
plot(shiftedVoltageData_y, 'b-', 'LineWidth', 2, 'DisplayName', 'Aligned X
Voltage');
plot(force_smooth, 'r-', 'LineWidth', 2, 'DisplayName', 'Force Data');
xlabel('Time(ms)');
ylabel('Amplitude');
title('Alignment of Force and Voltage Data');
legend('X Voltage', 'Y Voltage', 'Reference Force(N)');
grid on;

% Force Visuals
shiftedForceData_x =
((shiftedVoltageData_x.^2).*(shifted_coefficients_quadratic_x(1)))+(shifte
dVoltageData_x.*shifted_coefficients_quadratic_x(2))+shifted_coefficients_
quadratic_x(3);
shiftedForceData_y =
((shiftedVoltageData_y.^2).*(shifted_coefficients_quadratic_y(1)))+(shifte
dVoltageData_y.*shifted_coefficients_quadratic_y(2))+shifted_coefficients_
quadratic_y(3);

cubic_shiftedForceData_x =
((shiftedVoltageData_x.^3).*(shifted_coefficients_cubic_x(1)))+((shiftedVo
ltageData_x.^2).*shifted_coefficients_cubic_x(2))+(shiftedVoltageData_x.*s
hifted_coefficients_cubic_x(3))+(shifted_coefficients_cubic_x(4));
cubic_shiftedForceData_y =
((shiftedVoltageData_x.^3).*(shifted_coefficients_cubic_y(1)))+((shiftedVo
ltageData_y.^2).*shifted_coefficients_cubic_y(2))+(shiftedVoltageData_y.*s
hifted_coefficients_cubic_y(3))+(shifted_coefficients_cubic_y(4));

figure;
```

```
plot(originalTimeVector, force_smooth, 'r-', 'LineWidth', 2,
'DisplayName', 'Original Voltage');
hold on;
plot(originalTimeVector, shiftedForceData_x, 'b-', 'LineWidth', 2,
'DisplayName', 'Force Data');
xlabel('Time (seconds)');
ylabel('Amplitude');
title('Comparison of Voltage and Force Data with Phase Shift');
legend('Location', 'Best');
grid on;

% Hysteresis Visual - Quadratic
figure;
plot(shiftedVoltageData_x, force_smooth, 'b-', 'LineWidth', 2,
'DisplayName', 'Interpolated Force Data');
hold on;
plot(shiftedVoltageData_x, shifted_fittedLine_quadratic_x, 'r-',
'LineWidth', 2, 'DisplayName', 'Fitted Linear Line');
xlabel('Voltage(V)');
ylabel('Force(N)');
title('Correlation between Voltage and Force after Phase Shift');
legend('Interpolated Shifted Force Data', 'Fitted Quadratic Line');
grid on;

% Show Line
equationText_quad_shifted = sprintf('y = %.4x.^2 + %.4x + %.4f',
shifted_coefficients_quadratic_x(1), shifted_coefficients_quadratic_x(2),
shifted_coefficients_quadratic_x(3));
text(min(shiftedForceData_x), max(force_smooth) - 0.1,
equationText_quad_shifted, 'Color', 'r');

% Hysteresis visual - cubic
figure;
plot(shiftedVoltageData_x, force_smooth, 'b-', 'LineWidth', 2,
'DisplayName', 'Interpolated Force Data');
hold on;
plot(shiftedVoltageData_x, shifted_fittedLine_cubic_x, 'r-', 'LineWidth',
2, 'DisplayName', 'Fitted Linear Line');
xlabel('Voltage(V)');
ylabel('Force(N)');
title('Correlation between Voltage and Force after Phase Shift');
legend('Interpolated Shifted Force Data', 'Fitted Cubic Line');
grid on;

% Show Line
equationText_quad_shifted = sprintf('y = %.4x.^3 + %.4x.^2 + %.4x + %.4f',
shifted_coefficients_cubic_x(1), shifted_coefficients_cubic_x(2),
shifted_coefficients_cubic_x(3), shifted_coefficients_cubic_x(4));
text(min(shiftedForceData_x) - 0.2, max(force_smooth) - 0.1,
equationText_quad_shifted, 'Color', 'r');
```

```
% Error Calculations
abs_error = abs((shiftedForceData_x) - (force_smooth)) ./ (force_smooth)
.* 100;
valid_values = isfinite(abs_error);
percent_error = abs_error(valid_values);

average_percent_error = mean(percent_error);
average_percent_error_adj = mean(percent_error(500:6500));
median_percent_error = median(percent_error);
peak_percent_error = abs(max(shiftedForceData_x) - max(force_smooth)) ./
max(force_smooth) .* 100;
max_error = max(percent_error(500:6500));
norm_max_error = max_error ./ (max(force_smooth)-min(force_smooth));

disp(['Average Percent Error for the system: ',
num2str(average_percent_error), '%'])
disp(['Adjusted Average Percent Error for the system: ',
num2str(average_percent_error_adj), '%'])
disp(['Median Percent Error for the system: ',
num2str(median_percent_error), '%'])
disp(['Peak Force Percent Error for the system: ',
num2str(peak_percent_error), '%'])
disp(['Maximum Percent Error for the system: ', num2str(max_error), '%'])
disp(['Normalized Maximum Percent Error for the system: ',
num2str(norm_max_error), '%'])
```

Practical Testing Code

```
clc;
close all;
clear;

% Load voltage data
voltageDataF = readtable('FrontAnalysisPointDAQ.xlsx', 'ReadRowNames',
false);
voltageDataM = readtable('MiddleAnalysisPointDAQ.xlsx', 'ReadRowNames',
false);
voltageDataB = readtable('BackAnalysisPointDAQ.xlsx', 'ReadRowNames',
false);

% Extract relevant columns
% Front
% Make negative if tested in negative direction
voltageColumnx_F = voltageDataF.Volt;  % Replace 'Volt' with the actual
column name

% Make negative if tested in negative direction
voltageColumny_F = -voltageDataF.Volt_1;

% Make negative if tested in negative direction
voltageColumnz_F = voltageDataF.Volt_2;

% Extract relevant columns
% Middle
% Make negative if tested in negative direction
voltageColumnx_M = voltageDataM.Volt;  % Replace 'Volt' with the actual
column name

% Make negative if tested in negative direction
voltageColumny_M = -voltageDataM.Volt_1;

% Make negative if tested in negative direction
voltageColumnz_M = -voltageDataM.Volt_2;

% Extract relevant columns
% Back
% Make negative if tested in negative direction
voltageColumnx_B = voltageDataB.Volt;  % Replace 'Volt' with the actual
column name

% Make negative if tested in negative direction
voltageColumny_B = -voltageDataB.Volt_1;
```

```
% Make negative if tested in negative direction
voltageColumnz_B = voltageDataB.Volt_2;

% Set time vector
originalTimeVectorF = 1:length(voltageColumnz_F);
originalTimeVectorM = 1:length(voltageColumnz_M);
originalTimeVectorB = 1:length(voltageColumnz_B);

% Smooth data daq data
windowsize = 500;
xxF = movmean(voltageColumnx_F, windowsize);
yyF = movmean(voltageColumny_F, windowsize);
zzF = movmean(voltageColumnz_F, windowsize);

xxM = movmean(voltageColumnx_M, windowsize);
yyM = movmean(voltageColumny_M, windowsize);
zzM = movmean(voltageColumnz_M, windowsize);

xxB = movmean(voltageColumnx_B, windowsize);
yyB = movmean(voltageColumny_B, windowsize);
zzB = movmean(voltageColumnz_B, windowsize);

if xxF(1,1)~=0
    xxF = xxF - xxF(1,1);
end

if yyF(1,1) ~= 0
    yyF = yyF - yyF(1,1);
end

if zzF(1,1) ~= 0
    zzF = zzF - zzF(1,1);
end

if xxM(1,1)~=0
    xxM = xxM - xxM(1,1);
end

if yyM(1,1) ~= 0
    yyM = yyM - yyM(1,1);
end

if zzM(1,1) ~= 0
    zzM = zzM - zzM(1,1);
end
```

```
if xxB(1,1)~=0
    xxB = xxB - xxB(1,1);
end

if yyB(1,1) ~= 0
    yyB = yyB - yyB(1,1);
end

if zzB(1,1) ~= 0
    zzB = zzB - zzB(1,1);
end

% Create a plot of the aligned data
figure;
plot(xxF, 'g-', 'LineWidth', 2, 'DisplayName', 'Aligned X Voltage');
hold on;
plot(yyF, 'y-', 'LineWidth', 2, 'DisplayName', 'Aligned Y Voltage');
plot(zzF, 'b-', 'LineWidth', 2, 'DisplayName', 'Aligned Z Voltage')
xlabel('Time(ms)');
ylabel('Voltage(V)');
title('Voltage Data - Front');
legend('X Voltage', 'Y Voltage', 'Z Voltage');
grid on;

figure;
plot(xxM, 'g-', 'LineWidth', 2, 'DisplayName', 'Aligned X Voltage');
hold on;
plot(yyM, 'y-', 'LineWidth', 2, 'DisplayName', 'Aligned Y Voltage');
plot(zzM, 'b-', 'LineWidth', 2, 'DisplayName', 'Aligned Z Voltage')
xlabel('Time(ms)');
ylabel('Voltage(V)');
title('Voltage Data - Middle');
legend('X Voltage', 'Y Voltage', 'Z Voltage');
grid on;

figure;
plot(xxB, 'g-', 'LineWidth', 2, 'DisplayName', 'Aligned X Voltage');
hold on;
plot(yyB, 'y-', 'LineWidth', 2, 'DisplayName', 'Aligned Y Voltage');
plot(zzB, 'b-', 'LineWidth', 2, 'DisplayName', 'Aligned Z Voltage')
xlabel('Time(ms)');
ylabel('Voltage(V)');
title('Voltage Data - Back');
legend('X Voltage', 'Y Voltage', 'Z Voltage');
grid on;
```

```
% Convert back to force-cubic
force_x_cubic_F = ((xxF.^3).*(0.00016631)+((xxF.^2).*(-
.049283))+(xxF.*1.2484));
force_y_cubic_F = ((yyF.^3).*-1.4379)+((yyF.^2).*(3.7131))+(yyF.*0.13609);
force_z_cubic_F = ((zzF.^2).*(0.79819))+((zzF).*(0.071869));
figure;
plot(originalTimeVectorF, force_z_cubic_F, 'b-', 'LineWidth', 2,
'DisplayName', 'Interpolated Force Data');
hold on;
plot(originalTimeVectorF, force_x_cubic_F, 'g-', 'LineWidth', 2,
'DisplayName', 'Interpolated Force Data');
plot(originalTimeVectorF, force_y_cubic_F, 'y-', 'LineWidth', 2,
'DisplayName', 'Interpolated Force Data');
xlabel('Time(ms)');
ylabel('Force(N)');
title('Calculated Force Output - Front');
legend('Calculated Force Z', 'Calculated Force X', 'Calculated Force Y');
% equationText_cubic = sprintf('y = %.4x.^3 + %.4x.^2 + %.4x + %.4f',
coefficients_cubic_x(1), coefficients_cubic_x(2), coefficients_cubic_x(3),
coefficients_cubic_x(4));
% text(min(force_y_cubic) + 1, max(force_smooth) - 0.1,
equationText_cubic, 'Color', 'r');
grid on;

force_x_cubic_M = ((xxM.^2).*(-0.065227)+((xxM).*(.92249)));
force_y_cubic_M = ((yyM.^2).*1.6473)+((yyM).*(-.85318));
force_z_cubic_M = ((zzM.^2).*(0.51986)+((zzM).*(1.5348)));
figure;
plot(originalTimeVectorM, force_z_cubic_M, 'b-', 'LineWidth', 2,
'DisplayName', 'Interpolated Force Data');
hold on;
plot(originalTimeVectorM, force_x_cubic_M, 'g-', 'LineWidth', 2,
'DisplayName', 'Interpolated Force Data');
plot(originalTimeVectorM, force_y_cubic_M, 'y-', 'LineWidth', 2,
'DisplayName', 'Interpolated Force Data');
xlabel('Time(ms)');
ylabel('Force(N)');
title('Calculated Force Output - Middle');
legend('Calculated Force Z', 'Calculated Force X', 'Calculated Force Y');
% equationText_cubic = sprintf('y = %.4x.^3 + %.4x.^2 + %.4x + %.4f',
coefficients_cubic_x(1), coefficients_cubic_x(2), coefficients_cubic_x(3),
coefficients_cubic_x(4));
% text(min(force_y_cubic) + 1, max(force_smooth) - 0.1,
equationText_cubic, 'Color', 'r');
grid on;
```

```
force_x_cubic_B = ((xxB.^3).*(0.02432)+((xxB.^2).*(-
.6128))+(xxB.*3.3121));
force_y_cubic_B = ((yyB.^3).*0.15096)+((yyB.^2).*(-
0.70229))+(yyB.*2.2686);
force_z_cubic_B = ((zzB.^2).*(0.53724))+(zzB).*(5.4409);
figure;
plot(originalTimeVectorB, force_z_cubic_B, 'b-', 'LineWidth', 2,
'DisplayName', 'Interpolated Force Data');
hold on;
plot(originalTimeVectorB, force_x_cubic_B, 'g-', 'LineWidth', 2,
'DisplayName', 'Interpolated Force Data');
plot(originalTimeVectorB, force_y_cubic_B, 'y-', 'LineWidth', 2,
'DisplayName', 'Interpolated Force Data');
xlabel('Time(ms)');
ylabel('Force(N)');
title('Calculated Force Output - Back');
legend('Calculated Force Z', 'Calculated Force X', 'Calculated Force Y');

% equationText_cubic = sprintf('y = %.4x.^3 + %.4x.^2 + %.4x + %.4f',
coefficients_cubic_x(1), coefficients_cubic_x(2), coefficients_cubic_x(3),
coefficients_cubic_x(4));
% text(min(force_y_cubic) + 1, max(force_smooth) - 0.1,
equationText_cubic, 'Color', 'r');
grid on;
```